A Laser-induced Fluorescence Study of the Reaction $F + I_2 \rightarrow IF + I$.

ROBERT MALLOCH GLEN

Ph.D.

University of Edinburgh

1980

Declaration

I declare that this thesis is my own composition and that the work described herein is my own or where done in collaboration with others contains a substantial contribution from me. Where reported work was done mainly by others due credit is given and references are given to all other sources of information.

ACKNOWLEDGEMENTS

I am grateful to the Departments of Physics and Chemistry for the use of their facilities and to the Science Research Council for financial support.

To my supervisors, Prof. R.J. Donovan and Dr. M.A.D. Fluendy, I am much indebted. Robert Donovan's enthusiasm and counsel in times of adversity was an invaluable aid, while Malcolm Fluendy provided inspired reasoning in matters experimental and theoretical which was turely beyond description. My thanks also go to Dr. Alastair Rae for his sound practical advice, continual interest and rigorous criticism of the final draft.

I am pleased to acknowledge also the general help of my co-workers in this experiment. Doug (Heid the Ba') Fernie taught me much about how to conduct (and not conduct) research, while to Ross Wheeler go my inexpressible thanks for his tolerance and selfless assistance in extracting the necessary data. Many thanks also go to members (past and present) of the Molecular Beams and Kinetic Spectroscopy groups, in particular Dave Sutton and Geoff Black for numerous conversations at various levels of scientific sophistication.

Many technical personnel contributed to this work. Particular credit goes to Lewis Kennedy for his patient electronic wizardry, and Ronnie Proc for work on the laser cavity and other engineering jobs. Jimmy McKemmie while a late arrival in the group was always willing with advice and assistance.

Finally thanks to Chris Steven and Bob Reid of ICI Corporate Lab for respectively typing and proof-reading the final manuscript.

For Linda

ABSTRACT

An experimental arrangement for the study of internal energy partitioning in the reaction $F + I_2 \rightarrow IF + I$ ($\Delta D_o = 133$ kJ mol^{-1}) is described. The reagents were formed in a molecular beam system and vibrational levels of IF were detected by laser-induced fluorescence using a nitrogen laser pumped dye laser in the region 450 - 500 nm. The (6,0), (5,0), (8,1) and (8,2) bands were detected. The signal was found to be of low intensity ($<1s^{-1}$) but broadly in agreement with that predicted by a feasibility calculation. Because of the high noise rate, (laser induced afterpulsing in the photomultiplier) the data was of poor quality. A substantial improvement in signal-to-noise ratio is expected to arise mainly from improvements to the dye laser beam quality and an increase in the fluorine atom source intensity. Rotational lines in the spectra were not resolved due to the high laser linewidth ($\sim 2\text{Å}$). A simulation procedure was developed and used to extract the vibrational populations for v" = 0,1,2. This showed an inversion with a linear surprisal plot having $\lambda \simeq -5.3$ ($<f_v'> \simeq 0.6$). The rotational temperature was estimated by fitting trial distributions to the observed band profile and found to be $\sim 200 \pm 100$K ($<f_R'> \simeq 0.02$). This partitioning is not compatible with $<f_T'>$ determined from angular scattering measurements but shows some similarity to that of F + ICl → IF + Cl. Such results suggest a direct "early downhill" trajectory for this class of reactions.

CONTENTS

CHAPTER 1

INTRODUCTION

1.1 Reaction Dynamics

The determination of state-to-state reaction cross-sections is the main aims of reaction dynamics[1]. Conventional gas-phase 'bulb' experiments suffer from the defect that reactant energy states are sampled from a Boltzmann distribution and that product energy distributions are rapidly destroyed by energy transfer processes[2]. The reaction rate constant is thus the result of folding the initial distribution of states n at temperature T, $p(n;T)$ into the reactive cross-section for product formation $\sigma_R(n)$[3] in accordance with equ. 1.1.

$$k(T) = \sum_i p(n;T) \int \sigma_R(n) v P(v;T) dv \quad , \qquad 1.1$$

where $P(v;T)$ is the Boltzmann distribution of velocities at temperature T. The rate constant thus offers no information on which states, if any, have the greatest efficacy at promoting reaction.

Similarly, the cross-section $\sigma_R(n)$ is the result of summing the state-to-state cross-sections $\sigma_R(n;n')$ for product formation in the accessible states n'

$$\sigma_R(n) = \sum_{n'} \sigma_R(n;n') \quad , \qquad 1.2$$

the details of which are rapidly lost by thermalisation. As a result the selectivity of energy consumption from the reagent state n and the specificity of production of product states n' is washed out in the averaging in the canonical ensemble.

The behaviour of state-to-state cross-sections is of importance in a variety of areas of chemical interest. In particular the behaviour of elementary processes in the upper atmosphere[4] and the

continuing development of high power pulsed I.R. chemical lasers such as the HF laser[5] are highly dependent on such knowledge. The possibility of obtaining pulsed laser action in the visible spectrum, generated by purely chemical means[6] is also of current interest, as is that of producing an I.R. chemical laser based on an atomic transition[6,7]. In addition theoretical proposals leading to different forms of $\sigma(n;n')$ have a bearing on the interpretation of non-reactive interactions such as collisional quenching[8]. Specific excitation of product states has been applied to isotope separation[9] and state-selective synthetic methods are also forthcoming[10].

The determination of the quantities $\sigma(n,n')$ has been approached in two opposite directions; the production of selected reagent states and the analysis of product states before collisional relaxation. Historically, the latter proved more tractable[11], but with the development of pulsed IR gas lasers rapid development in the former has occurred[4].

In the case of product state analysis it is convenient to perform an average over the reagent states

$$\sigma_R(n') = \sum_n \sigma_R(n,n')$$

to obtain the cross-section for product formation in the state n'. By using the technique of supersonic molecular beam formation[12] the width of the reagent state distribution can be significantly reduced and the effect of the averaging minimised. Even where $p(n;T)$ is quite wide, the $\sigma_R(n')$ can still be significant.

In the remainder of this chapter some theoretical and experimental techniques relevant to the work in this thesis are described. A

recent review[13] has given a comprehensive account of the systems studied by these methods.

1.1.1 Theoretical methods and models

Theoretically the prediction of $\sigma(n;n')$ has been strongly associated with the concept of potential energy hypersurfaces[14]. In this approach the Born-Oppenheimer approximation is used to separate the wavefunctions for nuclear and electronic motion to yield the electronic eigenvalues U_i as a function of the nuclear co-ordinates. If the U_i are well separated their interaction can be neglected and the function $U_i(r_j)$ treated as the effective potential in which the nuclei move. Special methods are required if this condition is not met[15].

Since complete ab initio calculations of the potential U_i have been achieved only in the simplest systems ($H + H_2$ and isotopomeres), for reactions of more chemical interest recourse has to be made to semiempirical methods for the construction of the surface. A variety of such prescriptions have been detailed of which the most successful, for simple triatomic reactions, have been the diatomics in molecule (DIM) surface, and its derivative the London-Eyring-Polanyi-Sato (LEPS) surface. In this approach the necessary data are spectroscopic parameters describing the asymptotic behaviour of the species and adjustable parameters to vary the gross features of the surface, such as wells and barriers.

The effect on the $\sigma(n;n')$ caused by variation of such parameters is determined by the method of classical trajectory calculations[16]. For a given choice of initial conditions of the reactants (relative kinetic energy, vibrational phase, etc.) the classical equations of

motion are integrated along the reaction path through the surface, until product separation occurs. Random variation of the initial conditions then allows the distribution of product states to be built up, and their dependence on the nature of the surface to be determined. This approach, pioneered by J.C. Polanyi and co-workers, has led to the formulations of a set of correlation 'rules' for describing energy partitioning in reaction products as a function of the surface[14,17].

In a simple exothermic reaction of the type

$$A + BC \rightarrow AB + C \qquad A,B,C; \text{ atoms}$$

it is convenient to consider a cut through the hypersurface at constant angle θ (between r_{AB} and r_{BC}) to give a fixed angle surface (FAS) which is displayed as a contour diagram (Fig. 1.1). Polanyi divided the exothermicity ΔD_o of the reaction into attractive energy release (A_1), which is evolved in the entrance valley on a path parallel to the r_{AB} axis, and repulsive energy release (R_1), which is the remainder.

While this rectilinear method of classification is convenient for describing the surface alone, when dynamic behaviour is considered it is necessary to take into account the inertial properties of the reacting system. Inertial coupling arises because of the relative masses of the species, and is best considered in the skewed and scaled co-ordinate system that results from the diagonalisation of the kinetic energy[14] (Fig. 1.2). In the absence of inertial coupling such as occurs in the limit of B being much more massive than A (Fig. 1.2(a)), the representative point follows the line of steepest descent over the surface, which is initially along a line parallel to the Q_1 axis (the

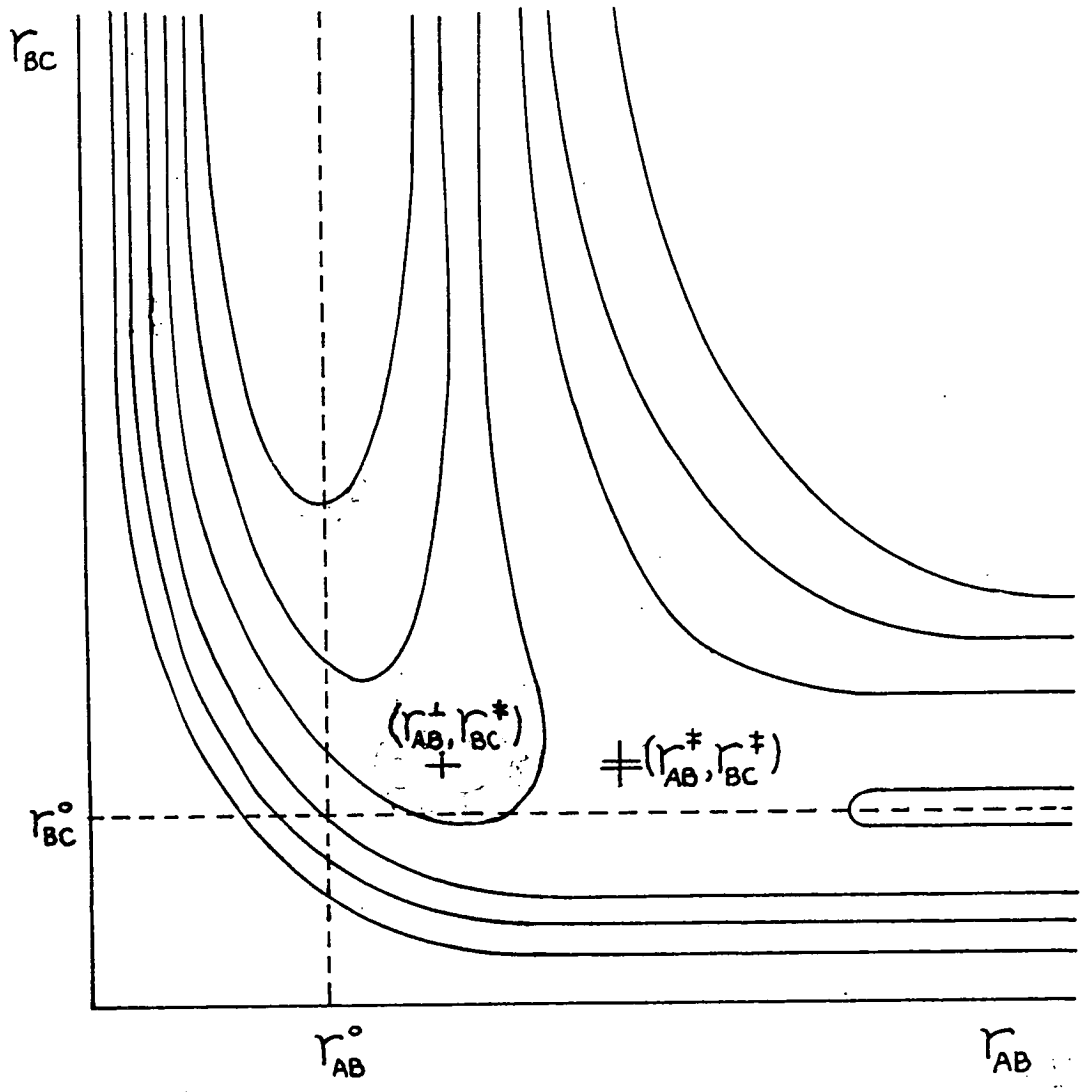

Fig. 1.1 Classification of Energy release in the rectilinear scheme $\ddagger$ is the barrier maximum and r_{AB}° and r_{BC}° are the asymptotic equilibrium internuclear distances in AB and BC. The attractive release is

$$A_{\perp} = \tilde{U}(r_{AB}^{\ddagger}, r_{BC}^{\ddagger}) - \tilde{U}(r_{AB}^{\perp}, r_{BC}^{\ddagger})$$

where r_{AB} is the point of minimum energy on the line $r_{BC} = r_{BC}$. The repulsive release is

$$R_{\perp} = \Delta D_{o} - E_{a} - A_{\perp}$$

where ΔD_{o} is the exothermicity and E_{a} the barrier height.

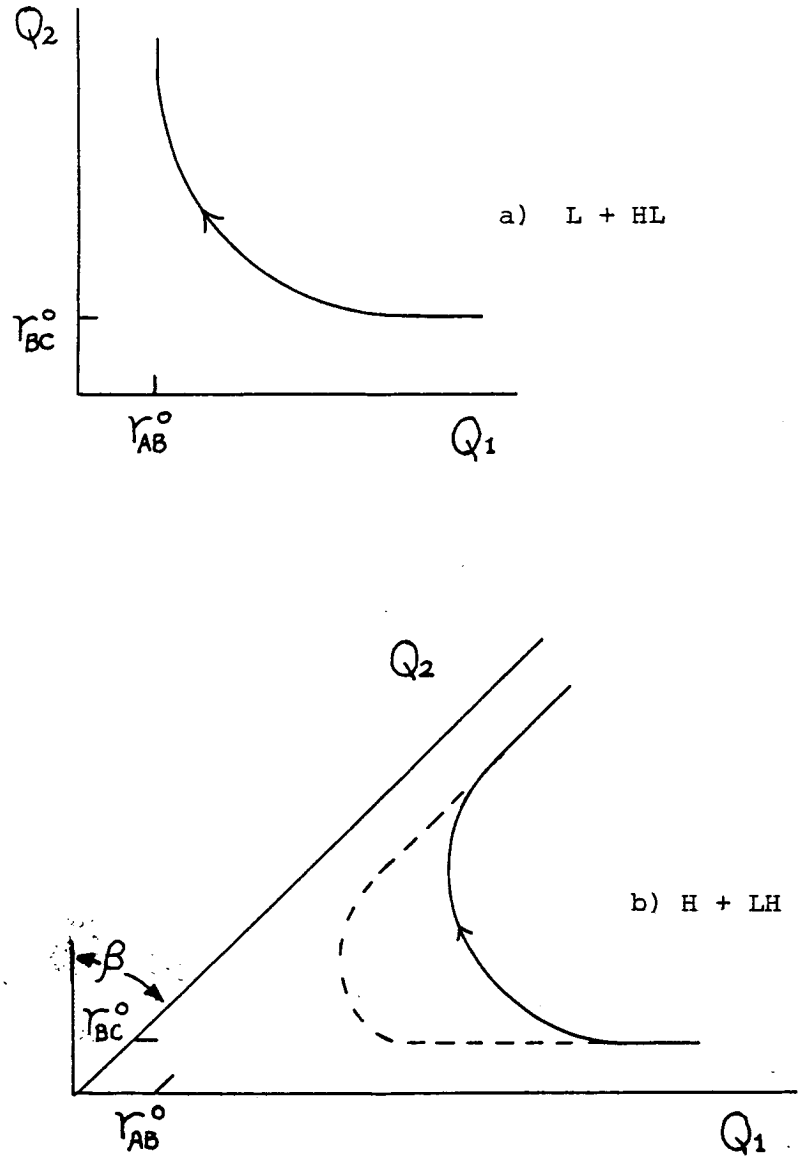

Fig. 1.2. Lines of steepest descent showing the effect of inertial coupling in the (Q_1, Q_2) co-ordinate system

a) If $M_B >> M_A, M_C$ then $\beta \simeq 0$ and the line of maximum force is determined only by the nature of the surface

b) If $M_B << M_A, M_C$ then $\beta \rightarrow 90^\circ$ and there is a component of force in the Q_2 direction which tends to pull the path away from the entry line. $\alpha \simeq 1$ in both cases.

entry line). As the coupling increases, the skew angle β, given by

$$\sin \beta = \left(\frac{m_A m_C}{m_{AB} m_{BC}} \right)^{\frac{1}{2}} , \qquad 1.3$$

increases and the path is pulled away from this line and bends gradually into the exit channel (Fig. 1.2(b)). The actual trajectory over the surface depends on the energy release. For early attractive release the momentum of the system is too great to allow the representative point to turn the corner and it tends to follow the entry line. The high velocity in the entrance channel becomes vibration of the AB bond. If the release is late then the line of steepest descent can be followed smoothly into the exit channel, and the energy release becomes relative translational energy of the products. When the release occurs in the region of the corner then the outcome depends on the relative masses in a second way (mixed energy release). If the scale factor, α, given by

$$\alpha = \left(\frac{m_{AB} m_C}{m_{BC} m_A} \right)^{\frac{1}{2}} , \qquad 1.4$$

scales the entrance co-ordinate relative to the exit co-ordinate then the force in the Q_2 direction is increased relative to that in the Q_1 direction, allowing the point to 'cut the corner' of the surface. Since this mechanism allows the representative point to avoid repulsive release, product vibration is favoured. The mass combination L + HH (L = light; H = heavy) shows the opposite effect in that the exit channel is stretched. The point thus tends to follow a more rectilinear trajectory, and show mainly repulsive release on a repulsive surface and mainly attractive release on an attractive one,

with little mixed release. This behaviour is known as the light atom anomaly[17], and means that this mass combination is more sensitive to the features of the surface than any other (Fig. 1.3).

Some degree of correlation between the gross features of the surface, as deduced by comparison of experiment and trajectory calculations, and molecular structure has been achieved using a naive molecular orbital theory[18]. Figure 1.4 shows schematic representations of bonding in HYZ and XYZ intermediates, as in H + Cl_2 and Cl + Br_2, in a near linear configuration. In the case of HYZ the highest occupied orbital is $2\sigma^*$. This orbital is more YZ antibonding and HY bonding than vice versa[11], so a strong Y-Z repulsion is induced is induced as the H-atom approaches. On the other hand approach of an O-atom or another halogen gives the configuration $s^2s^2 1\sigma^2 2\sigma^2 1\pi^4 2\pi^4 3\pi^{*4} 3\sigma^{*1/2}$. Since the antibonding $3\sigma^*$ orbital cannot offset the net bonding effect of the 1σ, 2σ orbitals, a bound state results, which is representated by a well in the surface, showing attractive release.

To bypass the computational excesses, associated with trajectory calculations, a number of statistical/dynamical and purely statistical theories have been evolved. Within this framework a division has been made between reactions which are known a posteriori to occur either via a complex or a direct mechanism. In the former a bound state is considered to be formed if the intermediate has a lifetime greater than a few rotational periods, whereas in the latter the lifetime is very much shorter.

Transition state theory[19,20] has been used to determine reaction rates, by calculating the rate of decomposition of the inter-

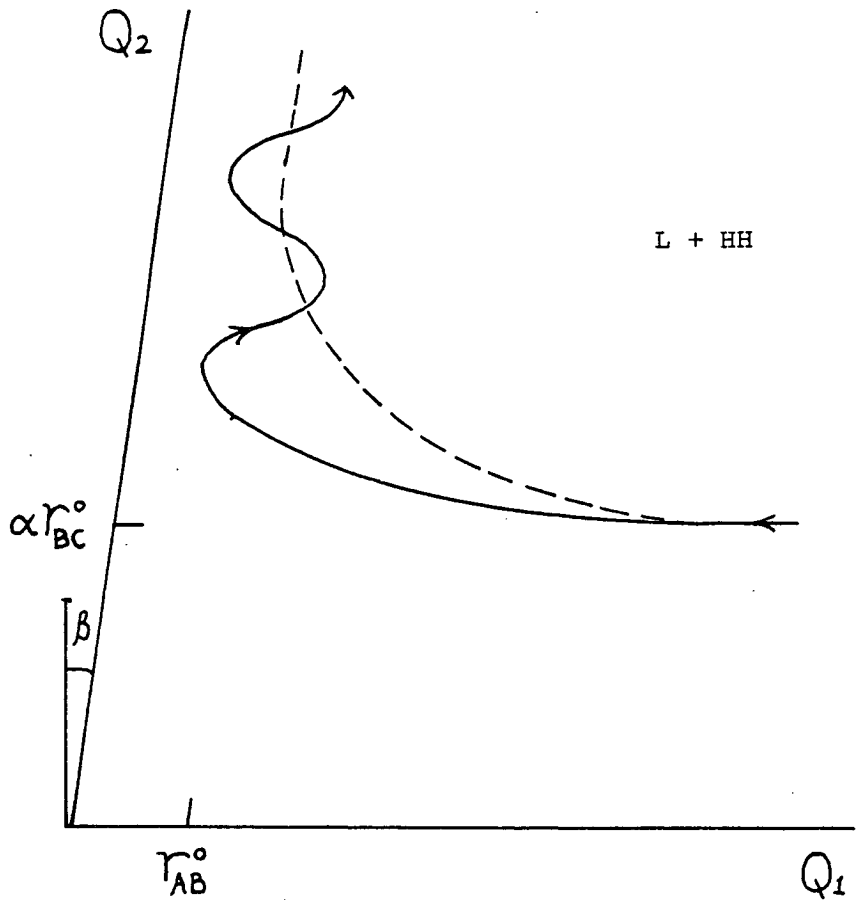

Fig. 1.3. Schematic of trajectory for $M_A << M_B, M_C$ in the (Q_1, Q_2) system on a surface with $A_1/\Delta D_o \simeq 1$. $\beta \simeq 0$, but the reduced force in the Q_1 direction, and high velocity in the entrance channel means that the representative point cannot follow the line of steepest descent (dotted) and enters the exit valley from the side.

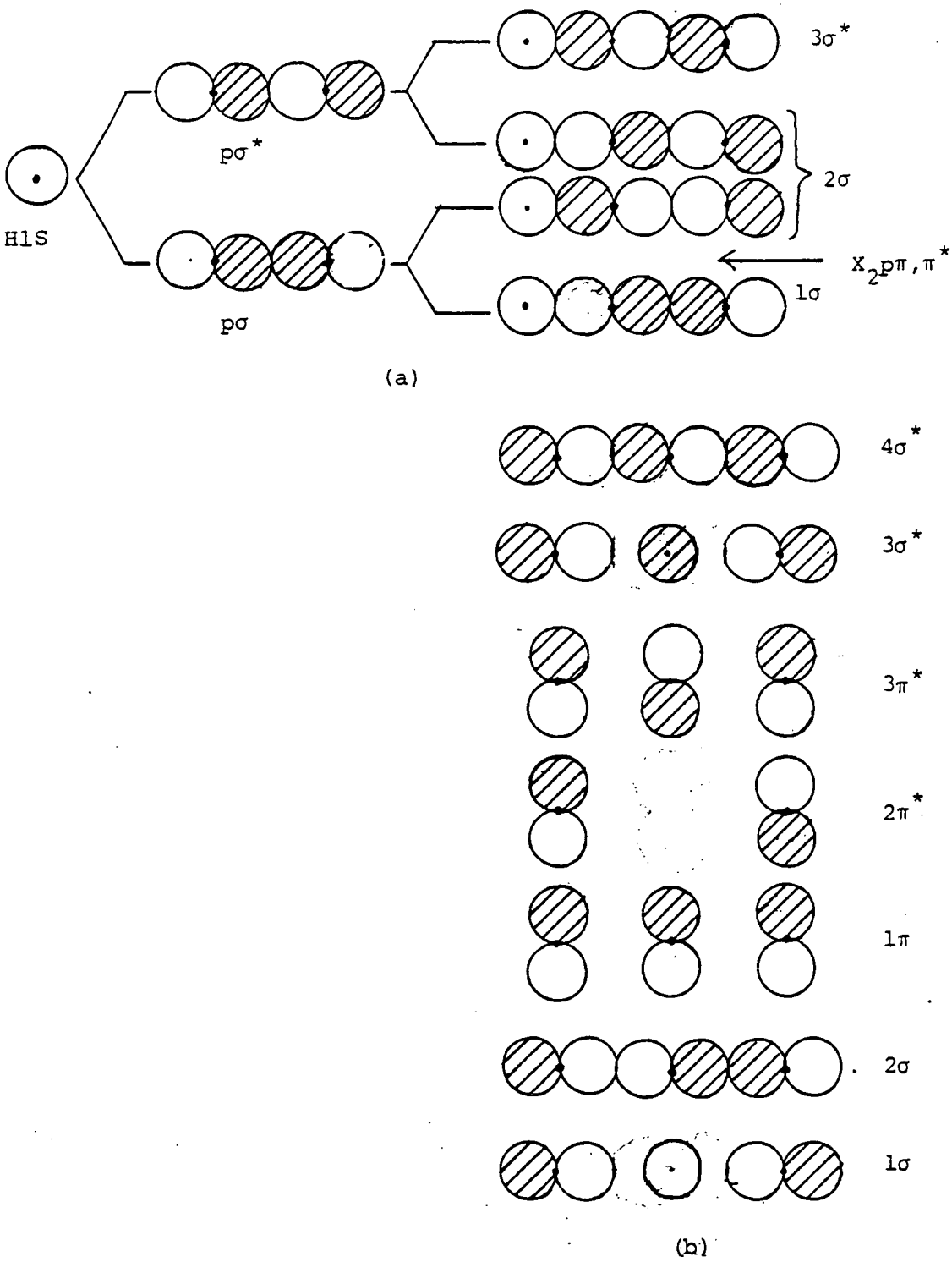

Fig. 1.4. Molecular orbital schemes

a) H + YZ

b) X + YZ

after Herschbach[11] and Grice[49]. See text for details

mediate in some critical configuration, usually a saddle point on the surface. To obtain product state distributions, dynamical information about the surface between the transition state and the asymptotic product limit is still required[21] however. If there exists more than one such critical region then a well must exist between them, and the details of the surface in the exit channel become less important.

For 'loose' transition states in which the activation energy is ∿zero the transition state is defined by the point at which the complex passes over the centrifugal barrier. Since no distortion of the complex structure occurs at such a point, the product energy distribution depends only on the density of states in each exit channel. Angular momentum conservation may restrict the accessible areas of phase space and this criterion was used in the phase space theory (PST) of Light and co-workers[22-23]. 'Tight' transition states in which E_a is non-zero and bond deformation occurs at the barrier, have also been investigated by incorporating dynamical information, as in the reactions of F + alkenes[26]. A simple theory based on the RRKM theory of unimolecular reactions[27] has been used for both loose and tight transition states. For loose states, equivalence with PST is claimed, although there is some disagreement in cases where the two have been applied[28]. Recently some progress has been made towards the unification of "complex" PST and "direct" transition state theory[29].

Statistical calculations based on density of states descriptions serve as useful yardsticks against which either internal state or velocity-angle distributions can be compared. A statistical theory of angular correlation distributions has also been formulated[30]. Using

information theory[31,32], truely dynamical effects in experimental data or trajectory calculations can be summarised by a few parameters. Compaction of the data is achieved by calculating the surprisal I(n') of the state distribution p(n') which is given by

$$I(n') = - \ln \frac{p(n')}{p^{o}(n')} \qquad 1.5$$

Here, n is the independent variable of the distribution, such as vibrational or rotational energy[33], angular momentum[34], macroscopic branching ratio[35] etc., and $p^{o}(n')$ is some reference distribution. $p^{o}(n')$ is often called the prior distribution and is the distribution for which the information content is minimal, i.e. for which the surprisal is zero and for which there are no dynamical constraints on the behaviour of the system. This statistical limit corresponds to[32]

$$p^{o}(E) = |\rho(E)|^{-1} \qquad 1.6$$

where $\rho(E)$ is the density of product states. The most probable distribution in the absence of constraints is the one in which all states are equally populated. Other priors can be chosen if the area of accessible phase space is restricted on kinematic grounds e.g. in the case of restriction by conservation of angular momentum PST may be a better prior. Recent work has helped to illustrate the differences in the surprisal resulting from various choices of $p^{o}(n')$[36]. The resulting surprisal I(n') is frequently found to be a linear function of n' or some simple function of n'. By such a method the behaviour of p(n') can be expressed by a few parameters.

1.1.2 Experimental methods

The determination of $p(n^+)$ under collision free conditions has relied heavily on the use of molecular beams[3,12], although 'bulk' techniques like flash photolysis[37] continue to provide useful results. Compared to bulk techniques the signal from beam systems is low, but considerable gains can be made in the control of reagent properties and relaxation of products. Here results from the three major techniques are outlined. These are

a) The determination of angular $I(\theta)$ and velocity $p(E'_t)$ distributions by particle counting (AVD)

b) The determination of vibration-rotation distributions $p(v',J')$ $(v' \neq 0)$ by observation of IR chemiluminescence (IRC)

c) The determination of $p(v')$ and occasionally other distributions by observation of laser-induced fluorescence (LIF)

Observation of visible and UV chemiluminescence has also given information on energy partitioning in electronically excited products[6].

A. Angular and velocity distributions[19]

Using mass spectrometric detection[38] a large number of reactions have had their angular scattering pattern and time of flight energy distribution analysed. The full angle velocity distribution is displayed as a polar contour map, and these have been classified according to various modes of limiting behaviour. Even in the absence of energy measurements, angular distributions may still show these general features, but assumptions about the dynamics are then only valid provided the total reactive cross-section does not change very much over the range of reactant energy[39].

The limiting behaviour patterns are as follows:

i) Symmetrical forwards and backwards peaking.

This has been interpreted in terms of complex formation[40] and observed in reactions like O + $I_2/Br_2/ICl$[41,42], and alkali + $SnCl_4/SF_6$[43]. In this model, if the complex survives for more than one rotational period, then the probability of dissociation at angle θ is uniform. When this is weighted to account for all possible planes of dissociation about the incident relative velocity vector a $(\sin\theta)^{-1}$ distribution results. The singularities at $\theta = 0,\pi$ are washed out by the requirement that AB carry away some angular momentum as rotation.

ii) Strong forward peaking.

This has been observed in reactions like K/Rb/Ba/Sr/Ca + $Cl_2/Br_2/ICl$[44-46] O + CS_2[47] and in Cl + Br_2[39] at high energies. In the spectator stripping model proposed to account for this, long range attraction with early energy release is assumed to hold in the entrance channel. The new bond forms when it is highly extended so considerable internal excitation is favoured. The non-reacting atom exerts very little effect on the departing molecule, so the incident momentum of A carries the AB product forward in an unperturbed trajectory. Various degrees of intermediate behaviour between stripping and complex formation occur, which have been attributed to the increasing lifetime of the intermediate, giving rise to a short-lived or osculating complex, as in O + Cl_2[48] and Cs + TlX[49].

iii) Strong backwards peaking.

This has been observed in reactions like H/CH_3 + Cl_2[50,51]. This distribution is presumed to arise from a rebound mechanism caused

by a late repulsive energy release, (as in Sec. 1.1.1). This is particularly so for H + Cl_2 which displays a strong light atom effect and yields high product translation. Variants of rebound behaviour occur if the preferred angle of attack changes from a linear to a bent configuration as in the series H + Cl_2, Br_2, I_2, when the peaking moves from backwards to sideways. The Walsh diagram, and simple molecular orbital theory for HXY systems predict that a linear configuration is preferred for H + Cl_2, but that as the electronegativity of the central atom decreases, there is an enhancement of the p-character of its orbitals, leading to an increased tendency to a bent intermediate as is observed. Similar considerations also predict that reaction at the least electronegative atom in a heteronuclear dihalogen is the preferred channel even if the other product is energetically more favourable. In Fig. 1.2(a), if Y is less electronegative than Z, the YZ antibonding orbitals are located mainly on Y, so the interaction is most favourable at the Y end. Stability of XYZ type intermediates is also greatest when the least electronegative atom is central[8,11]. This behaviour is known as the electronegativity ordering rule.

B. Infra-red chemiluminescence

Determination of ro-vibrational populations has been achieved by the method of arrested relaxation[52]. In this technique two low pressure jets of reagent are crossed in a well cryopumped chamber, and IR fluorescence of the product is observed using a spectrometer. With care vibrational relaxation is avoided and rotational relaxation is small. At present the technique is restricted to reactions in which the product molecule is HX (X = halogen, oxygen), as for heavier molecules the small spacing of the levels makes inter-

pretation of the spectra difficult. With light molecules however fully resolved distributions $p(v',J';T)$ can be obtained and hence $p(E_t';T)$ by conservation of energy. Results for reactions $H + X_2$ [53] give good general agreement with energy partitioning from AVD measurements [13], the variation of energy release between $H + Cl_2$ and $H + Br_2$ correctly reflecting changes in the qualitative features of the surface. Reactions of the type $X + HY \rightarrow HX + Y$ show mixed release on a repulsive surface [54] due to the influence of inertial coupling, although long range attraction may be invoked to explain the large cross-section. A similar mechanism, involving preferential attack at the end leading to the most stable intermediate followed by migration, has been used to explain the branching behaviour (both microscopic and macroscopic) of $H + XY$ reactions [55].

C. Laser-induced fluorescence

LIF was pioneered by Zare and co-workers [28,56], and has been used extensively for the determination of rotation-vibrational populations, mainly in reactions of group IIA atoms. Progress in this field up to 1977 was reviewed by Kinsey [57]. As this is the experimental technique used in this work, it will be examined in rather more detail than the two previous methods.

In LIF, product formed in a crossed beam or beam/gas arrangement is detected by excitation of a suitable electronic transition and observation of the subsequent fluorescence. The excitation is supplied by a tunable dye laser directed into the reaction zone. Pulsed systems [58] are normally used although lately CW lasers, for which a higher signal to noise ratio is claimed, [61] have been used [59-61].

Pulsed sources of 1GHz bandwidth ($\sim 10^{-2}$ Å in the visible) are capable of resolving individual (v,J) lines and by tuning the wavelength through the absorbtion bands these states can be picked out. The population in the absorbing state is related via an absorbtion strength factor to the observed fluorescence (See Chap. 2).

Like IRC, LIF has the advantage over AVD measurements of yielding total energy partitioning, (E_v', E_R', E_t'), parameters which are more directly related to features of the potential energy surface than angle velocity contour maps. The information supplied by these two distributions is complementary, but the information content is higher in the former[62]. In comparison with IRC it also has the advantage of yielding data on the v = 0 state, which can be important in statistical and near statistical distributions when this state is highly populated. It is also less restricted in the examinable product species. Detectively it is highly specific as each (v",J") is characterised by a set of exclusive excitation frequencies. This is a further advantage over mass spectrometric detection, where interfering reactions can yield products that crack to give the same species as the products of the main reaction[63,64]. The highly directional nature of the laser ensures detection is also spatially specific. With a good arrangement of collection optics signal recovery can be high (50%)[65]; it is thus very sensitive.

The major restrictions are that the product must have an absorbtion system susceptible to excitation by a tunable laser, and that sufficient spectroscopic data must be available for an unambiguous assignment of bands. The availability of Franck-Condon factors for the intensity factors can also be quite restrictive. It is often necessary

to calculate[66] or even guess[57] these before proceeding.

The intensity of fluorescence yields populations of the (v;J) states. To determine relative rate constants[57], the LAB frame velocity is required. For accurate conversion the angle-velocity map must be used to determine the distribution of LAB velocities, $\underline{v}'_{rel}$. If this is unavailable, the angular distribution can be treated as a variable from which a range of rate constants can be calculated. In many cases the resulting uncertainty may turn out to be quite small for reasonable assumptions about the angular distribution[66].

Results from LIF experiments have been interpreted in terms of type of energy release. The series Ba + HX[56] proceeds on a highly repulsive surface yielding a low fraction of energy in vibration $\langle f_v' \rangle$. Examples of complex formation have also been found as in the reactions Ba + O_2/CO_2[55], Sc/Y + NO/SO_2[66], and good agreement with the predictions of PST obtained.

A few reactions of non-metals have been considered. Notably H + $NO_2/ClO_2/O_3$[67,68], F + ICl[60], F + CH_3I/CF_3I[59]. H + NO_2 was found to occur on a highly attractive surface, in agreement with IRC experiments. High $\langle f_v' \rangle$ was found although there is some disagreement over the partitioning of energy between OH vibration and internal modes of NO. High $\langle f_R' \rangle$ was also observed suggesting H atom migration as in H + BrCl/ICl[54]. All reactions of the type H + ZO_2 show complex behaviour in AVD measurements. This has led to the suggestion that the lifetime for complex formation as described by angle-velocity maps is shorter than that required for a statistical distribution of internal energy. This has also been suggested elsewhere[26,55,60,70]. The reactions F + CH_3I/CF_3I[59] have been found to give a statistical

distribution. F + ICl is considered in the next section.

In addition to internal state distributions, LIF has been used to detect angular and angle-vibrational distributions[69-71], and to study the effects of reagent vibration on product distributions[65,72]. Even more informative data may be available using the technique of Fourier-transform doppler spectroscopy-LIF[73] which in principle is capable of yielding $p(v',J',E_t',\theta)$. A prescription for determining angular correlations using polarised LIF has also been described[74]. As yet, only the former of these two techniques has been implemented[171] although some work has been done on the determination of rotational orientations from the polarisation of fluorescence[75].

1.2 Reactions of Interhalogens

Reactions involving halogen atoms have provided a useful means of observing systematic trends in the dynamics of series like Ba + HX[65], H + X_2[50,52], X + HY[54], but data on interhalogen reactions of the type X + YZ (X,Y,Z all halogens) is scarce[13]. A considerable volume of work from discharge flow kinetics is available on production and handling of the species, as well as giving rate constants for the reactions[76]. Highly detailed spectroscopic studies of the diatomic halogens and interhalogens are also available[77,85], which should assist interpretation of LIF experiments, and the construction of LEPS surfaces for trajectory calculations.

1.2.1 Dynamics of interhalogen reactions

Apart from F_2 for which the dissociation energy, D_o", is anomalously low, D_o" for homonuclear interhalogens increases with decreasing molecular weight[85]. That of the heteronuclear interhalogens, XY, varies in the same fashion; for a given X, D_o" increases

as the atomic weight of Y decreases. Fluorine also fits this behaviour, and this data is summarised in Table 1.1.

Combining this data shows that there are in principle 16 inter-halogen reactions of the type X + YZ → XY + Z for which the exoergicity, $\Delta D_o''$ is negative, and these are listed in Table 1.2. Of these 9 have been studied so far at varying levels of detail[13] by mass spectrometric angular distribution measurements, a few of which have incorporated velocity analysis. In addition F + ICl has been studied by LIF.

Early angular distribution measurements were made with effusive beams[49,87-91], but experiments using velocity selection on the reaction Cl + Br_2[39] have shown that the reactive cross-section σ_R, does not vary much with energy. On the basis of this observation, and the similarity of angular distributions found for the reactions with X = Cl, Br the results of the earlier experiments appear to be correct. A caveat must be added on reactions where X = F, however, and such cases will be examined later.

For Cl + I_2/Br_2, Br + I_2 strong forward and weak backward peaking suggests behaviour lying between short-lived complex and stripping mechanisms, with Cl + Br_2 being more direct than Cl + I_2.

For Cl + IBr*, similar behaviour to Cl + I_2 is found although long lived complex formation has also been observed[91]. For Cl + BrI more forward scattering suggests a direct mechanism.

*The notation X + YZ is used when the product is XY and X + ZY when it is XZ.

D_o''/cm^{-1}	I	Br	Cl	F
F	22333 (83)	20600 (79)	21111† (20633)	12917
^{35}Cl	17366 (108)	18035*	19996	
^{81}Br	14659	15896		
I	12440			

Table 1.1. Dissociation energies of the ground state dihalogens. All data is from Coxon and sources therein[86] except where otherwise stated.

Notes : * Upper limit. A value of ∿18010 cm^{-1} is favoured.

† Dissociation products not unambiguously assigned. Upper figure corresponds to dissociation to $Cl(^2P_{3/2}) + F(^2P_{\frac{1}{2}})$, lower to $Cl(^2P_{3/2}) + F(^2P_{3/2})$.

	Reaction	$-\Delta D_o''/cm^{-1}$	$k_{298}/molec^{-1}cm^{-3}s$
A	$Cl + F_2 \rightarrow ClF + F$	<8194	$<10^{-14}$ (102)
B	$Br + F_2 \rightarrow BrF + F$	7683	
C	$I + F_2 \rightarrow IF + F$	9416	
D	$F + Cl_2 \rightarrow ClF + Cl$	<1115	1.6×10^{-10}
E	$F + Br_2 \rightarrow BrF + Br$	4704	3.1×10^{-10}
F	$F + I_2 \rightarrow IF + I$	9893	4.3×10^{-10}
G	$F + BrCl \rightarrow BrF + Cl$	>2565	
	$\rightarrow ClF + Br$ †	>3076	
H	$F + ICl \rightarrow IF + Cl$	4976	3.8×10^{-10}
	$\rightarrow ClF + I$ †	<3745	1.2×10^{-10}
I	$F + IBr \rightarrow IF + Br$	7674	
	$\rightarrow BrF + I$	5941	
J	$Cl + Br_2 \rightarrow BrCl + Br$	<2139	1.2×10^{-10} (104)
K	$Cl + I_2 \rightarrow ICl + Br$	4966	
L	$Cl + IBr \rightarrow ICl + Br$	2707	
	$\rightarrow BrCl + I$	2376	
M	$Br + I_2 \rightarrow IBr + I$	2219	
N	$Br + ICl \rightarrow BrCl + I$	<769	

Table 1.2. Exothermicities and bimolecular rate constants for the exothermic halogen + dihalogen reactions. $\Delta D_o''$ from Table 1.1. Rate constants from Appelmann and Clyne (103), except where otherwise stated

† = minor channel from electronegatively ordering rule

$1\ cm^{-1} \simeq 0.012.\ kJ\ mol^{-1}$.

For Br + ClI, a smaller cross-section with backward peaking was found suggesting a more repulsive interaction.

Such behaviour is in good agreement with that predicted by the electronegativity ordering rule. Decreasing stability of the intermediate is expected along the series

$$Cl + IBr,\ Cl + I_2,\ Br + I_2,\ Cl + Br_2,\ Cl + BrI,\ Br + ClI,$$

which is precisely what is observed. In Br + ClI the intermediate is significantly destabilised, with an energy barrier[18] and this is also in accord with observation. In all cases σ_R is less than the hardsphere value suggesting that although the initial interaction is repulsive it is also quite short range[39]. Alternately it may be attributable to a steric factor which only favours reaction within a restricted angle of approach. Trajectory calculations[92] made on a surface favouring colinear approach could not however be made to reproduce the observed behaviour by any sensible variation of surface parameters. It was also shown that although the surface did possess a well, its nature did not affect the results to any great extent.

There is some evidence to suggest that 21 electron species like XYZ may prefer a bent geometry although it is far from conclusive. Matrix isolated ClF_2 has been detected using raman spectroscopy[98] and a bond angle of 136^o found. Ab initio calculations[94] have given 145^o for ClF_2 and 159^o for Cl_3, but an IR spectrum of Cl_3[95] was interpreted in terms of $C_{\infty v}$ symmetry. Angular measurements on $F_2 + I_2$/ ICl/HI[96,97] also favour a bent geometry for FIX. The angle is expected to increase as the electronegativity of Y decreases as in $H + Cl_2/Br_2/I_2$[11].

When the attacking atom X, is fluorine additional effects have been predicted on the grounds of its extreme electronegativity and light mass. Greater repulsive release has been suggested on molecular orbital grounds[98] due to the increased YZ antibonding character of the $3\sigma^*$ orbital (See Fig. 1.2), as in CH_3, H + X_2. Charge transfer effects[99] have also been postulated, and would have the opposite effect of stabilising the intermediate and enhancing attractive energy release. Stable species of the form XIF (X = I,Cl,H,CH_3) have been detected mass spectrometrically[96,97], and the stability of I_2F and ClIF with respect to X + IF estimated as $\sim$12kJ mol^{-1} and 63 kJ mol^{-1} respectively.

Two studies of F + I_2[98,99] and one of F + ICl[98] have been made using angular scattering. (Unpublished data on F + IBr/Br_2[13] has also been obtained). Grice and co-workers found broad sideways to backwards scattering at 3.5 kJ mol^{-1}, whilst Wong and Lee found almost symmetrical forward backward peaking at $\sim$8 kJ mol^{-1}. The reliability of the former is suspect however[100] as the F-atom source was not well characterised and reactions like $F_2 + I_2 \rightarrow I_2F + F$ followed by fragmentation of I_2F in the detector may have interfered. A similar situation may presumably also hold for the latter. There appears therefore to be no completely reliable AVD measurements for these reactions.

1.2.2 LIF of interhalogen reaction products

Recent LIF work on the reaction F + ICl[60,61] has shown a significant vibrational inversion with $\langle f_v' \rangle \simeq 0.55$, and $\langle f_R' \rangle \simeq 0.14$. The possibility of obtaining IR laser action in the ground electronic state of product IF is most interesting. The partitioning strongly

suggests direct dynamics, in which the existence of a significant well of ∿63 kJ mol^{-1} has little effect. Interference from fluorescence in the ICl(A → X), ICl(B → X) and I_2(B → X) systems made modulation of the F-atom beam necessary in this experiment, but good band spectra were observed despite substantial fluorescence from reagents.

Information available on the spectroscopy of the interhalogens suggests there may be several other reactions examinable by LIF. Data on lifetimes and relative intensities of the B → X systems are summarised in Tables 1.3a), b). The main requirement in selecting feasible studies would be that the product molecule should not be much less efficient in fluorescence than the reactant in the spectral region of interest. Wavelength ranges of maximum fluorescence have been given by Clyne and McDermid[82] and these are summarised in Table 1.3c). Under normal crossed-beam conditions, where the dimensions of the reaction zone are a few mm, the residence time is sufficiently short to discriminate against fluorescence from the long-lived A-states[111, 112].

Based on these observations reactions E,F,G,H,I and L appear feasible. B and C may also be possible depending on the value of σ_R. I + F_2 appears to proceed via a rebound mechanism[13] and so is likely to have a small cross-section as in Br + ClI, and in agreement with the small rate constant for Cl + F_2. Thus σ_R may be too small for reactions B and C. Reaction D may also be possible depending on the absorbtion strength of ClF.

An alternative method for the suppression of reagent fluorescence which can be used with pulsed laser sources is that of lifetime discrimination. This has been used to separate product species in the

a)	I	^{81}Br	^{35}Cl	F
F	7 (83)	45 (105)	-	-
^{35}Cl	1 (79)	35 (106)	83 (84)	
^{81}Br	<1 (?)	12 (107, 174)		
I	~1 (109)			

b)	I	^{81}Br	^{35}Cl	F
F	5×10^3	10^2	WEAK*	-
^{35}Cl	3	0.5	1	
^{81}Br	WEAK*	20		
I	10^4			

c)	I	^{81}Br	^{35}Cl	F
F	440 (510)	483 (573)	-	-
^{35}Cl	600 (620)	550 ?	501 (543)	
^{81}Br	-	(514) (603)		
I	499 (630)			

Table 1.3. a) Lifetimes (μs) and b) relative intensities[87] of the B → X transitions of the dihalogens

* transition could not be detected via LIF under conditions where other species gave a significant signal[84,110]

c) Observed ranges of excitation which produce fluorescence[87] (nm). Upper figure is approximate predissociation limit and lower figure is the longest wavelength observed in a thermal distribution. If the upper figure is bracketed then predissociation has not been observed via LIF and corresponds to the observed range of significant intensity. For IBr there are expected to be no strong bands below the dissociation limit[78]

reactions Ca/Sr/Ba + BrCN[113] and is an advantage of pulsed over CW lasers. This could possibly be employed in F + I_2 for example.

As a contribution to the above scheme the reaction F + I_2, which is the subject of this thesis is considered to offer several specific advantages. The reaction is known to be fast and has a large exothermicity. IF has the next highest absorbtion co-efficient to I_2 of all the interhalogens and the B state is predissociated only above v' = 9. The lifetime (∿7μs) is suitable for detection with a gated system and is well coupled to the residence time in the reaction zone. Initially it is proposed to examine only the three lowest vibrational levels whose absorbtions lie above the onset of I_2 predissociation at ∿499 nm.

1.2.3 Spectroscopy and properties of IF

Historically IF was the last diatomic interhalogen to be discovered[114]. It has been observed in flames and flow tubes via chemiluminescence[112,114] and by laser induced fluorescence[80,83], following the reaction of F_2 or F with I_2. The former is believed to proceed via the formation of the stable I_2F intermediate[80] as follows

$$I_2 + F_2 \rightarrow I_2F + F \qquad \Delta U = +17 \text{ kJ mol}^{-1}$$

$$F + I_2F \rightarrow IF(A) + IF(X)$$

$$\rightarrow IF(B) + IF(X)$$

$$\rightarrow IF(X) + IF(X) \qquad \Delta U = -257 \text{ kJ mol}^{-1}$$

with emission occurring from the A and B states. Its transient nature is thought to be due to its kinetic instability in such systems to heterogeneous reaction on the vessel walls[103], either with an excess

of F-atoms or via disproportionation to yield Iodine polyfluorides. A value of $k_w \simeq 200\text{-}500\ s^{-1}$ was estimated. Only one synthetic preparation has been reported[115] via the reaction

$$I_2 + IF_3 \rightarrow 3IF$$

in pyridine solution at -35°C. Disproportionation to $IF_5 + I_2$ occurred above 0°C, for which $\Delta G \simeq -164\ kJ\ mol^{-1}$.

As in all heavy dihalogens the coupling of angular momenta approximates to Hund's case (c)[116]. The manifold of molecular states resulting from the combination of two ^2P_J atomic states has been given by Coxon[117]. The ordering of these states has been much discussed[112, 114,118] but is now fairly well established following the work of Clyne and McDermid[83]. This is shown schematically in Fig. 1.4.

The ground $X^1\Sigma(0^+)$ state correlates with two $^2P_{3/2}$ atoms. This combination also correlates with the first excited $A^3\Pi(1)$ state and a repulsive $Y^3\Pi(0^+)$ state. The second excited $B^3\Pi(0^+)$ state correlates diabatically with $I^2P_{\frac{1}{2}} + F^2P_{3/2}$ and adiabatically with $I^2P_{3/2} + F^2P_{3/2}$ via a strong interaction with the Y state. A weakly bound $C^3\Pi(0^+)$ state correlates with $I^2P_{3/2} + F^2P_{\frac{1}{2}}$, and intersects the B state below the crossing point with the Y state, at an energy between J' = 6 and J' = 7 in the v' = 9 level of the B state. Indirect predissociation is possible from these and higher levels via a second crossing of the C and Y states at large r. A stronger predissociation sets in above v' = 10 via the B-Y crossing. The first onset of predissociation occurs at ∿448 nm in the excitation spectrum. From the observation of the breaking off in the v' = 8 and v' = 9 levels the dissociation energy for the X state was determined as $22333.2 \pm 2.0\ cm^{-1}$.[83]

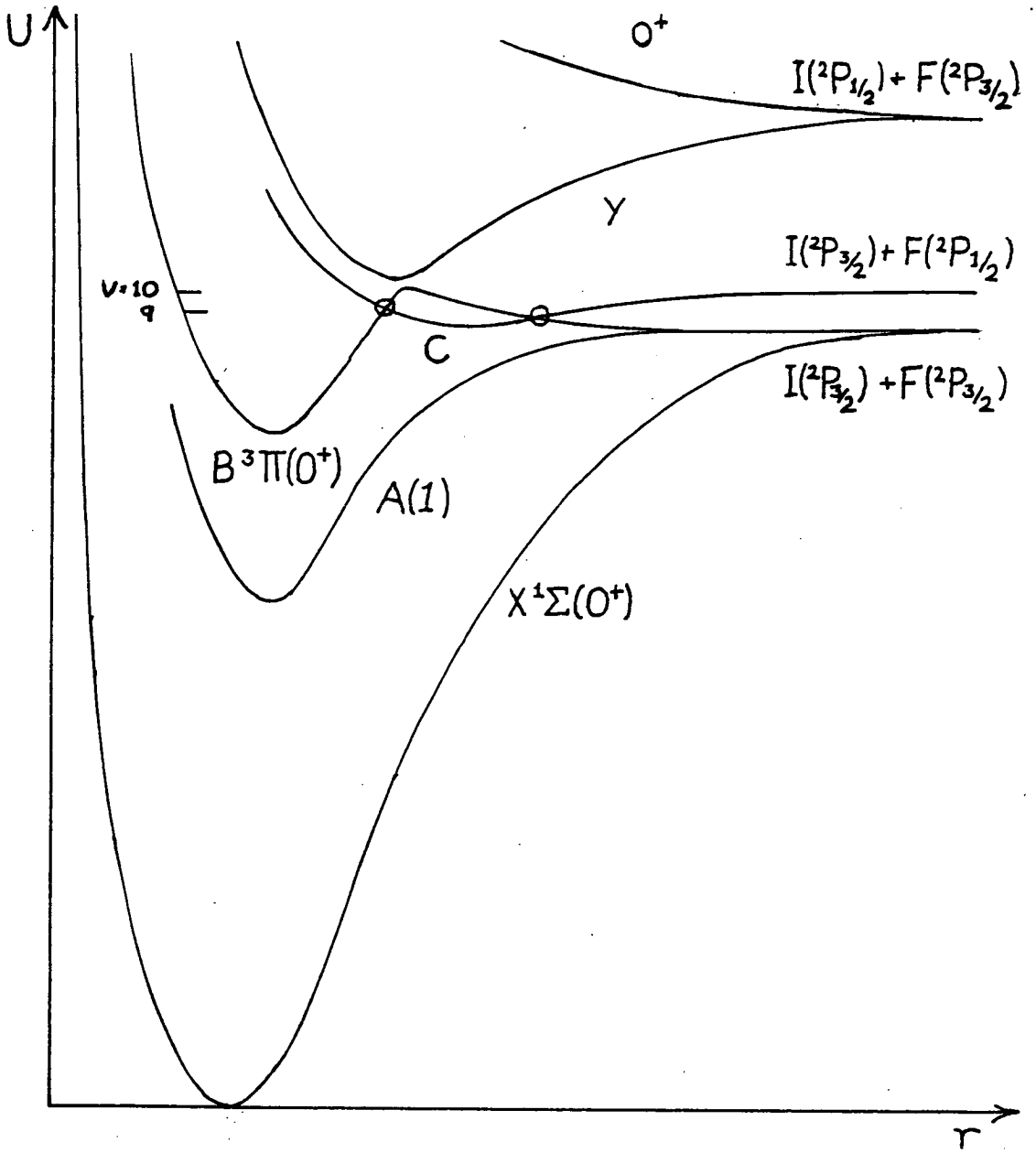

Fig. 1.4. Schematic diagram of the low-lying states of IF after Clyne and McDermid[83] and Birks et al.[118]. The weak interactions leading to the observed dissociation of $B^3\Pi(0^+)$ (v = 9) are shown by O.

($\sim$266.2 kJ mol^{-1}). This is the largest dissociation energy of the diatomic interhalogens.

1.3 Outline of Chapters 2 - 4

Chapters 2 - 4 of this thesis describe work done on a crossed molecular beam - LIF experiment, set up jointly by the Departments of Physics and Chemistry at the University of Edinburgh. The chosen system is the reaction $F + I_2 \rightarrow IF + I$. The experiment builds on the work described by Fernie[119], for the study of the reaction $O + I_2$ using the same method. Preliminary work, not described here, suggests that under the same conditions as those discussed here, this system is not feasible for such a study. This may be due to the low σ_R[42] compared with $F + I_2$. Since the original report[119] considerable changes have been made to the experimental arrangements and these are given in detail in Chapter 3.

The resulting set-up does not represent an optimum match of apparatus however. The two main constituents, the scattering chamber/vacuum system and laser system, were inherited from previous projects, and as will be shown there are serious restrictions arising from their deployment, particularly in the latter case. This thesis proposes only to establish the feasibility of using the apparatus for LIF work, and some calculations in support of this are also given in Chapter 3.

A comprehensive system of on-line control was developed and software has been written for this. Some justification for this and the details of its implementation are also given in Chapter 3.

The v" = 0,1,2 states of IF have been observed, although the data

is very noisy. A comparison of the predicted and actual performance of the apparatus is made in Chapter 3. It would appear that before any significant improvements in the data quality (i.e. signal to noise ratio) can be made, farther modifications of the apparatus will be required. Some suggestions in this area are made, in the light of experience which has been gained. Some of these are currently being implemented. Despite the low quality data some analysis is possible using simulated spectra. A computer program was written for this purpose. A detailed derivation of the simulation formula, and its limitations is presented in Chapter 2. Some simulations are shown and compared with work done elsewhere. By this means the accuracy of the program is assessed. The problems of using simulations to interpret low quality data are considered in Chapter 4. Lack of time prevented development of a rigorous fitting procedure, but qualitative considerations are shown to allow the extraction of population numbers. These are then analysed using the information theoretic approach. Some general conclusions are drawn in comparison with other ostensibly similar reactions, and a naive model is offered to interpret the observed differences in the dynamical behaviour.

Note added in proof (q.v. Table 1.3)

Recent work on the excitation spectrum of IBr has shown that the strongest absorbtions which are from v" = 2,3 (630 - 642 nm) have upper states which are strongly predissociated, with lifetimes of 10^{-7} - 10^{-8} s (172).

CHAPTER 2

SIMULATION OF LIF SPECTRA

2.1 Theory of LIF

The intensity of fluorescence resulting from excitation from a rovibronic state $\underline{i}$ to an intermediate state $\underline{j}$ followed by spontaneous emission to state $\underline{k}$ has been derived in outline from the Breit formula by Kinsey[57]. In the absence of any polarisation dependence in the response function of the detector, and assuming equal population of all magnetic sub-levels, this is given (in slightly altered notation*) by

$$I(\nu_{ij},\nu_{jk}) = R(\nu_{jk})\rho(\nu_{ij})B_{ij}N_i\Phi_{jk} \qquad 2.1$$

N_i is the population of level $\underline{i}$, B_{ij} is the Einstein co-efficient for the absorbtion $\underline{j} \leftarrow \underline{i}$, $\rho(\nu_{ij})$ is the energy density per unit bandwidth of the laser (SI units $Jm^{-3}Hz^{-1}$) and Φ_{jk} is the fluorescence yield of the emission $\underline{j} \rightarrow \underline{k}$. $R(\nu_{jk})$ is the sensitivity of the detector at the frequency of this emission. $I(\nu_{ij},\nu_{jk})$ thus refers to the number of photons observed per second at frequency ν_{jk}. Equation 2.1 refers to steady state conditions, whilst here and elsewhere pulsed sources are used. (In both cases the transition $\underline{j} \leftarrow \underline{i}$ is assumed not to be saturated). If the duration of the laser pulse Δt_L is considerably shorter than the mean lifetime of the state $\underline{j}$, it is convenient to

*Kinsey puts A_{jk} (the Einstein co-efficient) rather than Φ_{jk}. Since the dimensions of A and ρNB are s^{-1} and R is a pure number, his equation (6) is dimensionally incorrect. I must have the units photons s^{-1} (or photons $m^{-3}s^{-1}$ if ρNB is expressed as a density).

effect a separation into the absorbtion and emission processes. Thus $\rho(\nu_{ij})N_iB_{ij}$ is a rate of excitation and its integral over the pulse duration gives the total number of absorbtions. This can be accounted for by putting

$$\tilde{\rho}(\nu_{ij}) = \int_{\Delta t_L} \rho(\nu_{ij})dt \qquad 2.2$$

$\tilde{\rho}$ is now the integrated energy density (in the time sense).

Now the fluorescence signal is not resolved (in the frequency sense), so the emission part must be summed over all final states $\underline{k}$. Since

$$\Phi_{jk} = \frac{A_{jk}}{\sum_k A_{jk}} \qquad 2.3$$

where A_{jk} is the Einstein A co-efficient, this yields.

$$I(\nu_{ij}) = \sum_k I(\nu_{ij},\nu_{jk})$$

$$= N_i\tilde{\rho}(\nu_{ij})B_{ij}.\ \sum_k R(\nu_{jk})\left(\frac{A_{jk}}{\sum_k A_{jk}}\right) \qquad 2.4$$

The states $\underline{i},\underline{j},\underline{k}$ are now identified with rovibronic states having quantum numbers n,v,J with two, one and no primes respectively. It is convenient therefore to separate the three contributions to the intensity factors, by making the following assumptions. The electronic part of the transition moment, R_e, does not vary significantly in the transitions of $\underline{j} \rightarrow \underline{k}$ and the centrifugal coupling of the rotational and vibrational parts is negligible. Thus the vibrational contribution is given by the rotationless Franck-Condon factor

$$q_{v'v''} = |\langle v'|v''\rangle|^2$$

and the rotational part by the Honl-London factor

$$\frac{S_{J'J"}}{2J"+1}$$

where $S_{J'J"}$ is the rotational line strength. Farther, if emission occurs to only one electronic state n, then the electronic part of the transition moment cancels in the summation over k in equ. 2.4.

Substituting for A & B in equ. 2.4 then yields

$$I(\nu(v'J';v"J")) = kN_{v"J"}\tilde{\rho}(\nu(v'J';v"J"))q_{v'v"} \frac{S_{J'J"}}{2J"+1}$$

$$x \sum_{vJ}\left\{R(\nu(v'J';vJ)) \; x \; \frac{\left[\nu(v'J';vJ)\right]^3 q_{v'v} \frac{S_{J'J}}{2J'+1}}{\sum_{vJ}\left[\nu(v'J';vJ)\right]^3 q_{v'v} \frac{S_{J'J}}{2J'+1}}\right\} \qquad 2.5$$

with k a constant.

This is the equation from which most analyses have proceeded[66], but it is only as good as the approximations on which it is based. Only examination of the spectroscopic data can provide information as to its accuracy.

In principle therefore given the intensity of fluorescence and necessary data on frequencies and strengths of transitions equ. 2.5 can be solved to obtain the $n_{v"J"}$. In practice available data is not usually so detailed. Also the bandwidth of the laser is normally not sufficiently low to excite a single (v,J) transition, so that the observed intensity is the result of a convolution of the spectral

lineshape with the laser lineshape. As a result other methods of extracting $N_{v''J''}$ have been developed, depending on the detail of the observed spectrum.

For highly resolved spectra[67] observed intensities of individual rotational lines can be fitted to a laser frequency profile and $N_{v''J''}$ populations obtained directly. In the opposite limit of very poorly resolved structure, simple integration of the area under a band has been used[65] to obtain $N_{v''}$ populations.

In the intermediate range where only lines at high J are resolved, it is not possible to obtain $N_{v''J''}$ over a wide enough range of J" by the former method for a useful comparison with theory. It is then necessary to assume a functional form for the rotational distribution characterised by one or two parameters[66]. Alternately a numerical distribution can be obtained by allowing $N_{v''J''}$ to vary freely at several J"[67]. In both these latter cases, due to the number of variable parameters the simulated spectrum must be fitted to the observed one in a least squares fashion to obtain the best agreement. This is particularly true when band overlap occurs, for example due to highly rotationally excited products or closely spaced band origins. Even if a rigorous fitting procedure is not employed, simulated spectra can be used to obtain a qualitative description of the rotational envelope by direct comparison on a trial and error basis. In addition they are of use in a predictive sense using postulated distributions. For these reasons simulation calculations have also been employed in work on visible chemiluminescence[120] and energy transfer mechanisms[121].

2.1.1 Simplification of the fluorescence intensity

The principles of simulations of LIF spectra have been outlined by Dagdigian and Zare[69] and by Lieu and Parsons[66]. Simplifying approximations are applied to equ. 2.5 until it is reduced to a function of a few tractable variables which are appropriate to the experiment.

While still considering a single rovibronic excitation, put

$$\nu(v'J';vJ) \simeq \nu_o(v',v)$$

where ν_o is the relevant band origin, and after summing over each J term in both sums, the rotational intensity drops out to give

$$I(\nu(v'J';v''J'')) = kN_{v''J''}\tilde{\rho}(\nu(v'J';v''J''))q_{v'v''}\frac{S_{J'J''}}{2J''+1}$$

$$x \sum_v R(\nu_o(v',v))\left|\nu_o(v'v)\right|^3 q_{v'v}(\bar{\nu}^3_{v'})^{-1} \qquad 2.6$$

where $$\bar{\nu}^3_{v'} = \sum_v \left|\nu_o(v'v)\right|^3 q_{v'v}$$

Since the laser may excite several lines (possibly in different bands) simultaneously equ. 2.6 must be summed over a range of J" values, and possibly a range of v" values, to obtain

$$I(\nu_L;\Delta\nu_L) = \sum_{v''}\sum_{J''(v'')} I(\nu(v'J';v''J''))$$

$$= k\sum_{v''}\sum_{J''(v'')}\left\{ N_{v''J''}\tilde{\rho}(\nu(v'J';v''J''))q_{v'v''}\frac{S_{J'J''}}{2J''+1}\right.$$

$$\left. x \frac{1}{\bar{\nu}^3_{v'}}\sum_v R(\nu_o(v'v))q_{v'v}\nu_o(v'v)^3\right\} \qquad 2.7$$

where the sums over v" and J" are understood to be restricted by the

width of the laser line $\Delta\nu_L$ and its centre frequency ν_L.

Equation 2.7 must now be evaluated to yield $I(\nu_L;\Delta\nu_L)$ as a function of ν_L given $N_{v"J"}$. In addition, it is usually possible to separate the v" and J" dependences of the population numbers by assuming

$$N_{v"J"} = N_o P_v(v") P_R(J"|v") \qquad 2.8$$

where $P_v(v")$ is the vibrational distribution and $P_R(J"|v")$ is the conditional rotational distribution given v", and N_o is a normalising constant.

2.2 Simulation Program Structure

The evaluation of equ. 2.7 for any ν_L breaks down into six component steps as follows;

a) Given ν_L and $\Delta\nu_L$ determine (v',v") values and for each v", the range of J" values to be included in the sum.

b) Determine the "fluorescence factor" F(v') which is the last line of equ. 2.7 for the values of v' found in a).

c) Using either values of the molecular parameters (ω_e, B_e, etc.) to determine the line frequencies, or else data on the frequencies themselves, plus a functional description of $\tilde{\rho}(\nu)$, determine the value of $\tilde{\rho}(\nu(v'J';v"J"))$ for each of the transitions identified in a).

d) Given either functional forms or trial data on the v" and J" distributions calculate $n_{v"J"}$.

e) Multiply the results of steps b) - d) together with relevant Franck-Condon and Honl-London factors to form the term in braces in equ. 2.7, for each transition.

f) Sum the results of e) over the transitions determined in a).

Implementation of these steps will now be described in more detail, in the context of restrictions imposed by the availability of data for molecular species in general and efficiency in programming. It is intended that the program should eventually be useful for species other than the system studied in this thesis. There are however major restrictions in operation at present. All bands must be red-degraded, have simple P and R branches only, and show no perturbations. Since these conditions hold well for IF it is highly suitable for initial development.

The spectrum is defined by a start and end frequency (ν_1,ν_2) or their equivalent wavelength (λ_1,λ_2) together with a step interval $\Delta\nu_s$. Within this range several bands may be excited. To determine these an estimate of their frequency range is made. The high frequency end is defined by the band head. For the low frequency end an estimate of the highest J" state available must be made. In a dynamic situation this limit, J''_{max} is constrained by the reaction exo-ergicity, although in practice the limit is smeared out slightly by the thermal distribution of reactant energies. If however P(j") can be characterised by a Maxwell-Boltzmann distribution, then the limit is determined only by the point where the J" dependent parts become small enough to make a negligible contribution to the total intensity. This can be determined by finding the maximum value of $P(J'')S_{J',J''}/(2J''+1)$ and then the J" value at which this function becomes less than a certain fraction of this maximum value. Since the peaks in the spectra occur at or near the bandheads, which result from summing several terms, the true cut off fraction can be much less

than that determined this way. A value of $\sim 10^{-2}$ was found to give minimal discrepancies without causing an unreasonable run time. The corresponding J" is less than that resulting from ergicity restrictions for rotational temperatures up to ~1000K, and all but the highest vibrational states in the F + I_2 system. Once all the transitions in the spectrum have been identified the limit can be revised to take into account the v-dependent factors.

For each band the program calculates the factor F(v'). The curve R(λ) is approximated as a series of straight line segments over various wavelength intervals. For each v', there is a set of v levels, which make a significant contribution to the observed intensity. These are restricted in the summation by the curve R(λ) having a non-zero value. In addition there are restrictions imposed by the availability of Franck-Condon factors, and this also affects the calculation of $\bar{\nu}^3_{v'}$. In practice small additional terms do not make more than a few percent difference to both summations and so this is not too serious a problem.

Having determined the included bands, the program steps through (ν_2,ν_1) at intervals of $\Delta\nu_s$. To avoid having to recalculate or store and recall large numbers of line positions in each band it is easier to step through different sub-intervals of (ν_2,ν_1) for the range of each band. Intensity at each point is accumulated in an array of $(\nu_2 - \nu_1)/\Delta\nu_s$ elements, which is accessed sequentially with a resultant saving in time.

For each band the frequencies of lines from J" = 0 to $J"_{max}$ for each branch are calculated and inspected to determine those falling under the laser profile. A triangular lineshape is assumed. This

corresponds quite closely to that determined experimentally, and has the computational advantage of well-defined cut-off points. Under experimental conditions $\Delta\nu_L$ is much greater than the width of the absorbtion lines due to doppler broadening, so the latter may be taken as having delta function profiles.

The distribution P(v") is input as numerical data. This avoids complicated programming for the selection of different functions according to different dynamical models. The possible distributions of J" appear to be rather more restricted however, and either a one parameter, thermal distribution characterised by T_{rot} or a two-parameter function of the form

$$P(J") = (2J" + 1)\left\{1 + \left(\frac{J"}{J"_m}\right)^n\right\}^m \qquad 2.9$$

can be selected. J_m is the true exo-ergicity limit, and either T_{rot} or n and m can vary with v", and are input with P(v"). In the two parameter case J_m can be reduced in the manner described above, if n and m cause it to become sufficiently small at high J".

Rotational line strengths are taken from Hund's case (a) coupling conditions for intramultiplet transitions and are from Schlapp[122].

$$^1\Sigma^+ \rightarrow {}^3\Pi_o^+$$

P - branch	j"
R - branch	j" + 1

The operation of the program is summarised in the flow charts shown in Fig. 2.1 and 2.2, and a listing of the final version of the program appears in appendix 3.

Fig. 2.1. Flow diagram for simulation program.
The subroutine marked '*' is shown in detail in Fig. 2.2.

Fig. 2.2. Flow diagram for the determination of the intensity distribution within each band.

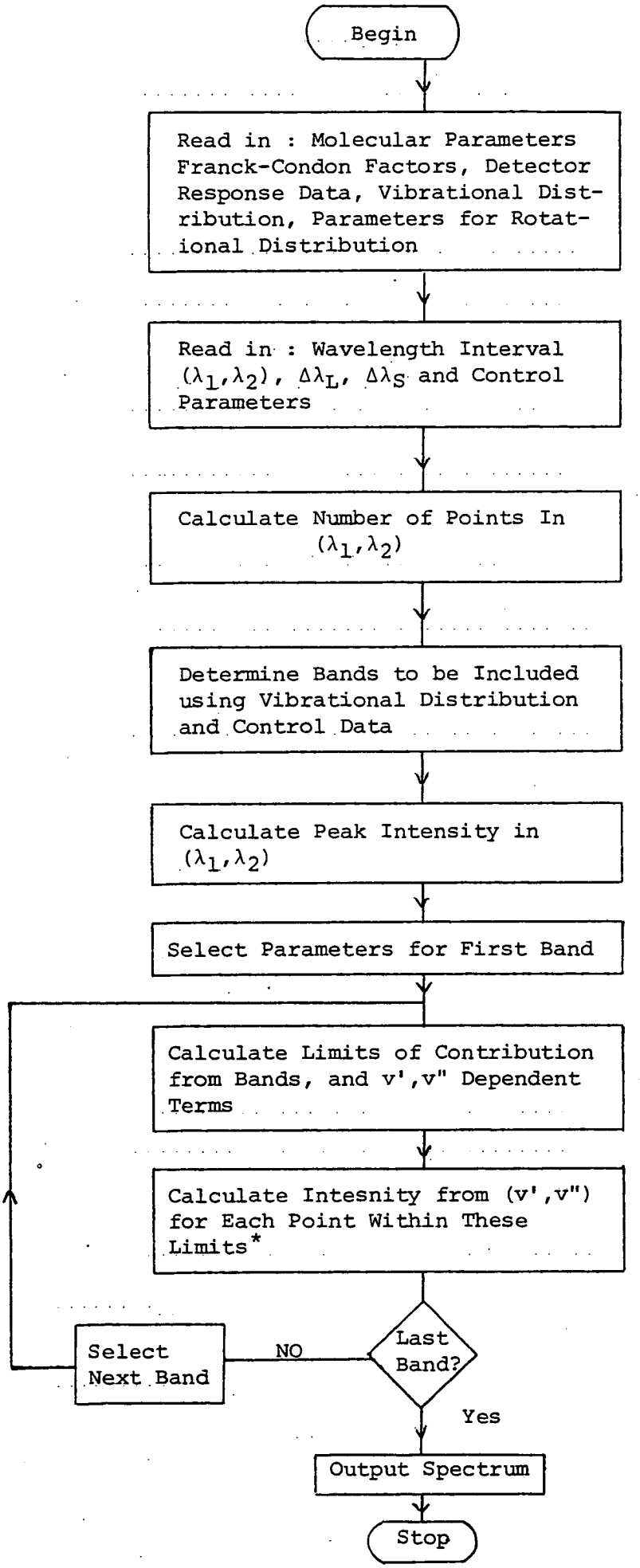
Begin
Read in : Molecular Parameters Franck-Condon Factors, Detector Response Data, Vibrational Distribution, Parameters for Rotational Distribution
Read in : Wavelength Interval (λ_1,λ_2), $\Delta\lambda_L$, $\Delta\lambda_S$ and Control Parameters
Calculate Number of Points In (λ_1,λ_2)
Determine Bands to be Included using Vibrational Distribution and Control Data
Calculate Peak Intensity in (λ_1,λ_2)
Select Parameters for First Band
Calculate Limits of Contribution from Bands, and v',v" Dependent Terms
Calculate Intesnity from (v',v") for Each Point Within These Limits*
Last Band?
NO
Select Next Band
Yes
Output Spectrum
Stop

Fig. 2.1

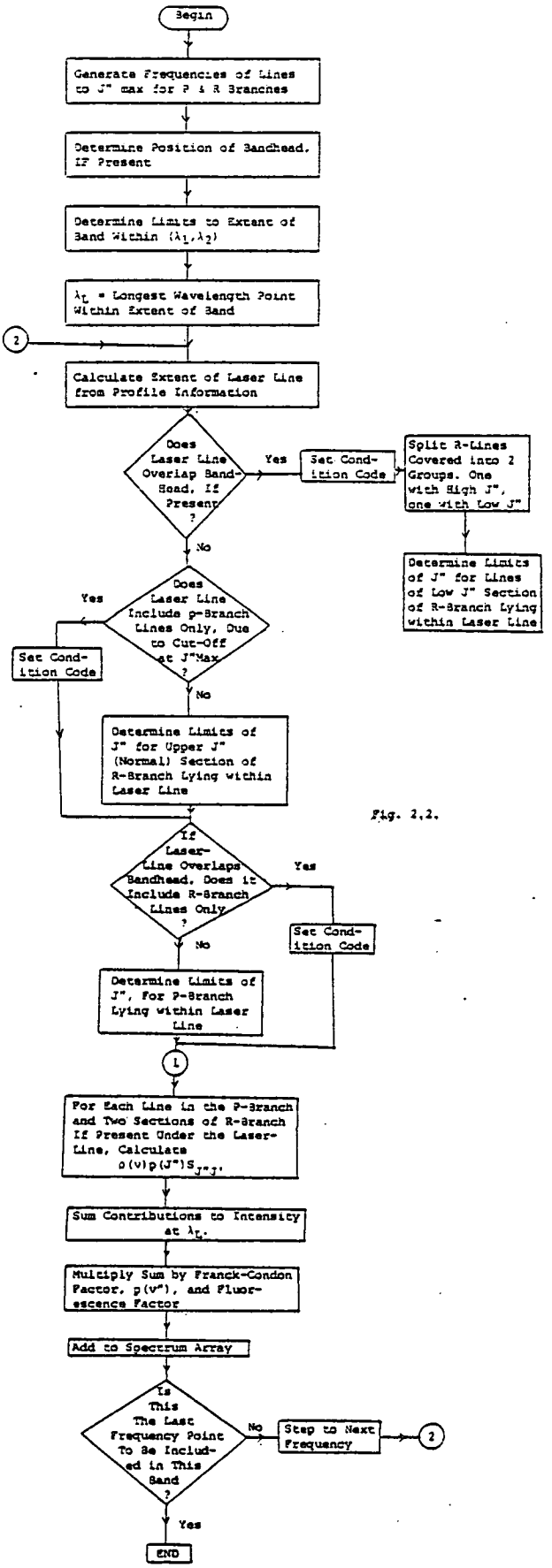
Begin
Generate Frequencies of Lines to J" max for P & R Brancnes
Determine Position of Bandhead, IF Present
Determine Limits to Extent of Band Within (λ_1,λ_2)
λ_L = Longest Wavelength Point Within Extent of Band
2
Calculate Extent of Laser Line from Profile Information
Does Laser Line Overlap Band-Head, If Present ?
Yes
Set Cond-ition Code
Split R-Lines Covered into 2 Groups. One with High J", one with Low J"
Determine Limits of J" for Lines of Low J" Section of R-Branch Lying within Laser Line
No
Does Laser Line Include p-Branch Lines Only, Due to Cut-Off at J"Max ?
Yes
Set Cond-ition Code
No
Determine Limits of J" for Upper J" (Normal) Section of R-Branch Lying within Laser Line
If Laser-Line Overlaps Bandhead, Does it Include R-Branch Lines Only ?
Yes
Set Cond-ition Code
No
Determine Limits of J", For P-Branch Lying within Laser Line
1
For Each Line in the P-Branch and Two Sections of R-Branch If Present Under the Laser-Line, Calculate $\rho(v)\rho(J")S_{J"J'}$.
Sum Contributions to Intensity at λ_L.
Multiply Sum by Franck-Condon Factor, p(v"), and Fluor-escence Factor
Add to Spectrum Array
Is This The Last Frequency Point To Be Includ-ed in This Band ?
No
Step to Next Frequency
2
Yes
END

Fig. 2.2.

2.3 Simulated Spectra

The program has been tested against previously published spectra for the molecule IF, and found to give good agreement. Additional tests against other systems satisfying the restrictions given earlier have not been possible due to lack of time. Provided the conditions are satisfied however there is no reason why the results should not be satisfactory.

The parameter which is most critical to successful execution is the laser linewidth $\Delta\nu_L$, which determines the number of lines summed over at frequency ν_L. This may involve up to three sequences of J" values depending on the position of the laser line with respect to the bandhead and tail, and the relative size of $\Delta\nu_L$ and the rotational spacing. In practice all the conditions can be tested for by allowing $\Delta\lambda_L$ to vary over the range $0.1 \sim 2\text{Å}$, which covers the usual range of $\Delta\nu_L$ in LIF experiments of this type. Below 0.1Å the delta function approximation of the absorption line begins to break down, while above 2Å no new conditions arise.

The step size $\Delta\lambda_s$ can be varied widely depending on how smooth the simulated spectrum is required to be. Continuous, as opposed to point by point, scans are well simulated by putting $\Delta\lambda_s$ equal to $\sim\dot{\lambda}\tau$, where $\dot{\lambda}$ is the scan rate and τ the intensity integration time. If $\Delta\lambda_s > \dot{\lambda}\tau$, the spectrum acquires an irregular appearance.

The program was tested in two modes. Under high resolution $\Delta\lambda_L \sim 0.2 - 0.5\text{Å}$, spectra of rotationally resolved bands could be created with $\Delta\lambda_s \sim 0.05 - 0.2\text{Å}$. These were compared with high resolution spectra from a LIF experiment on the reaction

$$F + CF_3I \rightarrow IF + CF_3$$

obtained by Stein et. al.[60] Under low resolution, $\Delta\lambda_L \sim 1\text{-}4\text{Å}$ $\Delta\lambda_S \sim 0.5 - 2\text{Å}$ several bands could be generated in a spectral region of typically 100 - 200Å. The peak heights and shapes could then be compared with observed spectra from the same source.

2.3.1 High resolution behaviour

An observed spectra of the (0,3) band against which the simulations will be compared is shown in Fig. 2.3. Figures 2.4,5 show high resolution simulations of this band with $\Delta\lambda_L = 0.4$ and $\Delta\lambda_S = 0.2$ and 0.1Å respectively. It can be seen that the smaller step size gives rise to a smoother rotational envelope. Figure 2.6 shows a simulation of this band using $\Delta\lambda_S$ and $\Delta\lambda_L$ chosen to match those of Stein et. al.[60] Figure 2.7 shows a similar simulation for the (0,6) band. In the experiment the rotational distribution was characterised by a temperature, but the product was shown to be partially relaxed, such that the intensities of lines with J" <30 contained a contribution from a distribution at 300K as well. This results in a shift of the most probable J" value and distorts the shape of the high frequency end of the band, so that simulation and experiment are not directly comparable. For J" > 30 the contribution to the intensity from the relaxed distribution is negligible and so allows a limited comparison. For J" <30 given that the extent of relaxation was estimated as ∿20%, the general shape and behaviour of the simulation is good. The main defect is that the height of resolvable lines at high J" are disproportionately higher with respect to the bandhead due to the relaxed contribution.

To test this a program was modified to incorporate a partially

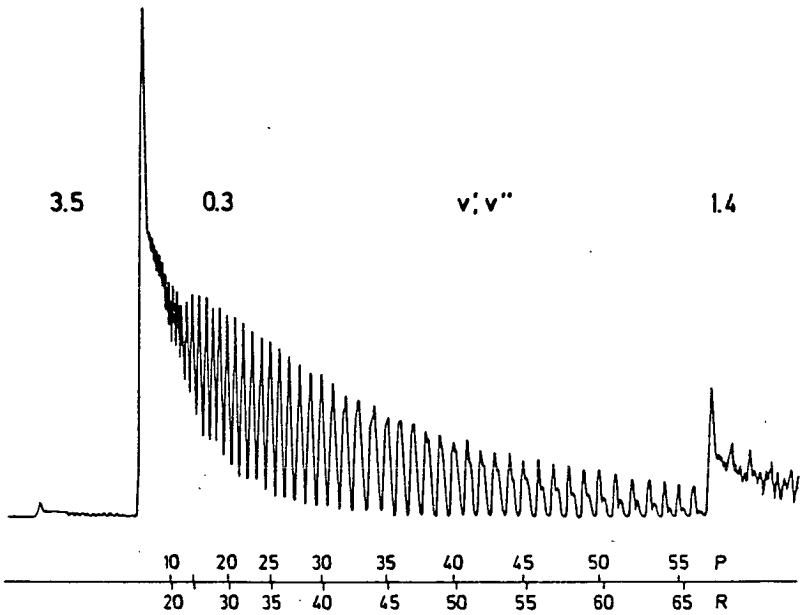

Fig. 2.3. Experimental LIF spectra of the (0,3) band of IF, reproduced from Stein et al[60]

Fig. 2.4. (page following) Simulation of the (0,3) band with $\Delta\lambda_L$ = 0.4Å and $\Delta\lambda_S$ = 0.2Å

Fig. 2.5. (page following) Simulation of the (0,3) band with $\Delta\lambda_L$ = 0.4Å and $\Delta\lambda_S$ = 0.1Å.

Fig. 2.6. (2nd page following) Simulation of the (0,3) band to match fig. 2.3.

Fig. 2.7. (2nd page following) Simulation of the (0,6) band. See text for details.

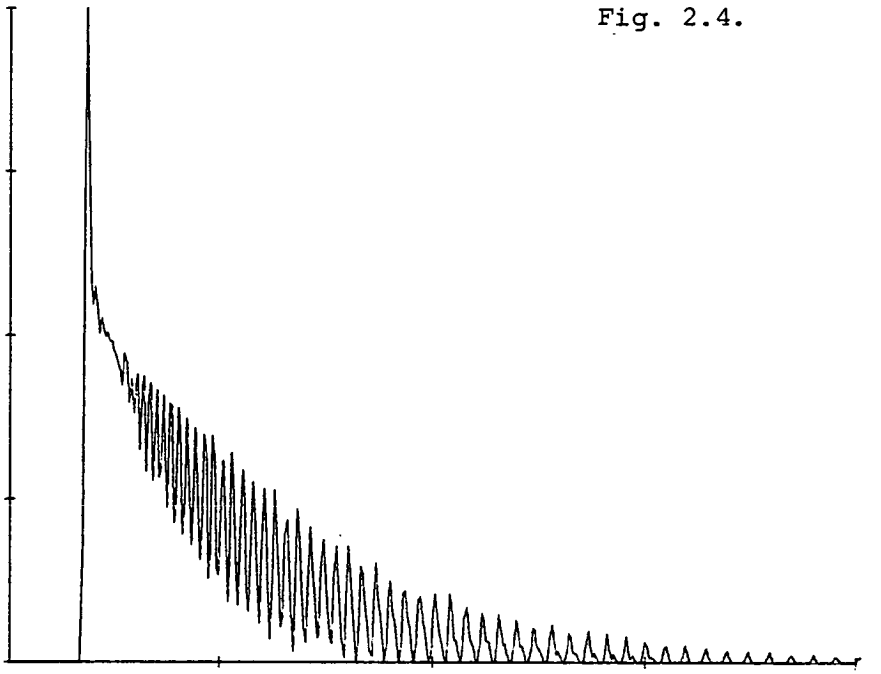

Fig. 2.4.

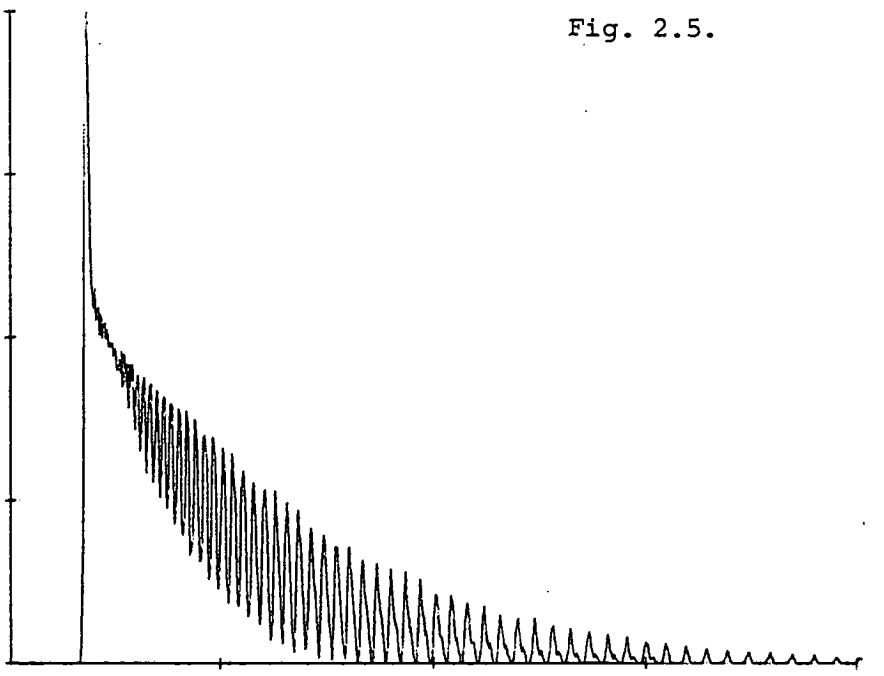

Fig. 2.5.

Fig. 2.6.

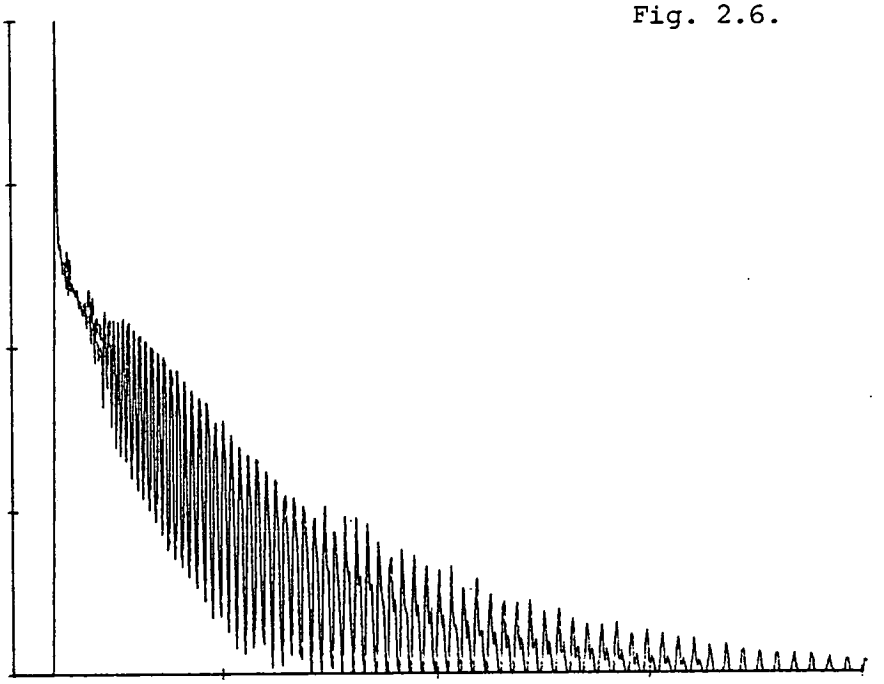

Fig. 2.7.

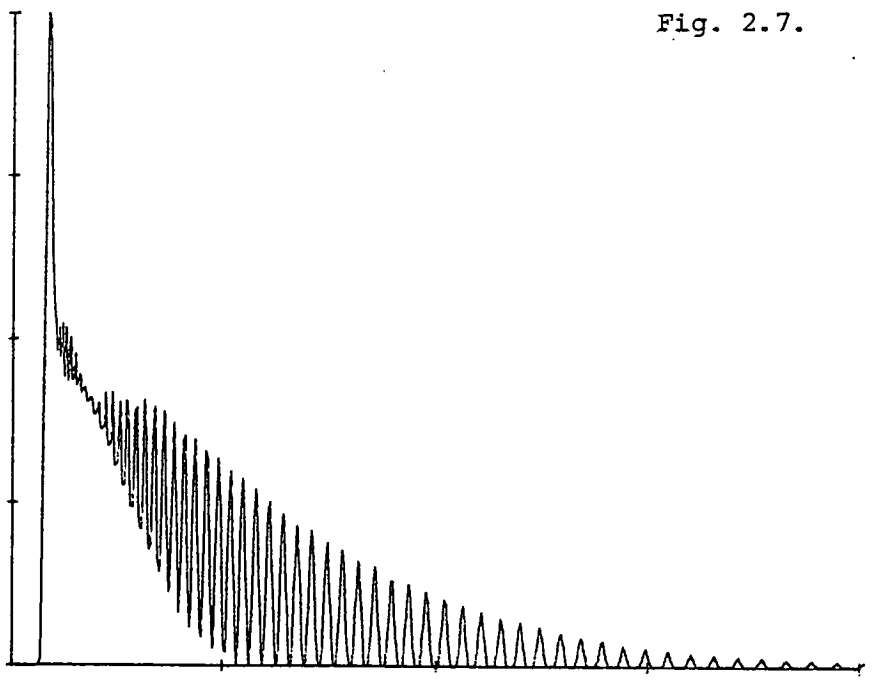

relaxed distribution of rotational states, which was assumed to be at 300K. The resulting spectra for two values of the fractional relaxation are shown for the (0,3) band in Figs. 2.8,9. These should be compared with the non-relaxed and totally relaxed simulations in Figs. 2.6 and 2.5 respectively. When the resulting simulations are normalised to the intensity at the bandhead, the result is the expected reduction of intensity at higher J" as the fractional relaxation increases.

Table 2.1 shows the intensity of various lines expressed as a fraction of the intensity of the bandhead and the P(15) line for the (0,3) band. It can be seen that best agreement is obtained for a fractional relaxation of $\sim$0.5. Within the limiting assumption that P(J") can be described as the sum of two thermal distributions, it is concluded that the program can reproduce such data to a good degree.

It should be noted however that the improved agreement resulting from the incorporation of a relaxed component in P(J") only demonstrates the possibility of the existence of such an effect. Other effects caused by the limitations of equ. 2.7 may be capable of reproducing the same discrepancy. In particular the use of rotationless Franck-Condon factors can be important in some cases[64] especially where high excitation (both rotational and vibrational) is involved. Several methods have been outlined for the estimation of the effect of centrifugal distortion on the intensity factors[123,124], but this has not been investigated further. It is clear however that such effects can only be estimated unambiguously when their behaviour is deduced from spectroscopic data or the form of P(J") is known to be well characterised, a situation not normally prevailing in crossed

Fig. 2.8. Simulation of (0,3) band.
Relaxation = 20%.

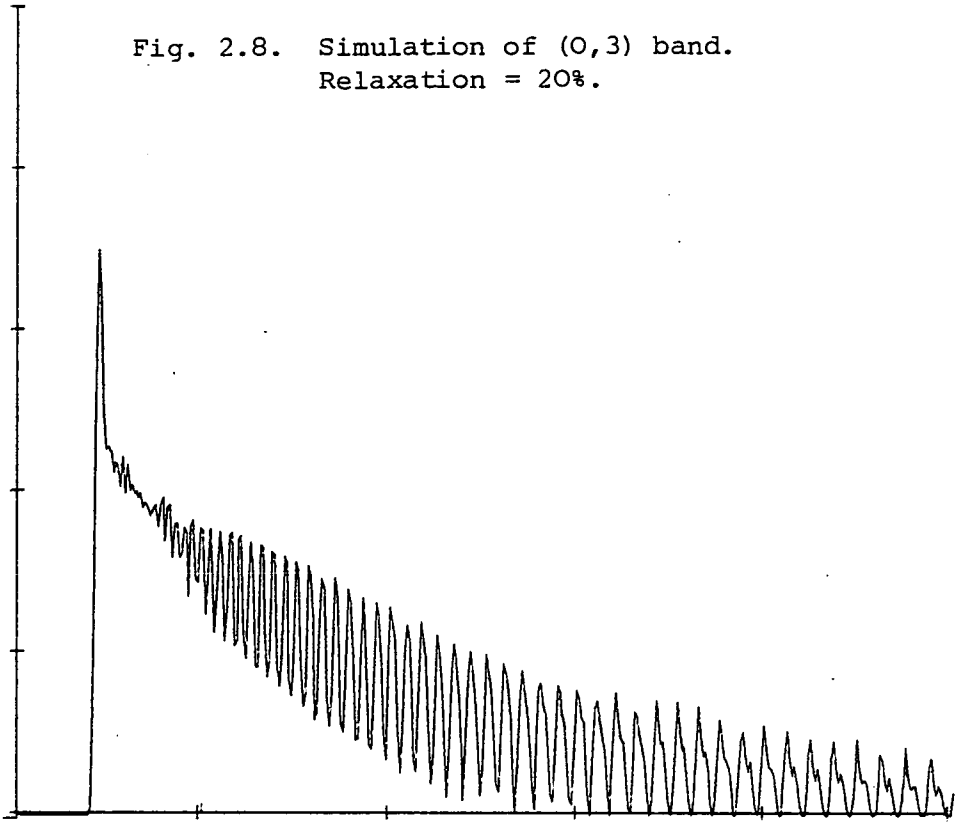

Fig. 2.9. Simulation of (0,3) band.
Relaxation = 50%.

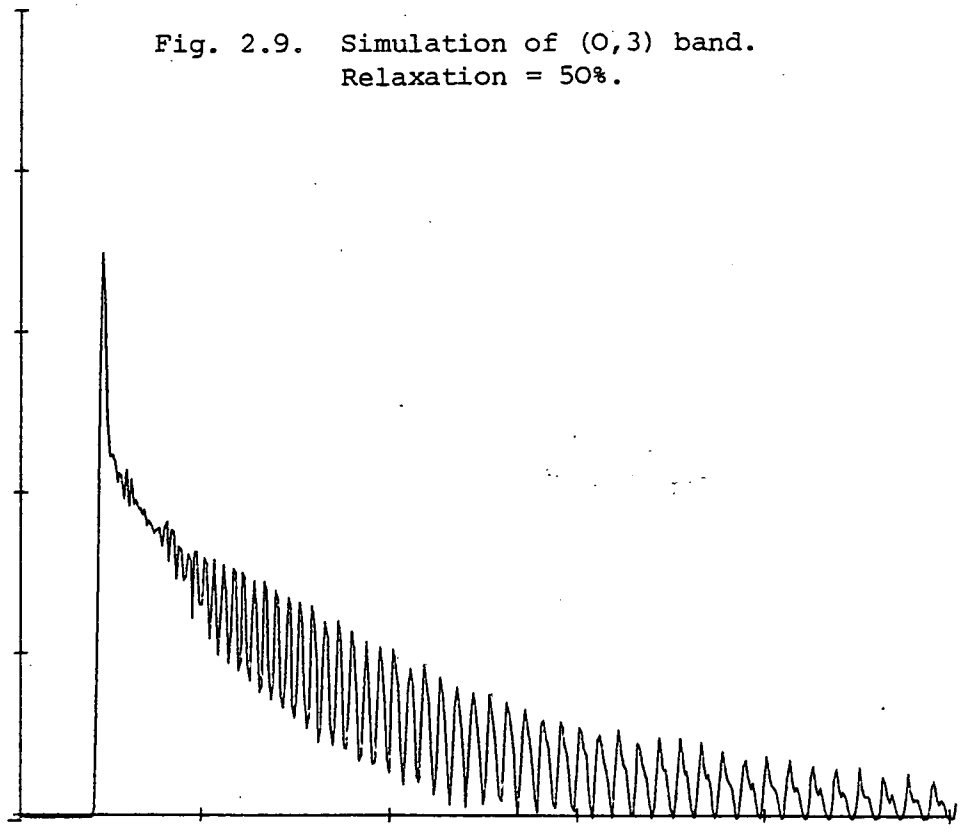

Line	Intensity as a Fraction of the Bandhead			
	Stein (60)	Relaxn.=0	Relaxn.=0.2	Relaxn.=0.5
P55	0.06	0.14	0.11	0.07
P40	0.15	0.24	0.22	0.15
P25	0.35	0.47	0.43	0.34
P15	0.44	0.54	0.50	0.44
	Intensity as a Fraction of the P15 Line			
P55	0.14	0.25	0.22	0.16
P40	0.33	0.46	0.45	0.31
P25	0.79	0.85	0.86	0.78

Table 2.1. Relative intensities of various lines as a function of fractional relaxation in the (0,3) band as compared with Stein et al[60]. Average uncertainty in ratio ≈ 0.2.

beam LIF experiments.

2.3.2 Low resolution behaviour

Direct comparison with low resolution observations is less straightforward than at high resolution. Due to the larger frequency ranges covered, information on the laser gain curve and detector response curve are required for consistent comparisons. A typical low resolution scan obtained by Stein et. al.[60] is shown in Fig. 2.10. Figures 2.11 - 13 show three regions of this system obtained from the P(v") and P(J") data of this work, with appropriate values for $\Delta\lambda_L$ etc. Rotational relaxation was not incorporated into the P(J") distribution as this would have been too difficult computationally. An approximate R(λ) variation typical of an S20 photocathode and a constant laser intensity within each section was used; detailed information on these functions was not available.

The main features for comparison are the relative heights and widths of the bands. As regards the latter it can be seen that the general shape of each band is in good agreement with the data. If anything the simulated bands appear rather too broad, especially for higher v", and this may be attributable to lack of rotational relaxation. Since this has been shown to be reproducible at high resolution, and no new algorithm is invoked which uses P(J") here, it is reasonable to conclude that the simulation can reproduce the observed profiles at low resolution also.

As regards the relative heights, Fig. 2.14 shows a complete simulation from 5200 - 5800Å. It is clear that there are severe differences between this and the observed data of Fig. 2.10. The effects of the varying dye gain curves can be at least partly removed

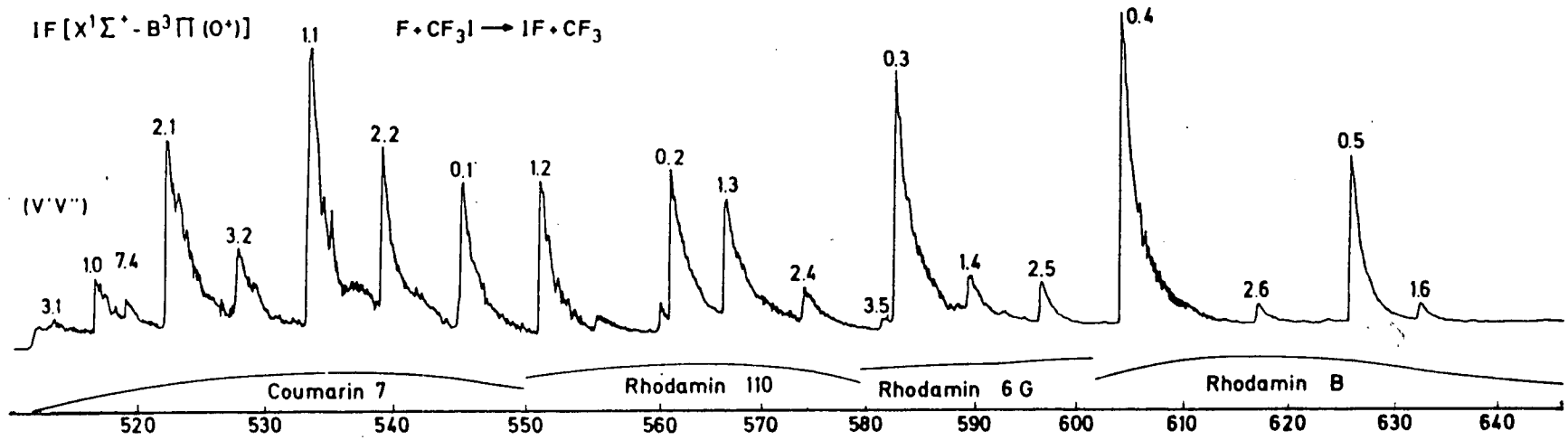

Fig. 2.10. Low resolution spectrum reproduced from Stein[60].

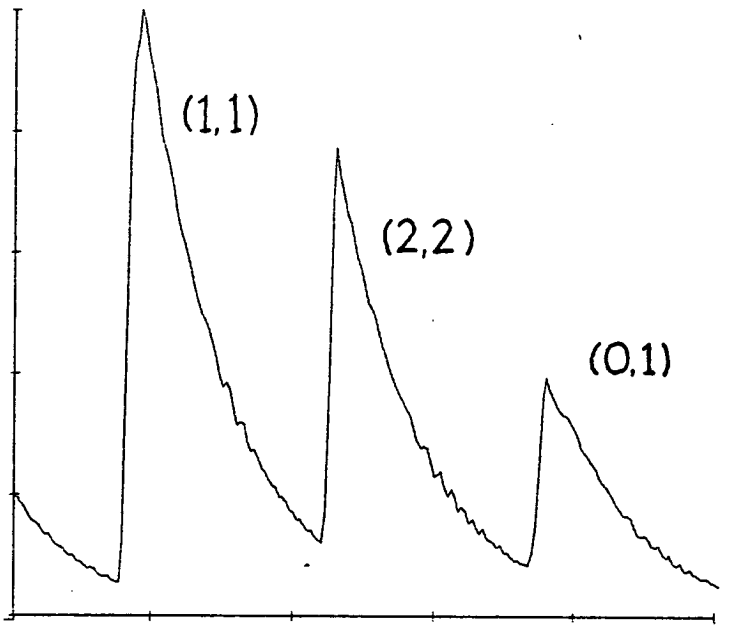

Fig. 2.11. Simulation of 530 - 550 nm

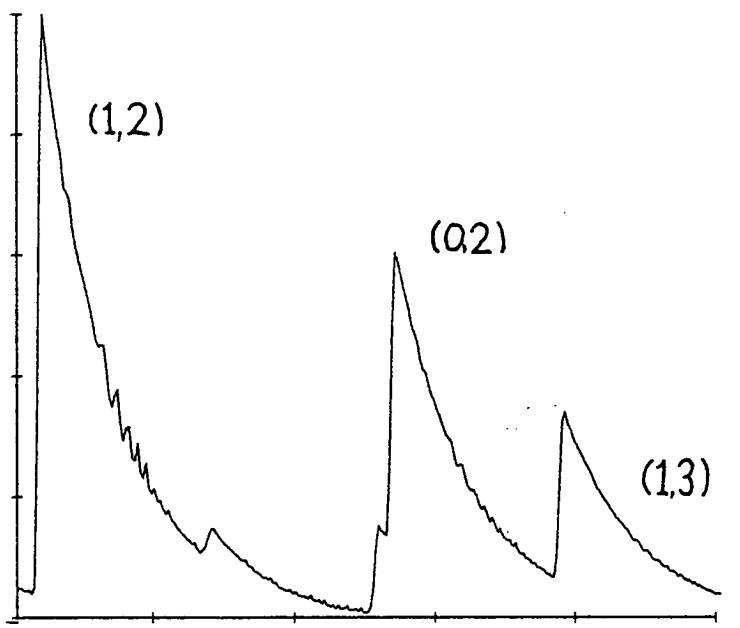

Fig. 2.12. Simulation of 550 - 575 nm

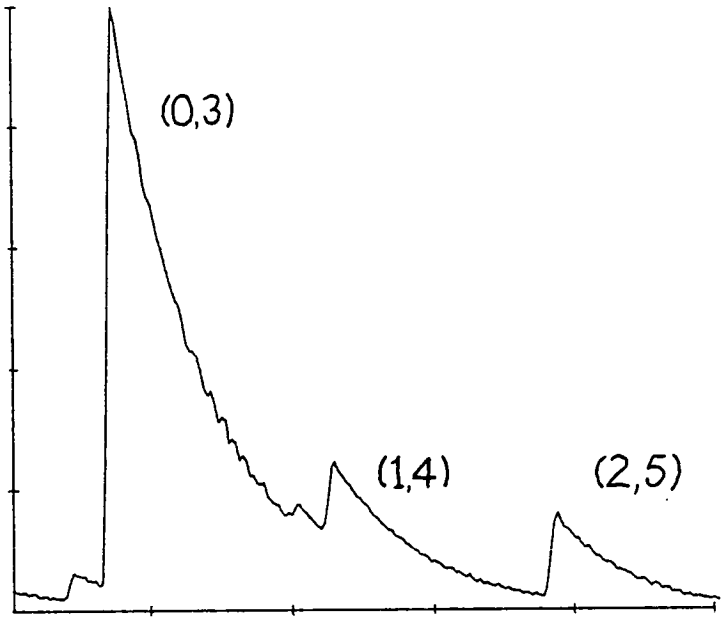

Fig. 2.13. Simulation of 580 - 600 nm

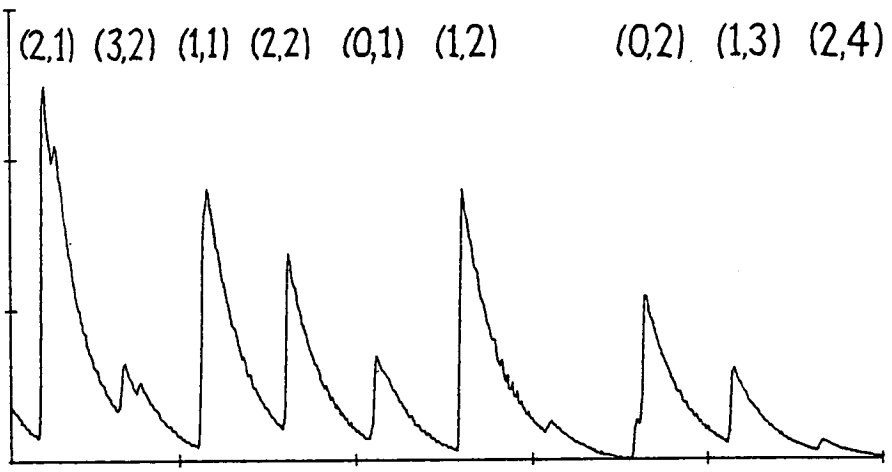

Fig. 2.14. Complete Simulation of 520 - 580 nm

by comparing adjacent bands in the regions where the gain curve can be assumed flat. Thus in Fig. 2.11 the (1,1) and (0,1) bands appear diminished with respect to the (2,2) band. Similarly in Fig. 2.12 the (0,2) band is diminished with respect to the (1,2) band. This is consistent with the simulated detector response curve being insufficiently sensitive to the red, as generally sensitivity increases with v'. Without more detailed information it is impossible to be more specific however.

2.3.3 Conclusions

Despite the reservations expressed in matching of low resolution simulations without adequate data on sensitivity and gain, the good agreement obtainable at high resolution leads to the conclusion that the simulation is capable of reproducing experiment sufficiently well for the extraction of meaningful data.

Note added in proof

Simulations of LIF spectra in product CS from the reaction $O + CS_2$ have highlighted the limitations discussed in Sec. 2.3.1[173]. Although the rotational distribution was thought to be relaxed at low J", the significance of possible departures from a thermal distribution at high J" could not be assessed because of uncertainty in the behaviour of $S_{J'J"}$ due to perturbations.

CHAPTER 3

EXPERIMENTAL

3.1 Experimental Details

3.1.1 Vacuum and beam systems

A: Scattering Chamber

The scattering chamber consists of a cylindrical stainless steel tank, shown in Fig. 3.1, of 1m diameter and 0.45m depth, with 1 cm walls. The scattering and detection zones are located at the geometric centre. A differentially pumped chamber (DPC) of volume ~16l. is located above the reaction zone, and is supported on legs mounted on an optical table which lies below the centre. The D.P.C. contains the body of the molecular cross-beam oven, and the atom nozzle beam assembly. Both these parts are mounted on a circular flat which is located in the base of the D.P.C. on the tank's axis. It is supported independently of the D.P.C. on three pins which screw into the optical table. This arrangement allows a considerably finer alignment of the beam assembly with the laser axis and fluorescence collection optics than is possible by moving the D.P.C. alone.

The atomic reagent is generated in a microwave discharge through a quartz pipe, outside the tank and passes through ports in the main chamber and D.P.C. to the beam assembly via pyrex tubing coated internally with PTFE. The nozzle is located in a cross piece which can be moved vertically on linear bearings, to vary the nozzle-skimmer distance, as shown in Fig. 3.2. The final connection of the gas tube is pushed directly into the nozzle and sealed inside by two 'O'-rings, which allows motion of the nozzle with respect to the fixed glassware. The skimmer is of stainless steel, and is fixed in the D.P.C. baseplate on the tank axis. With this arrangement the nozzle-skimmer distance can be varied to optimise the beam conditions.

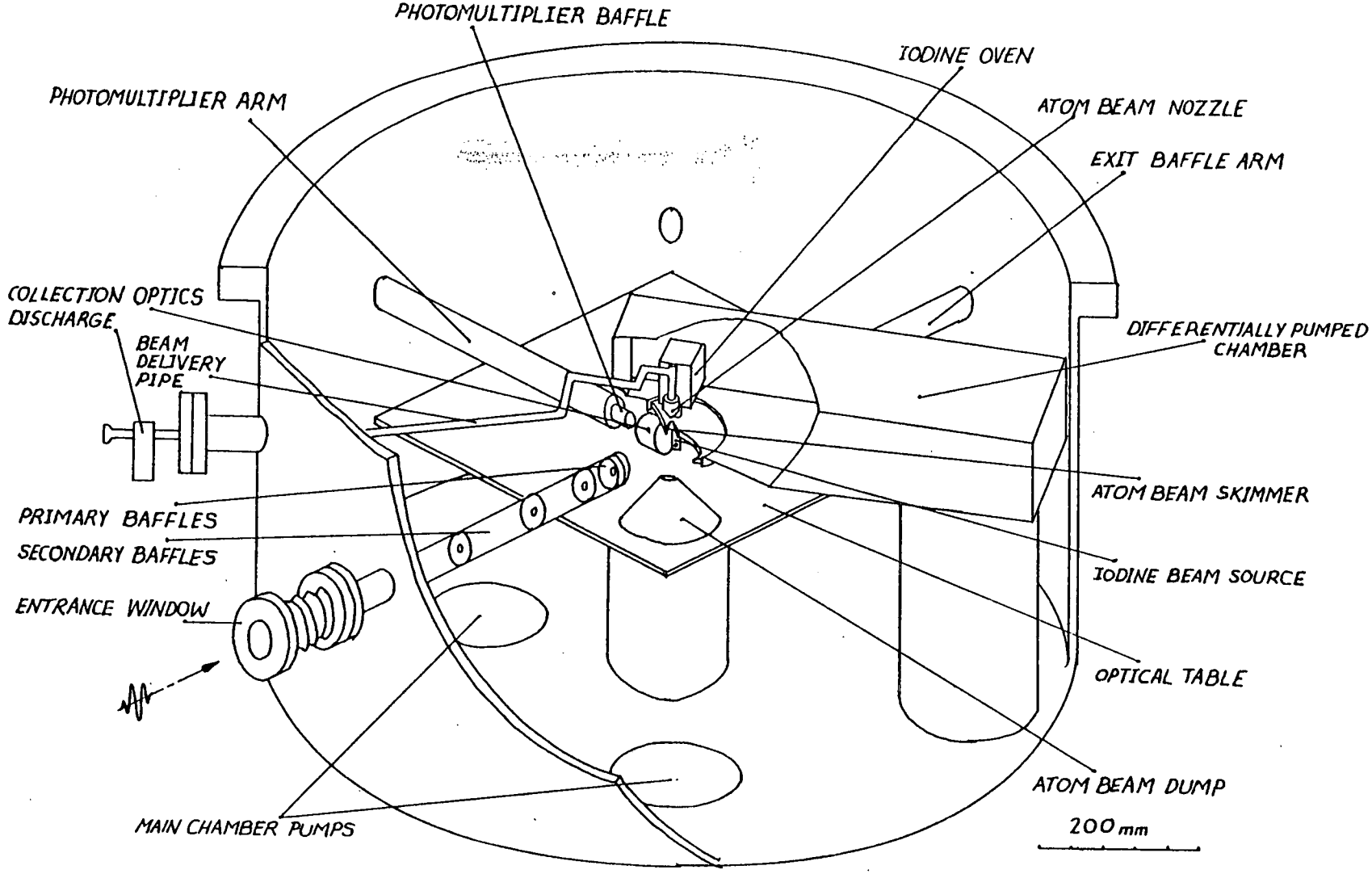

Fig. 3.1. Scattering chamber schematic

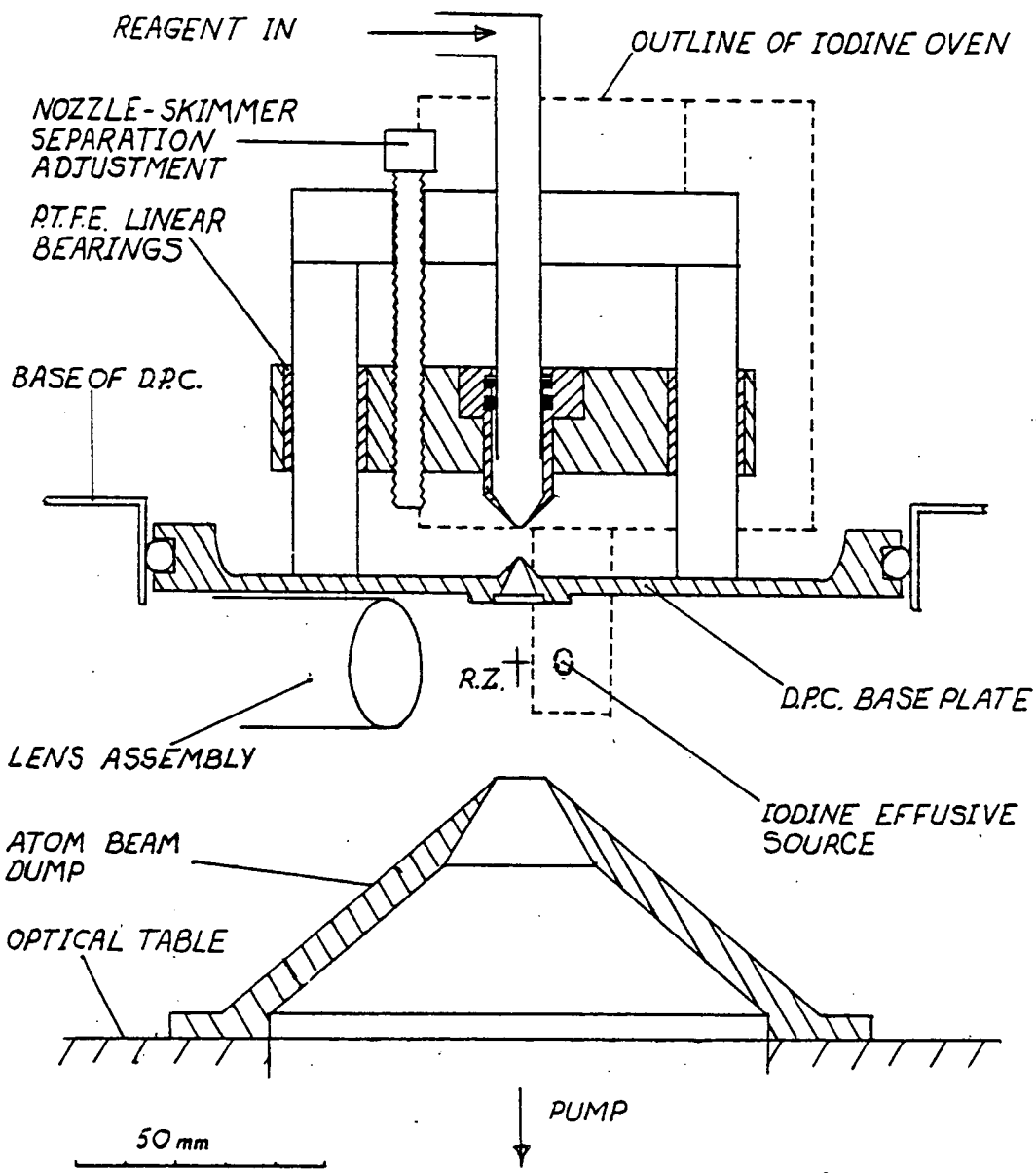

Fig. 3.2. Nozzle assembly schematic

RZ = Reaction zone

The cross-beam oven is supported on three pins screwed into the baseplate, on one side of the skimmer. The oven has a stem which passes through an 'O'-ring sealed hole in the baseplate and terminates 22 mm from the reaction zone. A microcapilliary array with a total orifice diameter of 1 mm in the side of this stem forms the source of molecular reagent.

From the skimmer of the atom beam to the reaction zone is ∿20 mm. Below the zone a beam dump consisting of a hollow stainless steel cone with an aperture of 10 mm is mounted on the optical table. This is separately pumped through a port in the table.

Around the side of the tank are arranged eight ports at the level of the reaction zone. Two of these allow the passage of the laser beam through the tank, and one at right angles to this supports the fluorescence detection photomultiplier and optics.

The main chamber is pumped directly by two Edwards E06 oil diffusion pumps (1400 ls^{-1}). Each pump is separated from the main chamber by two sets of cooled chevron baffles. The upper set is cooled by methanol circulating in a methanol/dry ice slush at -98°C, and the lower set by water. The main chamber is extensively cold-trapped by liquid nitrogen traps which are replenished automatically. The D.P.C. is pumped by a third E06, and the beam dump by a Leybold 501 oil diffusion pump (600 ls^{-1}). The two pumps on the main chamber are backed through two liquid N_2 traps by two Edwards rotary pumps (500 l min^{-1}). An Edwards EDM12 rotary pump (250 l min^{-1}) backs both the D.P.C. and dump through a third cold trap.

With this arrangement of pumps and traps, pressures of 2 x 10^{-5} torr in the main chamber and 2 x 10^{-3} - 10^{-2} torr in the D.P.C., were

attained with both beams running under typical conditions. The pressure in the main chamber was measured with Edwards IG3M and IG5K ionisation gaugeheads.

B: Iodine beam

The iodine cross-beam is formed from a glass micro-capillary array (10μm or 25μm pore diameter x 1 mm thickness, 75% transparency). The stem and oven are provided with independently variable heaters, with the stem normally kept 5 - 10 K hotter than the oven to prevent condensation and blocking of the capillary array. The corrosive nature of the iodine easily degraded the seal between the stem and the array, during a run of several days operation. The capillary was not usually reclaimable following this.

Under normal experimental conditions the oven was maintained at 60 - 70^{o}C corresponding to a vapour pressure of 5 - 10 torr. There was no direct means of monitoring the intensity of the beam experimentally. However, the background pressure in the tank was found to be stable once the oven temperature had stabilised, suggesting that any fluctuations in the beam intensity were small.

C: Fluorine atom beam

Discharge reagent is made up in a gas line before each experiment. A high pressure (760 torr) reservoir has a capacity of 20l., and gas is dispensed through a needle value to the microwave cavity. Typical operating pressures were 5 - 10 torr, as measured by a pirani gauge (Edwards PRCT 10, and Monitorr 162), and additional precision was available by using a digital readout. By adjusting the needle value to compensate for the slow decrease in the high pressure,

the low pressure could be kept constant to within a few percent.

Atomic fluorine reagent was obtained by discharging CF_4 diluted to ∿10% in He. CF_4 has the advantage over F_2 in being easily handled and non-toxic. An EMS type 214L cavity at a net power of ∿70W was used to discharge the mixture. This was external to the tank and the discharged mixture flowed a distance of 60 cm to the nozzle. Under these conditions the beam should consist mainly of He, CF_4, C_2F_6, F_2, and F[125], of which only atomic fluorine reacts directly with I_2 to give IF product. The nozzle is constructed of 'Teflon' and mounted as in Fig. 3.2. It has a diameter of 0.4 mm. The skimmer has a diameter of 1 mm with internal angle 25° and external angle 35°. The nozzle skimmer distance can be varied up to ∿15 mm.

3.1.2 Laser system

The laser system used is essentially that described by Fernie[119] so only a brief summary will be given. The nitrogen pump laser was built at Edinburgh and is of the parallel palte 'Blumlein' configuration. The discharge cavity is of ∿1 m length x 30 mm gap width x 3 mm electrode height, and operates at a gas pressure 30 - 50 torr. A hydrogen thyratron is used to discharge the capacitance across the gap at a repetition rate of 50 - 100 Hz, and yields a pulse width of ∿12 ns and a peak power output of ∿50 kW[119].

The output of the N_2-laser at 337.1 nm is focussed by a quartz lens onto the dye laser cell. This consists of a stainless-steel cell with quartz windows, through which the dye solution flows. The dye laser cavity is formed by a 50% reflecting concave output coupling mirror, a x10 beam expanding telescope and reflection grating (1200

lines mm^{-1}). This is mounted on a stepping motor (Unislide 4757) incorporating a divide by 20 gearing ratio to give a step length of ∿0.11 nm near the blaze wavelength of 450 nm.

The beam quality was found to be rather poor with this arrangement, having a non circular shape and irregular decrease in intensity. A 400μm diameter pinhole was positioned just in front of the output coupler to select only the core portion of the laser action. This resulted in better spatial definition of the beam, but also caused a drop in total power from 300 to 150μW. A circular diffraction pattern was also formed. The beam was allowed to expand from the output coupler, as shown in Fig. 3.3, to a diameter of 1-2 mm, and then collimated by a lens of 30 cm focal length. This resulted in a beam of low divergence (<1 mrad), and a uniform diameter of ∿2 mm in the reaction zone. The collimated beam was steared into the tank through a glass port. The various surfaces between output coupler and reaction zone result in a farther attenuation to 100μW power.

Along the laser path within the tank care must be taken to ensure that spurious pulses from the laser light are not accidentally counted. The use of a gated counting system prevents any photons scattered directly from the laser pulse being accepted, but exposure to such a (relatively) high intensity pulse of scattered laser light can cause secondary "afterpulse" effects in the photomultiplier[126]. These are caused by ionisation of the residual gas atoms in the cathode-first dynode space, by the initial photo-electron pulse. Ion bombardment of the cathode may liberate up to 20 secondary electrons, which appears as an afterpulse of varying size. The delay between the

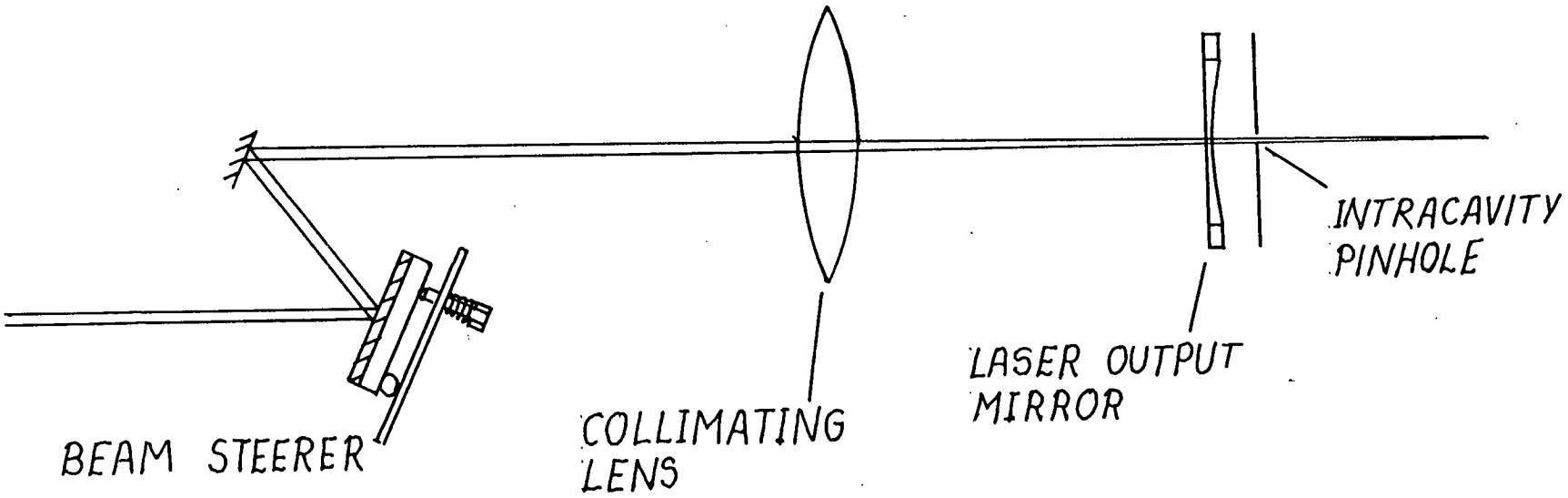

Fig. 3.3. Dye laser beam clean-up optics

initial multiphoton pulse and the secondary ion pulse is determined by the relatively low mobility of the ion, and is ∿1μs. This is also the timescale of the fluorescence signal. In the event of low signal rates it is important that this source of time-correlated noise is minimised.

Scattered light from the laser arises mainly from the entrance and exit windows. In addition there is the problem of diffraction rings caused by the intracavity pinhole. (The scattered light from this source was much less than that arising from the untrimmed beam). The beam passes through a series of 1 cm diameter apertures equispaced along the baffle arm, as shown in Fig. 3.4a). These serve to remove light scattered to wide angles at the windows, and higher order diffraction rings. Final shielding is performed by the primary baffles which are located in a demountable sleeve on the end of the baffle arm (Fig. 3.3). A variety of sizes and shapes of baffle and spacer were made and the optimum configuration determined over a period of several months. This is shown in Fig. 3.4b).

The use of baffles to reduce scattered light in this type of experiment has become a standard technique[79], and all such systems have relied on the fact that the beam is well defined spatially, and so is not spoiled on the baffles. In this experiment the diffraction rings were sufficiently intense to give rise to non-negligible scattering of the edges of the baffles however, and it was this that ultimately limited the reduction of the scattered light. The number of photons reaching the detector from the scattered light was estimated by viewing the resulting pulse on a fast oscilloscope. At a mean power of 100μW, this was between 1 and 10 photoelectrons

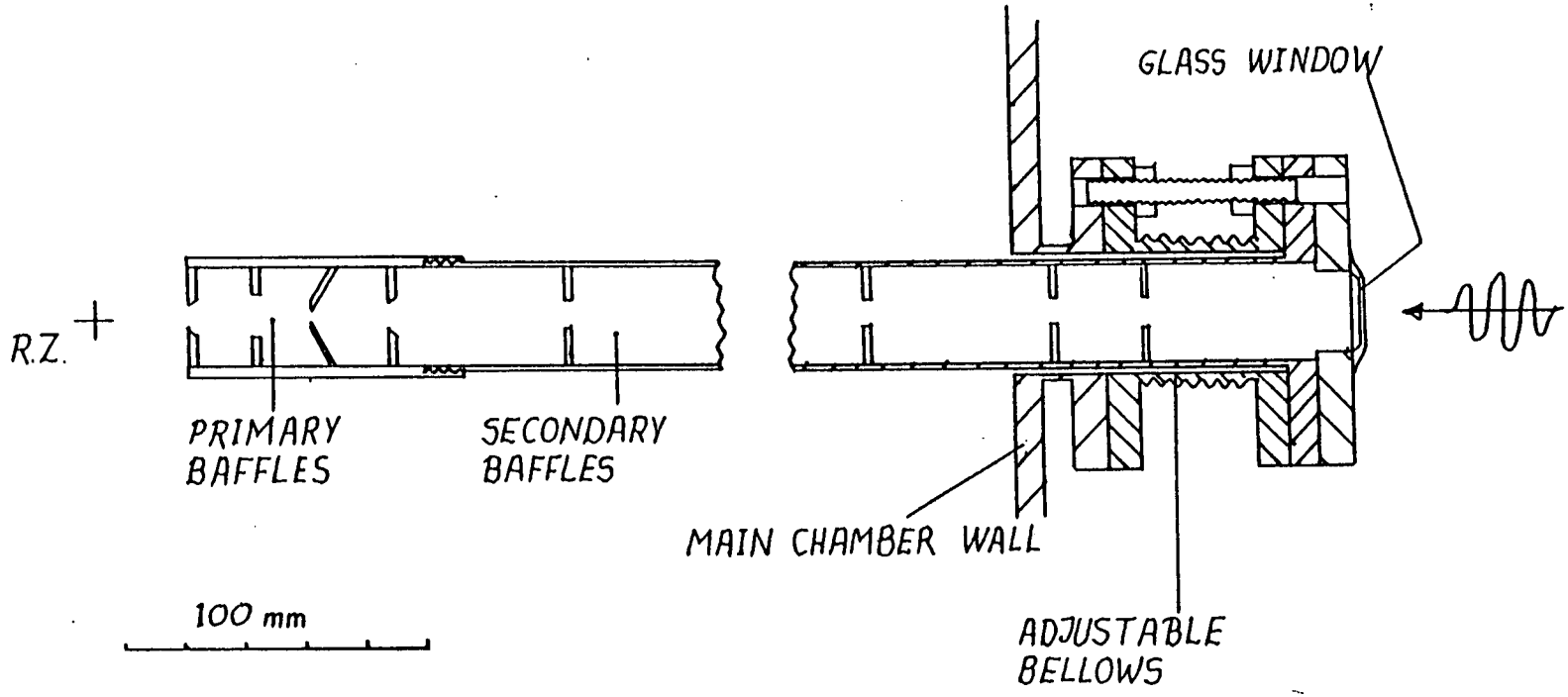

Fig. 3.4a) Baffle Arm

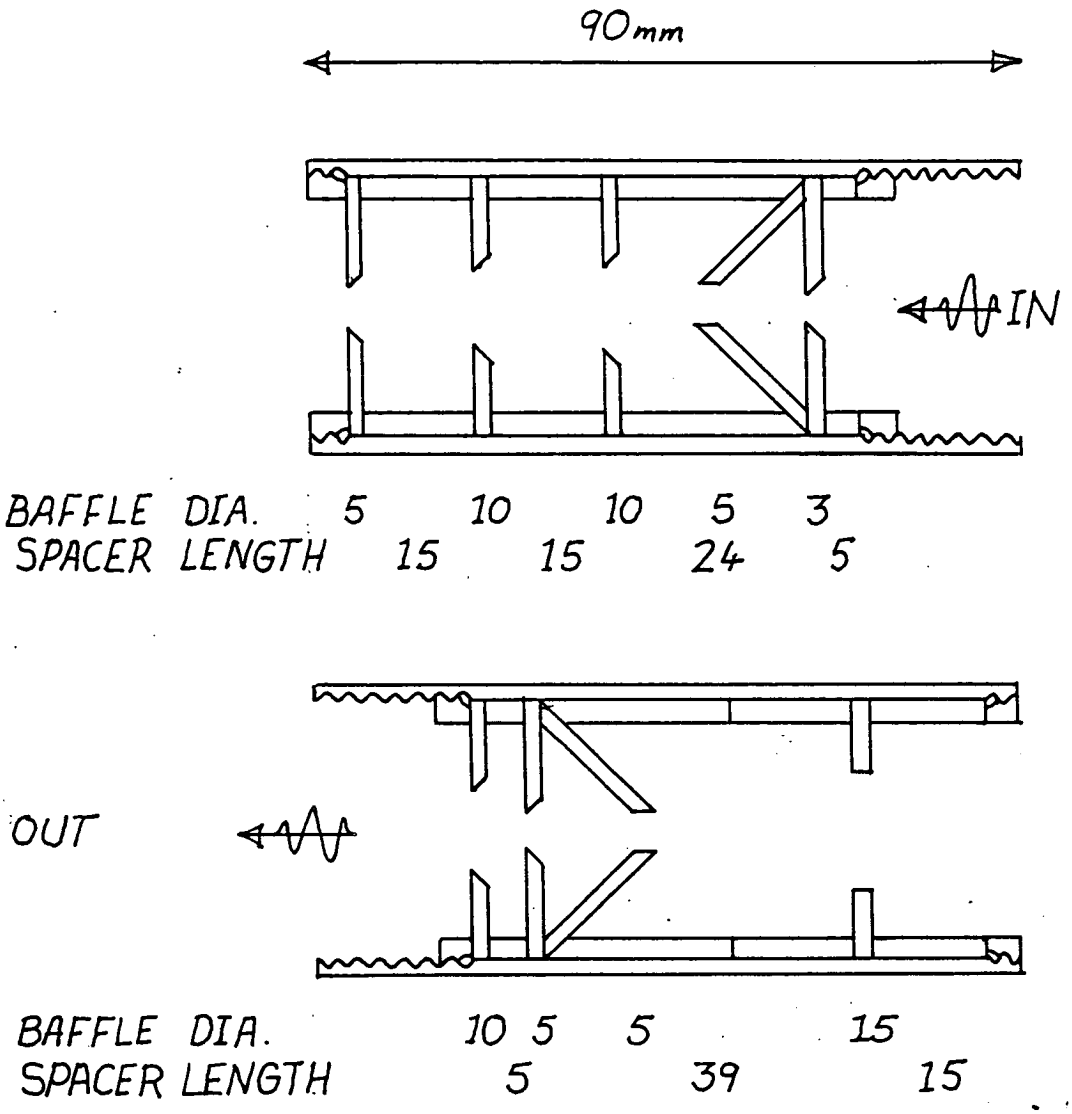

Fig. 3.4b) Baffle design

depending on the precision of alignment.

3.1.3 Measurement of dye laser parameters

The bandwidth, gain, and time duration of the dye laser pulse were all found to depend quite sensitively on the construction of the dye cell. There appeared to be no dominating cause i.e. one that could be correlated strongly with the observed variation in the above properties. Due to the limited lifetime of the dye cells, the following measurements are therefore approximate. Except where indicated however the numbers quoted are those relevant to the experiments in which conclusive data was obtained and as such are also used in the feasibility calculation.

A: Peak power and time duration

The time variation of the intensity was observed using a fast high voltage photodiode (I.T.L. Ltd.) and fast oscilloscope (Tektronix 7904 mainframe with 7B92 timebase and 7A21N direct access vertical deflection modules). The direct access unit was calibrated with a pulse generator (Lyons PG73N) and an internally calibrated oscilloscope (Hewlett Packard 142A). The sensitivity of the photodiode is a known function of wavelength. The peak power was determined as $\sim$320W, and the FWHM as $\sim$5ns. This corresponds to a pulse energy of $\sim$1.6μJ and a mean power of 80μW, or 3×10^{12} photons per pulse.

B: Bandwidth*

A scanning Fabry-Perot interferometer with a small plate separation was used to give a free spectral range of 5Å (25 cm^{-1}). By analysis of the hyperfine structure of the 546.1 nm Hg line, the finesse of the interferometer was found to be ∿50. To measure the laser bandwidth the output from an EMI 9824B photomultiplier was integrated with a time constant of 1s, and its output displayed as the Y co-ordinate of an X-Y plotter, the X-drive being obtained from the piezo-electric scan of the interferometer. The bandwidth of the associated electronics was determined from measurements on the Na D-lines to be ∿2 cm^{-1}.

Figure 3.5 shows laser line profiles obtained under various operating conditions, with two different dye cells. These results were reproducible for a given cell, and illustrate the effect of changing the cell, all other things being equal. Unfortunately, it did not prove possible to determine the bandwidth of all the cells used, due to the time involved in setting up the interferometer, but the results suggest that for pump laser operating voltages above ∿10 kV, the profile is approximately symmetrical and single peaked with a bandwidth of 3.2 ± 0.2Å. There is some evidence to suggest that the bandwidth decreases at higher pump powers. The use of much higher

* I am grateful to Ian Hutchison working under the supervision of Dr. A.G.A. Rae, for his measurements of the laser line profile, as part of a Carnegie Trust vacation scholarship.

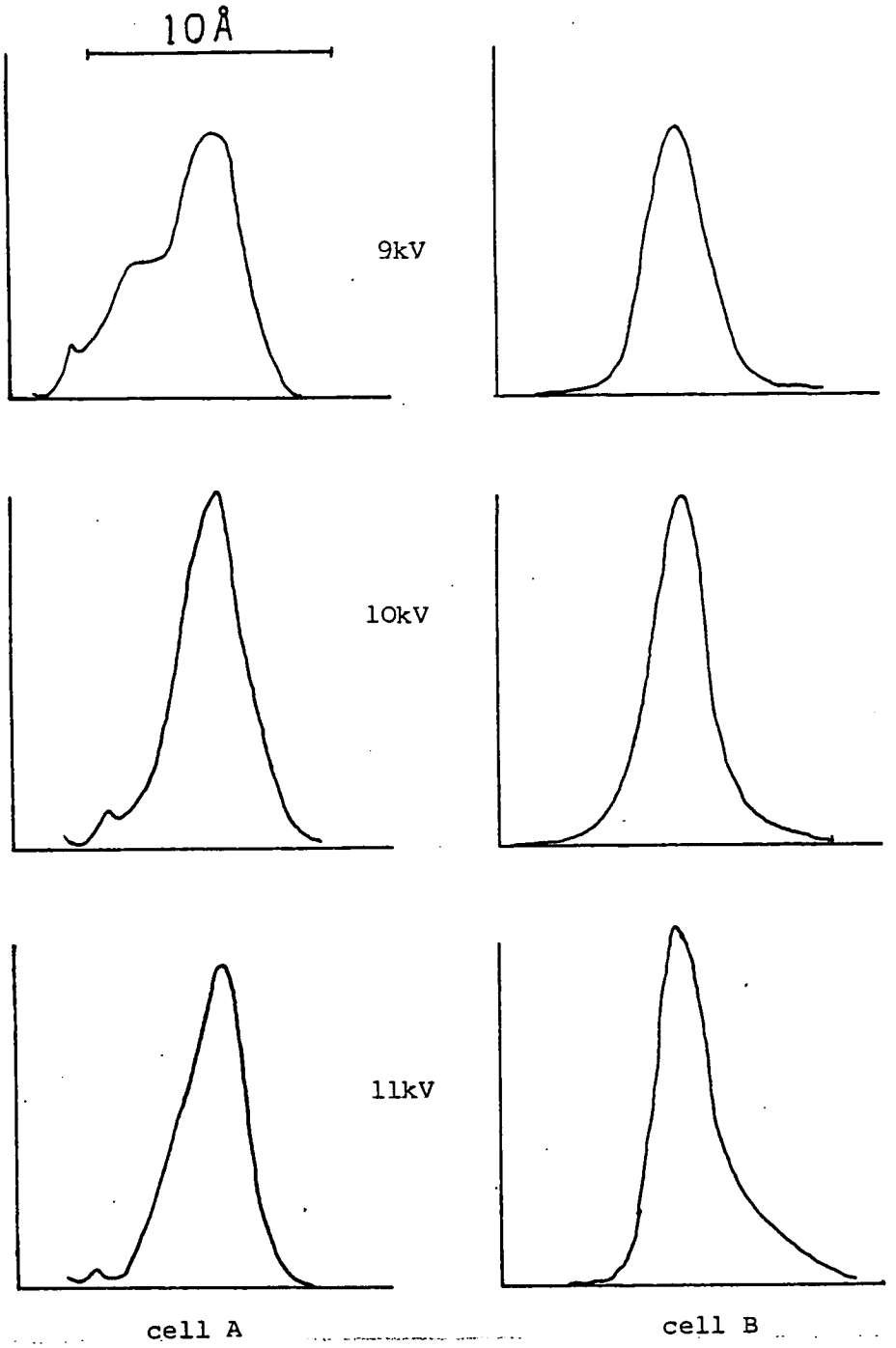

Fig. 3.5. Variation of dye laser bandshape with pump laser operating voltage for two dye cells

pump powers proved to be inexpedient however, as this significantly shortened the operating life of the nitrogen laser dielectric. The bandwidth was thus assumed to be $\sim 3\text{Å}$.

C: Wavelength stability and control

The wavelength of the laser could be determined using a Hilger Watts 30 cm spectrometer. This was calibrated over the range 450 - 590 nm using lines from Cd and Na discharge lamps, and found to be linear to within 1Å. Wavelength stability was tested by running the laser continuously for 4 hours. A mean drift of 1Å hr^{-1} was found. The consistency of the stepper motor was checked using the spectrometer. Some sticking and backlash was observed, which on small movements (<20Å) was found to be correctable with a high degree of reliability. Over long drives deviations from the predicted position of a few Å were typical, but less consistent. Normally the grating was operated under computer control, so after long drives the wavelength was checked and a correction applied as necessary.

D: Gain curve

The extent and shape of the gain curve was found to be highly dependent on the dye cell. As only coumarin 102 was used in the final sequences of the experiment, only the gain curve for this dye was analysed. This is shown in Fig. 3.6 for two different cells. Detailed knowledge of the gain curve is not required for interpretation of the data as the laser monitor provides information on the power levels during the course of the experiment. Variations in laser intensity occur dur to degradation of the dye and changes in the laser cavity as well as due to the gain curve.

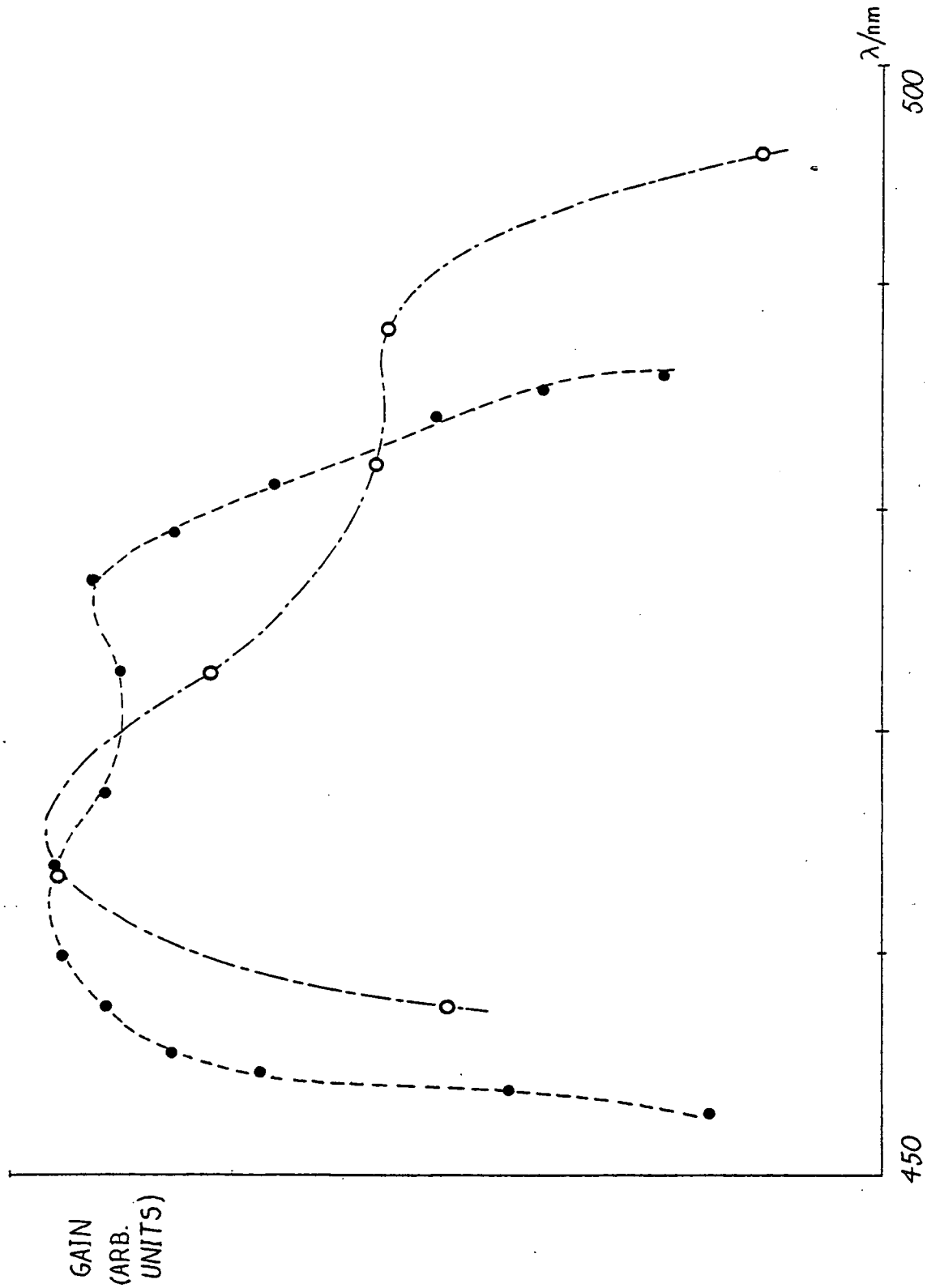

Fig. 3.6. Gain curves of Coumarin 102 using two different dye cells

3.1.4 Data Acquisition system

A: Fluorescence counting system

Fluorescence is viewed at right angles to the direction of the laser beam, as shown in Fig. 3.7. The photomultiplier (EMI 9824B) is mounted in a stainless steel tube which is attached via a flexible coupling to the external flange of the tank in a similar fashion to the laser baffle arms (Fig. 3.3). The photocathode is sealed against an 'O'-ring to the vacuum, as in Fig. 3.8. The fluorescence is collected by means of a simple lens system described by Clyne and McDermid[83]. The detection zone is located in the focal plane of an aspheric lens (dia. 30 mm, focal length 25 mm). A second such lens focuses the light through an aperture on to the photocathode. This focusing action assists rejection of spurious light which is not divergent from the reaction zone. This lens assembly is mounted in a brass cylinder which is bolted on to two of the DPC baseplate support legs. As the photomultiplier arm is not fixed with respect to the detection zone, the second lens is mounted on a screw coupling. This allows the focusing of the fluorescence through the pinhole to be optimised.

Pulses from the photomultiplier were amplified in two stages (Keithley 111A fast pre-amplifier and Hewlett-Packard 462A fast pulse amplifier) to give pulses of several hundred millivolts. These are accepted as input by a discriminator and passed to the gating system as standard 50Ω high level logic pulses. These three stages of processing were located as close to the photomultiplier as was possible. Substantial RF pickup at ∿12 MHz from the N_2-laser was observed on all

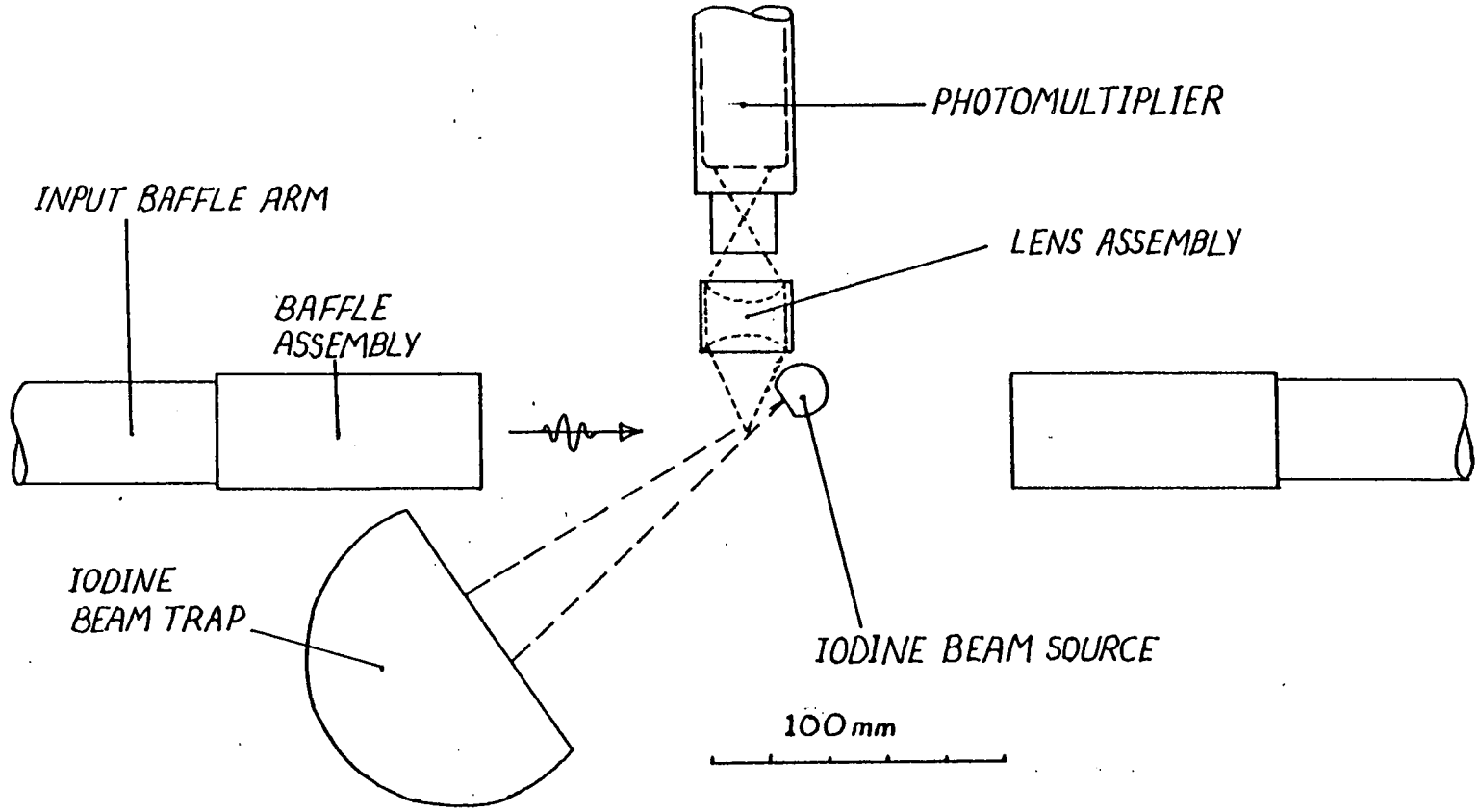

Fig. 3.7. Plan of reaction zone. Fluorine atom beam is into paper.

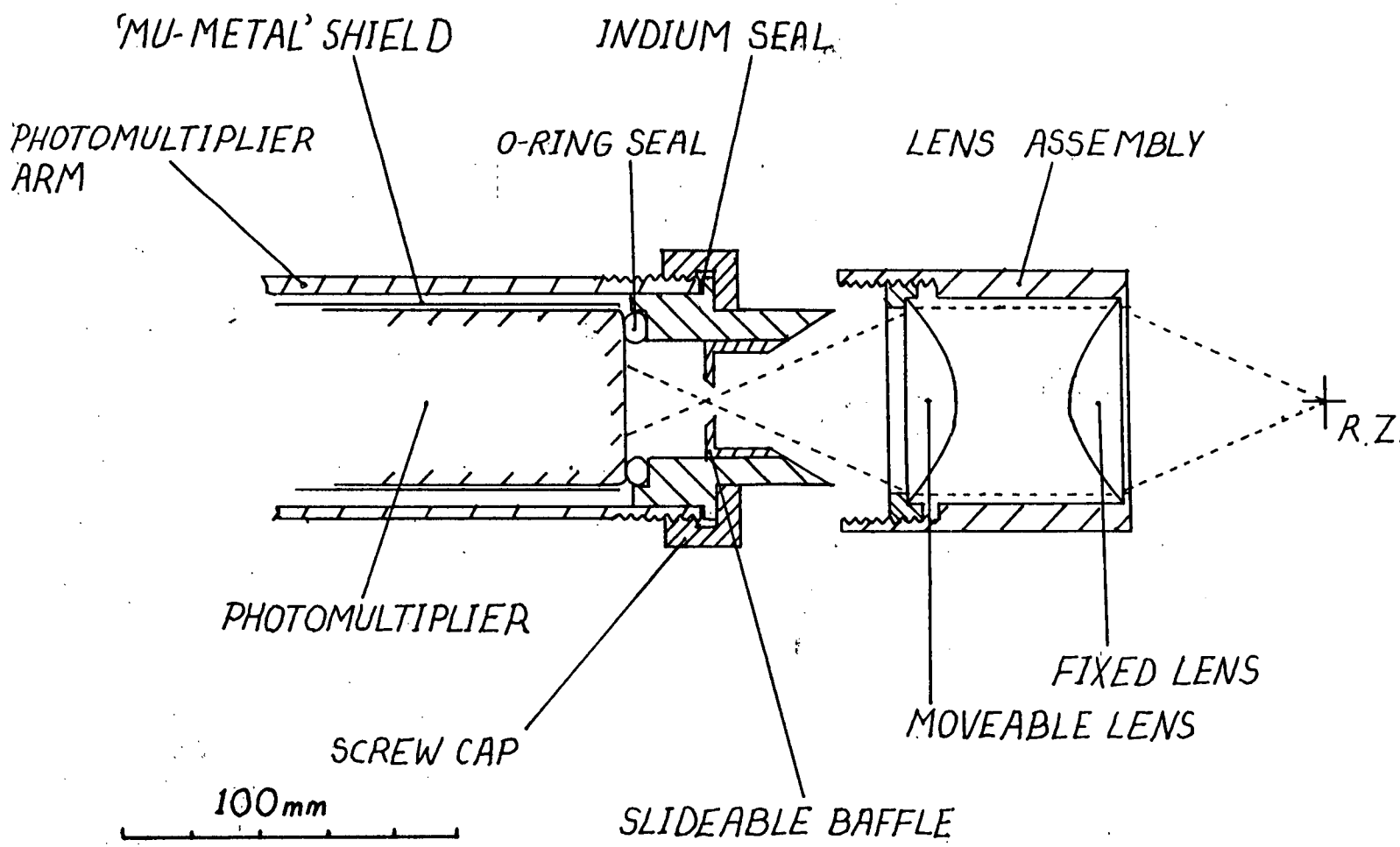

Fig. 3.8. Fluorescence collection optics

low level signal lines, and without shielding this was capable of masking the signal. Wrapping all the stages before the amplifier in in aluminium foil reduced this to <10 mV.

A schematic of the complete data collection system is given in Fig. 3.9.

Since a pulsed laser was used it was convenient to have a gated counting system. This has the advantage of enhancing the signal to noise ratio by a factor equal to the duty cycle if the main source of noise is uncorrelated in time with the signal. The gating pulse which defines the window during which pulses are counted is derived from part of the N_2-laser pulse illuminating a fast photodiode (I.T.L. Ltd.). The output from this is shaped, delayed and expanded to form the gating pulse. Discriminated pulses from the detector which arrive during the extent of the gate are amplified and counted in the scaler over a preset period of either, 1, 10, or 100 s. The pulse shaping and gating was performed using AIM units.

The timing and data logging were performed by a control unit specially built to interface the scaler to the departmental PDP11/45 minicomputer. This unit also performed various control operations and is described in section 3.2.

B: Laser monitor

The dye laser intensity was monitored during the course of an experiment by a second EMI 9824B photomultiplier, this time operating in the DC mode. At a repetition rate of 50 Hz the output of the photomultiplier could easily follow the pulsed input. The charge under each pulse was integrated on a sample and hold circuit with a time constant of 0.1 s, and the output displayed on an electrometer

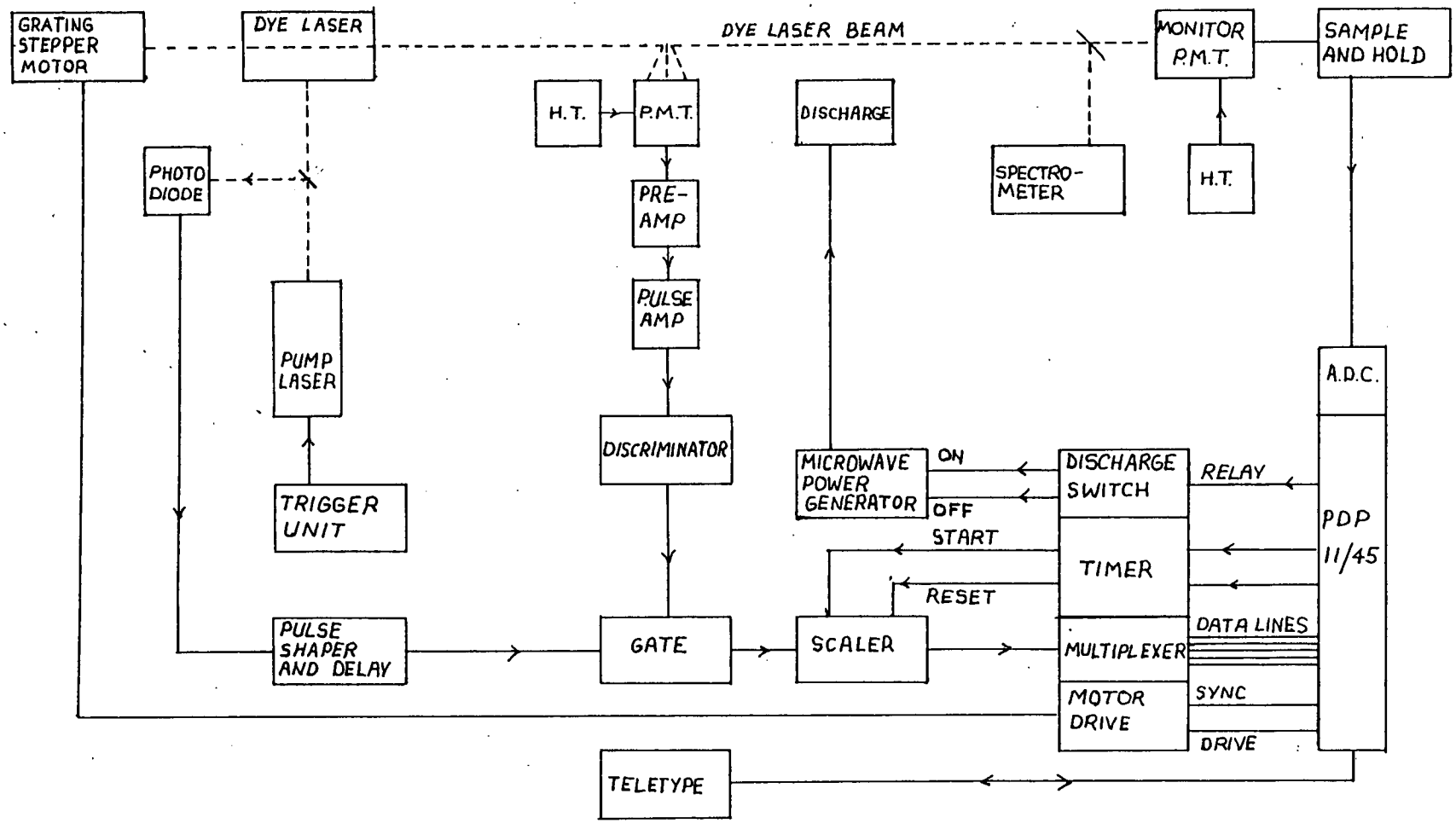

Fig. 3.9. Block diagram of data collection system.

(Keithley 602). The 0 - 1V output of this was connected to an analogue to digital converter which could be sampled under computer control at rates of up to 10^3 Hz.

The linearity of the monitor with respect to the incident intensity was checked using the fast photodiode and oscilloscope used for measuring peak power. The incident beam was attenuated using neutral density filters and the monitor signal and peak height measured. Correlation of these two measurements showed linear behaviour with a co-efficient of correlation of 0.98.

The use of two photomultipliers having the same response function allows for a possible simplification in normalising signal with respect to laser intensity provided certain conditions are satisfied. In general the intensity signal for a detector with response function $R(\lambda)$ is given by

$$S = \int_0^\infty R(\lambda) I(\lambda) d\lambda \qquad 3.1$$

where $I(\lambda)$ is the distribution of incident intensity. For laser radiation of intensity I_L, if $R(\lambda)$ is a slowly varying function of λ near the laser wavelength λ_L, over the laser bandwidth $\Delta\lambda_L$, then

$$S_L \simeq \int_0^\infty R(\lambda) I_L \delta(\lambda-\lambda_L) d\lambda = R(\lambda_L) I_L \qquad 3.2$$

For a fluorescence signal $I(\lambda)$ is determined by the Einstein A co-efficients as in equ. 2.4 and S has the form

$$S \alpha \sum_{jk} R(\lambda_{jk}) \left\{ \frac{A_{jk}}{\Sigma A_{jk}} \right\} I_L \qquad 3.3$$

with j,k referring to all possible (v,J) transitions. If $R(\lambda)$ does not vary much over the width of one band then this can be written as

$$S \alpha \sum_{v''} R(\lambda_{v'v''}) \frac{q_{v'v''} \bar{\nu}^3_{v'v''}}{\nu^3_{v'}} I_L \qquad 3.4$$

Only in two cases does this approach $R(\lambda_L)I_L$ as in equ. 3.2, and thus allow cancellation of the sensitivites in the normalisation with respect to I_L. These are:

a) if the fluorescence intensity is concentrated mainly in the band which is excited i.e.

$$q_{v'v''} \begin{cases} \simeq 1 & v'' = v''_o \\ \simeq 0 & v'' \neq v_o'' \end{cases}$$

where $v' \leftarrow v''_o$ is excited at λ_L.

b) If $R(\lambda)$ is approximately constant and $\simeq R(\lambda_L)$ in the range of significant fluorescence intensity.

For the B → X system of IF neither of these conditions holds particularly well. For absorbtion in the blue, fluorescence is distributed with significant intensity at wavelengths where $R(\lambda)$ is significantly different from $R(\lambda_L)$. Thus it is generally necessary to incorporate the response function into a simulation calculation as described in chapter 2. The correction to the monitor signal is applied to determine the true laser power before the intensity is incorporated into the simulation.

C: <u>The effect of laser induced noise</u>

The existence of time correlated laser induced afterpulsing was referred to in sec. 3.1.2. The strength of this effect is usually measured by the co-efficient β, which is the probability of afterpulse occurrence per photo-electron pulse. β is a function of the operating

voltage in the cathode - first dynode space and may be typically in the range 10^{-4} to 5×10^{-2}. Hence for scattered laser light of ∿5 photoelectrons per pulse, a noise rate of up to ∿12 s^{-1} may result from this source.

The requirement of high cathode sensitivity in the single photon counting mode directly opposes that of low afterpulsing. While the 9824 is not a particularly high gain device, it has a low dark count and a compact size, which enables a close proximity to the detection zone without the need for complex optics. Gains of up to 10^7 are achievable however. Several tubes of this type were tested for their afterpulsing properties. This was done by allowing a low level chaotic light source to be detected and using a time to amplitude converter and multichannel analyser to measure the distribution of pulse separation intervals over a 20μs range. This is shown schematically in Fig. 3.10. The delay shown is very short (∿ few ns) and merely serves to prevent the same pulse starting and stopping the converter. If a second pulse does not arrive within the 20μs range of the converter, it will not register a 'stop', but following the delay this same pulse will cause a new 'start'.

To prevent pulse pile-up distorting the time distribution, the probability of the occurrence of a second 'stop' pulse (i.e. of two pulses separated by <20μs) must be small. This is usually taken as meaning less than ∿5×10^{-2} [127] which gives a net loss of pulse pairs of ∿0.2% due to pile up[128]. At a count rate of 1000 s^{-1}, assuming Poisson statistics, the probability of one count arriving in a 20μs interval is $P_1 = 2 \times 10^{-2}$, so the above condition is satisfied at this rate.

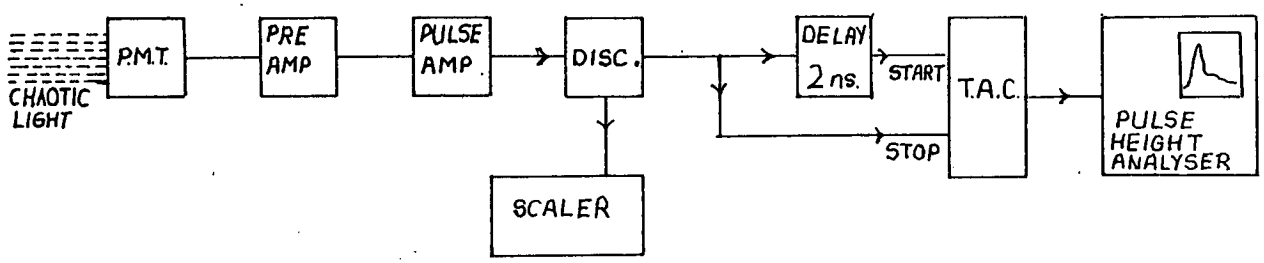

Fig. 3.10. Block diagram of system used for the determination of after-pulsing characteristics in photomultipliers.

The tubes were tested at a gain of 5×10^6, and the results are shown in Fig. 3.11(a). A rough estimate of β can be obtained by comparing the integrated area under the afterpulse peak with that under the random background level. This background represents the probability of two random pulses arriving within 20μs i.e. $P_2 = 2 \times 10^{-4}$. The ratio of the respective areas is ∿1:1, so the total afterpulse probability is 2×10^{-4}, and hence $\beta \simeq 10^{-2}$. Figure 3.11(b) shows a similar plot for a tube which was specially selected by EMI for its good afterpulse characteristics and no afterpulsing was observed. In practice it proved necessary to work at a gain of $\sim 2 \times 10^7$, which is near the limit of this tube type, and at this gain some afterpulsing was unavoidable. Typical behaviour under illumination by scattered laser light is shown in Fig. 3.12.

The time distribution of correlated noise can be used to determine best values for the delay and gatewidth. Figure 3.12 shows that although most of the afterpulsing is over ∿2μs after the laser flash, there is a tail which extends well into the region where fluorescence is expected. With a delay of 2μs and a gate of 10μs, the residual afterpulsing had an intensity of 0.2 - 0.5 s^{-1} or 0.4 - 1×10^{-2} per laser pulse. This noise source was found to behave approximately in a random manner with a standard deviation of approximately $\sqrt{N}$, where N is the rate per unit time.

D: Other sources of noise

With care all other sources of noise could be reduced effectively to zero. There was no evidence of any stray light from external sources. Stray light from the discharge could be reduced to <0.1 s^{-1}

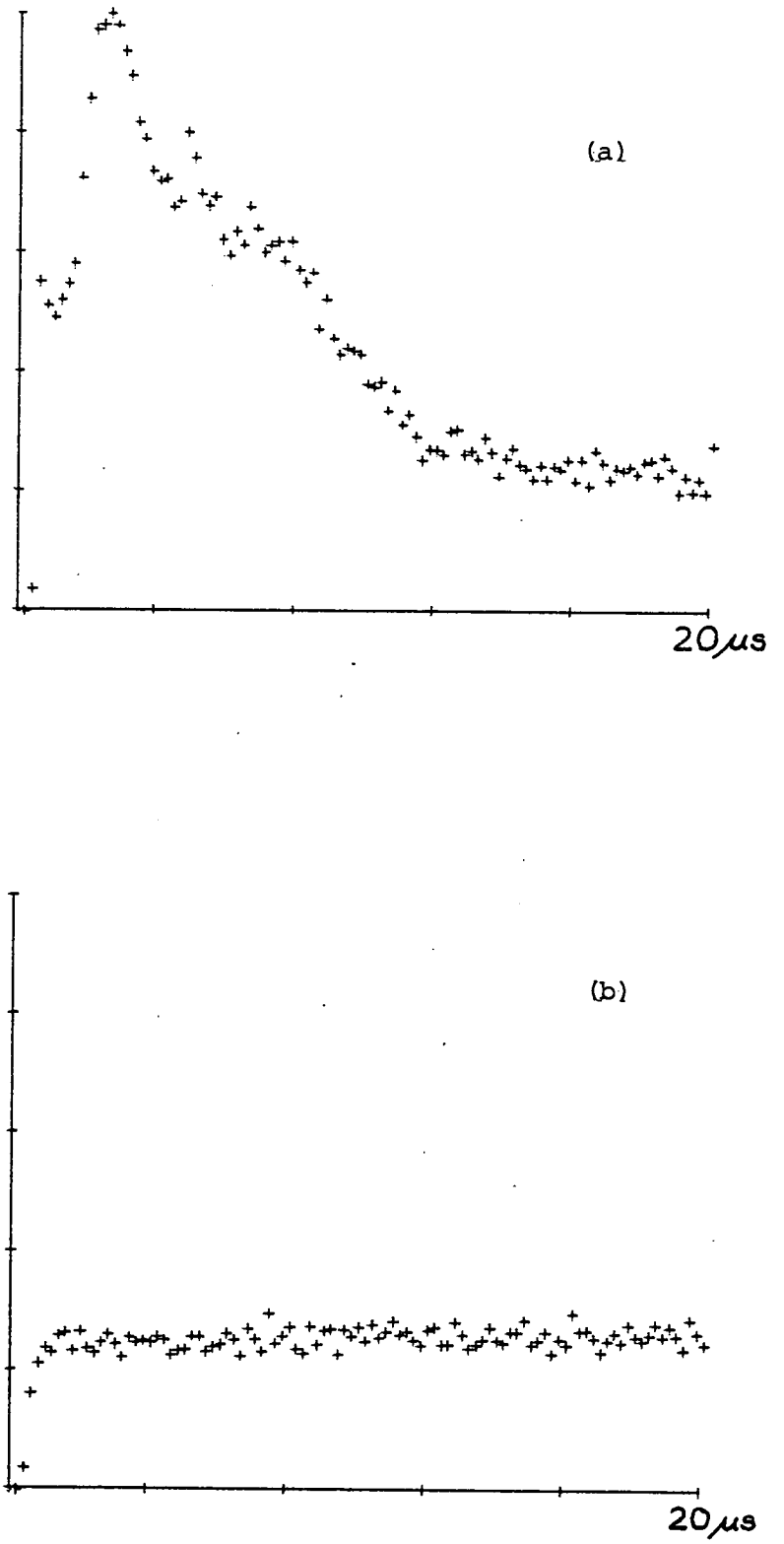

Fig. 3.11. Afterpulse distributions for two photomultipliers

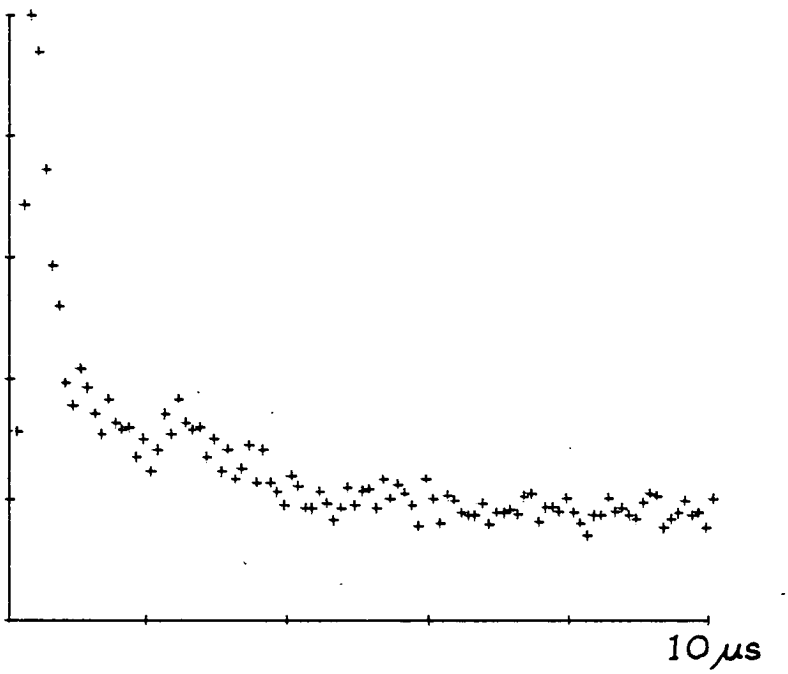

Fig. 3.12. Afterpulse distribution under illumination by laser pulses at high gain. (Note different scale to Fig. 3.11).

using woods horns on the gas pipe and by black painting the external surface with 'Nextel' (3M Corp.).

3.2 On-line Control System

3.2.1 Requirements

In experiments where long running times and the handling of large amounts of data are involved the use of on-line computer control is highly advantageous. In the experiment raw data is collected as pairs of pulse counts taken with the discharge alternately on and off over 1, 10 or 100 s. These pairs are collected in sets, each set corresponding to a given wavelength. In addition it is necessary to measure and store laser intensities and variations during collection, for normalisation purposes. This must be manipulated to yield preliminary values of true fluorescence signals and their errors as a function of wavelength so that the progress of the experiment can be monitored.

It is helpful also if the computer can perform simple routine control tasks, such as activating switches, monitoring pressures and giving warnings. This frees the experimenter from routine tasks and allows him to attend to more 'complex' checks such as laser wavelength, and gives him more time to make experimental decisions, and attend to 'emergencies'.

These considerations mean that software must satisfy certain requirements. It must be reliable (computer control is only worthwhile if it reduces problems), and allow for all possible assignments and combinations of conditions. It must not lead to any undefined states; all possible arithmetic errors must be rigorously trapped in any data analysis, and the results of hardware failure must be considered and

trapped. In all these situations the program must fail safe, so that the supervising subsystem cannot terminate execution and lead firstly to loss of data which may be core resident and secondly to the requirements of restarting the software with loss of time. In this connection it must be ensured that collected data is made permanent on disc space so that it will be preserved in the event of a subsystem crash. The frequency with which this is done must be decided in the context of how long a transfer takes and how often it is desirable to interrupt data collection.

It must also be flexible; data collection must not be interrupted for trivial reasons. This means that hardware faults which can be diagnosed by the software should have checking procedures and remedial action incorporated into the code if possible. Conversely care must be taken that such processes can terminate if more time is being spent attending to hardware faults than collecting data, so that the experimenter can intervene. None of the fault-attending code must interfere with the state of the collection code so that the same procedure can be resumed once the fault is fixed.

Software should be efficient. Since the main purpose is the accumulation of data, as little time as possible should be devoted to other tasks when this is not occurring. In practice the size of these intervals was determined by how long the experimenter took to decide on what to do next, based on feedback from the computer. The time during the collection periods can be used to monitor beam intensities, pressures etc., while the software would otherwise be idle. Other tasks like writing to the disc and moving wavelength were found to take negligible times in comparison, and so could be inserted where

convenient.

Finally it should be simple to operate, which means that operator input should be minimal. A series of one letter instructions from the teletype suffices. An interrupt facility, either through the hardware or from the terminal is also useful to abort the current operations and return to command level.

3.2.2 Structure and operation*

The data collection is organised round counting intervals of 1, 10 or 100 s during which the scaler accepts gated pulses from the detector electronics. The scaler is started by a signal from the computer after which control of the timing passes entirely to the interface hardware. The software must then wait until the timer clocks out. During this time the laser monitor signal is read a pre-set number of times and the mean and standard deviation calculated.

The software then waits for the end of the counting period, after which it reads the data. The data code is organised by the interface into twelve "bytes" of five bits each. The bytes are gated sequentially onto five parallel lines on receiving a sync pulse from the computer. In the computer the five bit code is read as an integer number into an array element. The first byte corresponds to an unambiguous bit pattern which is hard-wired into the scaler, and the software checks that this is the first element in the array. If this is not the case, then the array is cycled until it is. The

*For the detailed design and construction of the interface hardware, I am indebted to Mr. Douglas Munroe.

second byte is used to signal an interrupt request from the local hardware if necessary. The remaining ten elements contain the signal count code (up to 10^4 counts per interval). The software then decodes these elements. If they cannot be decoded due to a fault in the readout or encoding operations, an error message together with appropriate diagnostics is printed on the terminal. The software will then attempt to read the data a further ten times. If it is still unsuccessful, the counting and readout operation is repeated. Successive failures which result in repeated collections outnumbering successful collection within one wavelength set are deemed to warrant operator intervention and data collection is temporarily halted.

Every second counting period the microwave discharge is switched on by a relay in the interface and 5s allowed for it to stabilise before collection begins. One complete "round" of data thus consists of counts, mean monitor signal and deviation, for the discharge off and on. This process is repeated a number of times which the experimenter can set at will. At the end of a maximum of sixteen rounds all this data, together with variables describing the experimental details, time and wavelength, are organised into a binary block and written to the disc.

Occasionally it is necessary to collect a block of background data; that is with the laser blocked off, but otherwise identical to that above. In this mode true dark noise plus photon background is collected with the discharge off and stray light from the discharge with it on. Any offset due to ambient lighting is measured by the monitor. This data can then be used to correct the observed signal and

laser intensity. At the end of each block, the mean and error of the corrected, normalised signal, and noise are printed. Cumulative values of the signal and error are stored as a function of wavelength in arrays and the relevant entries are updated at the end of each block. In this way a preliminary profile of the spectrum is built up which the experimenter can interrogate between data collection sessions.

Another facility at this level is wavelength selection. The experimenter inputs the necessary increment in "stepper units" ($\sim$1Å). The software then corrects for sticking or backlash, drives the motor, and updates the wavelength code. Variables are provided for records of experimental conditions such as beam pressures, oven temperatures etc., which are not under computer control, and these may be explicitly updated by the experimenter. The commands also include a copying or clearing of the accumulated spectrum, and suspending or halting data collection. A block diagram for the global structure is given in Fig. 3.13. A listing of the program appears in appendix 4.

The structure of this program was built up over the period in which the experiment developed. In this way each stage could be tested and debugged at the correct level of experimental complexity. In addition many smaller programs were written to test individual routines, so that the limitations of the hardware could be assessed. Experience has shown that the final system has lived up to the requirements set out earlier. No data has ever been lost by software failure. Occasional individual data units have been lost through hardware failures over which the computer has no control, such as

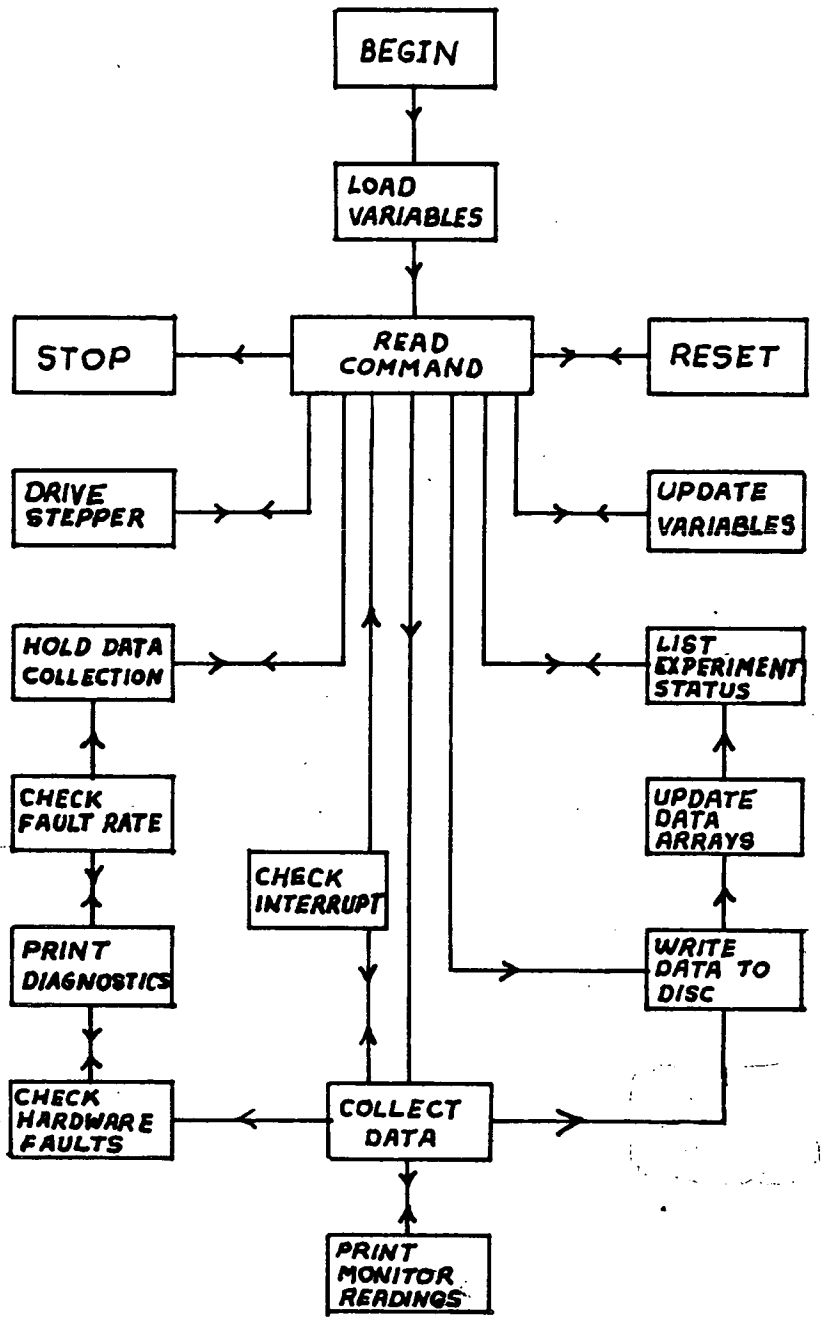

Fig. 3.13. Flow diagram for data collection program.

failure of the discharge to ignite. Monitoring of microwave power levels and pressures are areas where farther work will be necessary to ensure totally failsafe operation.

3.3 Feasibility Calculation

A detailed calculation to illustrate the feasibility of the proposed experiment will now be given. The calculation was made taking the experimental set-up described earlier as given, and numerical values are taken directly from the work described in the previous sections. In cases where values are not known a 'most pessimistic' choice was made. This ensures that the final estimate of the signal is a lower bound.

3.3.1 Molecular Iodine beam

This is formed from a microcapillary array. The flow rate $\dot{N}$ (in molecules s^{-1}) through a single tube of radius a and length L has been predicted by Giordmaine and Wang[129]. The large gas kinetic cross section of I_2 as derived from viscosity measurements[130], means that true Knudsen flow, where $\lambda >> a$ (λ is the mean free path) will occur along the entire length of the tube only at the pressures below 1 torr given typical values of a ($\sim$5μm). This would result in low flow rates. Useful collimation can still be achieved when the Knudsen flow condition holds only over a certain length, L_o, from the low pressure end of the tube, as long as $L_o >> a$. $\dot{N}$ and I(O), the differential angular intensity along the beam axis, cease to be proportional to source pressure ρ_o, according to the strict theory, however. In practice[131] it has been shown that with beams of He a linear variation of $\dot{N}$ with p_o still obtains in the regime where $a < \lambda_o$, where λ_o is the mean free path in the source.

The flow rate is then given by

$$\dot{N} = \frac{2\pi}{3} \frac{a^3 \bar{v} n_o}{L} \qquad 3.5$$

where $\bar{v}$ is the mean molecular velocity, and n_o the source density. Experimentally flow rates are found to be less than this by a factor of $\sim 2/3$.

The forward intensity and angular half width at half maximum are then found respectively from[129]

$$I(O) = \frac{1}{8} \left(\frac{3}{\sqrt{2\pi}} \right)^{\frac{1}{2}} \frac{\bar{v}^{\frac{1}{2}}}{\sigma} (\dot{N}a)^{\frac{1}{2}} , \qquad 3.6$$

and

$$\Delta\theta_{\frac{1}{2}} = \frac{2^{\frac{3}{4}} 3^{\frac{1}{2}}}{1.78} \frac{\sigma}{\bar{v}^{\frac{1}{2}}} \left(\frac{\dot{N}}{a} \right)^{\frac{1}{2}} \qquad 3.7$$

provided $\cos \Delta\theta_{\frac{1}{2}} \simeq 1$. σ is the collision diameter.

The measured values of $\Delta\theta_{\frac{1}{2}}$ are found to be a factor of ~ 2 greater. This has been interpreted as an end correction, but may include a contribution from scattering between molecules from different tubes, when an array is considered[131].

The highest efficiency of collimation is obtained by minimising $\Delta\theta_{\frac{1}{2}}$, but higher intensities at lower efficiency are obtainable by increasing n_o and/or a, subject to constraints on the pumping capacity.

Taking a driving pressure p_o of ~ 5 torr and a = 5μm, from equs. 3.1 - 3.3 it is found after applying the empirical corrections that

$$I(O) \simeq 1.2 \times 10^{13} \text{ sr}^{-1}\text{s}^{-1}$$

$$\Delta\theta_{\frac{1}{2}} \simeq 16^{\circ} \text{ FWHM}$$

a collision diameter of 6.5Å was assumed. The total forward intensity

is found by multiplying I(0) by the number of tubes M, contained in the orifice area, A, which is given by

$$M = \frac{A\varepsilon}{\pi a^2}$$

where ε is the transparency of the array, ($\sim$75%). For an orifice of 1 mm diameter $M \sim 7.5 \times 10^3$ so

$$I(0) \simeq 9 \times 10^{16} \text{ sr}^{-1}\text{s}^{-1}$$

The total flow rate is $\dot{MN}$ and is $\sim 3.4 \times 10^{16} \text{s}^{-1}$. This is well within the pumping capacity of the chamber, given the increased capacity due to cryotrapping, and allows some margin for increasing p_o if necessary.

At the reaction zone, which is $\sim$20 mm from the orifice, the density of reagent is

$$n_{I_2} = \frac{I(0)}{\bar{v}L^2}$$

$$\simeq 1.3 \times 10^{12} \text{ cm}^{-3}$$

3.3.2 Fluorine atom beam

Given the high reactivity of F atoms on glass a capillary array is not suitable as a source so a nozzle beam was chosen. Design criteria for nozzle sources have been discussed extensively[132,133], but the predictive capability of the theory is still limited. Accordingly, in discussing the operating conditions of this source, extensive approximations will be necessary.

The choice of operating conditions is determined initially by the amount of differential pumping available. The arrangement

described earlier has a maximum capacity of 6×10^{19} molecules s^{-1} at a load pressure of $5 \times 10^{-3} - 10^{-2}$ torr. This determines the upper limit of the total flow rate through the nozzle, $\dot{N}$. If $\dot{N}$ exceeds this value the pumping capacity begins to drop and the DPC pressure rises. Operating source density n_o and nozzle diameter D_o are then determined from

$$\dot{N} \simeq \tfrac{1}{4} n_o D_o^2 \bar{v}_o \qquad 3.9$$

where $\bar{v}_o$ is the mean molecular velocity in the source. Normal practice then dictates that the largest Mach numbers are obtained with the highest pressures across the nozzle, and thus with the smallest nozzle diameters compatible with equ. 3.9. A lower bound for D_o is however fixed by the mechanical construction of the nozzle. It was decided that the nozzle should be made of PTFE, due to its chemical inertness, and by trial and error the smallest diameter attainable was $\sim$0.02 cm. From equ. 3.9, the maximum source pressure is thus $\sim$200 torr.

As will be shown later, there are other requirements to do with the attenuation of F-atom concentration between discharge and nozzle, which favour a larger D_o. At this stage it is sufficient to say that a suitable compromise is a diameter of $\sim$0.1 cm, and pressure of 8 - 10 torr. A velocity of 10^5 cms^{-1}, which is appropriate for a beam seeded in He at room temperature, has been assumed. For an unseeded beam increased source pressures are possible.

Although stagnation pressures of $\sim$10 torr are low in comparison to those used in typical supersonic nozzle sources, it has been shown

that the resulting beam can still be well characterised in terms of a Mach number which gives a good description of its properties.[134]

The final state of the beam far from its source and skimmer is characterised by a terminal mach number M_T, which is given by

$$M_T \simeq 2\left(\frac{\varepsilon}{K_o}\right)^{0.4} \qquad 3.10$$

where K_o is the Knudsen number of the source ($= \lambda_o/D_o$) and ε is a collisional efficiency which describes the rate of decrease of thermal translational energy per molecule ($0 \leq \varepsilon \leq 1$), and which must generally be determined experimentally. Putting $\varepsilon = 1$, gives an upper limit to M_T which for $p_o \simeq 10$ torr and $D_o \simeq 0.1$ cm is $\sim$12.6. A mean free path of 10^{-3} cm in the source has been assumed. This is based on that of He, but rounded down by $\sim$20% to allow for a 10% concentration of other species, for which gas kinetic data are unavailable.

At some point downstream of the nozzle a transition from continuum to free molecular flow occurs. This distance L^* is given by[134]

$$\frac{L^*}{D_o} \simeq 0.24\left(\frac{\varepsilon}{K_n}\right)^{0.6} \qquad 3.11$$

Beyond this point flow continues with the density for a monatomic gas, at distance L given by

$$n \simeq 0.16\, n_o \left(\frac{L}{D_o}\right)^{2} \qquad L/D_o > 4 \qquad 3.12$$

Equation 3.11 predicts $L^* \simeq 2.2\, D_o$. Equation 3.12 will be used for the determination of n beyond L^*, even though the condition for its validity does not hold until some distance farther. The justification

for this is that a more sophisticated estimate of n beyond L^* is unwarranted here, and that L^*/D is not very much less than that required for Equ. 3.12 to hold, so n is not expected to be too inaccurate. In addition, Anderson and Fenn[134] have found that this procedure leads to good agreement with measured terminal Mach numbers, even for low density sources. (p_o = 5 torr, D_o = 0.8 mm).

It is clear then, that the source should function as a true nozzle, and that the surface of transition lies at 1-3 nozzle diameters from the source. Typically the skimmer is located at $\sim 5D_o$ from the source, and hence at the reaction zone, the source appears to be a distributed effusive source, whose molecules have a stream velocity determined by M_T superimposed on which is a thermal distribution. As has been indicated[133,134] provided skimmer interaction is negligible the intensity at a given point downstream of the skimmer becomes independent of nozzle-skimmer distance. Such interactions, which serve to reduce the observed intensity from that predicted theoretically have been attributed, in this low pressure regime, to a scattering of molecules from the walls of the skimmer. It has been shown that a good predictive parameter for the ratio of observed to predicted intensity is K_s/M_s, the ratio of Knudsen number to Mach number at the skimmer entrance. This has been verified over a wide range of p_o and D_s, for values of $K_s/M_s < 2$, although the exact range for the latter varies weakly with p_o and D_s, being greater for lower p_o and D_s. This breakdown has been attributed to scattering of beam reagent by background in the first differentially pumped chamber.

The effect of skimmer disturbance can be estimated as follows.

From equ. 3.12, the free stream density at the skimmer entrance is $\sim 2 \times 10^{15}$ cm^{-3}, and the mean free path there is thus ~ 0.2 cm. Assuming $D_s = 0.1$ cm, then $K_s \simeq 2$. M_s is more difficult to estimate, but given the maximum value of M_T is ~ 12, and assuming $\varepsilon \simeq 0.25$, gives the predicted attenuation, $K_s/M_s \simeq 0.5$. Reference to accumulated data[136] shows that this prediction is expected to be valid for this p_o and D_s. Skimmer interference is the major loss for the source. The density at the scattering zone is then calculated from equ. 3.12, and corrected by K_s/M_s. At 2.5 cm from the nozzle this is $\sim 3.7 \times 10^{13}$ cm^{-3}.

The angular FWHM of the intensity distribution is also rather difficult to estimate. Measurements of the radial distribution at various pressures have yielded Mach numbers in violent disagreement with those obtained from velocity measurements[134]. Other work[135,136] suggests that

$$\Delta\theta_{\frac{1}{2}} \simeq \frac{1}{2M_s} \qquad 3.13$$

is a good "rule of thumb". Using this estimate an angular half width of $\sim 12^{o}$ is obtained.

3.3.3 F-atom yield

The density of F-atoms in the beam is obtained by multiplying the beam density by the mole fraction of atomic fluorine, f_F. Initially, the decay of f_F between discharge and nozzle, due to reactions of F with the walls and other species will be ignored. This is an unlikely condition and its effects will be considered later. In the beam, selective concentration of heavier species along the axis[137] is also neglected.

In a discharge of pure CF_4 at 0.2 - 0.6 torr densities of F-atoms of 2.4 - 6 x 10^{14} cm^{-3} were observed 30 cm downstream by Kolbe and Kaufman[125]. The reagent was discharged in a cast alumina tube and flowed in a PTFE tube. It will be shown later that this corresponds to a dissociation of ∿10% in the discharge. This is assumed to be an attainable rate. No CF_3 was detected although F_2, CF_2, and C_2F_6 were present, in varying quantities. This is because the reaction rate of

$$2CF_3 \rightarrow C_2F_6$$

is fast[138,139] (k = 3 - 5.3 x 10^{12} cm^3 $mole^{-1}$ s^{-1}), and presumably faster than either

$$2F \rightarrow F_2$$

$$F + CF_3 \rightarrow CF_4$$

at these pressures. The concentration of F_2 was 3-10 times less than that of F.

The dominant mechanism for removal of F-atoms at these pressures is reaction at the walls of the tube[140], which results in its gradual errosion. This can be characterised by a first-order rate constant k_w given by[141]

$$k_w = \gamma \frac{\bar{v}}{2R} \qquad 3.14$$

where R is the tube radius, $\bar{v}$ the mean molecular velocity and γ the "sticking co-efficient". This results in an axial concentration gradient given by

$$n(x) = n(0)e^{-\xi x} \qquad 3.15$$

where n(0) is the concentration of active species just outside the discharge, and x, the displacement along the tube axis. ξ is an attenuation constant given by

$$\xi = \frac{k_w}{\bar{v}} \left(1 - \frac{\lambda k_w \bar{v}}{2\bar{v}_B^2}\right) \qquad 3.16$$

where $\bar{v}_B$ is the bulk flow velocity and λ the mean free path in the tube. If $k_w < 30$, at pressures of $\sim$1 torr or more then

$$\xi \rightarrow \frac{k_w}{\bar{v}_B} \qquad 3.17$$

Values of γ for F-atoms on a variety of surfaces have been determined[140]. Using the value of $\gamma = 2.5$ for PTFE it is possible to use equs. 3.14 - 17 to determine that 10% dissociation of CF_4 was obtained by Kolbe and Kaufman as stated earlier.

The effect of dilution of CF_4 in He is difficult to assess. The fractional dissociation will be assumed unchanged, so that for 10% CF_4 in He, a mole fraction of 1% of F-atoms is present in the discharge. The presence of He is not expected to affect the attenuation of reagent, since the third order homogeneous recombination of F-atoms in He is slow[140] ($k = 8 \pm 5 \times 10^{14}$ cm^6 mole^{-2} s^{-1}). Neglecting attenuation, the density of F-atoms in the beam is thus $\sim 3.7 \times 10^{11}$ cm^{-3}.

A <u>The effect of in-transit loss of F-atoms</u>

Some typical values of γ, ξ and the resulting attenuation over the 70 cm path from discharge to nozzle are given in Table 3.1. Reports of surface properties have often been contradictory however. Ogryzlo[142] reported good resistance for oxyacids baked at 250°C, but

Material	γ	ξ/cm^{-1}	Fractional Transmission
Pyrex	7×10^{-4}	7×10^{-2}	7×10^{-3}
Quartz	1.2×10^{-4}	1.2×10^{-2}	0.43
P.T.F.E. on quartz	7×10^{-5}	3.5×10^{-2}	1

Table 3.1. Variation of in-transit attenuation of F-atoms along a ~70 cm path on various surfaces. $\bar{v}_B$ from equ. 3.18 with d_o = 1 mm, D = 10 mm.

poor resistance for PTFE. Polanyi and Woodall[53] have successfully used "syrupy". H_3PO_4 provided several hours were allowed for fluorination. Several treatments of the pyrex gas pipe were used, and these will be discussed in sec. 3.4. This data qualitatively support PTFE as the most inert surface. It was not possible to estimate the absolute value of the attenuation, but its effect must be borne in mind when interpreting this calculation.

At this point it is worth noting that the attenuation is not entirely independent of the choice of nozzle parameters, as stated in sec. 3.3.2. By conservation of flux through any cross-section of the pipe-nozzle system, the linear flow velocity $\bar{v}_B$ is given by

$$D^2\bar{v}_B = d_o^2\bar{v} \qquad 3.18$$

where $D = 2R$ is the tube diameter. The choice of d_o as 1 mm rather than 0.2 mm increases $\bar{v}_B$ by a factor of 25 and thus decreases ξ by a similar factor. Since the attenuation depends exponentially on ξ through equ. 3.15, the increase in density of F-atoms in the reaction zone due to this factor, easily outweighs the loss due to the necessary decrease in stagnation pressure required by the pumping capacity.

3.3.4 Rate of product formation

In simple gas kinetic terms the rate of product formation is given by

$$Z = n_{I_2} n_F \sigma_R \bar{v}_{rel} \qquad 3.19$$

where n_{I_2} and n_F are the densities of the reagents in the intersection region, σ_R is the total cross-section for reaction into all product

states and $\bar{v}_{rel}$, the relative velocity.

The approximate geometry of the beam axes is shown in Fig. 3.14. O is the centre of the reaction and detection zone. S_1 is the atom nozzle and S_2 the I_2 effusive source. The distances S_1O and S_2O are 25 - 30 mm and 20 mm respectively. The detector is located along the y-axis. The axis of the I_2 beam is oriented at $\sim 60^{\circ}$ to the detector axis.

The beam densities at the reaction zone were determined in the previous sections to be;

$$n_{I_2} = 1.3 \times 10^{12} \text{ cm}^{-3}$$

$$n_F = 3.7 \times 10^{11} \text{ cm}^{-3}$$

Due to the higher velocity of the F-atoms, (10^5 cms^{-1} vs 2×10^4 cms^{-1}) the mean relative velocity is $\sim 10^5$ cms^{-1}. The total reaction cross-section is taken as 0.05 nm^2. This is based on evidence that the reactions Cl + I_2 and Cl + Br_2 proceed with $\sigma_R \sim 0.05 - 0.2$ nm^2 (143), and involves some degree of long range attraction*. Using these values in equ. 3.19 yields $Z = 2.4 \times 10^{13}$ cm^{-3} s^{-1}.

The shape of the detection zone is approximately cylindrical, with a diameter determined by the laser beam diameter and a length determined by the molecular beam half widths. Since the divergences

*The velocity averaged cross-section obtained from $\bar{\sigma}_R = k/\bar{v}_{rel}$ where k is the rate constant is 0.43 nm^2, but the low estimate has been chosen, so that the final result is a most pessimistic one.

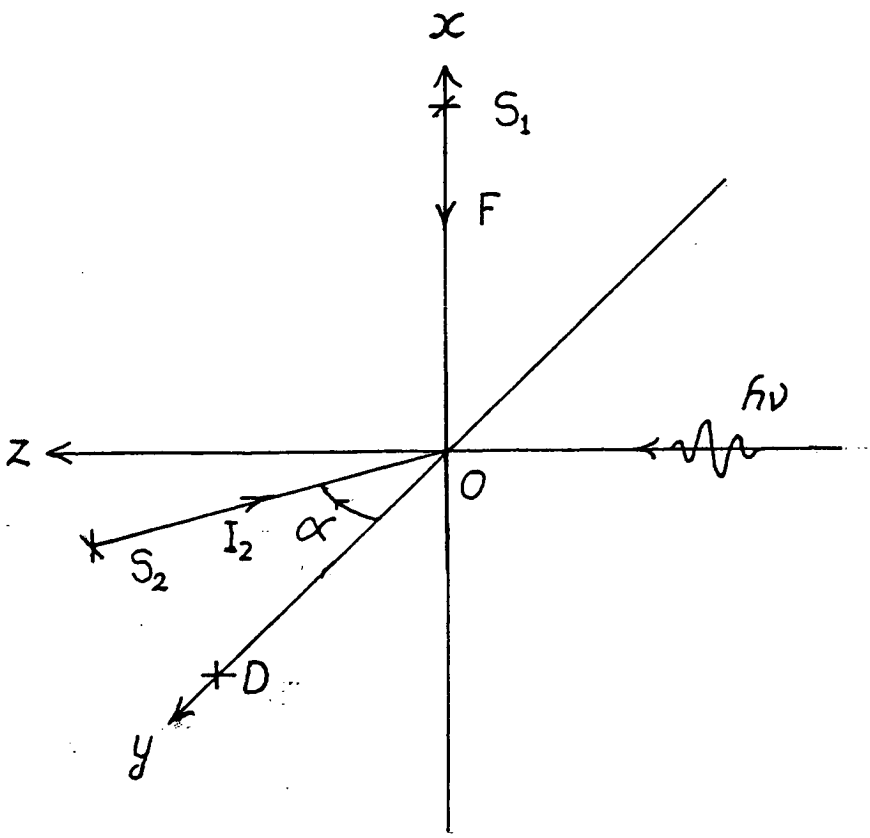

Fig. 3.14. Approximate geometry of beam axes

S_1 = F-atom source

S_2 = I_2 source

D = detector

O = Reaction zone

Scale : approx twice full size

of both beams are approximately equal ($\sim 15^{o}$) as are the distances S_1O and S_2O ($\sim$2.0 cm), the length of the detection zone is $\sim$0.5 cm. The cross-sectional area is $\sim 3 \times 10^{-2}$ cm^2, so its volume is $\sim 1.5 \times 10^{-2}$ cm^3.

The reaction zone on the other hand extends much further in the x and y directions. It must be considered as approximately a sphere of diameter 0.5 cm. Within this volume steady state conditions are assumed to hold. The mean free path of reactively produced species is sufficiently large to allow an uninterrupted trajectory out of this volume, and the flux of product through its surface, S, is assumed to be balanced by creation within the volume, V, i.e.

$$ZV = Sn_p\bar{v}' \qquad 3.20$$

where n_p is the product density and $\bar{v}'$ its mean velocity. From 3.20

$$n_p = \frac{1}{3} r \frac{Z}{\bar{v}'} \qquad 3.21$$

where r is the sphere radius. Substituting values for r,Z and $\bar{v}'$ = 0.9×10^5 cms^{-1} * yields. $n_p = 2.2 \times 10^7$ cm^{-3}.

3.3.5 Fluorescence yield

Given the product density n_p and a trial intensity distribution p(v",J"), the intensity of fluorecence can in principle be predicted using Equ. 2.5. A more tractable calculation results if

*This is essentially the relative velocity of the IF product after the collision (taken for the v = 0 state). Since the centroid velocity is small in comparison, the difference between the LAB and CM frame velocities is negligible (See Sec. 4.2.3).

the rate of excitation under the influence of a short pulse is considered first, followed by fluorescence with a quantum yield of unity.

The rate of absorption is given by

$$\dot{n} = \rho \, n \, B \qquad 3.22$$

where n is the density of the lower level and B and ρ have their usual meanings. A Boltzmann distribution of rotational states is assumed;

$$n = n_p p(v'') \frac{1}{Q_{v''}} e^{-J''(J''+1)B_{v''}/kT_r} \qquad 3.23$$

where $Q_{v''} = \frac{B_{v''}}{kT_r}$

is the rotational partition function. It is assumed that J''_{max} is sufficiently high not to affect the value of $Q_{v''}$. Using the separation of electronic, vibrational and rotational intensity factors yields

$$\dot{n}(\nu(v'J';v''J'')) = n_p p(v'') . K_{v''} \rho(\nu) \left| R_e(\bar{r}_{v'v''}) \right|^2 q_{v'v''} \times S_{J'J''} e^{-J''(J''+1)B_{v''}/kT_r} \qquad 3.25$$

where

$$K_{v''} = \frac{2\pi^2}{3\varepsilon_o h^2} \cdot \frac{B_{v''}}{kT_r} \qquad 3.26$$

is a constant whose value is $\sim 2.5 \times 10^{75}$ in SI units.

The laser bandwidth is large enough to cover several transitions. It is approximated by a square function of width $\delta\nu_L$ and intensity equal to the peak intensity, p_o. This gives

$$\dot{n}(\nu_L) = n_p p(v'') K_{v''} \rho_o q_{v'v''} \left| R_e(\bar{r}_{v'v''}) \right|^2 H_{J''} \qquad 3.27$$

$$\text{where} \quad H_{J"} = \sum_{\Delta J"} S_{J'J"} e^{-J"(J"+1)B_{v"}/kT_r} \qquad 3.28$$

Considering transitions in the bandhead allows the exponential factor to be put equal to unity, and summing line strengths over both branches gives

$$H_{J"} = \sum_{J"=0}^{J"_L} (2J" + 1) = J"_L{}^2 \qquad 3.29$$

where $J_L"$ is the highest transition covered by the laser line. For a not too densely packed bandhead $J_L" \simeq 15$, hence $H_{J"} \simeq 225$.

The factor ρ_o in Equ. 3.27 represents the energy density, and this can be estimated from measurements made on the laser beam, which are summarised in Table 3.2. The time profile is approximated to a square function of width Δt_L. The energy density is then given by

$$\rho_o = \frac{\bar{P}}{cf\Delta t_L \sigma_L \Delta\nu_L} \qquad 3.30$$

with c the velocity of light. From this equation it is found that $\rho_o = 4.6 \times 10^{-3}$ Jcm^{-3} MHz^{-1}.

Values of $R_e{}^2$ and $q_{v'v"}$ have been calculated for IF[77,83]. $R_e{}^2$ is constant to within 10% at 0.1 D^2 ($\simeq 10^{-60}$ C^2m^2). Substituting for $K_{v"}$, $H_{J"}$, $|Re|^2$, ρ_o and n_p into 3.27 yields. $\dot{n}(\nu_L) = 5.5 \times 10^{12}$ $\rho(v")q_{v'v"}$ cm^{-3}s^{-1}.

The observed rate of fluorescence assuming a long detector gatewidth is given by

$$S(\nu_L) = \dot{n}(\nu_L)\Delta t_L V' f\varepsilon \qquad 3.31$$

where V' is the volume of the detection zone and ε is the efficiency

of the fluorescence collection system.

From the geometry of the collection optics a solid angle of $\sim\pi/4$ sr is subtended by the detector. The mean quantum efficiency averaged over wavelengths of the fluorescence is $\sim$10%, so the observed rate is given by

$$S(\nu_L) \simeq 300 p(v'') q_{v'v''} \ s^{-1}$$

A Saturation of transitions

It is important that the intensity of the beam is not so high that the transitions become saturated, resulting in a loss of the linear dependence of fluorescence intensity on laser intensity and product density. While techniques exist to compensate for this[66], it is fairly simple to show that this does not apply here.

The condition for the sample to be unsaturated is that the peak rate of stimulated emission must be negligible in comparison to the spontaneous emission i.e.

$$B\rho << A \sim \tau_{rad}^{-1}$$

For the values of the intensity factors given for one (v,J) transition, $B\rho$ is $\sim 5 \times 10^3 \ s^{-1}$, whereas $A \geq 10^5 \ s^{-1}$. No correction for saturation is therefore required.

3.3.6 Signal to noise ratio

Here it is necessary to draw on observations made with the apparatus to determine typical noise count rates. If the only source of noise is dark noise, plus photon (background) noise, then an ungated rate of 50 s^{-1} is observed. This is fairly typical of this

type of experiment[67]. With a gated detector this noise rate is reduced by the duty cycle of the system (= fx gatewidth), which is 5×10^{-4}, so that a rate of a few counts in 100s is observed. (See Sec. 3.1.4). In this regime attainable S/√N ratios of 20 or more can be achieved for realistic combinations of p(v") and $q_{v',v"}$, as shown in table 3.3.

In practice the observed noise rate is much greater due to the presence of the time correlated afterpulsing. This is observed to give rise to a gated noise rate of up to 40 counts in 100s depending on the alignment of the laser beam, and its mean power. This has the effect of reducing the S/√N ratio attained over an equivalent count time, by a factor of ∿4. As is shown in table 3.3, now all but the lowest combinations of p(v") and $q_{v',v"}$ are seen to be attainable with reasonable S/√N ratios within 1000s count time.

3.4 Experimental Method

3.4.1 Optimisation of conditions

As far as was practicable operating conditions were optimised by observing the variation of fluorescence intensity of a strong bandhead e.g. (6,0), with a few easily adjustable parameters. The following observations were made;

i) Iodine oven temperature. The signal increased with increasing oven temperature over the range 30° - 70°C. Increasing beam divergence is also expected to occur, and this causes a significant rise in the background pressure beyond ∿80°C, at which point it reached $>10^{-4}$ torr. This was accompanied by a disappearance of the fluorescence signal, which was attributed to attenuation of the reagent beams by the ambient gas pressure.

Repetition rate	f	50 s^{-1}
Typical wavelength	λ	480 nm
Mean power	$\bar{P}$	100 μW
Pulse duration (FWHM)	Δt_L	12 ns
Bandwidth (FWHM)	$\Delta \nu_L$	0.3 nm = 0.4 THz
Beam cross-section	σ_L	3 x 10^{-2} cm^2

Table 3.2. Summary of laser parameters as used in the feasibility calculation.

	p	S/s^{-1}	Achievable S/ N ratios			
			Low noise: 2/100s		High noise: 40/100s	
			over 100s	over 1000s	over 100s	over 1000s
Strong Band	0.1	3	200	650	50	150
q ≃ 0.1	0.01	0.3	20	65	5	15
Weak Band	0.1	1	50	200	16	50
q ≃ 0.03	0.01	0.1	5	20	1.6	5

Table 3.3. Expected $S/N^{\frac{1}{2}}$ values for various regimes of $p_{v''}$, $q_{v'v''}$, and noise rate.

ii) Discharge power. The signal appeared to depend fairly critically on net discharge power, being maximised at ∿60W.

iii) Gas tube coating. It was not possible to give more than a general assessment on this. The following coatings were tried:

(a) Conc. HCl: Cleaning the tube with HCl was used in the early stages, and was found to give satisfactory, but rather weak (as compared with (c) below) signals.

(b) Conc. H_3PO_4: Coating the pipe with glacial H_3PO_4 resulted in a similar intensity, provided a 'burn-in' time of two to three hours was allowed. It was usually necessary to repeat this if the discharge was switched off for more than about ten minutes. As this was wasteful of time and discharge reagent it was not a very practicable coating. Also results tended to be erratic due to the difficulty of obtaining a uniform coating.

(c) PTFE film: 'Teflon' dispersion (Dupont FEP 856-200) was diluted to 50% in a 2% solution of wetting agent (Dupont VM-5336). The tube was cleaned in conc. KOH at 80°C for half an hour, rinsed out, neutralised with HCl and rinsed again with the wetting agent. A thin coating of dispersion was formed by slowly draining the tube of solution, and then sintered at 375°C for 45 minutes. This process should produce a layer of finish of ∿15μm thickness. Its performance with the 'water drop test'[144] was found to be very satisfactory. This process resulted in an increase of 3-4 in the resulting intensity, but the

quality of the coatings degraded between runs presumably because it possessed no mechanical strength.

As with all beam experiments alignment of the various beam axes was critical. The arrangement of oven and nozzle assembly ensures these two directions are automatically aligned. The alignment of laser axis with respect to the atom beam was made by arranging for a pin to be mounted at the location of the scattering zone. The laser was then adjusted until the pinhead was central in the beam. The position of the oven/nozzle assembly could then be adjusted sufficiently to ensure light scattered from the pin was visible centrally through the nozzle. The photomultiplier arm was then adjusted in a similar fashion. When this condition was achieved all four axes (atom, iodine, laser and detector) intersected at the detection zone.

The alignment of the laser beam proved to be particularly critical, as not only does deviation from optimum reduce the spatial overlap between beam and reaction zone, but also increases the laser-induced noise due to misalignment of the baffles. Occasionally, the laser axis was found to have wandered from its original alignment, and when this occurred it was necessary to relocate it, to ensure a clean passage through the reaction zone.

3.4.2 Experimental procedure

Experiments typically ran continuously for two to four days. Termination was caused either by exhaustion of iodine reagent in the oven or some catastrophic failure such as collapse of the dye cell or breakdown of the nitrogen laser dielectric.

Under normal operating conditions the laser was roughly tuned to the wavelength of a strong bandhead using the spectrometer, and a

cadmium emission lamp for calibration. The wavelength was then scanned to look for a signal. Once this was detected the wavelength was driven beyond the high frequency limit of the band and stepped towards lower frequency. Data was collected at a given wavelength until an acceptable signal to noise ratio appeared to have been developed, or until a given number of data pairs had been collected.

Once collection from one band appeared reasonably complete, the wavelength would be driven to another (normally weaker) band and the process repeated. Occasionally during searches for, and collections of weaker bands it was necessary to drive back to the stronger band and check the fluorescence intensity. This provides an internal check against long term drifts in beam intensity. External checks are provided by readings of beam pressure, tank pressure, discharge power, oven temperature, etc., made by the experimenter. While not uniquely definitive these are strongly suggestive of the internal behaviour of the apparatus. Normally these parameters could be held steady once established, for the entire duration of an experiment, and consistent values of each were obtained from one experiment to the next. This is important as it allows the possibility of data from different experimental runs to be combined to yield meaningful results.

Due to difficulties associated with reproducing large wavelength changes accurately by the grating control, it was found that the above method of scanning was much easier to operate than any other. Better compensation for drifts would be obtained by rapidly alternating between bands.

3.4.3 Organisation and processing of data

At the end of an experiment raw data is located in direct access files on the PDP11. A program was written to decode, analyse and list this data. Lists are then concatenated and sent to the Regional Computer Centre's ICL 4-75 system for archiving.

Data blocks which are associated with spurious events are discarded. Typical causes of these are excessive changes in laser intensity, tank pressure surges and laser beam wander.

The procedure followed in processing the data can be followed with reference to table 3.4. This shows a sequence of results obtained during one of the final experiments* in the region of the (8,1) band. Each 'block' consists of ten pairs of data collection intervals of length 10s. (Counts for discharge on and off). Each block except for background measurements is characterised by a step index which measures the laser wavelength with respect to some previously established point; one step being $\simeq$1.1Å. Blocks collected under similar conditions at the same wavelength are combined, and the means and standard deviations for the 'on' and 'off' counts for each group determined. In the case of table 3.3 groups consist of one, two or three blocks.

Within these larger data groups, inconsistently large counts are occasionally observed, which, result from RF pick-up from the laser and switching transients from nearby equipment. To eliminate these a simple filtering is performed, in which any individual counts outwith 2 standard deviations from the mean are rejected, and the mean and

*This is designated experiment II in Chapter 4.

Block No.	λ / nm	Elapsed Time/mins	Un-normalised Signal	Mean Laser Intensity	Normalised Signal
2	‡	0	-	(0.005)	-
3	469.6*	6.09	8.2 ± 1.5	0.37	6.6 ± 1.2
4		11.83			
5		18.84			
6	469.8	24.59	7.0 ± 0.9	0.36	5.8 ± 0.7
7		30.34			
8	467.4	40.48	1.6 ± 1.6	0.37	1.3 ± 1.3
9		46.25			
10	467.6	52.08	0.2 ± 1.4	0.37	0.2 ± 1.1
11		58.14			
12	469.6*	65.38	10.1 ± 2.2	0.38	7.9 ± 1.7
13		71.36			
14	467.8	77.12	3.0 ± 1.0	0.39	2.3 ± 0.7
15		82.89			
16	468.0	88.82	0.4 ± 1.0	0.39	0.3 ± 0.8
17		94.72			
18	469.6*	101.77	9.4 ± 2.3	0.39	7.3 ± 1.8
19	468.4	109.08	†	†	†
20		114.90			
21	468.4	120.72	2.0 ± 1.3	0.39	1.5 ± 1.0
22		126.47			
23	469.6*	132.35	8.4 ± 1.7	0.39	6.5 ± 1.3

Table 3.4. Sample of data collection in the region of the (8,1) band. (This data was later combined with other sets to yield the results shown in Fig. 4.3.)

* check readings on the (6,0) bandhead intensity

† data discarded due to pressure surge

‡ background (laser off) counts = 0.02 ± 0.04

Each block represents 10 x 10s; discharge on - discharge off

standard deviation recalculated. While this criterion is not statistically rigorous in terms of levels of confidence[145], since the sample size varies with wavelength, it provides a simple method of rejecting spurious data in a first approximation.

After the filtered means are calculated, the 'off' means are subtracted from the 'on' means to yield the signal. This is corrected for discharge background (if present), and this quantity is shown in column five of Table 3.4. The mean laser intensity for each group is also calculated, and the mean signal is normalised, with respect to a laser intensity of 0.300. The error in this normalised signal is calculated from the standard errors of the 'on' and 'off' counts in the usual manner.

Normalised signals from groups of blocks collected with different laser intensities can then be combined using

$$S = \frac{\Sigma N_i S_i}{\Sigma N_i} \qquad 3.34$$

$$\varepsilon = \frac{\{\Sigma N_i^2 \varepsilon_i^2\}^{\frac{1}{2}}}{\Sigma N_i} \qquad 3.35$$

where S_i and ε_i are the normalised signals and their errors and N_i, the number of entries in each group after filtering, and S, ε the final signal and its uncertainty. These $S \pm \varepsilon$ are then plotted as a function of λ to yield the observed spectrum.

3.5 Assessment of Experimental Performance

Here the data collection rate is compared with the predictions of Sec. 3.3, and some conclusions and recommendations drawn.

The typical signal rate for stronger bands e.g. $q_{50} \simeq 0.1$ was $<1\ s^{-1}$. Broadly speaking this is in agreement with the total rate predicted for low p(v") ($\simeq 10^{-2}$) in table 3.3. In Chapter 4 it will be shown that for the p(v") distribution obtained from the experiments, the expected value of p(0) is 0.01 - 0.03, so these figures appear to be consistent. Again from table 3.3 it is seen that given these conditions signal rates for weak bands e.g. $q_{81} \simeq 0.03$ are very low and longer count times are required to build up a satisfactory signal to noise ratio. This is roughly in agreement with what was observed; the (8,1), (8,2) bands ($q \simeq 0.03$) proving much more difficult to see than the (5,0), (6,0) bands ($q \simeq 0.1$). Anticipating the results shown in figure 4.9 shows that p(v") changes only slightly in the range v" = 0 - 2, so the decrease in absorbtion strength is not offset by an increased population as v" increases.

Also, it should be recalled that the predicted count rates obtain only at the bandhead. Away from this condition, the count rate again decreases resulting in significantly increased count times.

Some loss of intensity also occurs due to the gating system. In the case of a 2μs delay and 10μs gate there is a reduction of intensity by

$$e^{-2/\tau_R} - e^{-12/\tau_R} \simeq 57\%$$

where τ_R is the radiative lifetime, which is a significant loss. In practice the residence time in the detection zone may cut the gate off even earlier so this represents an upper limit to the reduction. The effect of laser induced noise prevents a reduction in the delay, or an increase of the effective aperture of the detector, both of which

would help to decrease this loss. Improvement in the quality of the laser beam is thus a necessary prerequisite to increasing the gate width.

To illustrate the importance of the different variables occurring in the feasibility calculation it is useful to restate and pull together equs. 3.19, 20, 27, 31 and 32.

$$Z = n_{I_2} n_F \sigma_R \bar{v}_{rel} \qquad 3.19$$

$$n_p = \frac{1}{3} \bar{r} \frac{Z}{\bar{v}'_{rel}} \qquad 3.20$$

$$\dot{n}(\nu_L) = n_p p(v'') K_{v''} \rho_o q_{v'v''} |Re.|^2 H_{J''} \qquad 3.27$$

$$\rho_o = \frac{\bar{p}}{cf\Delta t_L \sigma_L \Delta\nu_L} \qquad 3.31$$

$$S(\nu_L) = \dot{n}(\nu_L) \Delta t_L V' f\varepsilon \qquad 3.32$$

Substituting for Z into equ. 3.20; for n_p and ρ_o into 3.27; for $\dot{n}(\nu_L)$ into 3.32, and noting that

$$V' = \sigma_L \bar{r} \qquad 3.36$$

after collecting constants and cancelling, yields the observed signal in terms of useful variables.

$$S(\nu_L) \propto n_{I_2} n_F \left(\frac{\bar{v}_{rel}}{\bar{v}'_{rel}} \right) \left(\frac{\bar{p}}{\Delta\nu_L} \right) \bar{r}^2 . q_{v'v''} p(v'') . \varepsilon . \qquad 3.37$$

$H_{J''}$ has been taken as constant. The factors $(\bar{v}_{rel}/\bar{v}'_{rel})$ and $q_{v'v''}p(v'')$

are effectively fixed by the nature of the reactants and the system dynamics. Except for a variation in $\bar{v}_{rel}$ by seeding the beams these factors are not variable. The factor $\bar{P}/\Delta\nu_L$ is the mean power per unit bandwidth. It should be noted that while decreasing $\Delta\nu_L$ at constant $\bar{P}$ increases the signal according to equ. 3.37, there is a decrease in $H_{J''}$ which offsets this effect. It will be shown in Sec. 4.2 that reducing $\Delta\nu_L$ increases the efficiency with which the laser line covers the available transitions, at least near the bandhead, so $S(\nu_L)$ increases as $\Delta\nu_L$ decreases (at constant $\bar{P}$), although the effect is weak.

The variation of $S(\nu_L)$ with $\bar{r}^2$ is interesting. The steady state density of product increases linearly with the radius of the reaction zone, $\bar{r}$ (provided the beam flux is constant), since a larger number of incremental volumes in which formation occurs gives rise to more product passing through the remainder of the zone. In addition the number of excitation events increases linearly with $\bar{r}$, so the net result is a quadratic variation. Ultimately this variation is limited by the requirement that $\bar{r} << \lambda$.

Finally the signal varies linearly as expected with the density of reagents and ε. ε contains the gating effects discussed earlier as well as geometric and quantum contributions. Geometric efficiency could be improved considerably if the laser beam quality was improved.

Despite the generally good agreement between the predicted and observed signal, it is difficult to draw any firm conclusions about the accuracy of the feasibility calculation, due mainly to the uncertainty in the F-atom density. The fact that the experiment

certainly does not exceed the calculated performance is particularly disappointing in view of the choice of most pessimistic values for the variables. It is likely that the experimental deficiency arises mainly from an overestimation of the F-atom density. This may be due to still significant in-transit losses from wall recombination, poorly defined beam profile, or a combination of both. In any case it is likely that significant improvements would result from moving the discharge closer to the nozzle. This would allow an increase in stagnation pressure and decreased nozzle diameter to be used. Improved beam character would then result without the associated problems of wall recombination. Improved combined nozzle-discharge sources have recently been reported[146] and work is currently in progress on their application to this experiment[147].

CHAPTER 4

RESULTS AND DISCUSSION

4.1 General Considerations

Figure 4.1 shows a simulation of the region 450 - 500 nm for the excitation spectrum of IF. A uniform population of the three lowest vibrational levels and a rotational temperature of 300K was assumed. The v" = 0,1,2 are the only states which have bands accessible below the onset of I_2 absorption. This region is covered by the laser dyes coumarin 102 and coumarin 47. This simulation suggests that unless there is a very strong inversion in P(v") the strongest bands will arise from the v" = 0 state, due mainly to the higher Franck-Condon factors for these transitions.

Three experiments (subsequently called I, II, and III) were required to observe these three lowest states. All three used the apparatus and conditions discussed in Chapter 3. In I phosphoric acid coating was used on the gas tube, whereas in II and III teflon dispersion was employed; otherwise conditions were identical as far as could be discerned. The maximum signal was consistently low ($<1\ s^{-1}$).

In I the (6,0) band was observed. The low signal from this state suggested that long count times would be required for the v" = 1,2 states. The normalised signal as a function of laser wavelength in this experiment is shown in Fig. 4.2. In II the (6,0), (5,0) and (8,1) bands were observed, while in III the (5,0) and (8,2) bands were observed. These two sets of data form the totality of useful experimental results, and are shown later in this chapter (Fig. 4.7).

4.2 Determination of Results

The simulation program was used to generate fits to the observed data, as illustrated in Fig. 4.2. Traditional methods for determining vibrational populations from low resolution spectra have relied on

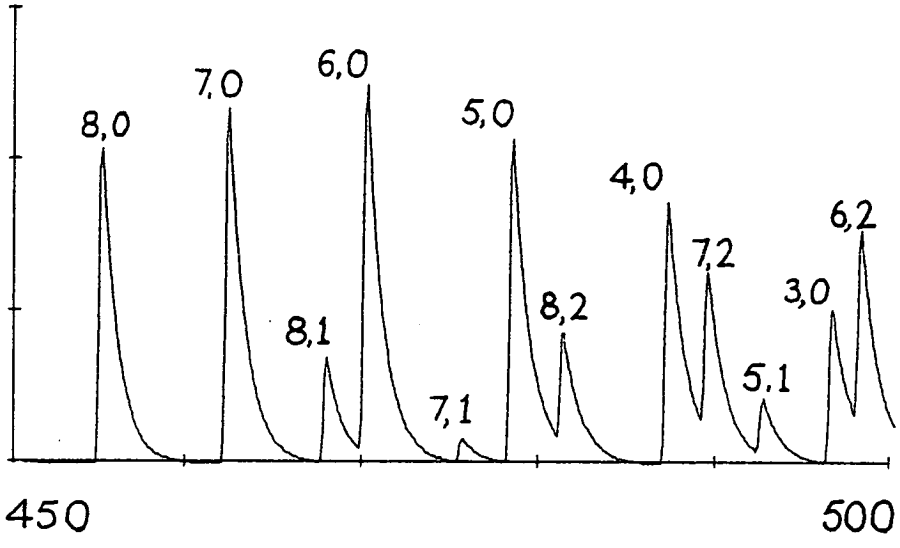

Fig. 4.1. Simulation of the excitation spectrum of IF in the region 450 - 500 nm assuming equipopulated v" = 0,1,2 states.

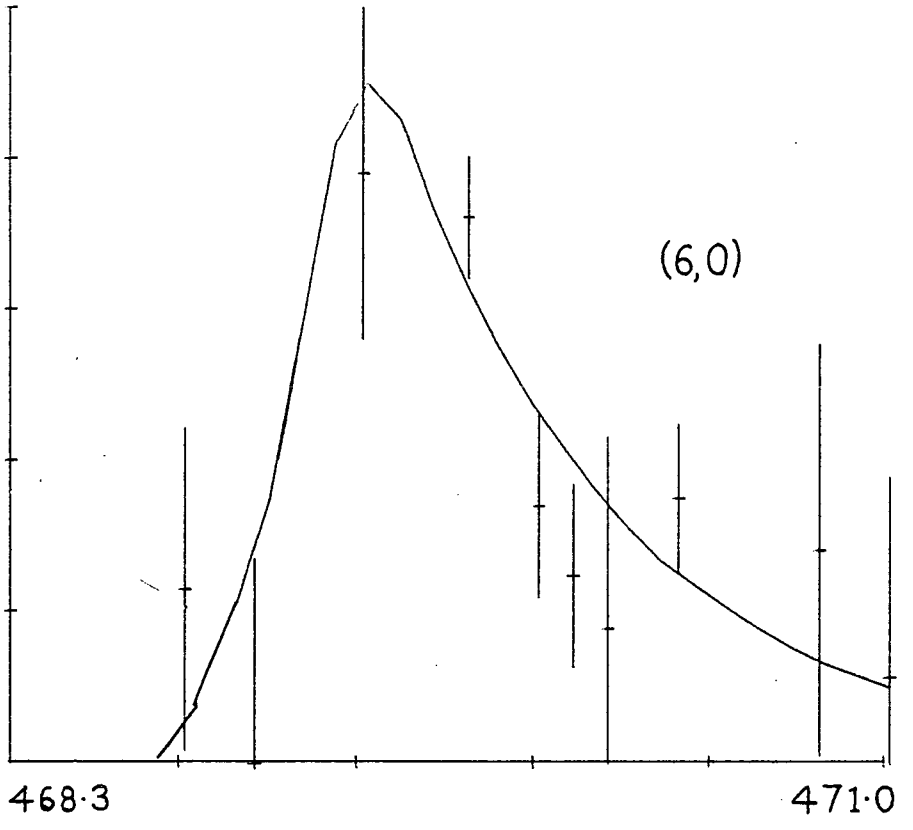

Fig. 4.2. Data of experiment I; (6,0) bandhead.

integrating the area under the band profile.[59,63]. Clearly the quality of the data presented here does not lend itself to such a treatment. The preferred method is thus that of obtaining simulated spectra which yield acceptable fits to the data, and hence the relative populations.

Ideally, the fitting procedure should be performed in a mathematically rigorous manner. By expressing $I(\lambda_L)$ as a function with quantities like $\Delta\lambda_L$, T_R, $N_{v''}$ as parameters a non-linear least squares fit could be performed to yield their optimum values. Unfortunately time considerations did not permit the extensive adaptation of the simulation program that this would involve. The alternative approach is to use good judgement combined with physical intuition to arrive at a qualitatively acceptable fit, which it is hoped is not too biased. It will be shown that the resulting range of parameter values is in fact fairly restricted so that the procedure is not entirely arbitrary.

In performing this fitting it was found easiest to proceed as follows. Since the (v',0) bands were most prominent, the four bands were fitted in pairs, with the (8,1) and (6,0) together and the (8,2) and (5,0) together. The number of $N_{v''}$ parameters is thus two since the populations can be taken with respect to N_0, i.e.

$$N'_{v''} = \frac{N_{v''}}{N_0} \qquad 4.1$$

Due to the large wavelength shift between bands it is convenient to have a shift parameter $\Delta\Lambda$, to take account of inaccuracies in the stepper motor drive. This allows the apparent positions of the band-heads to move with respect to each other.

The shape and extent of each band is then governed only by two remaining conditions; $\Delta\lambda_L$ and P(J"). $\Delta\lambda_L$ is in principle fixed by its measurement, but in view of the high degree of variability observed in the laser properties it is useful to allow $\Delta\lambda_L$ to vary within the 2-5Å range, between II and III.

For P(J") a normalised Boltzmann distribution was chosen i.e.

$$P(J) = \frac{1}{Q}(2J + 1)e^{-J(J+1)B_v/kT_R} \qquad 4.2$$

where $Q = B_v/kT_R$ is the rotational partition function. There is no a priori reason for this choice indeed it assumes canonical rather than microcanonical equilibrium. It is possible that a more flexible form like Equ. 2.4 would yield a better fit, but in view of the quality of the data here, the significance of any preferred choice, and its resulting parameters is dubious. Finally T_R in Equ. 4.2 is constrained to be the same for all v". This is equivalent to saying that the energy disposal criteria follow the frequently observed characteristic[1]

$$g'_R = \frac{f'_R}{1-f'_v} = \text{const}, \qquad 4.3$$

as shown in Fig. 4.3.

If in highly exothermic reactions it is assumed that f'_v does not change much for low v, then it follows that

$$f'_R \simeq \frac{\langle kT_R \rangle}{E_{TOT}} \simeq g'_R = \text{const}. \qquad 4.4$$

Hence a fixed T_R for low vibrational states is acceptable. Since the determination of P(J) and P(v) are independent of each other the restriction on f'_v can be checked once P(v) is determined.

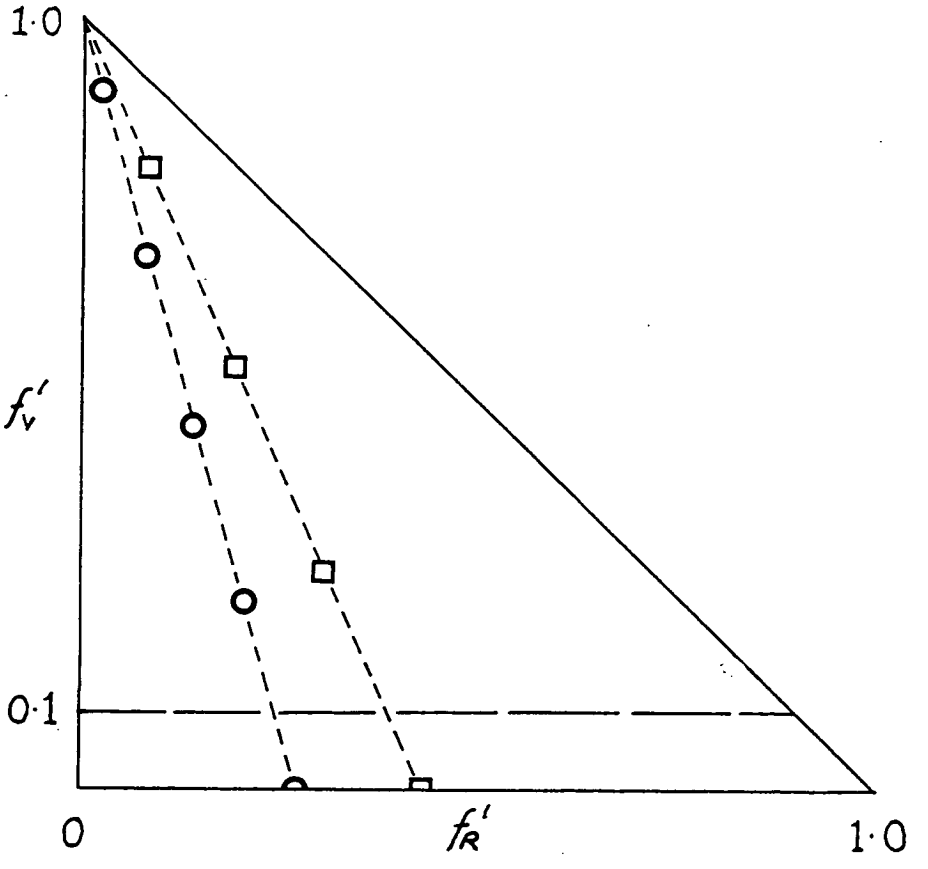

Fig. 4.3. Schematic energy characteristic for two exothermic reactions with high $\langle f_v' \rangle$, showing the slight variation of f_R' at low f_v'. The horizontal dashed line represents $f_v' \approx 0.1$, corresponding to v" = 2 in $F + I_2$

□ $F + HCl$ (169)

○ F / D_2 (170)

4.2.1 Effect of $\Delta\lambda_L$ and T_R

Before proceeding it is worth considering the effect of the shape parameters T_R and $\Delta\lambda_L$. Here it is demonstrated that the profile behaves much as expected as each is altered and that each affects the profile in a characteristic way that is independent of the value of the other. This feature greatly simplifies the fitting.

A: Variation of T_R

Figure 4.4a) shows the appearance of the (5,0) band taken with $\Delta\lambda_L$ = 1Å, and rotational temperatures of 100, 200, 300 and 400K. The simulations show the expected behaviour of increasing width and decreasing height as higher J levels fill up at the expense of lower ones. Figure 4.4b) shows the same distributions, but with the vibrational probability scaled up by 1,2,3 and 4 times, to yield approximately the same p(v,J) in the most probable state (except for the influence of the weakly dependent T_R factor in the exponent of Equ. 4.2). From this it can be seen that the rising part of the profile has a gradient that is independent of T_R, and that only the shape of the band tail is affected.

B: Variation of $\Delta\lambda_L$

Figure 4.5 shows the appearance of the (5,0) band at 300K with $\Delta\lambda_L$ = 1,2,3 and 4Å, the integrated laser energy density being held constant. Apart from the obvious loss of resolution as $\Delta\lambda_L$ increases, two other features are apparent. The gradient of the rising part of the profile decreases as $\Delta\lambda_L$ increases, and the falling parts of the profiles are virtually identical. (Indeed co-incidence is complete if the aritifical shift in Fig. 4.5 is removed). There is also a small decrease in peak intensity reflecting the lower efficiency with which

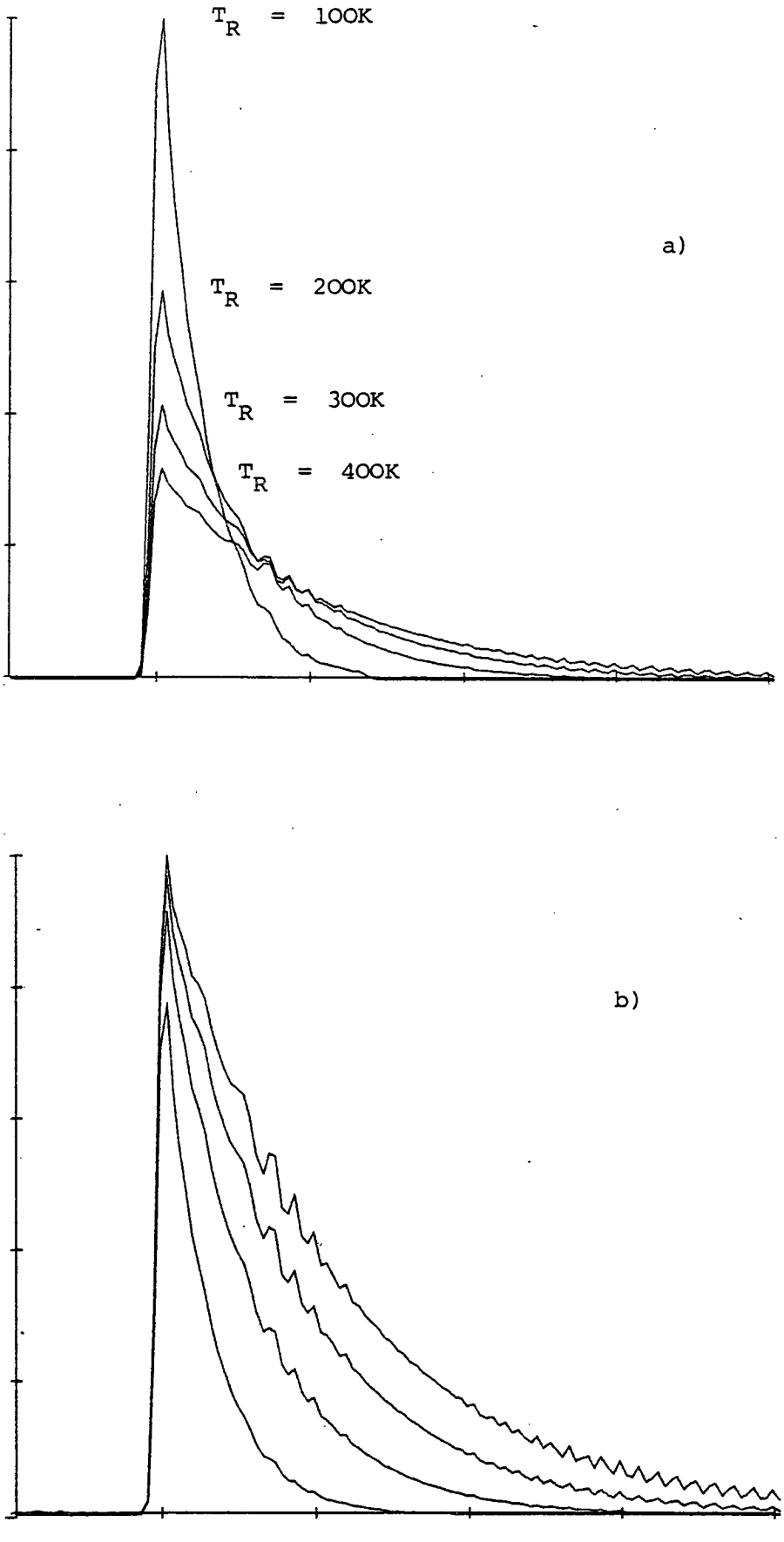

Fig. 4.4 (details over)

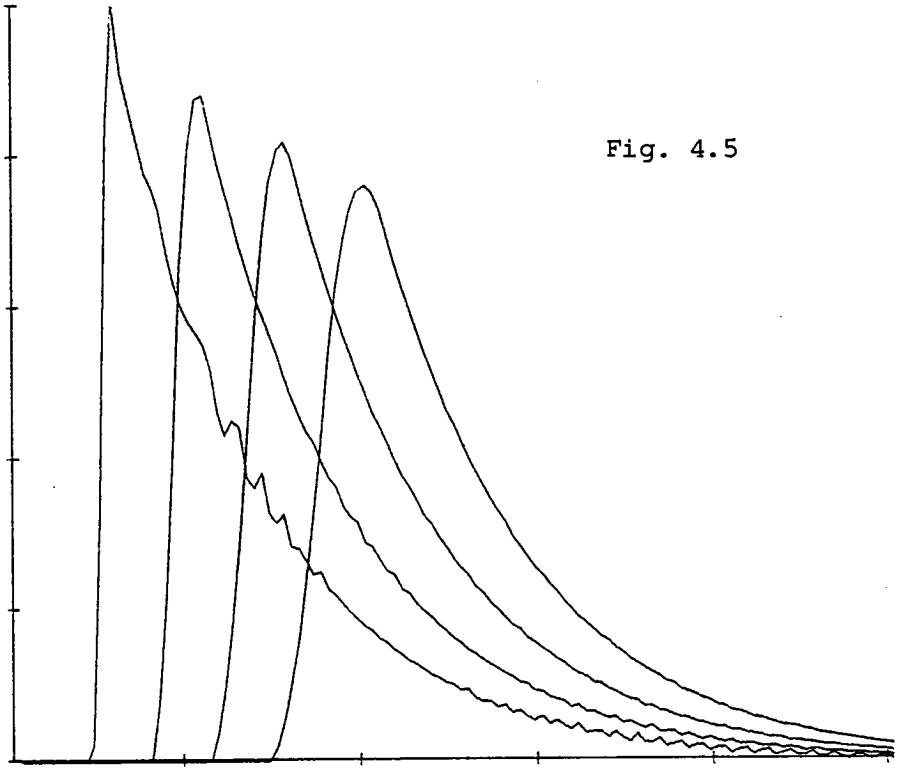

Fig. 4.5

Fig. 4.4. (previous page). Simulation of the (5,0) band of IF for various T_R

a) with correct normalisation

b) with normalisation removed showing the coincidence of the rising edge of the profile.

Fig. 4.5. (above). Simulation of the (5,0) band of IF for various values of $\Delta\lambda_L$. (An artificial shift of 5Å has been introduced between the profiles for clarity).

the laser bandwidth covers the bandhead, as presupposed in Sec. 3.5.

4.2.2 Fitting of Parameters

In determining which parameters generate the best fit, the following general procedure was followed. Simulations which passed through the greatest number of error bars were considered to be the best fits. These were constrained so that error bars which they did not pass through were, where possible, distributed equally above and below the fit. In some cases, points occur which cannot be incorporated into this general scheme by any sensible variation of parameters. When this problem has arisen, it has been assumed that this point is anomalous and it has been given less weight in determining the best fit than the others. This may appear to be a rather arbitrary scheme, but it is possible to consider it as a crude filter. The probability that such a point is likely to arise at random as a representation of the fit can be considered. If it lies outside the range of reasonable fits, then there is a good chance that it is caused by some anomalous event, and hence its lower weighting or rejection is justified. Clearly such a treatment is only justified if a large majority of points can be accommodated by the simulation. In the data presented here, there are perhaps two or three anomalous points only, so their scarcity supports this treatment.

The approximate uncertainty in the parameters is decided as follows. By varying the parameter in question an extreme fit which passes through some fraction of the number of non-anomalous points is found. The variation of the parameter to produce these fits is an estimate of its uncertainty. The fraction of points which yields such an estimate represents a compromise between allowing extreme fits which

reflect the large error bars, and rejecting fits which are extremely unlikely. A value of 60 - 70% seemed satisfactory.

The data for each band were first considered individually to establish working optimal values of T_R and $\Delta\lambda_L$, for use in the pairwise simulations later on. The data from II, i.e. (6,0) and (8,1) bands, were found to be best represented by $\Delta\lambda_L = 3\text{Å}$, whereas those from III, i.e. (5,0) and (8,2) bands were best fitted by $\Delta\lambda_L = 2\text{Å}$. There is no inconsistency here as the laser conditions were almost certainly different in these two experiments.

The individual bands could all be fitted to somewhat different optimal values of T_R. By considering the best fit to all bands a common value of T_R was established. This was found to be $\sim$200 ± 100K. As will be explained later, there is probably very little physical significance in the exact value of T_R.

Using these values of T_R and $\Delta\lambda_L$, the individual bands were used to determine the uncertainty in $N_{v''}$. This was done by varying a scaling parameter in the simulation graphics subroutines. With the best fit taken to represent a scale factor of unity, the uncertainty was determined by scaling the fit up and down, until the above condition was satisfied. Typical limits were ±0.1 - 0.2 of the best fit. These are shown for the four bands studied in Fig. 4.6. The resulting absolute errors in $N'_{v''}$ after allowing for scaling of one band with respect to another are given in Table 4.1.

The individual bands were then combined pairwise as described earlier to determine the $N'_{v''}$, which are given in Table 4.1. The best fits to these data are given in Fig. 4.7.

To normalise the two experiments with respect to each other, the

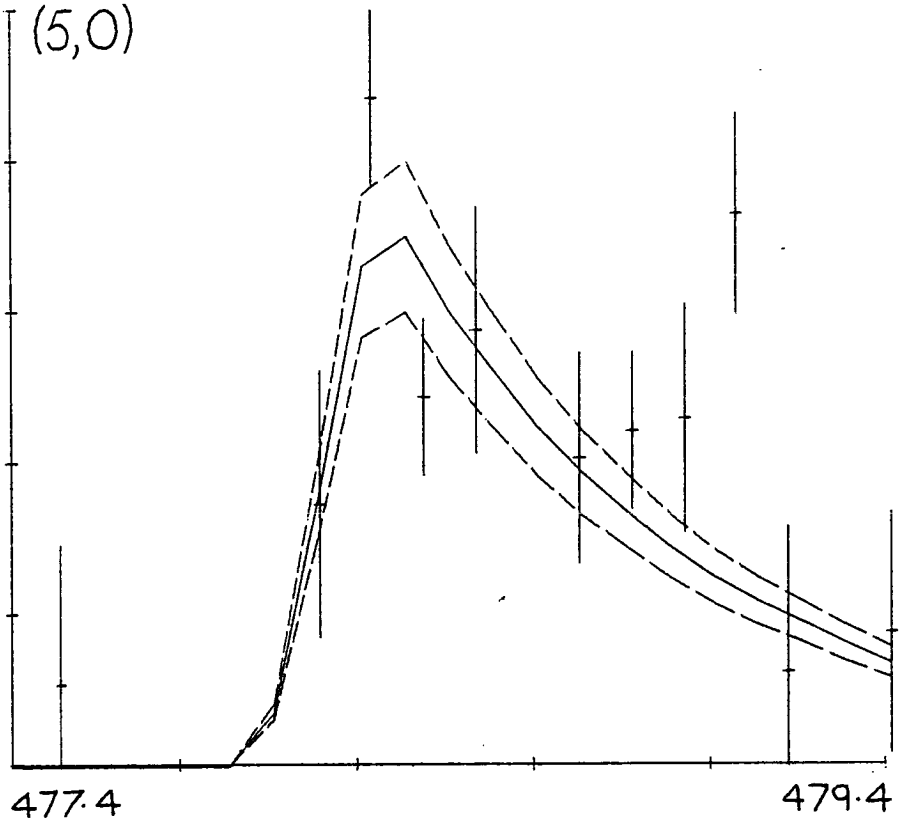

a)

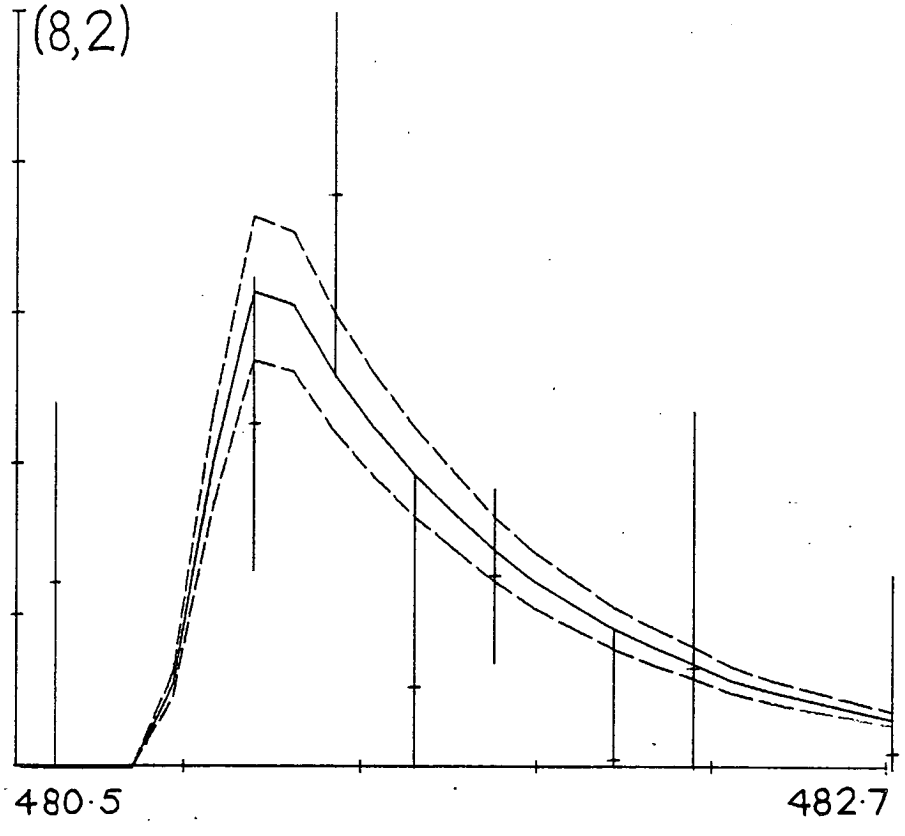

b)

Fig. 4.6. Best and most extreme fits of simulations to data for the observed bands of IF

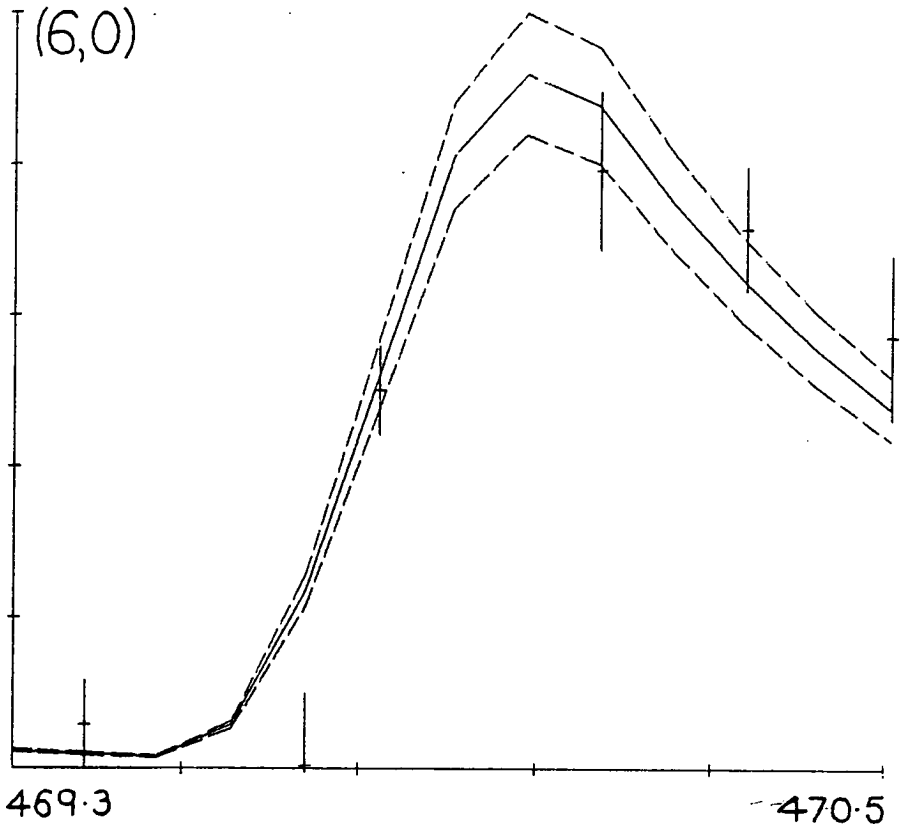

a)

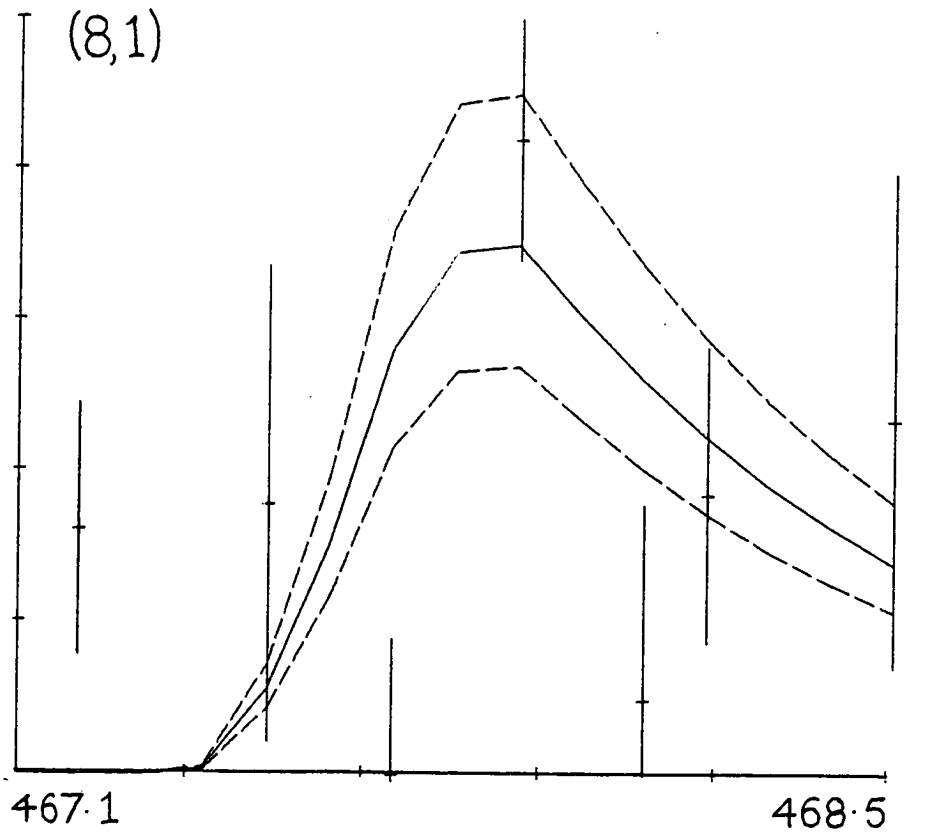

b)

Fig. 4.6. (contd.)

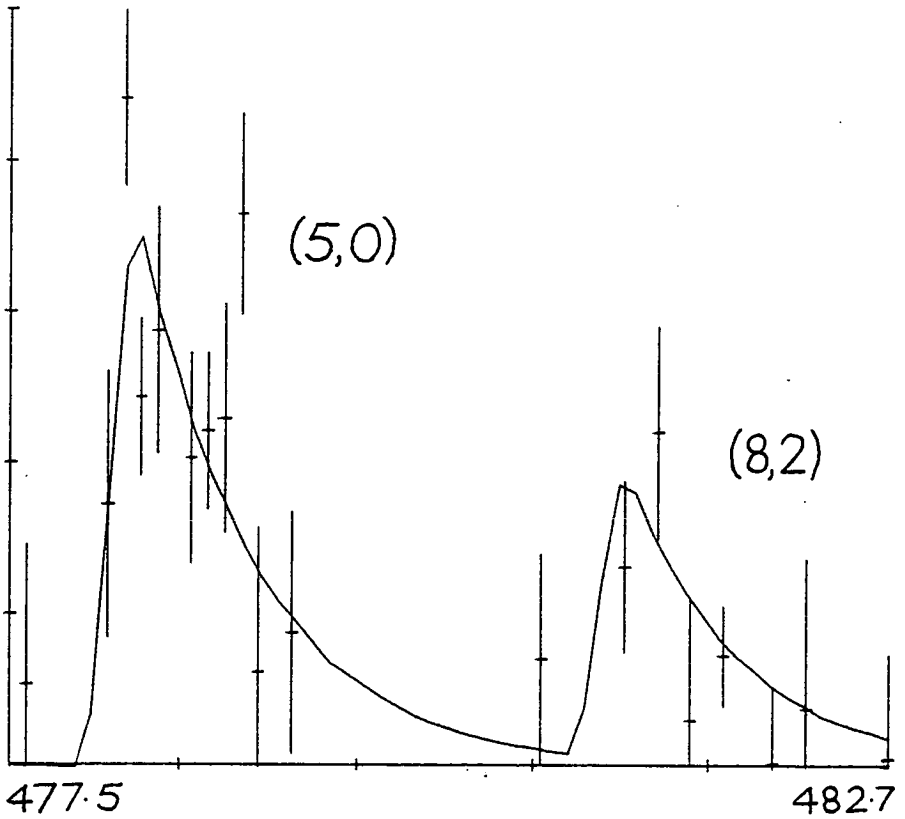

a)

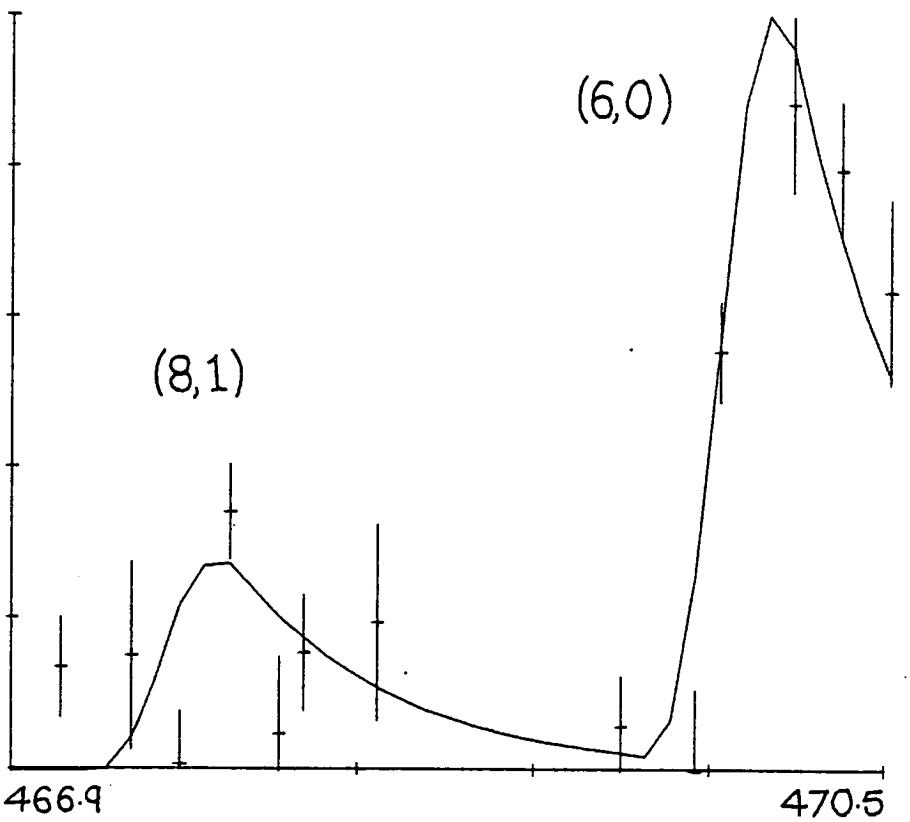

b)

Fig. 4.7. Pairwise fits of simulations to data

a) Experiment I, b) Experiment II.

Experiment	Band (v',v")	N''_v
II	(5,0)	1.00 ± 0.15
	(6,0)	1.16 ± 0.12
	(8,1)	1.38 ± 0.28
III	(5,0)	1.00 ± 0.15
	(8,2)	1.60 ± 0.24

Table 4.1. Ratios of populations and their uncertainties to that observed from the (5,0) band. The value of N'_1 is scaled up as determined by the ratio $N'_0(6,0)$: $N'_0(5,0)$ in II. Errors are determined as described in the text.

additional data on the (5,O) band collected in II was used to compare the populations derived from (5,O) and (6,O). The ratio of that from v' = 5 to v' = 6 was found to be 1:1.16. From the estimated uncertainties in Table 4.1 there is seen to be sufficient overlap to conclude that these results are consistent. On the assumption that the experimental conditions in II and III were similar (see Sec. 3.4.2) a route is provided for the direct comparison of data from the four observed bands. Thus, in calculating the final results of Table 4.1, the factor of 1.16 has been retained in the value of N_o from the (6,O) band, and used to correct the value of N_1', which was obtained by a pairwise simulation of the (8,1) and (6,O) bands.

4.2.3 Density to flux correction

To convert the population ratios in Table 4.1 to relative rate constants requires multiplication by the LAB velocity for each v" state. The product velocity in the CM frame is given by

$$u'_{IF} = \left\{ \frac{2(E_{TOT} - E'_R - E'_v)}{m_{IF}(1 + m_{IF}/m_I)} \right\}^{\frac{1}{2}} \qquad 4.5$$

From the Newton diagram in Fig. 4.8 it can be seen that for low v", u'_{IF} is greater than the centroid velocity, $\underline{v}_{CM}$, by a factor of ∿5. In the most extreme cases when $\underline{u}_{IF}$ is aligned parallel and antiparallel to $\underline{v}_{CM}$ the difference in the LAB velocity $\underline{v}_{IF}$ is ∿20% of its value when $\underline{v}_{CM}$ and $\underline{u}'_{IF}$ are perpendicular. In the absence of any reliable description of the angle-velocity map, the three limiting cases of stripping, rebound and complex behaviour can be considered. In all three the model angular distribution favours $\underline{u}'_{IF}$ parallel to $\underline{u}_F$, and hence perpendicular to $\underline{v}_{CM}$, when averaged over θ. In view of this the angle-

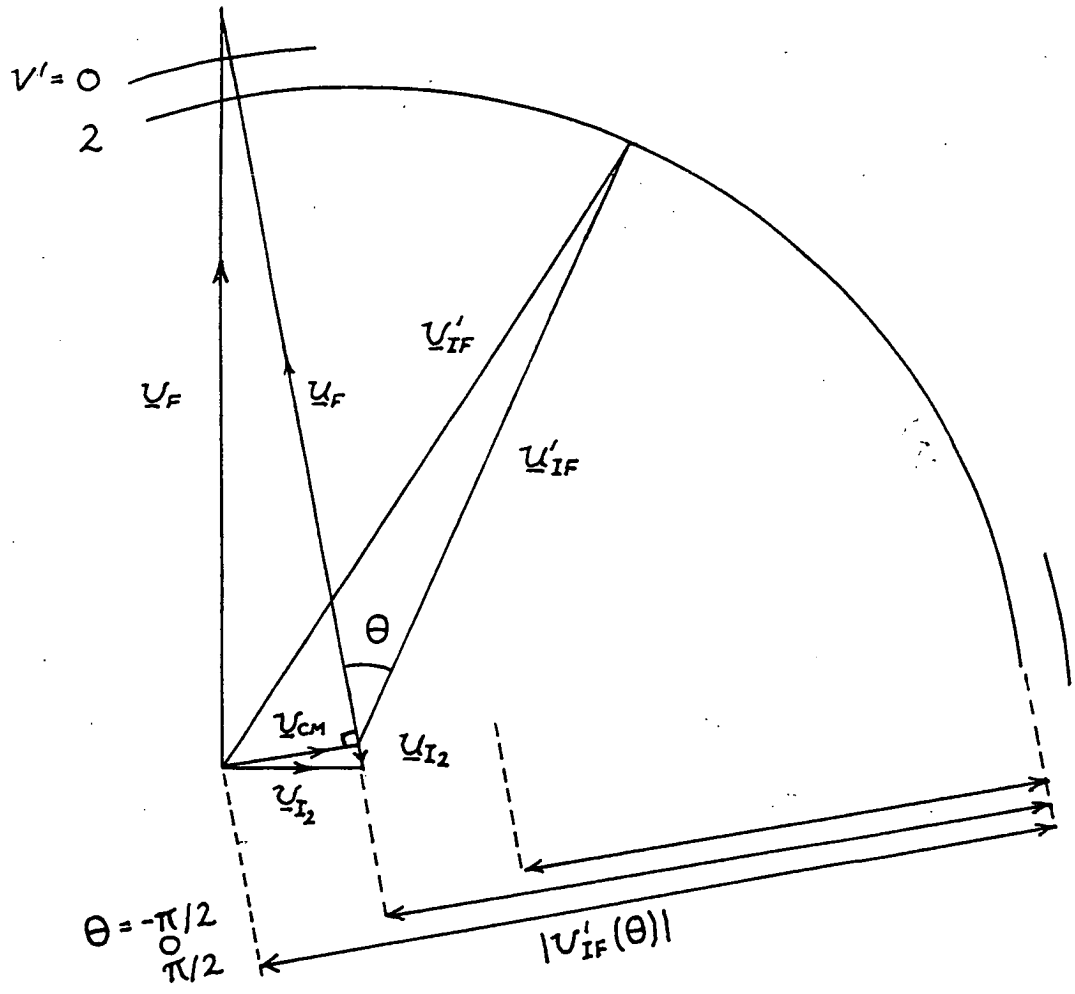

Fig. 4.8. Newton diagram for the reaction F + I_2 at a nominal total energy of 133 kJ mol^{-1} (11100 cm^{-1}).

averaged LAB velocity is unlikely to vary substantially for low v" and hence the $N'_{v"}$ can be taken directly as relative rate constants.

4.2.4 Effect of collisional relaxation

In considering the observed vibrational and rotational distributions the possibility of relaxation distorting the distributions must be considered. There are two sources of this;

(a) Rotational relaxation by R → T transfer to other species, within the reaction zone leading to a component with T_R equal to the reagent temperature

(b) Vibrational relaxation by V → T transfer or wall effects in the whole volume of the vessel, leading to a background component with T_V equal to that of the tank walls.

Since the density of IF in the reaction zone is low relaxation by V → V transfer in the zone itself is not a problem.

A: Rotational relaxation

In Section 3.2. the principal species present in the reaction zone were estimated to have densities

$$\text{He: } 3.7 \times 10^{13} \text{ cm}^{-1}$$

$$I_2\text{: } 1.2 \times 10^{12} \text{ cm}^{-3}$$

Hard sphere collision diameters are assumed as follows:

$$\text{He: } 2.6 \text{ Å}^{(83)}$$

$$I_2\text{: } 6.5 \text{ Å}^{*}$$

$$\text{IF: } 4.4 \text{ Å}^{(83)}$$

The rate of collisions of IF with He or I_2 is given by

*As in Section 3.2. This is likely to be an underestimate, but the final result is not very dependent on the exact value.

$$Z_{IF/Q} = \sigma_{IF/Q}\bar{v}_{rel}N_Q \qquad 4.16$$

where

$$\sigma_{IF/Q} = \frac{\pi}{4}(d_{IF} + d_Q)^2 \qquad 4.17$$

For low lying product IF vibrational states v'_{IF} is $\sim 10^5$ cms^{-1} as before. Typical collision conditions are taken to be right-angled, hence

$$v_{rel} = \{v_{IF}^2 + v_Q^2\}^{\frac{1}{2}} \qquad 4.18$$

Using suitable values for v_Q and equs. 4.16 - 18 yields

$$Z_{IF/He} \sim 2.0 \times 10^4 \ s^{-1}$$

$$Z_{IF/I_2} \sim 0.14 \times 10^4 \ s^{-1}$$

The mean free time between collisions is

$$\tau = (Z_{IF/He} + Z_{IF/I_2})^{-1} \qquad 4.19$$

$$\simeq 45\mu s$$

For a residence time in the reaction zone of $\sim 5\mu s$, the fraction of molecules that suffer collisions is $1-\exp(-5/45) \simeq 10\%$.

In practice the rate constant for rotational quenching is expected to be even less than the hard sphere value ($k_Q \simeq \sigma\bar{v} = 5.7 \times 10^{-10}$ cm^3 $molecule^{-1}$ s^{-1}). By modelling rotational relaxation of BrF via collisions with He, Clyne and McDermid determined k_Q to be 2.5×10^{-11} cm^3 $molecule^{-1}$ s^{-1} within a factor of 2 [85]. This is significantly less than the hard sphere value and it would be surprising if a similar situation did not hold for IF. On this basis it is concluded that rotationally relaxed product accounts for no more than 10% of the total.

This low value is due to the small size of the reaction zone and the high product velocity in the system.

B: Vibrational relaxation

The mole fraction of IF in the reaction zone is estimated from Sec. 3.2 as $x_{IF} \simeq 5.8 \times 10^{-7}$. The dispersion of product into the tank gives rise to a background of ground state molecules. Assuming, initially, no preferential pumping of IF, this background has a partial pressure $x_{IF}p_b$ where p_b is the total background pressure $\sim 4 \times 10^{-5}$ torr. Hence $p_{IF} \simeq 2.3 \times 10^{-11}$ torr or 7×10^5 cm^{-3}. This is about 3% of that in the reaction zone. This background is assumed to be vibrationally and rotationally thermalised at a temperature between that of the reagents, ~300K and that of the cold traps, ~77K. At 300K, about 4% of IF is in the v = 1 state, so interference from the background is only significant for v = 0. Anticipating the results shown in Fig. 3.10, the absolute probability for the production of IF in the v" = 0,1,2 states is seen to be ~0.01 - 0.02. Hence for v = 0 some 60% of signal may arise from the background. For v = 1 and 2, the figures are 8% and 0.6% respectively.

The mole fraction of IF in the background may be altered significantly from the above value by the cryo-trapping facilities however. This is believed to reduce x_{IF} for the following reasons. The vapour pressure of IF at 77K is likely to be very low. Since the thermochemical properties of IF are unknown, it is necessary to invoke comparisons with other interhalogens. The only species for which the necessary data are available are Br_2, I_2 and ICl. Use of the Clausius-Clapeyron equation with standard data[155-157] yields the vapour pressures at 100K as 10^{-6}, 10^{-29} and 10^{-17} torr respectively. Physically

IF is probably closest to ICl in size and structure, which suggests the background pressure will be low. While the arrangement of cryo-trapping probably leads to a range of surface temperatures, it is only necessary for the partial pressure to drop one order of magnitude to reduce the background contribution to fluorescence to a negligible amount. On the basis of the data for ICl, this is believed to be an achievable reduction.

Further supporting evidence comes from the observation in Sec. 3.4 that at background pressures above $\sim 1 \times 10^{-4}$ torr the fluorescence signal disappears*. If there was a significant contribution from a thermal background, the signal would only drop initially to ~60% of its low pressure value, and this would still be observable for the stronger v = 0 bands. Practically this means that the background fluorescence is less than the uncertainty in the signal caused by laser-induced noise and hence no correction has been applied.

4.3 Information - Theoretic Analysis

The data given in Table 4.1 will be analysed using the information theoretic approach of Levine and co-workers[31,32]. Since only the vibrational distribution is considered equ. 1.5 can be written explicitly as

$$I(f_{v'}) = - \ln \frac{p(f'_v)}{p^o(f'_v)} \qquad 4.6$$

where f'_v is the classical variable expressing the fraction of energy (above zero point) in product vibration

$$f'_v = \frac{E'_v}{E_{TOT}} \qquad 4.7$$

*Radiative quenching cannot be the cause of this since at 10^{-4} torr the collisional rate is $\sim 3 \times 10^3 s^{-1} << \tau_{rad}^{-1}$

$p^o(f'_v)$ can be evaluated in either the vibrating rotor (VR) or rigidly rotating harmonic oscillator (RRHO) approximations. In the former full interaction of anharmonic vibration and rotation is accounted for, whereas in the latter the vibration is assumed harmonic and uncoupled from rotation. For a diatomic product the RRHO approximation has a very simple form

$$p^o(f'_v) = \frac{5}{2}(1 - f'_v)^{3/2} \qquad 4.8$$

This is considered to be reasonably accurate for low lying (v,J) levels and has been used widely to generate prior distributions[32,67]. It has been shown[82] that if the surprisal $I(f'_v)$ is expanded as a polynomial of degree s in f'_v, i.e.

$$I(f'_v) = \lambda_o + \sum_{r=1}^{s} \lambda_r f'^r_v \qquad 4.9$$

then there are s + 1 constraints of the form

$$\langle f'^r_v \rangle = \sum_v f'^r_v p(f'_v) \qquad 4.10$$

which determine $p(f'_v)$. (One of these, for s = 0, is trivial, since it expresses conservation of probability). The $\langle f'^r_v \rangle$, $r \leq s$, are the independent moments of the distribution $p(f'_v)$. These, or alternatively, the co-efficients λ_r provide a compact way of describing the dynamics, which may then be related to features of the potential surface, for example by trajectory calculations.

Often, but not always[148-150] the surprisal is found to be linear in f_v indicating only one constraint of any importance, namely $\langle f'_v \rangle$, characterised by the parameter λ_1 (henceforth called simply λ_v). This

has been interpreted in terms of a 'microcanonical' temperature given by

$$T_v = \frac{E_{TOT}}{k\lambda_v}, \qquad 4.11$$

k being Boltzmann's constant. While this is a convenient (albeit confusing) method of representation, λ_v is still the more important, and general, parameter.

The surprisals for the first three vibrational levels of IF were calculated using equs. 4.6-8, and the data in Table 4.1. The total available energy is given by

$$E_{TOT} = E_T + E_R + E_v + \Delta D_o \qquad 4.12$$

where E_T, E_R and E_v are the reagent translational, rotational, and vibrational (in excess of zero point) energies, and ΔD_o the reaction exo-ergicity.

$$\Delta D_o = D_o(PRODS) - D_o(REACTS) \qquad 4.13$$

Typical conditions were assumed in evaluating the first three terms in equ. 4.12 as follows. E_T is given by $\frac{1}{2}\mu v_{rel}^2$ where μ is the reduced mass of the reacting system and v_{rel}, the reactant relative velocity in the CM frame. From Fig. 4.8, $v_{rel} \simeq v_F \simeq 10^5$ cms^{-1}. The internal energy of I_2 is calculated for the v = 0, J = 58 state of I_2. This is approximately the most populated state at ~360K; a typical operating temperature of the oven. The various contributions to E_{TOT} are detailed in Table 4.2.

Based on this data a value of $E_{TOT} \simeq 1.38$ eV (133 kJ mol^{-1}, 11100 cm^{-1}) is obtained. On this basis, states up to v = 20 can be populated, although there are only 20 vibrational states with energy

	eV*
$D_o(I_2)$ (116)	1.54
$D_o(IF)$ (78)	2.81
E_T	0.09
E_v	0.00
E_R	0.15

Table 4.2. Reagent energy composition for the reaction $F + I_2 \rightarrow IF + I$.

*1eV ≃ 96 kJ mol^{-1} ≃ 8050 cm^{-1}

$\lesssim \Delta D_o$.

Surprisal values calculated for the four observed $N'_{v''}$ values are given in Table 4.3., and are plotted in Fig. 4.9. A least mean squares analysis of this data yielded $\lambda_v = -5.3$, with extreme limits of -3.1 and -6.9. This corresponds to $T_v = -3000K$ with limits -5200 and -2300K respectively.

Qualitatively the results indicate a vibrational population inversion, but the quantitative behaviour of $p(f'_v)$ changes substantially between the limits of λ_v, when extrapolated over the entire range of f'_v. This is shown in Fig. 4.10. These curves were synthesised using

$$p(f'_v) = \frac{p^o(f'_v)\exp\{\lambda_v f'_v\}}{p^o(f'_v)\exp\{\lambda_v f'_v\}} \qquad 4.14$$

with $p^o(f'_v)$ given by equ. 4.8.

There are serious restrictions on how reliable such a gross extrapolation can be considered to be. The use of equ. 4.14 hinges on the assumption that $I(f'_v)$ varies linearly over the entire range of f'_v, i.e. that equ. 4.9 is well satisfied for $s = 1$. Clearly, co-efficients of higher powers of f'_v which might not be detectable within the uncertainty of the data at low f'_v would make a considerable difference at high f'_v. There is however sufficient evidence to suggest this is unlikely to happen in $F + I_2$. Information theory has been used to determine surprisal values for a variety of reactive and non-reactive processes. Non-reactive processes, like vibrational and rotational energy transfer and photochemical decomposition[151] frequently show non-linear surprisal plots[152]. Reactive processes show linear[153],

(v',v")	$f_{v"}$	$I(f_{v"})$		
		MIN	TYP.	MAX.
(5,0)	0	-0.162	0.000	0.139
(6,0)	0	0.039	0.148	0.247
(8,1)	0.054	0.179	0.405	0.590
(8,2)	0.108	0.479	0.642	0.782

Table 4.3. Limiting and typical values of $I(f_v)$ obtained from the data of Table 4.2.

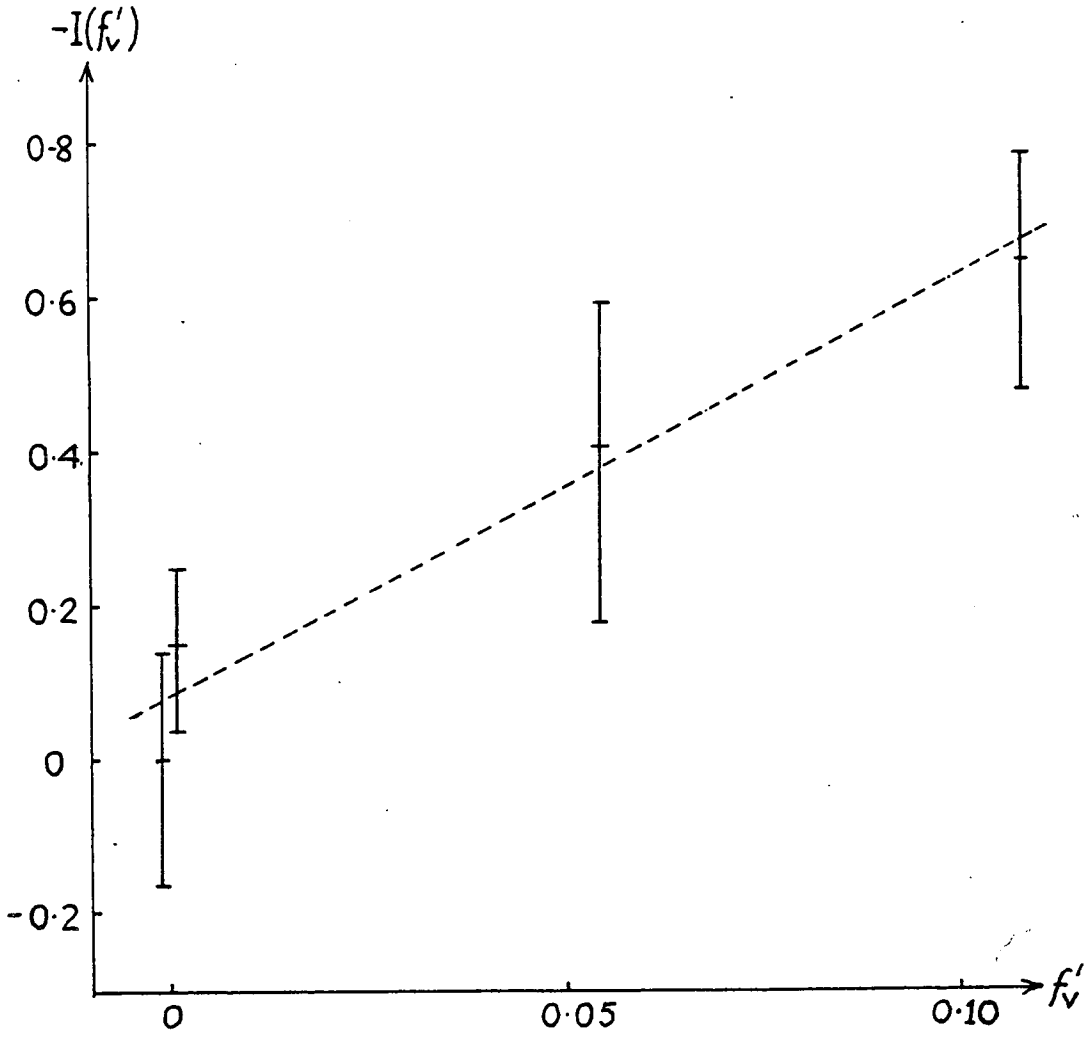

Fig. 4.9. Surprisal plot for the reaction F + I_2 (The two points at f'_v = 0 are displaced slightly for clarity).

Fig. 4.10. (over)

Extrapolated vibrational distributions corresponding to the range of λ_v determined for F + I_2

■ ; λ_v = -3.1

◆ ; λ_v = -5.3

● ; λ_v = -6.9

The dashed line is the synthetic distribution for F + ICl (λ_v = -5.7) normalised with respect to E_{TOT}.

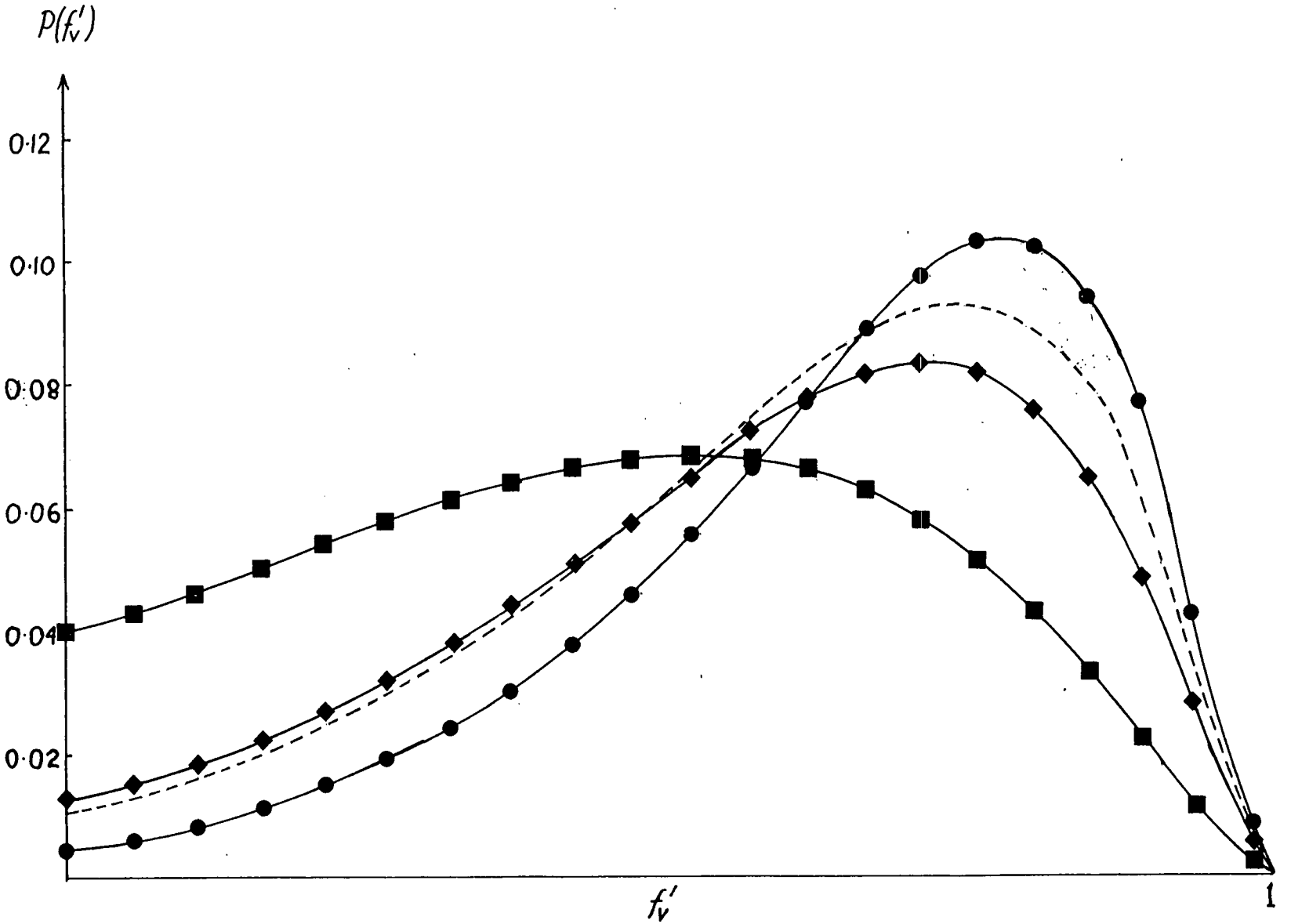

Fig. 4.10.

and non-linear behaviour[150,154]. Non-linear behaviour has been correlated with reactions showing significant repulsive energy release and large $\langle f_T' \rangle$ such as H + $Cl_2/Br_2/I_2$, and Ba + HX, and this is thought to be connected with a kinematic restriction on the transfer of momentum. If $\langle f_T' \rangle$ is low, non-linear effects are small, and this holds for reactions showing attractive and mixed release such as Cl + HI/DI, F + H_2/D_2. From the work of Stein et al[60,61] an estimate of the behaviour of $p(f_v')$ for the reaction F + ICl in the range v = 3-10 can be made. This shows $I(f_v')$ to be linear in f_v' with $\lambda_v = -5.7$ and a correlation of >98%. Since the range and quality of this data is better than that presented here, this is felt to strongly support a linear surprisal plot for F + I_2.

The mean fraction of total energy appearing in vibration is given by

$$\langle f_v' \rangle = \frac{\Sigma p^o(f_v') f_v' \exp\{\lambda_v f_v'\}}{\Sigma p^o(f_v') \exp\{\lambda_v f_v'\}} \qquad 4.15$$

This, and other parameters for the reactions F + I_2/ICl are summarised in Table 4.4.

4.4 Discussion

The data presented in the previous section has shown that a significant vibrational inversion exists in the lowest lying states of IF product in the reaction F + I_2. If this behaviour is extrapolated to the exo-ergicity limit some 60% of the total energy appears as vibration. The rotational distribution was found to be cold consisting of only a few percent of E_{TOT}. By subtraction the remaining ~40% is partitioned into product translation. This is significantly different

		F + I_2		
	F + ICl	MIN	TYP.	MAX.
E_{TOT}/cm^{-1} [a]	5520 [b]	-	11100	-
λ_v	-5.7	-3.1	-5.3	-6.9
T_v/K	-1400K	-5200	-3000	-2300
$\langle f_v \rangle$	0.60 [c]	0.48	0.59	0.67
$\langle v \rangle$ [d]	6	9	12	13
$\hat{f}_v$ [e]	0.75	0.52	0.71	0.78
$\hat{v}$ [e]	7	10	14	15
$\langle f_R \rangle$	0.14 ± 0.07	-	∿0.02	-
T_R/K	1200 ± 600	-	∿200	-
$\hat{J}$ [e]	39	-	11	-
$\langle f_T \rangle$ [f]	0.26	∿0.5	∿0.4	∿0.3

Table 4.4. Summary of product energy analysis for F + I_2 and F + ICl.

Notes: a) 1 $cm^{-1} \simeq 1.2 \times 10^{-2}$ kJ mol^{-1}.

b) There appears to be some discrepancy over the exact value of E_{TOT} for this reaction. This figure uses ΔD_o obtained in Chap. 1, and $E_v = 0$. The result (∿66 kJ mol^{-1}) is less than that quoted by Stein et al (∿70 kJ mol^{-1}) [60,61]. This is due i) to the use here of a more recent (and higher) value for D_o (ICl) [108] and ii) the fact that Stein erroneously included the zero point vibrational energy of ICl (in equ. 4.9) in his caluclation of E_{TOT}.

c) This is the synthetic value of $\langle f'_v \rangle$ as calculated from Equ. 4.15. The measured value of ∿0.55 [60,61] does not include the contribution from unobserved states.

d) $\langle v \rangle$; vibrational state closest to $\langle f_v \rangle$

e) $\hat{f}_v$; the most probably f_v, and $\hat{v}$; the nearest state. $\hat{J}$; the most probable rotational state at temperature $T_R = \langle f_R \rangle kE_{TOT}$

f) $\langle f_T \rangle = 1 - \langle f_R \rangle - \langle f_v \rangle$

to $\langle f'_T \rangle$ as determined by AVD measurements which have yielded $\lesssim 15\%$ [97,100] in the range E_T = 3 - 8 kJ mol^{-1}. While some caution should be exercised with the AVD data due to the apparent variation of the angular distribution over this energy range, it is unlikely that it can be reconciled with the results presented here, even allowing for the error bounds on $\langle f'_v \rangle$.

This data is of interest in comparison with the work of Stein et al [59-61] on F + ICl. A significant vibrational inversion was observed for this reaction also, but the rotational distribution was estimated as having a temperature of 600 - 1800K, which is considerably greater than that obtained here for F + I_2. No time of flight studies have been reported for this reaction so an independent estimate of $\langle f'_T \rangle$ is unavailable. A tentative angular distribution has been obtained which suggests the possible existence of a long-lived complex [18].

Rationalisation of the similarities in, and differences between these two reactions in terms of the potential surface topography is difficult without the aid of realistic dynamical calculations. There has been no comprehensive study of systems which approximate to F + I_2 either inertially or dynamically since the early work of Bunker and Blaise [158,159]. This is surprising in view of the suitability of the LEPS-type surfaces for these systems*. Bunker and Blaise used on entirely empirical surface to study the effects of mass variation, but restricted their attention to 2D only. The mass combination M + HM

*Preliminary calculations in 2D using a LEPS surface for F + I_2/ICl has suggested that the energy partioning may indeed be well accounted for [147].

(M = 16 a.m.u.) used in that work is close to that of F + I_2, but no separate rotational distributions were presented. Full 3D calculations have been made for the combination M + MM only. In general these have shown that 2D calculations tend to underestimate $\langle f'_R \rangle$[159,160], a situation which has been noticed in various other circumstances[119,161].

In practice the mass combination of F + I_2 is more likely to resemble L + MM than M + MM, and may thus be expected to exhibit the light atom effect, although more weakly than the archetypal H/D + X_2 series. The scale factor, α, is $\simeq 2$, and is similar to that of D + F_2 for which the effect has been propounded[162]. F + ICl cannot be considered as approaching this limit however ($\alpha \simeq 1.3$).

A second difference may result from the proposed well of depth $\sim$60 kJ mol^{-1} in the F + ICl surface[96,163]. This compared with $\sim$13 kJ mol^{-1} for F + I_2. When considered with the respective total energies, the RRK lifetime formula

$$\frac{\tau}{\tau_v} = \left\{ \frac{\varepsilon + E_{TOT}}{E_{TOT}} \right\}^3 \qquad 4.20$$

yields a lifetime τ, of the intermediate $\simeq 6\tau_v$ for FICl and $\sim\tau_v$ for F + I_2, where τ_v is the vibrational period of the intermediate. A longer lifetime is thus expected for the intermediate in F + ICl, but this is still considerably less than $\tau \gtrsim \tau_R$ required for the observation of long-lived complex (LLC) behaviour in the angle-velocity map. F + I_2 may thus be more like Cl + I_2, proceeding by a direct mechanism, with a large cross-section and high exothermicity.

Another system worthy of brief comment is O + I_2. This is inertially very similar to F + I_2 yet has very different dynamical features[42]. LLC behaviour observed in AVD measurements has been

attributed to a substantial well in the surface. Recent trajectory calculations by Fernie[119] have shown however that angular scattering patterns, ostensibly indicating LLC behaviour can in fact result from fairly brief encounters ($\lesssim$2ps) and are not incompatible with a vibrationally inverting mechanism, even when the surface has a substantial well. For this M + HH combination the angular distribution is determined by the repulsion in the BC bond together with the preferred geometry of the ABC intermediate. Such distributions are thus not very informative, although this explanation does help to rationalise the data on F + I_2/ICl.

The question of the relative timescales for statistical energy partitioning and true LLC behaviour in the angular distribution is thus still open, as regards triatomic intermediates. Certainly for systems like F + CH_3I/CF_3I both criteria hold[59,61,63], but the definite polyatomic nature of the intermediate allows fast intramolecular energy exchange via strong coupling of normal modes, and the departing tetratomic acts as an energy sink. Since such a facility is not available in triatomics, statistical partitioning may be an infrequent process except for very long lived intermediates. In the Ba + O_2 system[55] for example statistical partitioning may be the result of an extended lifetime due to special features of the surface. Such features are unlikely to figure in the F + XY systems however[164].

The various relevant properties of the systems discussed above are summarised in Table 4.5.

Of the salient features of the two reactions F + I_2/ICl, it is well established that vibrational excitation is substantial in both

	ΔD_o/ kJ mol^{-1}	ε/ kJ mol^{-1}	σ_R/ Å	α (Scale factor)	β (Skew angle)	$\langle f_T \rangle$	$\langle f_v \rangle$	$\langle f_R \rangle$
F + I_2	122	12	38[a]	2.0	14°	0.4[b] 0.15-0.2)[c]	0.6[b]	0.02
F + ICl	60	63	43[a]	1.3	10°	0.26[b]	0.6[b]	0.14
Cl + I_2	59	~0	18[c]	1.5	19°	0.3[c]	-	-
O + I_2	73	‹150(?)›	8[c] (?)	2.1	14°	0.3[c]	-	-

Table 4.5. Summary of properties of four reactions discussed in the text.

Notes: a) from velocity averaged rate constant (See Chap. 1).

b) from LIF

c) from AVD measurements

cases. Both surfaces are thus expected to show "early downhill" behaviour, i.e. attractive release in the entrance channel. For F + I_2 $\langle f'_v \rangle$ may correlate with the attractive release ($A_\perp$) and $\langle f'_T + f'_R \rangle$ with the repulsive release ($R_\perp$), by virtue of the light atom effect. F + ICl may be expected to avail itself of some mixed energy release and thus given reaction on the same surface a higher $\langle f'_v \rangle$ is expected. Unfortunately the data presented here is not good enough to corroborate or refute this proposal.

As regards rotation it is possible that the differing values of $\langle f'_R \rangle$ may be explicable by kinematic effects only, as described in the next section. Only after this question is considered can dynamical contributions to $\langle f'_R \rangle$ be assessed unambiguously.

4.4.1 Sources of product rotation

Theoretical work on sources of rotation is not nearly so detailed as that on vibration and translation. It is obviously inadequate to invoke conservation of energy for angular momentum restrictions may be important, even in the statistical limit. Some progress in understanding how $\langle f'_R \rangle$ is determined has been made by Hijazi and Polanyi[165,166] using classical trajectory studies.

While energy release in the new AB band in general becomes vibration, release in the old BC bond generates rotation and translation. The correlation of non-repulsive release with $\langle f'_v \rangle$ has been shown to hold fairly well for all mass combinations[17]. The partitioning between $\langle f'_R \rangle$ and $\langle f'_T \rangle$ is thus the mechanism of interest. Product translation results from repulsion along the line of the centre of mass of AB and C, while rotation requires the action of torques. These result from the angular variation of the potential U, and hence it is

useful to use the FMS representation. This again necessarily restricts the picture to 2D, but for qualitative considerations this is not a serious restriction.

A: Attractive surfaces

In 2D on attractive surfaces $\langle f_R' \rangle$ is generally found to be higher than on repulsive ones[17,161], but the behaviour of $\langle f_R' \rangle$ with changes in mass, energy release, or initial angle of approach is complex and difficult to elucidate. In a naive model of a direct encounter with attractive release the main source of $\underline{J}'$ is the relative motion of A with respect to B. If the BC bond is severed while A is still a large distance away ($>r^o_{AB}$) then C does not exert much influence on the internal motion of the incipient AB diatom. Thus initial orbital angular momentum ($\underline{L}$) is transformed into $\underline{J}'$. This effect is greatest when A is heavy and B and C light[165], as A can then carry a lot of $\underline{L}$ and the contraction of the Q_2 co-ordinate allows C to escape the interaction rapidly, and hence minimally perturb the AB collision. When the attacking atom is light this $\underline{L} \rightarrow \underline{J}'$ transformation is weakened by "spiralling in". A is now more susceptible to the action of torques caused by the BC potential, and as it approaches, $\underline{L}$ is taken up by rotation of the intermediate while A is constrained to approach along the direction in which $U(\theta)$ is a minimum. This situation is worst in the L + HH/LH case as C departs only slowly, and hence A experiences maximal torque. The final dissociation of AB·C produces $\underline{L}'$ derived from $\underline{J}$ and $\underline{L}$. This mixing is further facilitated when BC has a high moment of inertia, as in L + HH (as opposed to L + LH), since $\underline{J}$ can now increase significantly for only small amounts of attractive energy

release. The heavy BC molecule thus acts as an angular momentum sink, and the resulting $\underline{J}'$ is small.

If the attractive release is high however A may be travelling too fast to follow the path of maximum descent in the FMS so that the mixing is incomplete. Thus for high A_T, $\underline{J}'$ may increase, and some dependence of $\underline{J}'$ on impact parameter or angle of approach is expected. This holds provided the repulsive release (R_T) is small, as otherwise repulsive contributions (see below) can obscure these trends. On very attractive surfaces $\langle f_R' \rangle$ may become very large due to secondary encounters.

In general it is difficult to estimate the value of $\underline{J}'$ resulting from the attractive part of the trajectory due to its curvature on the FMS. This contribution is formally given by

$$J_A' = \mu_{AB} r_{AB}^* v_{rel}^* \sin \gamma^* \qquad 4.21$$

where the co-ordinates are as shown in Fig. 4.11 and the superscript '*' refers to the value at the time of BC separation. The difficulties clearly arise because r_{12}^*, v_1^*, and γ^* cannot be obtained from their initial values without a detailed knowledge of the surface, and so the above qualitative considerations must suffice. In general trajectory calculations have supported these[17].

B: Repulsive surfaces

In this case the repulsive release itself provides a source of $\underline{J}'$. If the BC band is not severed until the A-atom has approached to near r_{AB}^o, then BC repulsion cause a torque on B about A. This torque is maximised when the intermediate is highly bent and $\underline{J}'$ is greatest when A is heavy and B light. The corollany of this is that in

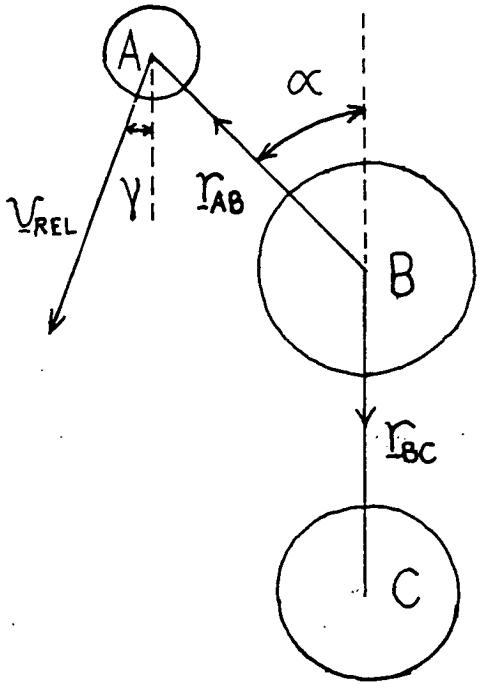

Fig. 4.11. Co-ordinates used in the explanation of sources of rotational excitation (see text for details).

L + HH/HL reactions low $\underline{J}'$ values may result even from bent configurations.

The influence of $\underline{L}$ on $\underline{J}'$ in repulsive encounters is thus much diminished from that in attractive ones for the normal L + LL case, whereas for H + HL the $\underline{L} \rightarrow \underline{J}'$ kinematic conversion is still dominant[166]. For L + HH there is an indirect effect only. Here the orbiting motion of BC tends to continue undisturbed by the attack of A and hence the important conversion is $\underline{J} \rightarrow \underline{L}'$. This is rather less in repulsive encounters or at higher energies where the A-BC interaction can influence BC motion to a greater extent. Since $\underline{J}'$ can be low it follows that when $\underline{L}$ is low and the A-BC interaction weak an apparent $\underline{L} \rightarrow \underline{J}'$ transformation may appear. That this is merely accidental has been illustrated in calculations by increasing $A_{\perp}$ or E_T, both of which result in increased $\underline{J}'$[166].

Repulsive release lends itself more easily to predictions of energy partitioning than attractive release, as attention can be focussed on the outcome of AB-C repulsion from a known configuration and the initial (attractive) part of the trajectory ignored. A number of models have been suggested for this process[167] and used to predict angle and velocity distributions. The DIPR model[161,168] has been used with some success to predict rotational distributions in 2 and 3 dimensions[161] but only in systems where a harpooning mechanism is postulated. In this case BC repulsion begins while A is still quite remote and decays monotonically with time, whereas in a covalent interaction the repulsive force is expected to pass through a maximum and onset at smaller AB separations. Even assuming this restriction is

not problematic, the prediction of trends in $\underline{J}'$ due to kinematic effects is difficult because of a number of parameters which cannot be estimated easily.

Instead therefore, an ultra-simplified impulsive model is offered here, in which the effect of the monotonically decreasing force in the DIPR model is replaced by an instantaneous impulse in the BC bond which releases energy ε. This is partitioned between rotation and translation only and $\langle f_R' \rangle$ and $\langle f_T' \rangle$ determined by conservation laws. ε is not merely the repulsive release R_T in the Polanyi scheme as it must account for part of the mixed release as well. Its exact nature is of no importance to the final predictions however.

In appendix 1 it is shown that the rotational energy derived from this source is given by

$$\langle E_R' \rangle = \varepsilon(1 + \Gamma \operatorname{cosec}^2\alpha^*)^{-1} \left(\frac{r_{AB}^*}{r_{AB}^o} \right)^2 \qquad 4.22$$

where

$$\Gamma = \frac{M_A}{M_B M_C} \cdot \frac{M^3}{\Delta M^2}$$

with $M = M_A + M_B + M_C$, $\Delta M = M_A + M_B - M_C$.

α^* is the ABC angle at the moment of impulse. As expected $\langle E_R' \rangle$ increases with AB bond length and ABC angle. The factor Γ carries the inertial information and is tabulated in Table 4.6 for various mass combinations. From this it is apparent that at a given α^*, $\langle E_R' \rangle$ should increase along the series

L + HH, L + HL, H + LH, H + HL, L + LL, (L + LH, H + LL)

This trend is in relatively good agreement with that found in

H +			L +			
LL	LH	HL	LL	LH	HL	HH
1	$8\,\frac{M_H}{M_L}$	$2\,\frac{M_H}{M_L}$	27	1	$\frac{M_H}{M_L}^2$	$8\,\frac{M_H}{M_L}^3$

Table 4.6. Limiting behaviour of the factor Γ if $M_H >> M_L$ for various mass combinations.

trajectory calculations for small A_T [17]. As A_T increases other contributions to $\langle E_R' \rangle$ (Equ. 4.21) tend to wash out these differences.

If Γ is large then

$$\langle E_R' \rangle \alpha \quad \frac{\sin^2\alpha^* \; r_{AB}^*}{\Gamma} \qquad 4.23$$

The factor Γ for $F + I_2/ICl$ are $\sim 3 \times 10^3$ and $\sim 10^2$ respectively, so that on kinematic grounds alone product rotation in $F + I_2$ is expected to be diminished with respect to F + ICl, even for a repulsive release.

The correct prediction of the trends m $\langle f_R' \rangle$ with changes in inertial property by such a simple model is perhaps surprising. The impulse approximation is the limiting case of the DIPR model as the time during which the force in the BC bond acts tends to zero. This is obviously quite a good approximation for covalent collisions, and is expected to be best for nearly rectilinear trajectories (as in L + HH) where reflection off the repulsive wall of the FAS maximises $\partial U/dr_{BC}$ and hence minimises its time duration.

4.5 Summary and Conclusions

The reaction $F + I_2 \rightarrow IF + I$ produces vibrationally excited, but rotationally cold, product. Kinematic arguments have been preserved which suggest a low $\langle f_R' \rangle$ can result from either attractive or mixed/repulsive energy release for the L + HH mass combination. The AVD measurements, while conflicting with those presented here may not be very informative. $\langle f_R' \rangle$ measurements do not yield any information on $\langle A_T \rangle$ or $\langle R_T \rangle$ for this reaction either, so the nature of the surface, and the role of the light atom effect remains unclear. A more accurate determination of $\langle f_v' \rangle$ for this reaction is thus required. When coupled

with trajectory calculations on realistic surfaces (also for F + ICl) this should yield the desired information. There is also a requirement for further investigations (both theoretical and experimental) into the origin of product rotation.

The discussion has centred mainly on kinematic arguments, but various dynamical problems remain unresolved. In particular the variation of interbond angle in trihalogen intermediates has yet to be considered, and this may only become available when full angle-velocity contour maps are obtained. Similarly the effectiveness (or non-effectiveness) of the well in F + ICl in producing high $\langle f_R' \rangle$ needs analysing theoretically.

Five years ago Grice first wrote of the possible influences on the dynamics of trihalogen reactions[18]. These would still appear to be one of the most rewarding classes of reactions for study, and as such deserve a further investigation.

APPENDIX 1. Classical rotational angular momentum from an impulsive force

In the classical calculation, repulsion of AB is restricted to take place in 2D from an intermediate ABC with co-ordinates given in Fig. A1.1. The centre of mass of ABC is the point $K(x_c,y_c)$ and of AB is $K'(x_c',y_c')$. A, B and C have masses M_1, M_2 and M_3 respectively. The origin of the co-ordinate system is at the midpoint of the BC band. The AB diatom recedes with velocity v_{12} directed parallel to the y-axis, while C recoils with velocity v_3. The translational and rotational energy is assumed to arise only from the impulsive release ε in the BC bond, with vibration of AB ignored. This is assumed to arise from the attractive part of the potential.

Hence

$$\varepsilon = E_T' + E_R' \qquad \text{A1.1}$$

$$= \tfrac{1}{2}\mu_{123}' v_{rel}^2 + \frac{J_{12}^2}{2I_{12}} \qquad \text{A1.2}$$

μ_{123}' is the reduced mass of the AB + C system and v_{rel} its velocity of separation (= $|v_{12}|+|v_3|$). J_{12} and I_{12} are the rotational angular momentum of BC (J') and its moment of inertia.

Thus from A1.2

$$v_{REL}^2 = \frac{2}{\mu_{123}'}\left(\varepsilon - \frac{J_{12}^2}{2I_{12}}\right) \qquad \text{A1.3}$$

Conservation of linear momentum gives

$$v_{12} = \frac{M_3}{M} v_{rel} \quad , \quad v_3 = \frac{M_1 + M_2}{M} v_{rel} \qquad \text{A1.4,5}$$

and of angular momentum

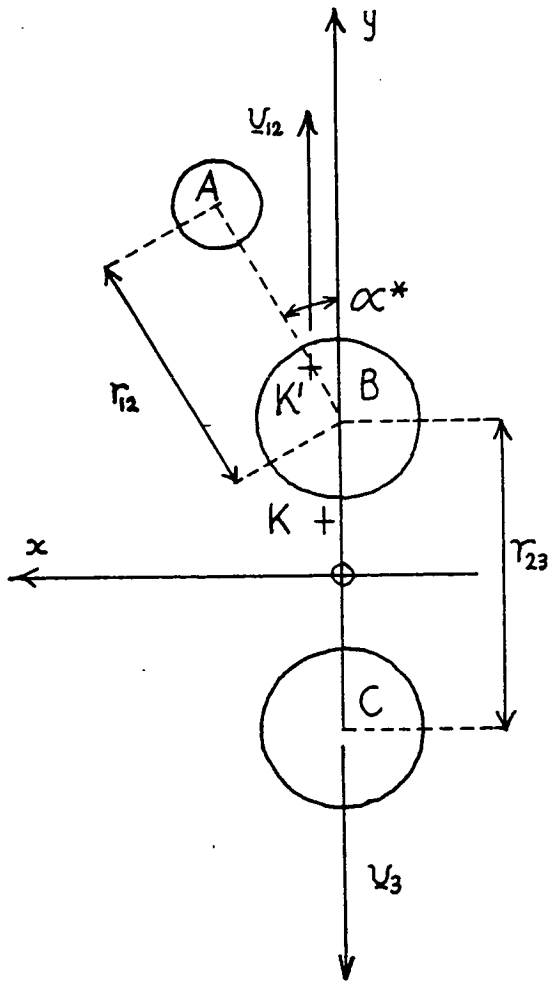

Fig. A1.1. Parameters used in the determination of J' using the impulsive model.

$$-M_3 v_3 x_c + (M_1 + M_2) v_{12} (x'_c - x_c) + J_{12} = 0 \qquad \text{A1.6}$$

from which

$$J_{12} = x_c m_3 (v_3 - v_{12}) \qquad \text{A1.7}$$

From equs. A1.4,5

$$J_{12} = x_c \frac{M_3}{M} v_{rel} \cdot \Delta M \qquad \text{A1.8}$$

where

$$\Delta M = m_1 + m_2 - m_3 \qquad \text{A1.9}$$

Eliminating v_{rel}^2 between A1.3 and A1.8 gives

$$\frac{2\varepsilon}{\mu'_{123}} = J_{12}^2 \left\{ \frac{1}{\mu'_{123} I_{12}} + \frac{M}{m_3}^2 \frac{1}{x_c^2} \frac{1}{\Delta M^2} \right\} \qquad \text{A1.10}$$

Using $x_c = \frac{m_1}{M} r^*_{12} \sin\alpha^*$ and $I_{12} = \frac{1}{\mu_{12} r_{12}^o}$ in A1.10

gives

$$\frac{J_{12}^2}{2\mu_{12} r_{12}^{o2}} = \varepsilon \left(\frac{r^*_{12}}{r_{12}^o} \right)^2 \left(1 + \frac{\Gamma}{\sin^2\alpha^*} \right)^{-1} \qquad \text{A1.11}$$

where $\Gamma = \frac{m_2}{m_1 m_3} \frac{M^3}{\Delta M^2}$ A1.12

APPENDIX 2 : Simulation Program

```
1     %BEGIN
2         %REALSLONG
3         %INTEGER JMAX,OJ,V1MAX,V2MAX,IMELEC,MFLAG
4         %INTEGER K,KHEAD,KR1,KR2,KP1,KP2,KR1A,KR2A,KOR,KOP,KMAX
5         %INTEGER FLAG1,FLAG2,FLAG3,FLAG4,CFLAG1,CFLAG2,CFLAG,HFLAG,VIFLAG
6         %INTEGER NS,VV,NPTS
7         %INTEGER IW,I,NSTEPS,JJ,NJJ,IJ,NB1,NB2,IJMAX,IGCO
8         %INTEGER V1,V2
9         %REAL GCMAX,EGC
10        %REAL LAMBDA1,LAMBDA2,LAMBDAB1,LAMBDAB2,DLAMBDA,LAMBDAC
11        %REAL FFMAX,IJL,FFI,FV
12        %REAL W1,W2,WB1,WB2,WL,WL1,WL2,DWL
13        %REAL WHEAD,WOR,WOP,WV,WE,W0,WLIM
14        %REAL NN,MM,TROT,ZROT,FJLIM,ETOT,MELEC,RNS
15        %REAL FVLIM,FFLIM,FVIBMAX
16        %REAL Q,Q1,Q2,S
17        %REAL BE1,BE2,DE1,DE2,ALPHAE1,ALPHAE2,BETAE1,BETAE2,  %C
C               GAMMAE1,GAMMAE2,OMEGAE1,OMEGAE2,OMEGAXE1,OMEGAXE2,  %C
C               OMEGAYE1,OMEGAYE2,  %C
C               TE1,TE2,G1,G2,AV1,AV2,B1,B2,D1,D2
18        %EXTERNALROUTINESPEC PROMPT(%STRING(15) S)
19        %EXTERNALROUTINESPEC DEFINE(%STRING(63) S)
20        %EXTERNALROUTINESPEC READFILENAME(%STRINGNAME NAME)
21        %EXTERNALINTEGERFNSPEC EXIST(%STRING(63) FILE)
22        %EXTERNALINTEGERFNSPEC RESPONSE(%INTEGERARRAYNAME A, %INTEGER N)
23        %EXTERNALROUTINESPEC GRAPH(%INTEGER N)
24        %EXTERNALREALFNSPEC EXPREAL(%REAL X,Y)
25        %EXTERNALSTRINGFNSPEC ITOS(%INTEGER I)
26        %REALFNSPEC ILASER(%REALNAME W)
27        %REALFNSPEC GAIN(%REAL W)
28        %REALFNSPEC PROT(%INTEGER J)
29        %REALFNSPEC FROT(%INTEGER J)
30        %REALFNSPEC HL(%INTEGERNAME K)
31        %REALFNSPEC LINE(%INTEGER K,OJ)
32        %REALARRAY L(0:20),ISENS(0:20),GC(0:20),WGC(0:20)
33        %OWNINTEGERARRAY REP1(1:2)='Y','N'
34        %OWNINTEGERARRAY REP2(1:2)='T','D'
35        %STRING(8) DATAFILE,OUTFILE,SPECFILE,FCFFILE,VIBINFILE,DETFILE,GAINFILE
36        %CONSTREAL KK=0.6943
37        ! BOLTZMANN'S CONSTANT IN(CM)-1(K)-1 !
38        !
39        ! DEFINE STREAMS:
40        ! ST10--DATA IN:MOLECULAR PARAMS ETC.
41        ! ST11--RESULT OUT:WAVELENGTH DIFFERENCE FROM START
42        !                  VS. RELATIVE INTENSITY
43        ! ST12--ADDITIONAL INFO ON SPECTRA.
44        ! ST14--TOTAL NUMBER AND DETAILS OF AVAILABLE
45        !       FRANK-CONDON FACTORS.
46        ! ST15--VIBRATIONAL PROBABILITIES AND BAND DESCRIPTORS
47        ! ST20--DETECTOR SENSITIVITY CURVE
48        ! ST21--LASER GAIN CURVE
49        !
50        START:
51        NEWLINE;PROMPT('DATAFILE:')
52        READFILENAME(DATAFILE) %UNTIL EXIST(DATAFILE)=1
53        DEFINE('ST10,'.DATAFILE)
54        NEWLINE
55        PROMPT('FCF FILE:')
56        READFILENAME(FCFFILE) %UNTIL EXIST(FCFFILE)=1
57        DEFINE('ST14,'.FCFFILE)
58        SELECTINPUT(10)
59        SETMARGINS(10,15,80)
60        READ(MELEC)
61        ! TOTAL AN.MOMMENTUM. I.E. OMEGA IN COUPLING
```

```
62          ! CASES (A) & (C).
63          READ(TE1);READ(TE2)
64          READ(BE1);READ(BE2)
65          READ(DE1);READ(DE2)
66          READ(ALPHAE1);READ(ALPHAE2)
67          READ(BETAE1);READ(BETAE2)
68          READ(GAMMAE1);READ(GAMMAE2)
69          READ(OMEGAE1);READ(OMEGAE2)
70          READ(OMEGAXE1);READ(OMEGAXE2)
71          READ(OMEGAYE1);READ(OMEGAYE2)
72          READ(V1MAX) ;!PREDISSOCIATION LIMIT
73          SELECTINPUT(0)
74          CLOSESTREAM(10)
75          !
76          ! READ IN SENSITIVITY VS WAVELENGTH. INTERVALS DO NOT
77          ! HAVE TO BE REGULARLY SPACED. NPTS IS THE NUMBER OF ENTRIES
78          ! AND SHOULD NOT EXCEED 21.
79          !
80          NEWLINE;PROMPT('DET. DATA FILE:')
81          READFILENAME(DETFILE) %UNTIL EXIST(DETFILE)=1
82          DEFINE('ST20,'.DETFILE)
83          SELECTINPUT(20)
84          READ(NPTS)
85          %CYCLE I=0,1,NPTS-1
86          READ(L(I));READ(ISENS(I))
87          %REPEAT
88          SELECTINPUT(0)
89          NEWLINE;PROMPT('LASER NORM?')
90          %IF RESPONSE(REP1,2)='Y' %THENSTART
91          FLAG4=1
92          !READ IN GAIN CURVE
93          !SAME COMMENTS APPLY AS FOR DETECTOR SENSITIVITY CURVE
94          NEWLINE;PROMPT('LASER FILE:')
95          READFILENAME(GAINFILE) %UNTIL EXIST(GAINFILE)=1
96          DEFINE('ST21,'.GAINFILE)
97          SELECTINPUT(21)
98          GCMAX=0
99          READ(IGC0)
100         %CYCLE I=0,1,IGC0-1
101         READ(EGC)
102         WGC(I)=1.0@8/EGC
103         READ(GC(I))
104         %IF GC(I)>GCMAX %THEN GCMAX=GC(I)
105         %REPEAT
106         %CYCLE I=0,1,IGC0-1
107         GC(I)=GC(I)/GCMAX
108         %REPEAT
109         %FINISHELSE FLAG4=0
110         !
111         !READ AVAILABLE FRANC-CONDON FACTORS !
112         !
113         SELECTINPUT(14)
114         CLOSESTREAM(20)
115         READ(NJJ)
116         %BEGIN
117             %INTEGER LFLAG
118             %INTEGERARRAY FV1(1:NJJ),FV2(1:NJJ)
119             %INTEGERARRAY FV2LIM(0:V1MAX)
120             %REALARRAY FCF(1:NJJ)
121             ! NJJ IS THE NUMBER OF BANDS FOR WHICH INFO ON FCF'S IS AVAILABLE
122             %REALFNSPEC SENS(%REAL X)
123             %REALFNSPEC SCORR(%INTEGER J)
124             %REALFNSPEC FCFACTOR(%INTEGER I1,I2)
125             %CYCLE V1=0,1,V1MAX
```

```
126             FV2LIM(V1)=0
127             %REPEAT
128             %CYCLE JJ=1,1,NJJ
129             READ(V1);READ(V2);READ(FCF(JJ))
130             FV1(JJ)=V1;FV2(JJ)=V2
131             %IF V1<=V1MAX %THENSTART
132             %IF V2>FV2LIM(V1) %THEN FV2LIM(V1)=V2
133             %FINISH
134             %REPEAT
135             SELECTINPUT(0)
136             CLOSESTREAM(14)
137             !
138             NEWSPEC:
139             OFLAG1=0;OFLAG2=0
140             SELECTINPUT(0)
141             NEWLINE; PROMPT('START:');READ(LAMBDA1)
142             NEWLINE; PROMPT('FINISH:');READ(LAMBDA2)
143             NEWLINE; PROMPT('INTERVAL:'); READ(DLAMBDA)
144             NEWLINE; PROMPT('LASER FWHM:'); READ(DWL)
145             NEWLINE;PROMPT('THERM OR DYN:')
146             %IF RESPONSE(REP2,2)='T' %THENSTART
147             NEWLINE;PROMPT('FRAC.LIM.TO J:');READ(FJLIM)
148             NEWLINE;PROMPT('HOMONUC?')
149             %IF RESPONSE(REP1,2)='Y' %THENSTART
150             NEWLINE;PROMPT('2*NUC.SPIN:');READ(NS)
151             OFLAG2=1
152             %IF NS-(NS//2*2)=0 %THEN RNS=(NS//2+1.)/(NS//2)  %C
  C              %ELSE RNS=(NS/2.)/(NS/2.+1)
153             ! RNS IS THE RATIO OF POPULATIONS OFSTATES OF EVEN
154             ! ROTATIONAL A.M. TO THOSE OF  ODD ROTAIONAL A.M., ASSUMING THAT
155             ! THE GROUND ELECTRONIC STATE IS TOTALLY SYMMETRIC.
156             !
157             %FINISH
158             NEWLINE;PROMPT('FRAC.LIM.TO V:');READ(FVLIM)
159             %FINISHELSESTART
160             NEWLINE;PROMPT('ETOT:');READ(ETOT)
161             OFLAG1=1
162             %FINISH
163             NEWLINE;PROMPT('OUTPUT FILE:');READFILENAME(OUTFILE)
164             DEFINE('ST12,'.OUTFILE)
165             SELECTOUTPUT(12)
166             %IF OFLAG1=1 %THENSTART
167             PRINTSTRING('DYNAMIC SIMULATION FROM DATAFILE ');PRINTSTRING(DATAFILE)
168             NEWLINE;PRINTSTRING('TOTAL ENERGY =');PRINTFL(ETOT,4)
169             %FINISHELSESTART
170             PRINTSTRING('THERMAL SIMULATION FROM DATAFILE ');PRINTSTRING(DATAFILE)
171             NEWLINE;PRINTSTRING('FRACTIONAL LIMIT TO ROTATIONAL SENSITIVITY =')
172             ;PRINT(FJLIM,1,3)
173             NEWLINE;PRINTSTRING('FRACTIONAL LIMIT TO VIBRATIONAL SENSITIVITY =')
174             PRINT(FVLIM,1,3)
175             %FINISH
176             NEWLINE;PRINTSTRING('START OF SPECTRA = ');PRINT(LAMBDA1,4,2)
177             NEWLINE;PRINTSTRING('END OF SPECTRA = ');PRINT(LAMBDA2,4,2)
178             NEWLINE;PRINTSTRING('INTERVAL = ');PRINT(DLAMBDA,2,2)
179             NEWLINE;PRINTSTRING('LASER FWHM = ')
180             PRINT(DWL,4,2)
181             NEWLINES(2)
182             PRINTSTRING('VIBRATIONAL BANDS SUMMED OVER')
183             NEWLINES(2)
184             PRINTSTRING('V1 V2  JMAX PROB. TROT   HEAD   ORIGIN   LIMIT       FCF')
185             LAMBDAC=(LAMBDA1+LAMBDA2)/2.
186             DWL=1.@8*DWL/LAMBDAC/LAMBDAC
187             NSTEPS=INT((LAMBDA2-LAMBDA1)/DLAMBDA)
188             W1=1.@8/LAMBDA1
```

```
189             %2=1.@6/LAMBDA2
190             IMELEC=INTPT(MELEC+0.001)
191             MFLAG=INTPT(MELEC-IMELEC+0.6)
192             ! MFLAG=1 IF MELEC IS HALFINTEGERAL
193             ! MFLAG=0 IF MELEC IS INTEGERAL
194             KOR=IMELEC
195             KOP=IMELEC+1
196             NEWLINES(2);PROMPT("VIB. DATA FILE:")
197             READFILENAME(VIBINFILE) %UNTIL EXIST(VIBINFILE)=1 %OR VIBINFILE=".TT"
198             %IF VIBINFILE=".TT" %THEN VIFLAG=1 %ELSE VIFLAG=0
199             DEFINE("ST15,".VIBINFILE)
200             SELECTINPUT(15)
201             %IF VIFLAG=1 %THEN PROMPT("V2 MAX:")
202             READ(V2MAX) ;! EXOERGICITY OR OTHER LIMIT
203             VV=(V2MAX+1)*(V1MAX+1)
204             !
205             %BEGIN
206                 %REALARRAY FVIB(0:V2MAX),TROTI(0:V2MAX)
207                 %INTEGERARRAY NNI(0:V2MAX),MMI(0:V2MAX),JL(0:V2MAX)
208                 %INTEGERARRAY JV1(1:VV),JV2(1:VV)
209                 %REALARRAY N(0:NSTEPS)
210                 %CYCLE IW=0,1,NSTEPS
211                 N(IW)=0
212                 %REPEAT
213                 %CYCLE V2=0,1,V2MAX
214                 %IF VIFLAG=1 %THEN PROMPT(ITOS(V2).":")
215                 READ(FVIB(V2))
216                 %IF OFLAG1=0 %THEN READ(TROTI(V2))  %C
  C              %ELSESTART
217                 READ(MMI(V2))
218                 READ(NNI(V2))
219                 %FINISH
220                 %REPEAT
221                 IJ=0
222                 FFMAX=0
223                 %CYCLE V2=0,1,V2MAX
224                 !
225                 !DETERMINE APPROX. J VALUE OF MOSTINTENSE CONTRIBUTION
226                 ! HL FACTOR IS ASSUMED TO BE PPNL. TO J.
227                 !
228                 AV2=V2+0.500000000000
229                 G2=OMEGAE2*AV2-OMEGAXE2*AV2*AV2  %C
  C              +OMEGAYE2*AV2*AV2*AV2
230                 B2=BE2-ALPHAE2*AV2+GAMMAE2*AV2*AV2
231                 D2=DE2+BETAE2*AV2
232                 !
233                 %IF OFLAG1=0 %THENSTART
234                 TROT=TROTI(V2)
235                 ZROT=B2/KK/TROT
236                 ! MAX VALUE OF J*FROT IS:
237                 K=INTPT(SQRT(1+8/ZROT)/4)
238                 IJL=FROT(K)*K
239                 JL(V2)=K
240                 %UNTIL K*FROT(K)<FJLIM*IJL %THEN K=K+1
241                 %FINISHELSESTART
242                 MM=MMI(V2);NN=NNI(V2)
243                 %IF G2>ETOT %THEN ->STARTSIM
244                 JMAX=INTPT(SQRT((ETOT-G2)/B2))
245                 !MAX. VALUE OF J*PROT IS:
246                 K=INTPT(JMAX*EXPREAL(MM*NN+1,-1/NN))
247                 IJL=PROT(K)*K
248                 JL(V2)=K
249                 %UNTIL K*PROT(K)<FJLIM*IJL %THEN K=K+1
250                 %FINISH
```

```
251             JMAX=K
252             ! FIRST ESTIMATE OF ROTATIONAL LIMIT
253             !
254             %CYCLE V1=0,1,V1MAX
255             !
256             AV1=V1+0.500000000000000
257             G1=OMEGAE1*AV1-OMEGAXE1*AV1*AV1  %C
  C             +OMEGAYE1*AV1*AV1*AV1
258             B1=BE1-ALPHAE1*AV1+GAMMAE1*AV1*AV1
259             D1=DE1+BETAE1*AV1
260             WV=G1-G2
261             WE=TE1-TE2
262             W0=WE+WV
263             !
264             WLIM=LINE(JMAX*IMELEC,1)+W0
265             !ESTIMATE BANDHEAD
266             K=IMELEC
267             %WHILE LINE(K,1)>LINE(K+1,1) %THEN K=K+1
268             WHEAD=LINE(K,1)+W0
269             ! SEE IF BAND LIES IN INTERVAL(W1,W2)
270             %IF WHEAD>W2 %AND WLIM<W1 %THENSTART
271             !ACCEPTED BAND
272             IJ=IJ+1
273             JV1(IJ)=V1
274             JV2(IJ)=V2
275             FFI=FCFACTOR(V1,V2)*FVIB(V2)
276             %IF FFI>FFMAX %THEN FFMAX=FFI
277             %FINISH
278             %REPEAT
279             %REPEAT
280             STARTSIM:IJMAX=IJ
281             !NO. OF BANDS IN SPEC
282             ! NOW REVISE LIMITS FOR ACCEPTED BANDS
283             !AND CALCULATE SPECTRUM
284             FVIBMAX=0
285             %CYCLE IJ=1,1,IJMAX
286             V1=JV1(IJ);V2=JV2(IJ)
287             AV2=V2+0.500000000000
288             G2=OMEGAE2*AV2-OMEGAXE2*AV2*AV2  %C
  C             +OMEGAYE2*AV2*AV2*AV2
289             B2=BE2-ALPHAE2*AV2+GAMMAE2*AV2*AV2
290             D2=DE2+BETAE2*AV2
291             AV1=V1+0.500000000000000
292             G1=OMEGAE1*AV1-OMEGAXE1*AV1*AV1  %C
  C             +OMEGAYE1*AV1*AV1*AV1
293             B1=BE1-ALPHAE1*AV1+GAMMAE1*AV1*AV1
294             D1=DE1+BETAE1*AV1
295             WV=G1-G2
296             WE=TE1-TE2
297             W0=WE+WV
298             LFLAG=0
299             %IF FVIB(V2)>FVIBMAX %THEN FVIBMAX=FVIB(V2)
300             FV=FCFACTOR(V1,V2)*FVIB(V2)/FFMAX
301             %IF LFLAG=1 %THEN -> OUTPUT
302             K=JL(V2)
303             S=SCORR(V1)
304             ! DETECTOR SENSITIVITY TO FLUORESCENCE CORRECTION
305             %IF OFLAG1=0 %THENSTART
306             TROT=TROTI(V2)
307             ZROT=B2/KK/TROT
308             IJL=K*FROT(K)
309             FFLIM=FJLIM*FROT(K)*K/FV
310             %IF IJL<FFLIM %THEN ->NEXT
311             %UNTIL K*FROT(K)<FFLIM %THEN K=K+1
```

```
312                 %FINISHELSESTART
313                 MM=MMI(V2);NN=NNI(V2)
314                 FFLIM=FJLIM*PROT(K)*K/FV
315                 %IF IJL<FFLIM %THEN K=K+1
316                 %FINISH
317                 !
318                 JMAX=K
319                 !
320                 KMAX=JMAX+IMELEC
321                 SELECTINPUT(0)
322                 CLOSESTREAM(15)
323                 !
324                 ! FROM HERE ON K LABELS THE INTEGRAL PART OF THE TOTAL
325                 ! ANG.MOMMENTUM (ELECTRON SPIN+MOTION PLUS NUCLEAR MOTION).
326                 ! K0R AND K0P ARE THE LABELS FOR THE STRANSITIONS STARTING
327                 ! AT THE LOWEST VALUE OF J(TOTAL A.M.) COMPATIBLE WITH CONSERVATION
328                 ! REQUIREMENTS. NOTE HOWEVER THAT JMAX  IS A NUCLEAR
329                 ! ROTATIONAL Q.NO.,WHEREAS KMAX IS ALABEL FOR THE TRANSITIONS STARTING
330                 ! FROM THE VALUE OF J WHICH HAS ROTATIONAL A.M. JMAX.
331                 ! THE AUTHOR APOLOGISES FOR THE AMPLE ROOM FOR CONFUSION HERE.
332                 !
333                 %BEGIN
334                     !
335                     %REALARRAY P(K0P:KMAX),R(K0R:KMAX)
336                     ! FREQUENCIES OF LINES IN BRANCHES !
337                     !
338                     DJ=1
339                     %CYCLE K=K0R+1,KMAX
340                     R(K)=LINE(K,DJ)+W0
341                     %REPEAT
342                     !
343                     DJ=-1
344                     %CYCLE K=K0P+1,KMAX
345                     P(K)=LINE(K,DJ)+W0
346                     %REPEAT
347                     %CYCLE K=K0R+1,KMAX-1
348                     %IF R(K)>R(K+1) %THENSTART
349                     KHEAD=K
350                     WHEAD=R(KHEAD)
351                     HFLAG=1
352                     -> FIXORIGIN
353                     %FINISH
354                     %REPEAT
355                     ! NO BANDHEAD
356                     WHEAD=W0R
357                     KHEAD=K0R
358                     HFLAG=0
359                     FIXORIGIN:W0P=P(K0P)
360                     W0R=R(K0R)
361                     WLIM=P(KMAX)
362                     ! TEST TO SEE IF BAND LIES IN THE INTERVAL(W1,W2) !
363                     %IF WLIM>W1 %THEN -> SKIPGEN
364                     %IF WHEAD<W2 %THEN -> SKIPGEN
365                     ! DETERMINE POSITION WHICH WILL JUST INCLUDE THE
366                     ! LINES AT THE HIGHEST AND THE LOWEST FREQUENCIES.
367                     WB1=WHEAD+DWL
368                     LAMBDAB1=1.@8/WB1
369                     NB1=INTPT((LAMBDAB1-LAMBDA1)/DLAMBDA)
370                     NB1=0 %IF NB1<0
371                     WB2=WLIM-DWL
372                     LAMBDAB2=1.@8/WB2
373                     NB2=INTPT((LAMBDAB2-LAMBDA1)/DLAMBDA)+1
374                     NB2=NSTEPS %IF NB2>NSTEPS
375                     !
```

```
376                     ! SUM STATES FOR THEIS BAND
377                     !
378                     %CYCLE IW=NB1,1,NB2
379                     WL=1.88/(LAMBDA1+IW*DLAMBDA)
380                     WL1=WL-DWL
381                     WL2=WL+DWL
382                     ! CHECK TO SEE IF LASER LINE IS AT TOO HIGH
383                     ! A FREQUENCY TO CONTAIN ANY LINES
384                     %IF WL1> WHEAD %THEN G=0 %AND -> ADDUP
385                     FLAG3=1
386                     ! ASSUME THAT  R(KMAX) IS LESS THAN THE LOWEST LASER
387                     ! FREQUENCY. IF NOT THEN FLAG3 WILL BE SET=0 LATER.
388                     ! CHECK TO SEE IF THE LASER LINE PROFILE WILL CONTAIN
389                     ! ANY LINES IN THE BANDHEAD.
390                     %IF WL2>WOR %AND HFLAG=1  %THEN -> ABNORMAL %ELSESTART
391                     FLAG2=0
392                     ! SINGLE SUM IN R-BRANCH
393                     FLAG1=1
394                     ! CONTRIBUTION FROM P-BRANCH
395                     ! UNLESS WL1>WOP.
396                     ! CHECK FOR THIS NOW.
397                     %IF WL1>WOP %THEN FLAG1=0 %AND -> L20
398                     K=K0P
399                     TESTKP2:%IF P(K)>WL2 %THENSTART
400                     %IF K=KMAX %THEN -> SETKP2
401                     K=K+1
402                     -> TESTKP2
403                     %FINISH
404                     SETKP2:KP2=K
405                     TESTKP1:%IF P(K)>WL1 %THENSTART
406                     %IF K=KMAX %THEN -> SETKP1
407                     K=K+1
408                     -> TESTKP1
409                     %FINISH
410                     SETKP1:KP1=K
411                     ! CHECK TO SEE IF LASER LINE LIES BEYOND KMAX
412                     ! CUTOFF IN R-BRANCH
413                     %IF WL2<R(KMAX)%THENSTART
414                     FLAG3=0
415                     ! NO CONTRIBUTION FROM R-BRANCH
416                     -> L100
417                     %FINISH
418                     L20:K=K0R
419                     TESTKR2:%IF R(K)>WL2 %THENSTART
420                     %IF K=KMAX %THEN -> SETKR2
421                     K=K+1
422                     -> TESTKR2
423                     %FINISH
424                     SETKR2:KR2=K
425                     TESTKR1:%IF R(K)>WL1 %THENSTART
426                     %IF K=KMAX %THEN -> SETKR1
427                     K=K+1
428                     -> TESTKR1
429                     %FINISH
430                     SETKR1:KR1=K
431                     -> L100
432                     %FINISH
433                     !
434                     ABNORMAL:
435                     ! VARIOUS CONDITIONS FOR WAYS IN WHICH PART OF THE LASER
436                     ! LINE PROFILE MY OVERLAP THE BANDHEAD NOW FOLLOW.
437                     !
438                     FLAG1=1
439                     ! ASSUME CONTRIBUTION FROM P-BRANCH. IF THIS IS NOT SO FLAG1
```

```
440                     ! WILL LATER BE SET=0.
441                     FLAG2=1
442                     ! THERE WILL BE TWO SETS OF LINES IN THE R-BRANCH TO BE
443                     ! SUMMED OVER IF THE LASER LINE OVERLAPS THE BANDHEAD.
444                     !
445                     %IF WL1<=W0P %AND W0R<WL2<WHEAD %THENSTART
446                     ! CASE B:2 DISCONTINUOUS SUMS IN R-BRANCH
447                     !        :NORMAL SUM IN P-BRANCH
448                     KR1A=K0P
449                     KP2=K0P
450                     K=K0P
451                     %WHILE P(K)>WL1 %THENCYCLE
452                      K=K+1
453                     %IF K=KMAX %THEN KP1=KMAX+1 %ANDEXIT
454                     %REPEAT
455                     KP1=K-1
456                     K=K0R
457                     %WHILE R(K)<WL2 %THENCYCLE
458                      K=K+1
459                     %IF K=KMAX %THEN KR2A=KMAX+1 %ANDEXIT
460                     %REPEAT
461                     KR2A=K-1
462                     K=KHEAD
463                     %WHILE R(K)>WL2 %THENCYCLE
464                      K=K+1
465                     %IF K=KMAX %THEN KR2=KMAX+1 %ANDEXIT
466                     %REPEAT
467                     KR2=K
468                     %WHILE R(K)>WL1 %THENCYCLE
469                      K=K+1
470                     %IF K=KMAX %THEN KR1=KMAX+1 %ANDEXIT
471                     %REPEAT
472                     KR1=K-1
473                     ->L100
474                     %FINISH
475                     !
476                     %IF W0P<WL1<WHEAD %AND W0R<WL2<WHEAD %THENSTART
477                     ! CASE C:2 DISCONTINUOUS SUMS IN R-BRANCH
478                     !        :NO SUM IN P-BRANCH
479                     K=K0R
480                     %WHILE R(K)<WL1 %THENCYCLE
481                      K=K+1
482                     %IF K=KMAX %THEN KR1A=KMAX+1 %ANDEXIT
483                     %REPEAT
484                     KR1A=K
485                     %WHILE R(K)<WL2 %THENCYCLE
486                      K=K+1
487                     %IF K=KMAX %THEN KP2A=KMAX+1 %ANDEXIT
488                     %REPEAT
489                     KR2A=K-1
490                     K=KHEAD
491                     %WHILE R(K)>WL2 %THENCYCLE
492                      K=K+1
493                     %IF K=KMAX %THEN KR2=KMAX+1 %ANDEXIT
494                     %REPEAT
495                     KR2=K
496                     %WHILE R(K)>WL1 %THENCYCLE
497                      K=K+1
498                     %IF K=KMAX %THEN KR1=KMAX+1 %ANDEXIT
499                     %REPEAT
500                     KR1=K-1
501                     FLAG1=0
502                     ! NO SUM OVER THE P-BRANCH !
503                     -> L100
```

```
504                     %FINISH
505                     !
506                     %IF WL1<=WOP %AND WL2>=WHEAD %THENSTART
507                     ! CASE D:2 CONTINUOUS SUMS IN R-BRANCH
508                     !        :NORMAL SUM INP-BRANCH
509                     KP2=KOP
510.                    KR1A=KOR
511                     KR2A=KHEAD
512                     KR2=KHEAD+1
513                     K=KOP
514                     %WHILE P(K)>WL1 %THENCYCLE
515                      K=K+1
516                     %IF K=KMAX %THEN KP1=KMAX+1 %ANDEXIT
517                     %REPEAT
518                     KP1=K-1
519                     K=KHEAD
520                     %WHILE R(K)>WL1 %THENCYCLE
521                      K=K+1
522                     %IF K=KMAX %THEN KR1=KMAX+1 %ANDEXIT
523                     %REPEAT
524                     KR1=K-1
525                     -> L100
526                     %FINISH
527                     !
528                     %IF WOP<WL1<WHEAD %AND WL2>=WHEAD %THENSTART
529                     ! CASE E:2 CONTINUOUS SUMS IN R-BRANCH
530                     !        :NO SUM IN P-BRANCH
531                     KR2A=KHEAD
532                     KR2=KHEAD+1
533                     K=KOR
534                     %WHILE R(K)<WL1 %THENCYCLE
535                      K=K+1
536                     %IF K=KMAX %THEN KR1A=KMAX+1 %ANDEXIT
537                     %REPEAT
538                     KR1A=K
539                     K=KHEAD
540                     %WHILE R(K)>WL1 %THENCYCLE
541                      K=K+1
542                     %IF K=KMAX %THEN KR1=KMAX+1 %ANDEXIT
543                     %REPEAT
544                     KR1=K-1
545                     FLAG1=0
546                     %FINISH
547                     !
548                     L100:
549                     ! YES FOLKS HERE IT IS AT LAST!
550                     ! SUM CONTRIBUTIONS FOR THE VARIOUS PARTS OF THE TWO BRANCHES.
551                     !
552                     DJ=1
553                     Q=0
554                     ! SUM CONTRIBUTION FROM R=BRANCH IF PRESENT
555                     %IF FLAG3=1 %THENSTART
556                     %IF KR1<KR2 %THEN -> L120
557                     ! THESE "INVERSE" ASSIGNMENTS OCCUR WHEN THE LASER
558                     ! FWHM IS SO SMALL OR THE LINE SPACING IN ANY ONE
559                     ! BRANCH SO LARGE THAT THERE ARE NO LINES UNDER THE
560                     ! LASER LINE PROFILE IN WHICH CASE THE CONTRIBUTION
561                     ! IS ZERO.
562                     %IF KP2=KR1 %THENSTART
563                     Q1=ILASER(R(KR1))*HL(KR1)
564                     %IF OFLAG1=1 %THEN G1=G1*PROT(KR1-IMELEC) %ELSE Q1=G1*FPOT(KR1-IMELEC)
565                     Q=Q+Q1
566                     -> L120
567                     %FINISH
```

```
568                 %CYCLE K=KR2,1,KR1
569                 G1=ILASER(R(K))*HL(K)
570                 %IF OFLAG1=1 %THEN G1=G1*PROT(K-IMELEC) %ELSE G1=G1*FROT(K-IMELEC)
571                 G=G+G1
572                 %REPEAT
573                 %FINISH
574                 L120:
575                 !
576                 ! NOW SUM CONTRIBUTION FROM LOWER K PART OF R=BRANCH.
577                 !
578                 %IF FLAG2=1 %THENSTART
579                 %IF KR1A>KR2A %THEN -> L140
580                 %IF KR1A=KR2A %THENSTART
581                 G1=ILASER(R(KR1A))*HL(KR1A)
582                 %IF OFLAG1=1 %THEN G1=G1*PROT(KR1A-IMELEC) %ELSE G1=G1*FROT(KR1A-IMELEC
583                 G=G+G1
584                 -> L140
585                 %FINISH
586                 %CYCLE K=KR1A,1,KR2A
587                 G1=ILASER(R(K))*HL(K)
588                 %IF OFLAG1=1 %THEN G1=G1*PROT(K-IMELEC) %ELSE G1=G1*FROT(K-IMELEC)
589                 G=G+G1
590                 %REPEAT
591                 %FINISH
592                 L140:
593                 !
594                 ! NOW SUM CONTRIBUTION FROM P-BRANCH.
595                 !
596                 DJ=-1
597                 %IF  FLAG1=1 %THENSTART
598                 %IF KP1<KP2 %THEN -> ADDUP
599                 %IF KP1=KP2 %THENSTART
600                 G1=ILASER(P(KP1))*HL(KP1)
601                 %IF OFLAG1=1 %THEN G1=G1*PROT(KP1-IMELEC) %ELSE G1=G1*FROT(KP1-IMELEC)
602                 G=G+G1
603                 -> ADDUP
604                 %FINISH
605                 %CYCLE K=KP2,1,KP1
606                 G1=ILASER(P(K))*HL(K)
607                 %IF OFLAG1=1 %THEN G1=G1*PROT(K-IMELEC) %ELSE G1=G1*FROT(K-IMELEC)
608                 G=G+G1
609                 %REPEAT
610                 %FINISH
611                 ADDUP:
612                 !
613                 ! THE NUMBER OF EXCITATIONS CAUSED BY THE LASER LINE
614                 ! AT THE FREQUENCY CORRESPONDING TO IW IS THEN----
615                 !
616                 G2=G*FCFACTOR(V1,V2)
617                 G2=G2*FVIB(V2)*S
618                 N(IW)=N(IW)+G2
619                 !
620                 %REPEAT
621                 SKIPGEN:
622                 %END !!LEVEL 4

623               !
624               OUTPUT:SELECTOUTPUT(12)
625               NEWLINE;WRITE(V1,2);WRITE(V2,2)
626               %IF LFLAG=0 %THEN WRITE(JMAX,4) %ELSE PRINTSTRING('  N.A. ')
627               ;PRINT(FVIS(V2)/FVISMAX,1,3)
628               PRINT(TROTI(V2),4,1)
629               %IF LFLAG=0 %THEN PRINT(1.28/WHEAD,4,2) %ELSE PRINTSTRING('   N.A.  ')
630               PRINT(1.28/W0,4,2)
```

```
631             %IF LFLAG=0 %THEN PRINT(1.C@8/WLIM,4,2)%ELSE PRINTSTRING('  N.A.  ')
632             %IF LFLAG=0 %THENSTART
633             SPACES(3)
634             PRINT(FCFACTOR(V1,V2),1,4)
635             %FINISHELSE PRINTSTRING('N.A.')
636             NEXT:%REPEAT
637             !
638             SELECTOUTPUT(0)
639             CLOSESTREAM(12)
640             NEWLINE;PROMPT('SPECTRA FILE:');READFILENAME(SPECFILE)
641             DEFINE('ST11,'.SPECFILE)
642             SELECTOUTPUT(11)
643             %CYCLE IW=0,1,NSTEPS
644             NEWLINE;PRINT(IW*DLAMBDA,2,2);PRINTFL(N(IW),4)
645             %REPEAT
646             SELECTOUTPUT(0)
647             CLOSESTREAM(11)
648             %END ;!LEVEL 3

649         !
650         SELECTOUTPUT(0)
651         CFLAG=0
652         NEWLINE;PRINTSTRING(' SIMULATION COMPLETE')
653         NEWLINE;PROMPT('GRAPH?')
654         %IF RESPONSE(REP1,2)='Y' %THEN GRAPH(NSTEPS+1)
655         NEWLINE;PROMPT('CONTINUE?')
656         %IF RESPONSE(REP1,2)='Y' %THENSTART
657         NEWLINE;PROMPT('SAME SYSTEM?')
658         %IF RESPONSE(REP1,2)='Y' %THEN -> NEWSPEC %ELSE CFLAG=1
659         %FINISH
660         !
661         %REALFN FCFACTOR(%INTEGER V1,V2)
662             ! FINDS FCF'S FROM LIST  ARRAY FCF USING INDEX ARRAYS FV1,FV2
663             ! IF FCF IS UNAVAILABLE RETURNS VALUE = 0 AND SETS LFLAG=1
664             !
665             %INTEGER I
666             %CYCLE I=1,1,NJJ
667             %IF FV1(I)=V1 %AND FV2(I)=V2 %THENRESULT=FCF(I)
668             %REPEAT
669             LFLAG=1
670             %RESULT=0
671             %END ;! FCFACTOR

672         !
673         %REALFN SENS(%REAL LAMBDA)
674             %REAL S1,S2,DS,L1,L2,DL
675             %CYCLE I=0,1,NPTS-1
676             %IF L(I)>LAMBDA %THEN -> INTERP
677             %REPEAT
678             %RESULT=0 ;! SENSITIVITY=0 AT LONGEST WAVELENGTHS.
679             !
680             INTERP:
681             S1=ISENS(I-1);S2=ISENS(I)
682             L1=L(I-1);L2=L(I)
683             DS=S2-S1
684             DL=L2-L1
685             %RESULT=S1+DS*(LAMBDA-L1)/DL
686             %END ;!SENS

687         !
688         %REALFN SCORR(%INTEGER V1)
689             %REAL U,S,SIGMA,G2,W0,W03,W3
690             %INTEGER V2
691             SIGMA=0
```

```
692                 %3=0
693                 %CYCLE V2=0,1,FV2LIM(V1)
694                 U=V2+0.5000000000
695                 G2=OMEGAE2*U-OMEGAXE2*U*U+OMEGAYE2*U*U*U
696                 W0=(TE1-TE2)+(G1-G2)
697                 W03=W0*W0*W0*1.0@-12
698                 W3=W3+W03*FCFACTOR(V1,V2)
699                 LFLAG=0
700                 %REPEAT
701                 V2=0
702                 %CYCLE
703                 U=V2+0.500000000000
704                 G2=OMEGAE2*U-OMEGAXE2*U*U+OMEGAYE2*U*U*U
705                 W0=(TE1-TE2)+(G1-G2)
706                 W03=W0*W0*W0*1.0@-12
707                 S=SENS(1.0@8/W0)
708                 %IF S<1.0@0@-3 %THENEXIT
709                 SIGMA=SIGMA+S*FCFACTOR(V1,V2)*W03
710                 V2=V2+1
711                 LFLAG=0 ;! SUPRESS TEMP. FCF FAULT.
712                 %REPEAT
713                 %RESULT=SIGMA/W3
714                 %END ;!SCORR

715             !
716             %END ;!LEVEL 2.

717         %IF CFLAG=1 %THEN -> START
718         !
719         %REALFN ILASER(%REALNAME W)
720             !
721             ! CALCULATES THE INTENSITY OF THE LASER "LINE" AT FREQUENCY
722             ! W (IN (CM)-1), ASSUMING A TRIANGULAR LINE PROFILE WITH
723             ! FWHM=DWL.
724             !
725             %REAL DW,ILMAX
726             %IF FLAG4=0 %THEN ILMAX=1 %ELSE ILMAX=GAIN(W)
727             ! UNNORMALISED LASER PEAK INTENSITY !
728             DW=MOD(W-WL)
729             %IF DW>=DWL %THENRESULT=0 %ELSERESULT=ILMAX*(DWL-DW)/DWL
730             %END ;!ILASER!

731         !
732         %REALFN PROT(%INTEGER J)
733             !
734             ! CALCULATES  A 2-PARAMETER ROTATIONAL DISTRIBUTION
735             ! OF A LIEU AND PARSONS TYPE (SEE J. CHEM. PHYS.
736             ! VOL 67.,1814,(1977).
737             ! NOTE THAT WHEN THIS FUNCTION IS CALLED ABOVE THE
738             ! QU. NO. K-1  GIVES THE ROTATION OF THE NUCLEUS, -N
739             ! IN HERZBERG'S NOTATION FOR CASE (A) COUPLING . SEE VOL 1.
740             ! P.219
741             !
742             %REAL R
743             R=1-EXPREAL(J/JMAX,NN)
744             %IF R>0 %THENRESULT=EXPREAL(R,MM) %ELSERESULT=0
745             %END ;!PROT

746         !
747         %REALFN FROT(%INTEGER J)
748             !
749             ! THIS ROUTINE CALCULATES THERMAL ROTATIONAL
750             ! DISTRIBUTIONS ACCORDING TO BOLTZMANN'S LAW
751             ! SAME COMMENTS APPLY TO PARAMETERS AS IN PROT.
```

```
752             !
753             %REAL A
754             A=EXP(-ZROT*J*(J+1))*ZROT
755             ! NORMALISED PROB. FOR COMPARISON OF BANDS
756             ! AT DIFFERENT TROT.
757             %RESULT=A %IF OFLAG2=0
758             ! NO NUCLEAR SPIN RESTRICTIONS
759             %IF J-(J//2*2)=0 %THENRESULT=RNS*A %ELSERESULT=A
760             ! SCALING FOR EVEN LEVELS
761             %END ;!FROT

762         !
763         %REALFN HL(%INTEGERNAME K)
764             !
765             ! CALCULATES HOML-LONDON FACTORS GIVEN THE PARAMETER K.
766             ! THE TOTAL A.M. IS GIVEN BY K+1/2.
767             ! THE EXPRESSIONS USED ARE FROM HERZBERG VOL 1. P.208.
768             ! SIMPLIFIED FOR PURE CASE(A) OR (C) COUPLING
769             ! DJ=+1 :R-BRANCH
770             ! DJ=-1 :P-BRANCH
771             !
772             %REAL J,JA
773             J=K+MFLAG/2
774             JA=J+0.50000000000 +DJ/2
775             %RESULT=JA
776             %END ;!HL

777         !
778         %REALFN LINE(%INTEGER K,DJ)
779             !
780             ! CALCULATES FREQUENCY OF LINES FROM SPECTROSCOPIC
781             ! CONSTANTS.
782             !
783             %REAL J1,J2,T1,T2
784             J2=K+MFLAG/2
785             J1=J2+DJ
786             T1=B1*J1*(J1+1)-D1*J1*J1*(J1+1)*(J1+1)
787             T2=B2*J2*(J2+1)-D2*J2*J2*(J2+1)*(J2+1)
788             %RESULT=T1-T2
789             %END ;!LINE

790         !
791         %REALFN GAIN(%REAL W)
792             %REAL W1,W2,DW,G1,G2,DG
793             %IF W>WGC(0) %OR W<WGC(IGC0-1) %THENRESULT=0
794             %CYCLE I=0,1,IGC0-1
795             %IF W>WGC(I) %THEN ->INTERP
796             %REPEAT
797             !
798             INTERP:W1=WGC(I)
799             W2=WGC(I-1)
800             G1=GC(I)
801             G2=GC(I-1)
802             DW=W1-W2
803             DG=G1-G2
804             %RESULT=G2+DG*(W-W2)/DW
805             %END ;! GAIN

806         !
807         !
808         %ENDOFPROGRAM
```

APPENDIX 3 : Data Collection Program

The main program begins on line 403. Lines 1-402 are system subroutines and functions and are included only for completeness.

I am grateful to the system staff of the Department of Physics PDP11/45, Peter McInnes and Steven Hayes for their help in implementing this program.

```
1       %BEGIN
2          !
3          %INTEGERFN VOLT(%INTEGER CHAN,GAIN)
4             LACC(CHAN<<8+GAIN<<3)
5             *EMT_363
6             %RESULT=ACC
7             %END ;! FN VOLT
8          !
9          %REALFN RTIME
10            %INTEGER A,B
11            *MOV_R1,-(SP)
12            *EMT_321 ;! TIME IN R0,R1
13            *MOV_R1,R5
14            *MOV_(SP)+,R1;!RESTORE R1
15            *MOV_R0,34.(R1);!HIGH ORDER IN A
16            *MOV_R5,36.(R1);!LOW ORDER IN B
17            A=A+1 %IF B<0 ;!SIGN BIT?
18            %RESULT=(A*65536.+B)/3000 ;! MINUTES
19            %END ;!OF RTIME
20         !
21         %ROUTINE SETPOT(%INTEGER X,UNIT)
22            !
23            !     X=UNIT => ON, X=0 => OFF
24            !
25            !  RELAY9 -- START COUNTING
26            !  RELAY10 -- RESET TIMER
27            !
28            *MOV_R1,-(SP)
29            *MOV_14.(R1),R0 ;! X
30            *MOV_16.(R1),R1 ;! UNIT
31            *EMT_352
32            *MOV_(SP)+,R1
33            %END ;! SETPOT
34         !
35         %INTEGERFN IABS(%INTEGER I)
36            I=-I %IF I<0
37            %RESULT=I
38            %END ;!IABS
39         !
40         %REALFN ABS(%REAL B)
41            B=-B %IF B<0
42            %RESULT=B
43            %END ;!ABS
44         !
45         %ROUTINE WAIT(%INTEGER X)
46            !WAITS X/50 SECS AND THEN RETURNS
47            !X SHOULD NOT EXCEED 32,767
48            LACC(X)
49            *EMT_375
50            %END
51         !
52         %ROUTINE RINGBELL(%INTEGER I)
53            %INTEGER K
54            %CYCLE K=1,1,I
55            PRINT SYMBOL(7)
56            ! BELL IS CTRL G ON TT
57            %REPEAT
58            %END;! OF RINGBELL
59         !
60         %REALFN MAKEREAL(%INTEGER AD)
61            %REAL X
62            *MOV_14.(R1),R2
63            *MOV_#36.,R3
64            *ADD_R1,R3
```

```
65          *MOV_(R2)+,(R3)+
66          *MOV_(R2)+,(R3)+
67          %RESULT=X
68          %END;! MAKEREAL
69      !
70      %ROUTINESPEC PRINTFL(%REAL X,%INTEGER N)
71      %REALFN MOD(%REAL X)
72          *_BIC_#100000,14.(R1)
73          %RESULT=X
74          %END ; ! OF FN MOD
75      %ROUTINE PRINT(%REAL X,%INTEGER N,M)
76          %OWNINTEGER IMAX=32767; !MAX INTEGER IN ONE WORD.
77          %REAL Y,Z,ROUND
78          %INTEGER I,J,L,SIGN,DP;          ! DP=DECIMAL POINT
79          M=4 %IF M>4; DP=0;                    ! DEAL WITH STUPID PARAMS
80          %IF N<=0 %THEN N=1;              ! DEAL WITH STUPID PARAMS
81          Y=MOD(X);                        ! ALL WORK DONE WITH Y
82          ROUND= (1/2)/10**M;                ! ROUNDING FACTOR
83          %IF Y>IMAX %THEN %START
84          PRINTFL(X,M); %RETURN; %FINISH
85          I=0;Z=1; Y=Y+ROUND;
86          COUNT LEADING PLACES:
87          I=I+1;Z=10*Z;                    ! NO DANGER OF OVERFLOW HERE
88          %IF Y>=Z %THEN -> COUNT LEADING PLACES
89          SPACES(N-I);                     ! O.K FOR ZERO OR -VE SPACES
90          SIGN=' ';                        ! '+' IMPLIED
91          %IF X<0 %THEN SIGN='-'
92          PRINT SYMBOL(SIGN)
93          J=I-1; Z=10**J
94          NEXT DIGIT:
95          L=INT PT(Y/Z);                   ! OBTAIN NEXT DIGIT
96          Y=Y-L*Z;Z=Z/10;                    ! AND REDUCE TOTAL
97          PRINT SYMBOL(L+'0')
98          J=J-1
99          %IF J>=0 %THEN -> NEXT DIGIT
100         %IF M=0 %THEN %RETURN;           ! NO DECIMAL PART TO BE O/P
101         %IF DP=0 %THEN %PRINTTEXT'.'
102         DP=1; J=0; Z=1
103         Y=10*Y; M=M-1; -> NEXT DIGIT
104         %END
105     %ROUTINE PRINTFL(%REAL X,%INTEGER N)
106         %REAL SIGN,ROUND,FACTOR
107         %INTEGER COUNT,INC
108         N=4 %IF N>4
109         ROUND=.5/10**N
110         SIGN=1
111         %IF X=0 %THEN -> ZERO .
112         %IF X < 0 %THENSTART
113         X=-X; SIGN=-SIGN; %FINISH
114         INC=1; COUNT=0; FACTOR=1/10
115         %IF X <= 1 %THENSTART
116         FACTOR=10; INC=-1; %FINISH
117         SCALE: %IF 1<=X+ROUND %AND X+ROUND<10 %THEN -> PRINTOUT
118         X=X*FACTOR; COUNT=COUNT+INC
119         -> SCALE
120         ZERO: COUNT=-99
121         PRINTOUT: PRINT(SIGN*X,1,N)
122         %PRINTTEXT'@'
123         WRITE(COUNT,2)
124         %END
125     %ROUTINE READF(%REALNAME XX)
126         %INTEGER ADR
127           *_MOV_14.(R1),36.(R1);  ! ADR=ADDR(XX)
128         !
```

```
129             !
130             %ROUTINESPEC READ(%INTEGER ADR,PARM)
131             %ROUTINESPEC SKIP SYMBOL
132             %INTEGERFNSPEC NEXT SYMBOL
133             %SWITCH SW(1:6)
134             %INTEGER CH,P,PT,DIG,STATE
135             %INTEGERARRAY L(1:72)
136             %OWNINTEGERARRAY A(0:48)=  %C
          2, -1, -1,  5, -1, -1, -1,
137               2,  2,  3,  5,  6, -1, -1,
138               1,  0,  0,  4,  0,  0,  0,
139               1,  0,  0, -1,  0,  0,  0,
140              -1, -1,  4, -1, -1, -1, -1,
141               3,  3, -1, -1, -1, -1, -1,
142              -1, -1, -1, -1, -1, -1, -1
143             %INTEGER ROW
144               -> FIRST
145             RESET:
146               %PRINTTEXT'WRONG';NEWLINE
147             FIRST:
148               P=0
149               STATE=1
150             INSCH:
151               READ SYMBOL(CH)
152               P=P+1
153               L(P)=CH
154               ROW=0
155               %IF CH='+' %OR CH='-' %THEN -> OUT
156               ROW=ROW+1
157               %IF '0'<=CH %AND CH<='9' %THEN -> OUT
158               ROW=ROW+1
159               %IF CH=' ' %THEN -> OUT
160               ROW=ROW+1
161               %IF CH=10 %THEN -> OUT
162               ROW=ROW+1
163               %IF CH='@' %THEN -> OUT
164               ROW=ROW+1
165               %IF CH='.' %THEN -> OUT
166               ROW=ROW+1
167             OUT:
168               STATE=A(7*ROW+STATE-1)
169               -> INSCH %IF STATE>0
170               -> RESET %IF STATE<0
171               PT=1
172               READ(ADR,1)
173             !
174             !
175             !
176             %ROUTINE READ(%INTEGER ADR,PARM)
177                %INTEGER FLAG,CURSYM; ! FLAG= 0FOR'-',1 FOR '+'
178                %INTEGER IVALUE,J
179                %REAL RWORK,SCALE,WK2
180                %OWNREAL IMAX=32767.0
181                         FLAG=1
182                         -> TEST SIGN
183                IGNORE LEADING SPACES:
184                         SKIP SYMBOL
185                TEST SIGN:CURSYM=NEXT SYMBOL;          ! CARE NOT TO READ TERMINATOR
186                         -> IGNORE LEADING SPACES %IF CURSYM=' ' %OR CURSYM=10
187                         -> PASS SIGN %IF CURSYM='+'
188                         -> DIGIT %UNLESS CURSYM='-'
189                MINUS:   FLAG=0;                       ! RECORD INITIAL MINUS
190                PASS SIGN: SKIP SYMBOL;                ! MOVE OVER SIGN ONCE IT HAS
191                         CURSYM=NEXT SYMBOL;           ! BEEN RECORDED IN FLAG
```

```
192             DIGIT:    -> DIGIT NOT FIRST %UNLESS '0'<=CURSYM %AND CURSYM<='9'
193                       RWORK=CURSYM-'0';                ! KEEP TOTAL IN RWORK
194             LOOP:     SKIP SYMBOL
195                       CURSYM=NEXT SYMBOL
196                       -> NOT DIG %UNLESS '0'<=CURSYM %AND CURSYM<='9'
197                       RWORK=10*RWORK+(CURSYM-'0');  ! CONTINUE EVALUATING
198                       -> LOOP
199             NOT DIG:  -> TRY AT %UNLESS CURSYM='.'
200                       SCALE=10
201             FPART:    SKIP SYMBOL
202                       CURSYM=NEXT SYMBOL
203                       -> TRY AT %UNLESS '0'<=CURSYM %AND CURSYM<='9'
204                       RWORK=RWORK+(CURSYM-'0')/SCALE
205                       SCALE=10*SCALE; -> FPART
206             TRY AT:
207             ! THE VALUE HAS NOW BEEN READ INTO RWORK. THERE MIGHT BE AN EXPONENT
208             ! E.G. '1.7@ 10'  IS VALID DATA FOR READ
209                       -> FIX %UNLESS CURSYM='@'
210                       SKIP SYMBOL;                     ! MOVE PAST THE '@'
211                       READ( ADDR(IVALUE),0); ! RECURSIVE CALL TO FIND EXPONENT
212                       %IF IVALUE<=-99 %THENSTART
213                          RWORK=0
214                          -> FIX
215                          %FINISH
216                       WK2=10.0
217                       %IF IVALUE<0 %THENSTART
218                          IVALUE=-IVALUE
219                          WK2=0.1
220                          %FINISH
221                       -> FIX %IF IVALUE=0
222                       %CYCLE J=1,1,IVALUE
223                       RWORK=RWORK*WK2
224                       %REPEAT
225             FIX:
226             ! KNOCK NUMBER INTO RIGHT FORM
227                       -> INT READ %IF PARM=0
228                       %IF FLAG=0 %THEN RWORK=-RWORK
229                       !REAL(ADR)=RWORK
230                       !J=ADDR(RWORK)
231                       !INTEGER(ADR)=INTEGER(J)
232                       !!INTEGER(ADR+2)=INTEGER(J+2)
233             *_MOV_#46.,R0
234             *_ADD_R1,R0    ; ! R0=ADDR(RWORK)
235               *_MOV_14.(R1),R3
236               *_MOV_(R0)+,(R3)+
237               *_MOV_(R0)+,(R3)+
238                       %RETURN
239             INT READ:
240                       !IVALUE= INT(RWORK)
241                       WK2=0.5
242                       %IF RWORK<0 %THEN WK2=-0.5
243                       IVALUE=INTPT(RWORK+WK2)
244                       %IF FLAG=0 %THEN IVALUE=-IVALUE
245                       !INTEGER(ADR)=IVALUE
246                       *_MOV_42.(R1),@14.(R1)
247             %RETURN
248             DIGIT NOT FIRST:
249             ! CAN HAVE  .73 AS VALID IMP NO
250                       SKIP SYMBOL
251                       CURSYM=NEXT SYMBOL
252                       RWORK=(CURSYM-'0')/10
253                       SCALE=100; -> FPART
254                       %END; ! READ
255           %ROUTINE SKIPSYMBOL
```

```
256                 PT=PT+1
257                 %END; ! SKIP SYMBOL
258               %INTEGERFN NEXT SYMBOL
259                 %RESULT=L(PT)
260                 %END; ! NEXT SYMBOL
261                     %END; ! READF
262             %ROUTINE READ(%INTEGERNAME I)
263               %REAL X
264               ! USE READF FOR INTEGERS SINCE IT IS IMMUNE TO SYMBOL IN DATA
265               READF(X)
266               %IF X>30000. %THENSTART ; ! INTPT FAILS FOR X>2**15
267               I=30000;%RETURN;%FINISH
268               X=X-1 %IF X<0 ;!COMPENSATE FOR ERROR IN INTPT
269               I=INTPT(X+.001)
270               %END
271             !
272             %REALFN SQRT(%REAL X)
273               %REAL Y,Z
274               %IF X<=0 %THENSTART
275               %IF X=0 %THEN %RESULT=0
276               NEWLINE;%PRINTTEXT' NEG ARG IN SQRT'
277               ;NEWLINE
278               %RESULT=1.
279               %FINISH
280               Y=(1+X)/2
281               1:Z=(Y+X/Y)/2
282               %IF Z>=Y %THEN %RESULT=Y
283               Y=Z
284               ->1
285               %END;! OF FN SQRT
286             !
287             ! DIRECT ACCESS FILE ROUTINES
288             !
289             %ROUTINE CREATE(%INTEGERARRAYNAME FILE)
290               LACC(ADDR(FILE(2)))
291               *MOV_R1,-(SP)
292               *MOV_(R0),R2
293               *MOV_-(R0),R1
294               *MOV_-(R0),R0
295               *EMT_345 ;! CREATE
296               *MOV_(SP)+,R1 ;! RESTORE R1
297               %END ;! CREATE
298             %INTEGERFN FIRSTBLOCK(%INTEGERARRAYNAME FILE)
299               LACC(ADDR(FILE(2)))
300               *MOV_R1,-(SP)
301               *MOV_(R0),R2
302               *MOV_-(R0),R1
303               *MOV_-(R0),R0
304               *EMT_344 ;! UDEX
305               *MOV_(SP)+,R1 ;! RESTORE R1
306               %RESULT=ACC
307               %END ;! FIRSTBLOCK
308             %INTEGERFN NEXTBLOCK(%INTEGER BLOCK)
309               LACC(BLOCK)
310               *MOV_R1,R5
311               *EMT_340
312               *MOV_R5,R1
313               %RESULT=ACC
314               %END ;! NEXTBLOCK
315             %INTEGERFN FILESIZE(%INTEGERARRAYNAME FILE)
316               %INTEGER I,J
317               I=0
318               J=FIRSTBLOCK(FILE)
319               1: %RESULT=I %IF J=0 %OR I=4000
```

```
320             I=I+1
321             J=NEXTBLOCK(J)
322             ->1
323             %END ;! FILESIZE
324         !
325         %INTEGERFN BLOCKNOF(%INTEGER FIRST,N)
326             %INTEGER I
327             %RESULT=0 %IF N<1 %OR N>4000
328             I=FIRST
329             1:%IF N=1 %OR I=0 %THEN %RESULT=I
330             I=NEXTBLOCK(I)
331             N=N-1
332             ->1
333             %END ;! BLOCKNOF
334         !
335         !
336         %OWNINTEGER DABLOCK
337         %OWNINTEGER DAPROTEC
338         %ROUTINE OPENDA(%INTEGERARRAYNAME FILE)
339             ! OPEN FOR READ OR WRITE
340             1:LACC(ADDR(FILE(2)))
341             *MOV_R1,R5
342             *MOV_(R0),R2
343             *MOV_-(R0),R1
344             *MOV_-(R0),R0
345             *EMT_344 ;! UDEX
346             *MOV_R1,-(SP)
347             *MOV_R5,R1 ;! RESTORE R1
348             DABLOCK=ACC
349             *MOV_(SP)+,R0
350             DAPROTEC=ACC
351             %RETURNIF DABLOCK#0
352             CREATE(FILE)
353             ->1
354             %END;! OPENDA
355         %ROUTINE WRITEDA(%INTEGER BLOCK,X)
356             ! X IS ADDRESS OF START OF 512 BYTE BLOCK
357             %INTEGER DWBLOCK,I,J
358             %IF BLOCK<0 %OR BLOCK>200 %THENSTART
359             %PRINTTEXT' BAD BLOCK NUMBER';NEWLINE
360             *EMT_372
361             %STOP;%FINISH
362             %IF DABLOCK=0 %THENSTART
363             %PRINTTEXT' DAFILE NOT OPEN';NEWLINE
364             *EMT_372
365             %STOP;%FINISH
366             2:DWBLOCK=BLOCKNOF(DABLOCK,BLOCK)
367             %IF DWBLOCK=0 %THENSTART;!FILE TOO SMALL
368             LACC(DAPROTEC)
369             *MOV_R0,-(SP)
370             LACC(DABLOCK)
371             *MOV_R1,R5
372             *MOV_(SP)+,R1
373             *EMT_341 ;! APPEND
374             *MOV_R5,R1
375             ->2
376             %FINISH
377             LACC(X)
378             !ADDRESS
379             *MOV_R0,-(SP)
380             LACC(DAPROTEC);! PROTEC
381             *MOV_R0,-(SP)
382             LACC(DWBLOCK);! BLOCK NUMBER
383             *MOV_R1,R5
```

```
384             *MOV_(SP)+,R3
385             *MOV_#-400,R2
386             *MOV_(SP)+,R1
387             *EMT_330;! WRITE
388             *MOV_R5,R1
389             %END ;! WRITEDA
390         !
391         !
392         ! TEXT FILE OUTPUT
393         !
394         %ROUTINE DEFINE OUTPUT(%INTEGERARRAYNAME A)
395             LACC(ADDR(A(0)))
396             *MOV_#UTFIL,R5
397             *MOV_(R0)+,(R5)+
398             *MOV_(R0)+,(R5)+
399             *MOV_(R0)+,(R5)+
400             %END ;!DEFINEOUTPUT
401         !
402         !
403         %ROUTINESPEC COLLECTDATA
404         %ROUTINESPEC SETOUTPUT
405         %ROUTINESPEC GETDATA
406         %ROUTINESPEC DECODE
407         %ROUTINESPEC WRITECODE
408         %ROUTINESPEC STOPPROG
409         %ROUTINESPEC WRITETODISC
410         %ROUTINESPEC ANALYSE(%REALARRAYNAME D1,%REAL M1,LIM,%REALNAME MEAN,%C
        SIGMA,%INTEGERNAME N1)
411         %ROUTINESPEC WAITPROG
412         %ROUTINESPEC CHECKINTERRUPT
413         %ROUTINESPEC LOADVARS
414         %ROUTINESPEC INITIALISE
415         %ROUTINESPEC WRITESPEC
416         %ROUTINESPEC MONITOR
417         %ROUTINESPEC DRIVEGRATING
418         %ROUTINESPEC SUMMARISE(%INTEGER STEP)
419         %ROUTINESPEC CHECKERROR
420         %REALFNSPEC READLASER
421         %INTEGER I,P,CTIME,COUNTS,COUNTS0,COUNTS1,RINT,MINT,MONIT,T1,DTIME
422         %INTEGER ERRCD,NSETS,ERRCD1,IMONIT,SFLAG,IFLAG
423         %INTEGER FLAG1,FLAG2,FLAG3,FLAG4
424         %INTEGER ISET,STEPS,SEQNO,IINST,ISTEP,NC,NC1,NC2,NC0,QFLAG,IE,RTI
425         %REAL MM,LL,TIMEIN,TIMEOUT
426         %INTEGER NBLOCK,FBLOCKS,SPECNO
427         %INTEGER OLDDIR,NEWDIR
428         %REALARRAY P1(1:16)
429         %REALARRAY PP1(1:16)
430         %REALARRAY P0(1:16)
431         %REALARRAY PP0(1:16)
432         %REALARRAY ILASER(1:50)
433         %REAL LPOW,LPOW1,LSIGMA,LFAC1,LFAC2,LSCALE
434         %REAL MP0,MP1,MPP0,MPP1,Q0,Q1,QQ0,QQ1
435         %REAL MTIME,DNOISE,SUMERR,FFAULT,FTIME
436         %INTEGERARRAY A(0:11)
437         %INTEGERARRAY STORE(0:11)
438         %INTEGERARRAY S0(1:16)
439         %INTEGERARRAY S1(1:16)
440         %INTEGERARRAY FNAME(0:2)
441         %INTEGERARRAY TNAME(0:2)
442         %INTEGERARRAY NACC(-50:50)
443         %REALARRAY SIGNAL(-50:50)
444         %REALARRAY ERROR(-50:50)
445         %REALARRAY EXPVAR(0:31)
446         %OWNINTEGERARRAY REPLY(1:9)='K','E','C','R','D','F','B','U','S'
```

```
%SWITCH EXEC(1:9)
PRIME:NEWLINES(2) ;%PRINTTEXT' PRIME INTERFACE? '
FLAG2=0;FLAG3=0
READSYMBOL(P)
%IF P#'Y' %AND P#'N' %THENSTART
%PRINTTEXT' INVALID RESPONSE'
->PRIME
%FINISH
%IF P='Y' %THENSTART
SETPOT(256,256)
SETPOT(512,512)
%FINISH
IINST=9
RINT=3
! ENTRY TO PROGRAM HERE
! INITIALISE VARIABLES
ISET=0
CTIME=0
SPECNO=0
SEQNO=0
NSETS=0
NBLOCK=1
QFLAG=1 !!DEFINE DAFILE ON FIRST PASS
LPOW=1;LSIGMA=1
IFLAG=0
%CYCLE I=0,1,31
EXPVAR(I)=999
%REPEAT
LOADVARS
NEWSCAN:%CYCLE I=-50,1,50
NACC(I)=0
SIGNAL(I)=0
ERROR(I)=0
%REPEAT
STEPS=0;DNOISE=0
CHANGE:INITIALISE
%CYCLE I=1,1,16
S0(I)=0;S1(I)=0
P0(I)=0;P1(I)=0
PP0(I)=0;PP1(I)=0
%REPEAT
PROMPT:NEWLINE;%PRINTTEXT' :'
READSYMBOL(P)
!
! VALID PROCEEDURES:K=KILL PROGRAM
!                   :W=WAIT PROGRAM
!                   :C=COLLECT FLUORESCENCE
!                   :R=WRITE COLLECTED DATA TO DISC
!                   :D=DRIVE TO NEW WAVELENGTH
!                   :F=FEEDBACK ON CURRENT SCAN
!                   :B=COLLECT BACKGROUNDS
!                   :U=UPDATE EXPVARS WITHOUT WRITING TO DISC
!                   :S=SELECT NEW SCAN
!
NEXTSTEP:
%CYCLE IE=1,1,IINST
%IF P=REPLY(IE) %THEN ->EXEC(IE)
%REPEAT
NEWLINE;%PRINTTEXT' INVALID'
->PROMPT
EXEC(1):STOPPROG
EXEC(2):
WAITPROG
->PROMPT
```

```
511         EXEC(9):WRITESPEC
512         ! OUTPUT OLD SPECTRUM TO SPEC__
513         -> NEWSCAN
514         EXEC(4):
515         WRITETODISC ;->PROMPT
516         EXEC(5):
517         DRIVEGRATING
518         -> PROMPT
519         EXEC(6):NEWLINE;%PRINTTEXT' STEP INDEX:'
520         READ(ISTEP)
521         -> PROMPT %IF ISTEP=-999
522         FLAG2=1 %IF ISTEP=30000 ;! STEP CODE FOR BACKGROUND
523         SFLAG=1
524         SUMMARISE(ISTEP)
525         SFLAG=0;FLAG2=0
526         ->EXEC(6)
527         EXEC(8):INITIALISE
528         -> PROMPT
529         EXEC(7):FLAG2=1
530         ISTEP=30000
531         ! PROCEED TO COUNTING EVENT
532         EXEC(3):COLLECTDATA
533         FLAG2=0;->PROMPT
534         !
535         %ROUTINE COLLECTDATA
536            SELECTOUTPUT(0)
537            TIMEIN=RTIME
538            SUMERR=0
539            FLAG1=1 ;!ENTRY WITH BEAM ON
540            NC=0 ;!NO OF PAIRS AT THIS W.
541            COUNTS0=0;COUNTS1=0
542            %IF FLAG2=0 %THEN ISTEP=STEPS
543            RESET:%IF IFLAG=1 %THENSTART
544            CHECKINTERRUPT
545            %RETURNIF RTI=0
546            %FINISH
547            %IF FLAG1=1 %THEN NC=NC+1
548            SKIPINC:IFLAG=0
549            SETPOT(0,512)
550            SETPOT(512,512)
551            ERRCD=0;COUNTS=0
552            %IF FLAG1=1 %THENSTART
553            SETPOT(0,1024) ;!TESLA ON,DISCHARGE ON
554            WAIT(DTIME*120) ;!WAIT FOR TESLA OFF AND BEAM SETTLE
555            %FINISH
556            SETPOT(0,256)
557            SETPOT(256,256)
558            %IF IMONIT=0 %THENSTART
559            WAIT(CTIME*50+1)
560            ->NOLASER
561            %FINISH
562            MTIME=RTIME
563            LPOW1=LPOW ;!OLD LASER POWER
564            ERRCD1=0
565            MONITOR
566            MTIME=(RTIME-MTIME)*3000
567            T1=INTPT(CTIME*50-MTIME)
568            WAIT(T1+1) %IF T1>0
569            NOLASER:
570            %IF FLAG1=1 %THEN SETPOT(1024,1024) ;! DISCHARGE OFF
571            GETDATA
572            DECODE
573            %IF ERRCD#0 %THEN CHECKERROR
574            %IF ERRCD#0 %THEN -> SKIPINC
```

```
575             %IF FLAG1=1 %THENSTART
576             COUNTS1=COUNTS
577             S1(NC)=COUNTS1
578             P1(NC)=LPOW
579             PP1(NC)=LSIGMA
580             FLAG1=0;! DISCHARGE OFF
581             WAIT(100) ;! WAIT FOR BEAM TO SETTLE
582             -> RESET
583             %FINISH
584             ! FLAG1=0 FOR THIS DATUM HERE,SO PROCESS ONE PAIR OF COUNTS
585             COUNTS0=COUNTS
586             S0(NC)=COUNTS0
587             P0(NC)=LPOW
588             PP0(NC)=LSIGMA
589             INC:%IF NC=NC0 %THENSTART
590             TIMEOUT=RTIME
591             SFLAG=0
592             SUMMARISE(ISTEP)
593             SETPOT(0,512)
594             SETPOT(512,512)
595             WRITETODISC
596             %RETURN
597             %FINISH
598             ! PROCEED TO BEAM ON
599             FLAG1=1
600             ->RESET
601             %END ;! COLLECTDATA
602         !
603         %ROUTINE GETDATA
604             ! READS BINARY DATA (12 BYTES OF 5 BITS EACH) FROM INTERFACE
605             %INTEGERFNSPEC READBIN
606             %INTEGER I
607             %CYCLE I=0,1,11
608             A(I)=21;STORE(I)=21
609             %REPEAT
610             %CYCLE I=0,1,11
611             STORE(I)=READBIN
612             WAIT(RINT)
613             %REPEAT
614             %INTEGERFN READBIN
615                 *EMT_336
616                 *MOV_12. (R1),R1
617                 *RTS_PC
618                 %END ;!READBIN
619             %END ;!GETDATA
620         !
621         %ROUTINE DECODE
622             %INTEGER I,J,N,R,II,K,IC1
623             %OWNINTEGERARRAY PRIORITY(0:11)=0,1,0,1,0,1,0,1,0,1,0,1
624             %OWNINTEGERARRAY IMAXD(0:5) = 7,6,7,2,3,0
625             %INTEGERARRAY BIT(0:4)
626             %INTEGERARRAY SETBIT(0:11)
627             %INTEGERARRAY DIGIT(0:5)
628             IC1=0
629             %CYCLE I=0,1,11
630             %IF STORE(I)=31 %THENSTART
631             NEWLINE
632             RINGBELL(10)
633             %PRINTTEXT' MODE FAULT'
634             ERRCD=1
635             K=0
636             -> TRANSFER
637             %FINISH
638             %REPEAT
```

```
639           %CYCLE I=0,1,11
640           %IF STORE(I)=20 %THEN ->PERM ;!START CODE IN HIGHEST BYTE
641           %REPEAT
642           %RETURNIF FLAG3=1
643           RINGBELL(10);%PRINTTEXT' STARTCODE FAULT'
644           ERRCD=4
645           K=0
646           -> TRANSFER
647           PERM:
648           %CYCLE II=I,1,11
649           A(II-I)=STORE(II)
650           %REPEAT
651           -> CHECK RANK %IF I=0 ;! NO CYCLING OF ELEMENTS
652           K=11-I+1
653           TRANSFER:%CYCLE II=K,1,11
654           A(II)=STORE(II-K)
655           %REPEAT
656           %IF ERRCD#0 %THENSTART
657           WRITECODE
658           %RETURN
659           %FINISH
660           CHECKRANK:
661           %IF A(1)=10 %THENSTART
662           IFLAG=1 ;!INTERRUPT REQUEST CODE
663           IC1=2 ;!SKIP RANKCHECK IN FIRST  DECADE
664           %FINISH
665           %CYCLE I=IC1,1,11
666           %IF PRIORITY(I)=0 %AND ((A(I)=0 %AND A(I+1)=0) %OR     %C
          (A(I)#0 %AND A(I+1)#0)) %THENSTART
667           %RETURNIF FLAG3=1
668           NEWLINE
669           RINGBELL(10)
670           %PRINTTEXT' READOUT FAULT'
671           WRITECODE
672           ERRCD=2
673           %RETURN
674           %FINISH
675           %REPEAT
676           %CYCLE I=2,1,11 ;! SKIP STARTCODE
677           %IF A(I)=0 %THEN -> PASSBYTE
678           %CYCLE J=0,1,4
679           BIT(J)=A(I)<<J&16                ;!GET BIT
680           %IF BIT(J)=16 %THENSTART         ;!TEST FOR SET BIT
681           SETBIT(I)=4-J                    ;!POSITFLAG1 OF SET BIT
682           N=5-(I-(PRIORITY(I)))//2    ;!POWER OF TEN
683           DIGIT(N)=SETBIT(I)+5*(1-(PRIORITY(I)))
684                                            ;!VALUE OF BYTE
685           %FINISH
686           %REPEAT
687           PASSBYTE:%REPEAT
688           N=4
689           TESTDIGIT:R=DIGIT(N)-IMAXD(N)
690           %IF R<0 %THEN -> COUNTSCK
691           %IF R=0 %AND N#0 %THENSTART
692           N=N-1
693           -> TESTDIGIT
694           %FINISH
695           %RETURNIF FLAG3=1
696           NEWLINE
697           RINGBELL(10)
698           %PRINTTEXT' OVERFLOW FAULT'
699           ERRCD=3
700           WRITECODE
701           %RETURN
```

```
702             COUNTSOK:%CYCLE N=0,1,4
703             COUNTS=COUNTS+DIGIT(N)*10**N
704             %REPEAT
705             ERRCD=0 %IF FLAG3=1.
706             FLAG3=0
707             %END ;! DECODE
708         !
709         %ROUTINE MONITOR
710             %INTEGER I
711             %REAL MM,LL
712             %CYCLE I=1,1,MONIT
713             ILASER(I)=READLASER
714             WAIT(MINT)
715             %REPEAT
716             MM=0
717             LL=30000
718             %IF MONIT=1 %THENSTART
719             LPOW=ILASER(1)
720             ->SKIPANALYSIS
721             %FINISH
722             ANALYSE(ILASER,MM,LL,LPOW,LSIGMA,MONIT)
723             SKIPANALYSIS:%RETURNIF FLAG2=1
724             %IF ABS(1-LPOW/LPOW1)>LFAC1 %THENSTART
725             %RETURNIF NC=1 ;! NO DIAG ON FIRST PASS
726             NEWLINE;RINGBELL(5)
727             %PRINTTEXT' LASER POWER CHANGED FROM';PRINTFL(LPOW1,4);NEWLINE
728             %PRINTTEXT' TO ';PRINTFL(LPOW,4)
729             ERRCD1=1
730             %FINISH
731             %IF MONIT=1 %THENRETURN
732             %IF LSIGMA>LPOW*LFAC2 %THENSTART
733             NEWLINE;RINGBELL(5)
734             %PRINTTEXT' LASER POWER VARYING OVER';PRINTFL(LSIGMA,4)
735             %PRINTTEXT' ABOUT ';PRINTFL(LPOW,4)
736             ERRCD1=ERRCD1+2
737             %FINISH
738             %END ;!MONITOR LASER
739         !
740         %ROUTINE ANALYSE(%REALARRAYNAME D1,%REAL M1,LIM,%REALNAME MEAN,%C
                SIGMA,%INTEGERNAME N1)
741             %INTEGER NA,NB,C
742             %REAL E,M2,SD
743             NA=1
744             NB=N1
745             SD=0.
746             M2=0
747             C=0
748             %IF LIM<=0. %THEN LIM=.0001 ;! SMALL PERTURBATION
749             %CYCLE I=NA,1,NB
750             E=D1(I)
751             %IF ABS(E-M1)<LIM %THENSTART
752             M2=M2+E
753             C=C+1 ;! ACCEPTED ELEMENTS
754             %FINISH
755             %REPEAT
756             ->OK %UNLESS C<2
757             RINGBELL(10)
758             NEWLINE ;%PRINTTEXT' DIVISION BY ZERO IN ANALYSE';NEWLINE
759             WRITE(C,4);WRITE(NA,4);WRITE(NB,4)
760             NEWLINE
761             PRINT(M1,6,4);PRINT(LIM,6,4);PRINT(E,6,4);NEWLINE
762             MEAN=1;SIGMA=1
763             %PRINTTEXT' DATA COLLECTION STOPPED'
764             WAITPROG
```

```
765             %RETURN
766             OK:M2=M2/C ;! NEW ESTIMATE OF MEAN
767             %CYCLE I=MA,1,NB
768             E=D1(I) ;! SUBTRACT MEAN TO AVOID LOSS OF PRECISFLAG1
769             %IF ABS(E-M1)<LIM %THEN SD=SD+(E-M2)*(E-M2)
770             %REPEAT
771              N1=C
772             MEAN=M2
773             SIGMA=SQRT(SD/(C-1)) ;! STANDARD DEVN.
774             %END ;!ANALYSE
775         !
776         %ROUTINE WRITECODE
777             NEWLINE
778             %CYCLE I=0,1,11
779             WRITE(A(I),2) ;SPACES(2)
780             %REPEAT
781             %END ;!WRITECODE
782         !
783         %ROUTINE STOPPROG
784             NEWLINE;WRITE(NSETS,3)
785             %PRINTTEXT'DATA SETS CREATED';NEWLINE
786             %PRINTTEXT'LAST SEQ NO. = ';WRITE(SEQNO,4)
787             NEWLINES(2)
788             *EMT_372
789             %END ;!STOPPROG
790         !
791         %ROUTINE INITIALISE
792             %INTEGER IDEFN,IMAX,I,JJ
793             QFLAG=0
794             IDEFN=27
795             IMAX=0
796             JJ=1
797             NEWLINE;%PRINTTEXT' TYPE INDEX=-1 TO END ALTERATIONS'
798             READINDEX:NEWLINE
799             %PRINTTEXT'INDEX NO:';READ(I)
800             %IF I<=0 %THEN -> CHECKVARS
801             %IF I>31 %THENSTART
802             %PRINTTEXT'OUT OF RANGE'
803             -> READINDEX
804             %FINISH
805             %IF I>=23  %AND I<=27 %THENSTART
806             NEWLINE;%PRINTTEXT' NOT ACCESSIBLE'
807             ->READINDEX
808             %FINISH
809             %IF I>IDEFN %THENSTART
810             %PRINTTEXT'WARNING-VARIABLE NO.';WRITE(I,3)
811             %PRINTTEXT'NOT DEFINED'
812             %FINISH
813             %IF I=18 %THEN QFLAG=1
814             READVARS:
815             %PRINTTEXT'VAR.SETTING:';READF(EXPVAR(I))
816             %IF I>IMAX %THEN IMAX=I
817             JJ=JJ+1
818             -> READINDEX
819             CHECKVARS:%IF IMAX>IDEFN %THEN ISET=IMAX %ELSE ISET=IDEFN
820             EXPVAR(0) =ISET
821             ! CHECK FOR FAULTY PARAMS
822             LSCALE=EXPVAR(9)
823             %IF LSCALE<0.001 %OR LSCALE>10.0 %THENSTART
824             NEWLINE;%PRINTTEXT'INVALID MONITOR FSD'
825             I=9;JJ=JJ-1
826             ->READVARS
827             %FINISH
828             DTIME=INTPT(50*EXPVAR(16)+0.001)
```

```
829             CTIME=INTPT(EXPVAR(17)+0.001)
830             %IF CTIME#1 %AND CTIME#10 %AND CTIME#100 %THENSTART
831             NEWLINE;%PRINTTEXT'INVALID COUNT TIME';NEWLINE
832             I=17;JJ=JJ-1
833             ->READVARS
834             %FINISH
835             SEQNO=INTPT(EXPVAR(18)+0.001)
836             %IF SEQNO=0 %OR SEQNO>999 %THENSTART
837             NEWLINE;%PRINTTEXT 'INVALID SEQ.NO.';NEWLINE
838             I=18;JJ=JJ-1
839             ->READVARS
840             %FINISH
841             MONIT=INTPT(EXPVAR(19)+.01)
842             %IF MONIT<0 %OR MONIT>50 %THENSTART
843             %PRINTTEXT'INVALID NO. OF MONITORINGS';NEWLINE
844             I=19;JJ=JJ-1
845             ->READVARS
846             %FINISH
847             LFAC1=EXPVAR(20)
848             LFAC2=EXPVAR(21)
849             NCO=INTPT(EXPVAR(22)+0.001)
850             %IF NCO>16 %OR NCO<1 %THENSTART
851             %PRINTTEXT'INVALID NO OF DATA POINTS';NEWLINE
852             I=22;JJ=JJ-1
853             ->READVARS
854             %FINISH
855             FLAG4=INTPT(EXPVAR(28)+0.001)
856             %IF FLAG4#0 %AND FLAG4#1 %THENSTART
857             %PRINTTEXT'INVALID VARIABLE 28-FLAG';NEWLINE
858             I=28;JJ=JJ-1
859             ->READVARS
860             %FINISH
861             !
862             ! ALTER OUTPUT STREAM IF SEQNO HAS BEEN CHANGED
863             !
864             %IF QFLAG=1 %THENSTART
865             SETOUTPUT
866             QFLAG=0
867             %FINISH
868             %IF MONIT=0 %THENSTART
869             NEWLINE;%PRINTTEXT' LASER MONITORING OFF';NEWLINE
870             IMONIT=0;%RETURN
871             %FINISH
872             IMONIT=1
873             MINT=INTPT(CTIME/MONIT*50+0.001);! LASER MONITORING INTERVAL
874             %END ;!INITIALISE
875         !
876         %ROUTINE WRITE TO DISC
877             %REALARRAY DA(0:127)
878             %INTEGER I,K,ADR,K0
879             NEWLINE
880             %CYCLE K=0,1,127
881             DA(K)=0
882             %REPEAT
883             DA(0)=NBLOCK
884             DA(1)=STEPS
885             DA(2)=NC
886             DA(3)=TIMEIN
887             DA(4)=TIMEOUT
888             K0=5
889             %CYCLE K=0,1,31
890             DA(K+K0)=EXPVAR(K)
891             %REPEAT
892             K0=K0+K
```

```
893             ADR=ADDR(S0(1))
894             %CYCLE K=1,1,8
895             DA(K+K0)=MAKEREAL(ADR)
896             ADR=ADR+4
897             %REPEAT
898             K0=K0+K
899             ADR=ADDR(S1(1))
900             %CYCLE K=1,1,8
901             DA(K+K0)=MAKEREAL(ADR)
902             ADR=ADR+4
903             %REPEAT
904             K0=K0+K
905             %CYCLE K=1,1,16
906             DA(K+K0)=P0(K)
907             %REPEAT
908             K0=K0+K
909             %CYCLE K=1,1,16
910             DA(K+K0)=PP0(K)
911             %REPEAT
912             K0=K0+K
913             %CYCLE K=1,1,16
914             DA(K+K0)=P1(K)
915             %REPEAT
916             K0=K0+K
917             %CYCLE K=1,1,16
918             DA(K+K0)=PP1(K)
919             %REPEAT
920             WRITEDA(NBLOCK,ADDR(DA(0)))
921             %PRINTTEXT' BLOCK NO. ';WRITE(NBLOCK,6)
922             %PRINTTEXT' WRITTEN TO  DISC';NEWLINE
923             NBLOCK=NBLOCK+1
924             NSETS=NSETS+1
925             %END ;!WRITETODISC
926         !
927         %ROUTINE SETOUTPUT
928             %INTEGER N,I
929             %INTEGERARRAY DIG(0:2)
930             SELECTOUTPUT(0)
931             N=SEGNO
932             %CYCLE I=0,1,2
933             DIG(I)=INTPT(N/10**(2-I))
934             N=N-DIG(I)*10**(2-I)
935             DIG(I)=DIG(I)+48
936             %REPEAT
937             ! DIG(I) CONTAINS THE DIGITAL PART OF THE OUTPUT FILE NAME
938             FNAME(0)='I'<<8+'L'
939             FNAME(1)=DIG(0)<<8+'F'
940             FNAME(2)=DIG(2)<<8+DIG(1)
941             NEWLINE
942             %PRINTTEXT' OUTPUTFILE IS LIF'
943             %CYCLE I=0,1,2
944             PRINTSYMBOL(DIG(I))
945             %REPEAT
946             NEWLINE
947             !OPEN FILE
948             OPENDA(FNAME)
949             FBLOCKS=FILESIZE(FNAME)
950             NEWLINE;%PRINTTEXT' FILE CONTAINS ';WRITE(FBLOCKS,6)
951             %PRINTTEXT' BLOCKS'
952             NBLOCK=FBLOCKS+1
953             %PRINTTEXT' NEXT BLOCK NO.=';WRITE(NBLOCK,6)
954             NEWLINE
955             %END ;!SETOUTPUT
956         !
```

```
957         %ROUTINE LOADVARS
958            %INTEGER I
959            SELECTINPUT(21) ;!FILE LIF000
960            %CYCLE I=0,1,31
961            READF(EXPVAR(I))
962            %REPEAT
963            SELECTINPUT(20)
964            CLOSESTREAM(21)
965            %END ;!LOADVARS
966         !
967         %REALFN READLASER
968            !
969            !     READS LASERBEAM MONITOR ON ADC CHANNEL 5
970            !     USES AUTO RANGING FOR MAX PRECISION
971            !
972            %OWNREALARRAY FACT(0:3)= 10.,5.,2.5,1.25
973            %INTEGER GAIN,VAL
974            GAIN=3 ;! START ON MOST SENSITIVE RANGE
975            1: VAL=VOLT(5,GAIN)
976            %IF MOD(VAL)>1000 %THENSTART
977            GAIN=GAIN-1
978            ->1 %IF GAIN>=0 ;! KNOCK DOWN GAIN
979            NEWLINE
980            RINGBELL(40)
981            %PRINTTEXT'  OUTPUT CLOSE TO 10 VOLTS';NEWLINE
982            %PRINTTEXT' LEVEL TAKEN AS 10 VOLTS';NEWLINE
983            GAIN=0
984            VAL=1023
985            %FINISH
986            %RESULT=VAL*FACT(GAIN)/1023*LSCALE ;! MULTIPLY IN RANGE FACTOR & NORMALISE
987            %END ;! READLASER
988         !
989         %ROUTINE DRIVEGRATING
990            %INTEGER DSTEPS,DD
991            %ROUTINESPEC DRIVEMOTOR(%INTEGER UNIT,STEPS)
992            NEWLINE;%PRINTTEXT' STEPS:';READ(DSTEPS)
993            %RETURNIF DSTEPS=0
994            NEWDIR=DSTEPS//IABS(DSTEPS)
995            !NEWDIR=+1:=>RED
996            !      =-1:=>BLUE
997            %IF NEWDIR=OLDDIR %THEN  DD=1 %ELSE DD=3
998            STEPS=STEPS+DSTEPS
999            DSTEPS=DSTEPS+NEWDIR*DD ;!COMPENSATION
1000           OLDDIR=NEWDIR
1001           DRIVEMOTOR(1,DSTEPS)
1002           !
1003           %ROUTINE DRIVEMOTOR(%INTEGER UNIT,STEPS)
1004              *MOV_R1,-(SP)
1005              *MOV_14.(R1),R0
1006              *MOV_16.(R1),R1
1007              *EMT_355
1008              *MOV_(SP)+,R1
1009              %END ;!DRIVEMOTOR
1010           !
1011           %END ;!DRIVEGRATING
1012        !
1013        %ROUTINE CHECKINTERRUPT
1014           %INTEGER P,IREP
1015           NEWLINE;%PRINTTEXT' INTERRUPT REQUEST:'
1016           ! TYPE 'C' TO CONTINUE
1017           ! TYPE X TO RETURN TO PROCEEDURE SELECT
1018           READINT:READSYMBOL(P)
1019           %IF P#'X' %AND P#'C' %THEN -> READINT
1020           NEWLINE
```

```
1021            %IF P='X' %THEN RTI=0
1022            %IF P='C' %THEN RTI=1
1023            ! CHECK INTERRUPT DISABLED
1024            IREP=0
1025            CHECK:
1026            IFLAG=0
1027            GETDATA
1028            DECODE
1029            %RETURNIF IFLAG=0
1030            -> CHECK %IF IREP=1
1031            %PRINTTEXT' INTERRUPT FAULT';NEWLINE
1032            IREP=1
1033            WAIT(250)
1034            ->CHECK
1035            %END ;!CHECKINTERRUPT
1036        !
1037        %ROUTINE WAITPROG
1038            NEWLINE
1039            *EMT_301
1040            NEWLINE
1041            %END ;!WAITPROG
1042        !
1043        %ROUTINE SUMMARISE(%INTEGER STEPI)
1044            %ROUTINESPEC RECAP
1045            %INTEGER I,J,N2,N3
1046            %REALARRAY DUM(1:16)
1047            %REALARRAY DUM0(1:16)
1048            %REAL MM,LL,M,D,E,M0,D0,E0,SNRAT,F0,F1
1049            %REAL S2,S3,E2,E3,B
1050            J=0;MM=0;LL=10000.
1051            %IF SFLAG=1 %THENSTART
1052            %IF FLAG2=1 %THENSTART
1053            NEWLINE;%PRINTTEXT' DISCHARGE NOISE=';PRINT(DNOISE,3,4)
1054            %FINISHELSE RECAP
1055            %RETURN
1056            %FINISH
1057            NEWLINE
1058            WAIT(50) ;! WAKE UP TT!
1059            %PRINTTEXT'BLOCKNO.=';WRITE(NBLOCK,6)
1060            NEWLINE;%PRINTTEXT'SEQ. NO.=';WRITE(SEQNO,4)
1061            NEWLINE;%PRINTTEXT'TIME=';PRINT(TIMEOUT,4,4)
1062            %IF FLAG2=0 %THENSTART
1063            NEWLINE;%PRINTTEXT'STEPS=';WRITE(STEPI,4)
1064            %FINISH
1065            NEWLINE;%PRINTTEXT'ENTRIES=';WRITE(NC,3)
1066            NEWLINE
1067            %IF NC<2 %THENSTART
1068            NEWLINE;%PRINTTEXT' NO ANALYSIS AVAILABLE'
1069            %RETURN
1070            %FINISH
1071            %IF IMONIT=0%OR FLAG4=0 %THENSTART
1072            F1=1;F0=1
1073            ->CALCULATE %IF IMONIT=0
1074            %FINISH
1075            ANALYSE(P0,MM,LL,MP0,MPP0,NC)
1076            ANALYSE(P1,MM,LL,MP1,MPP1,NC)
1077            %IF FLAG2=1 %THENSTART
1078            Q0=MP0;Q1=MP1;! LASER MONITOR OFFSETS
1079            QQ0=MPP0;QQ1=MPP1
1080            EXPVAR(23)=Q1
1081            EXPVAR(24)=Q0
1082            EXPVAR(25)=QQ1
1083            EXPVAR(26)=QQ0
1084            F0=1;F1=1;!NO NORMALISATION OF COUNTS
```

```
1085          %FINISH
1086          NO UPDATE;%IF FLAG2=1 %THEN B=0 ;! NO BACKGROUND TO SUBTRACT
1087          NEWLINE;%PRINTTEXT' MONITOR'
1088          %IF FLAG2=1 %THENPRINTTEXT' OFFSET';%PRINTTEXT'   ON      OFF'
1089          NEWLINE;%PRINTTEXT'   INTENS.';PRINT(MP1,1,4);PRINT(MP0,1,4)
1090          NEWLINE;%PRINTTEXT'  VARN.      ';PRINT(MPP1,1,4);PRINT(MPP0,1,4)
1091          CALCULATE:J=0
1092          %CYCLE I=1,1,NC
1093          %IF FLAG2=1 %OR IMONIT=0 %OR FLAG4=0 %THEN -> NORMALISE
1094          F0=P0(I)-Q0
1095          F1=P1(I)-Q1
1096          NORMALISE:
1097          B=BNOISE %IF FLAG2=0
1098          DUM0(I)=S0(I)/F0
1099          DUM(I)=(S1(I)-B)/F1-DUM0(I)
1100          ! NORMALISED SIGNAL
1101          %REPEAT
1102          MM=0;LL=1000000.
1103          ANALYSE(DUM,MM,LL,M,D,NC)
1104          ANALYSE(DUM0,MM,LL,M0,D0,NC)
1105          %IF FLAG2=1 %THENSTART
1106          BNOISE=M
1107          EXPVAR(27)=BNOISE
1108          %FINISH
1109          E=D/SQRT(NC)
1110          E0=D0/SQRT(NC)
1111          NEWLINE;%IF FLAG2=0 %THENSTART
1112          SPACE;%IF IMONIT=0 %OR FLAG4=0 %THENPRINTTEXT'UN'
1113          %PRINTTEXT'NORMALISED DATA'
1114          %FINISHELSEPRINTTEXT' BACKGROUND'
1115          NEWLINE;%PRINTTEXT' MEAN SIG=';PRINTFL(M,4)
1116          NEWLINE;%PRINTTEXT' ERROR=';PRINTFL(E,4)
1117          NEWLINE;%PRINTTEXT' NOISE LEV=';PRINTFL(M0,4)
1118          NEWLINE;%PRINTTEXT' FLUCTN=';PRINTFL(D0,4)
1119          %RETURNIF FLAG2=1
1120          %IF M0<0.0001 %THEN SNRAT=999.99 %ELSE  %C
      SNRAT=M/SQRT(M0/NC)
1121          NEWLINE;%PRINTTEXT' S/N=';PRINTFL(SNRAT,4)
1122          %IF STEPI<-50 %OR STEPI>50 %THENSTART
1123          NEWLINE;%PRINTTEXT' DATA ARRAY RANGE EXCEEDED'
1124          %RETURN
1125          %FINISH
1126          N2=NACC(STEPI)
1127          S2=SIGNAL(STEPI)
1128          E2=ERROR(STEPI)
1129          N3=N2+NC
1130          S3=(N2*S2+NC*M)/N3
1131          E3=SQRT(N2*N2*E2*E2+NC*NC*E*E)/N3
1132          NACC(STEPI)=N3
1133          SIGNAL(STEPI)=S3
1134          ERROR(STEPI)=E3
1135          RECAP
1136          !
1137          %ROUTINE RECAP
1138             NEWLINE;%PRINTTEXT'      CUMULATIVE RESULTS'
1139             NEWLINE;%PRINTTEXT' ENTRIES=';WRITE(NACC(STEPI),5)
1140             NEWLINE;%PRINTTEXT' SIGNAL=';PRINTFL(SIGNAL(STEPI),4)
1141             NEWLINE;%PRINTTEXT' ERROR=';PRINTFL(ERROR(STEPI),4)
1142             %END ;!RECAP
1143          !
1144          %END ;!SUMMARISE
1145       !
1146       %ROUTINE CHECKERROR
1147          %INTEGER J,H
```

```
1148            FLAG3=1;H=10( ;!DISABLE FAULT DIAG
1149            H=CTIME %IF ERRCD=1
1150            %CYCLE J=1,1,1(
1151            ERRCD=0
1152            WAIT(H)
1153            GETDATA
1154            DECODE
1155            %IF ERRCD=0 %THEN -> DIAG
1156            %REPEAT
1157            DIAG:FTIME=RTIME
1158            NEWLINE;%PRINTTEXT' TIME=';PRINT(FTIME,4,4)
1159            %PRINTTEXT' PAIRS=';WRITE(NC,4);WRITE(FLAG1,2);NEWLINE
1160            %IF ERRCD=0 %THEN -> OK
1161            SUMERR=SUMERR+1
1162            FFAULT=SUMERR/NC
1163            %IF NC>3 %AND FFAULT>0.5 %THENSTART
1164            NEWLINE;%PRINTTEXT' FAULT RATE EXCEEDED'
1165            WAITPROG
1166            %FINISH
1167            %RETURN
1168            OK:NEWLINE;%PRINTTEXT' READOUT AFTER ';WRITE(J,3)
1169            %PRINTTEXT' ATTEMPTS'
1170            %END ;!CHECKERROR
1171        !
1172        %ROUTINE WRITESPEC
1173            %INTEGER I,J
1174            %INTEGERARRAY DIG(0:1)
1175            READSPECNO:
1176            NEWLINE;%PRINTTEXT' SPECFILE NO:';READ(SPECNO)
1177            %IF SPECNO<0 %OR SPECNO>99 %THENSTART
1178            %PRINTTEXT' INVALID';-> READSPECNO
1179            %FINISH
1180            %CYCLE I=0,1,1
1181            DIG(I)=INTPT(SPECNO/10**(1-I))
1182            SPECNO=SPECNO-DIG(I)*10**(1-I)
1183            DIG(I)=DIG(I)+48
1184            %REPEAT
1185            TNAME(0)='P'<<8+'S'
1186            TNAME(1)='C'<<8+'E'
1187            TNAME(2)=DIG(1)<<8+DIG(0)
1188            NEWLINE
1189            DEFINEOUTPUT(TNAME)
1190            SELECTOUTPUT(1)
1191            %CYCLE J=-50,1,50
1192            %IF NACC(J)#0 %THENSTART
1193            WRITE(J,4)
1194            WRITE(NACC(J),4)
1195            PRINTFL(SIGNAL(J),4)
1196            PRINTFL(ERROR(J),4)
1197            NEWLINE
1198            %FINISH
1199            %REPEAT
1200            SELECTOUTPUT(0)
1201            CLOSESTREAM(1)
1202            %END ;!WRITESPEC
1203        !
1204        %ENDOFPROGRAM
```

W#9919

APPENDIX 4 : List of commonly used abbreviations and page reference for definition

	Page Ref.
LIF : Laser-induced fluorescence	13
IRC : Infra-red chemiluminescence	13
AVD : Angle-velocity distribution	13
LLC : Long-lived complex	14
FAS : Fixed angle surface	See Ref. (14)
FMS : Fixed molecule surface	See Ref. (14)
PST : Phase space theory	11

APPENDIX 5 : Publication

An abbreviated account of this work appeared in Donovan et. al., Chem. Phys. Letts. 69, 472 (1980) and is reproduced here.

Volume 69, number 3 CHEMICAL PHYSICS LETTERS 1 February 1980

ENERGY PARTITIONING IN THE REACTION F + I_2

R.J. DONOVAN, D.P. FERNIE, M.A.D. FLUENDY, R.M. GLEN, A.G.A. RAE and J.R. WHEELER
Department of Physics, University of Edinburgh, Edinburgh EH9 3JJ, UK

Received 8 November 1979

The vibrational populations and rotational temperature of the IF product formed in the reaction F + I_2 → IF + I have been measured using a crossed-beam laser-induced fluorescence technique. The relative collision energy was 90 meV. Measurements of the relative populations in the v = 0, 1 and 2 levels showed a strong population inversion with an effective temperature of −3000 K, corresponding to a fraction of the total energy, $\langle f_v \rangle = 0.6 \pm 0.1$, appearing in product IF vibration. In contrast, the product was rotationally cold with $\langle f_R \rangle \approx 0.02$. The results are consistent with a direct dynamical process for this reaction.

1. Introduction

The F + I_2 reaction is of interest as one of a series for which quite detailed dynamical information is now available. The reaction has been studied at thermal energies [1] and a rate constant corresponding to a reaction cross section σ_R = 43 Å^2 found. Molecular beam scattering experiments [2,3] on this system have produced rather disparate results. Grice et al. [2] observed predominantly backwards and sideways product scattering at an initial collision energy of 35 meV while at the higher collision energy of 100 meV Wong and Lee [3] observed a more isotropic distribution with some excess forward scattering. Both groups reported a fraction $\langle f_T \rangle \approx 0.15$ of the total energy appearing in product translation.

In the closely analogous reaction F + ICl [4] substantial IF product excitation was observed with $\langle f_v \rangle$ = 0.63 indicating a very nonstatistical energy disposal probably as a result of a direct dynamical process. The reactions Cl + I_2 and Cl + Br_2 have also been studied by beam scattering methods [5–7]. The former reaction showed stripping dynamics with $\langle f_T \rangle \approx 0.3$, while the Cl + Br_2 reaction proceeded via a short-lived complex again with $\langle f_T \rangle \approx 0.3$.

As might be expected from the greater density of accessible states the process F + CH_3I → FI + CH_3 has been shown to proceed via a long-lived complex at thermal collision energies and the lifetime of this complex has been estimated from molecular scattering measurements for a range of initial collision energies [8,9]. In the long-lived complex regime approximately 30% of the total energy appeared as translational motion of the products. Laser-induced fluorescence measurements [10] confirmed the expected statistical distribution of energy, the CH_3 fragment emerging with about 40% of the total energy and 30% being evenly divided between rotation and vibration in the IF product.

This family of reactions reveals an interesting graduation of behaviour at thermal collision energies, spanning the range from direct to long-lived complex dynamics. The system investigated here, F + I_2, will thus be of interest in exploring the effects of changes in the mass ratio and in revealing any novel features in the potential surface associated with fluorine atom reactions.

2. Experimental

The experiment was performed in a crossed molecular beam laser induced fluorescence apparatus. An effusive I_2 beam was produced using a 10 μm microcapillary array with the reagents supplied from a reservoir at 370 K (≈10 Torr). F atoms were generated by a microwave discharge in a mixture of 10% CF_4 in He, at a total pressure of 5 Torr and were delivered to a nozzle of diameter 1 mm, mounted in a differentially pumped chamber, via a glass pipe coated in "Teflon" (Dupont

FEP 856-200) [11]. The reaction zone was approximately spherical in shape with diameter ≈5 mm and the IF concentration was estimated to be $\approx 10^7$ cm^{-3}. The background pressure with beams running was $\approx 4 \times 10^{-5}$ Torr. The reaction zone was illuminated by a tuneable dye laser. This was pumped by a nitrogen laser of original design [12] operated at a 50 Hz repetition rate. The dye laser pulse was <5 ns (fwhm) in duration and had a band width of 2–3 Å. Rotational structure was thus not resolvable. The dyes used were Coumarin 47 and Coumarin 102 (Applied Photophysics Ltd.) covering the region 460–490 nm. In this region the (5,0), (6,0), (7,0), (8,1), (8,2) bands have Franck–Condon factors >0.03 [13]. Beyond 500 nm fluorescence from IF is obscured by that from the I_2. The fluorescence from the product was viewed at right angles to the laser beam through an aspheric lens and aperture system and was detected by a photomultiplier (EMI 9824). The photon-counting system was gated open 2 μs after each laser flash and closed 10 μs later. Since the IF(B) lifetime is about 8 μs [14] this technique helps to discriminate against noise from other species and against after-pulsing in the photomultiplier. Data was accumulated in this way for 10 or 100 s periods with the laser and F atom discharge each alternately on and off. The count accumulated in each mode together with a measurement of the laser intensity, taken with a sample and hold A–D converter, was captured by a PDP11/45 computer.

Noise from both photomultiplier dark count and stray light was negligible (< 0.1 s^{-1}) and the main noise arose from laser-induced after-pulsing in the photomultiplier. This resulted from a rather poor beam profile and amounted to about 1 s^{-1}. The signal rate was also low, due principally to the low mean laser power (≈100 μW), being comparable with or less than the noise rate. Counting times were therefore long and data could only be collected at a few selected wavelengths to map out the gross features of the vibrational distribution. Bands with $v = 0$ were relatively easy to see but $v = 1$ and 2 were more difficult due to the small Frank–Condon factors from these levels.

3. Results

The (5,0), (6,0), (8,1) and (8,2) bands have been observed. The net signal, the difference in the signals with the F atom discharge on and off, was corrected for background and normalised using the recorded laser intensity (corrected as necessary for wavelength sensitivity). The results are shown as a function of wavelength in fig. 1. The error bounds are largely determined by the after-pulsing effects discussed previously.

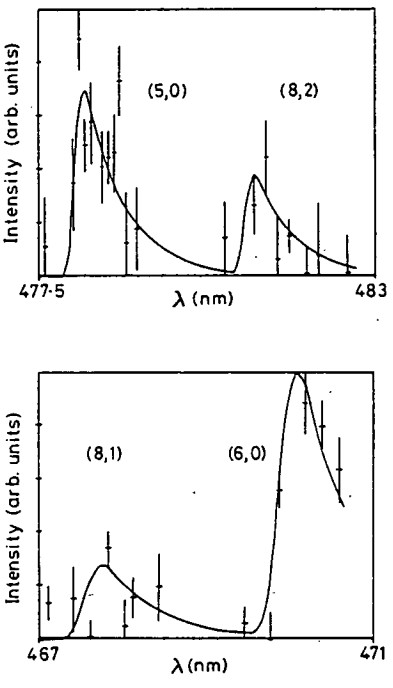

Fig. 1. Fluorescence intensity in the (5,0), (8,2), (8,1) and (6,0) bands of IF product as a function of the wavelength of the incident laser light.

The data have been fitted to a simulated spectrum [15] calculated by convoluting the line frequencies with a triangular laser bandwidth function determined experimentally and using the Franck–Condon factors reported by Clyne et al. [13]. A Boltzmann distribution of rotational states was assumed and all the bands were constrained to the same rotational temperature. The only variable parameters in the fit were the level populations, $N(v)$, which are proportional to the cross sections for the reaction into that channel. The population ratios calculated in this way, relative to $N(0) = 1.0$, are shown in table 1. Good agreement is observed for independent estimates via the (6,0) and (5,0) bands and a rotational temperature of about 200 K satisfactorily describes all the observed levels. The rotational temperature could not be determined to better than 100 K.

Table 1
Population observed in various vibrational levels

Band $v' \leftarrow v''$	$N(v'')$
(5,0)	1.00 ± 0.15
(6,0)	1.16 ± 0.12
(8,1)	1.38 ± 0.28
(8,2)	1.60 ± 0.24

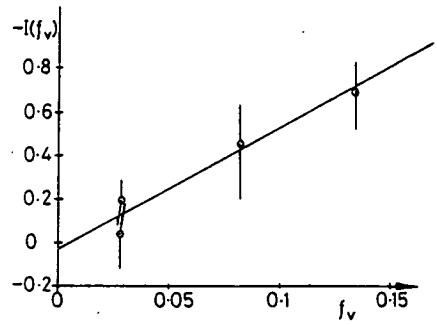

Fig. 2. Plot of the surprisal $-I(f_v)$ against f_v for the four observed bands of IF.

4. Discussion

The relative populations in the 0, 1 and 2 vibrational states of the IF product, as shown in table 1, reveal a substantial population inversion. Higher states, up to $v = 19$ are energetically available but are not measurable experimentally due to predissociation, which sets in at $v' = 9$, and interference by fluorescence from the I_2 reagent. Nevertheless, an effective vibrational temperature for the product can be estimated via the surprisal plot, fig. 2. Such plots are very frequently linear [16] over most of the energetically accessible range and so can provide an estimate of the population in the higher states. The gradient in fig. 2 corresponds to an effective vibrational temperature of −3000 K and a most probable vibrational state of $v = 13$–14 in the product. This extrapolation then yields a fraction of total energy in vibration $\langle f_v \rangle = 0.6 \pm 0.1$.

The rotational temperature is less well defined since individual rotational transitions cannot be resolved. However, information on the average rotational temperature is available from the band profile. The accuracy of this estimate is contingent on relaxation effects but except in the case of the $v = 0$ state, where signals from cold product in the background might interfere, this should not be a substantial effect. The average rotational temperature observed, about 200 K, is equivalent to a rotational fraction $\langle f_R \rangle \approx 0.02$. The energy disposal estimated from these measurements is compared with that for analogous reactions in table 2.

The F + I_2 reaction releases the major fraction of its exothermicity as product vibration and in this respect is similar to the ICl reaction. The disposal is highly nonstatistical and this pattern is characteristic of direct dynamics of reaction with a substantial attractive energy release in the entrance valley of the potential surface. For L + HH mass ratios the relative vibrational and translational disposals can be expected to correlate with the attractive entrance and repulsive exit behaviour of the potential.

The rotational excitation observed is much smaller than in ICl. This may arise from the mass ratio since the exit I atom carries away most of the incident angular momentum associated with I_2 rotation as orbital

Table 2
Energy disposal

Disposal fraction	System				
	F + I_2	F + ICl	Cl + I_2	Cl + Br_2	F + CH_3I
$\langle f_v \rangle$	0.6	0.55 [b]	–	–	0.15 [d]
$\langle f_R \rangle$	0.02	0.14 [b]	–	–	0.14 [d]
$\langle f_T \rangle$ beam measurement	0.15 [a]	–	≈0.3 [c]	≈0.3 [c]	≈0.3 [e]
$\langle f_T \rangle$ by difference	0.4	0.31	–	–	(0.4 in CH_3) [d]

[a] Refs. [2,3]. [b] Ref. [4]. [c] Ref. [6]. [d] Ref. [10]. [e] Ref. [8].

angular momentum and acts as an effective sink for angular momentum. The low rotational excitation observed may also be associated with a much slower relaxation, compared with ICl, of the I_2^- bond during the collision.

References

[1] E.H. Appelman and M.A.A. Clyne, J. Chem. Soc. Faraday I 71 (1975) 2072.
[2] C.F. Carter, M.R. Levy, K.B. Woodall and R. Grice, Faraday Discussions Chem. Soc. 55 (1973) 381.
[3] Y.C. Wong and Y.T. Lee, Faraday Discussions Chem. Soc. 55 (1973) 383.
[4] L. Stein, J. Wanner, H. Figger and H. Walther, in: Laser induced processes in molecules, Springer series in chemical phys. Vol. 6, eds. K.L. Kompa and S.D. Smith (Springer, Berlin, 1974) p. 232.
[5] Y.T. Lee, P.R. LeBreton, J.D. McDonald and D.R. Herschbach, J. Chem. Phys. 51 (1969) 455.
[6] H.J. Loesch and D. Beck, Ber. Bunsenges. Physik. Chem. 75 (1971) 736.
[7] Y.T. Lee, J.D. McDonald, P.R. LeBreton and D.R. Herschbach, J. Chem. Phys. 49 (1968) 2447.
[8] J.M. Farrar and Y.T. Lee, J. Chem. Phys. 63 (1975) 3639.
[9] J.J. Valentini, M.J. Coggiola and Y.T. Lee, Faraday Discussions Chem. Soc. 62 (1977) 232.
[10] L. Stein, J. Wanner and H. Walther, J. Chem. Phys., to be published.
[11] H.C. Berg and D. Kleppner, Rev. Sci. Instr. 33 (1962) 248.
[12] D.P. Fernie, unpublished.
[13] M.A.A. Clyne and I.S. McDermid, J. Chem. Soc. Faraday II 72 (1976) 2242.
[14] M.A.A. Clyne and I.S. McDermid, J. Chem. Soc. Faraday II 74 (1978) 1644.
[15] R.M. Glen, Ph.D. Thesis, University of Edinburgh, to be published.
[16] R.D. Levine and J.C. Kinsey, in: Atom–molecule collision theory, ed. R.B. Bernstein (Plenum Press, New York, 1979).

REFERENCES

1. R.D. Levine and R.B. Bernstein, Molecular Reaction Dynamics. (Oxford University Press, New York, 1972).

2. A.B. Callear, Specialist Periodical Reports; Gas Kinetics and Energy Transfer Vol. 3. P.J. Ashmore and R.J. Donovan, Eds. (The Chemical Society, London, 1978).

3. J.I. Steinfeld and J.L. Kinsey, Progr. Reaction Kinetics 5, 1 (1970).

4. H.S. Johnstone, Ann. Rev. Phys. Chem. 26, 315 (1975).

5. M.J. Berry, J. Chem. Phys. 59, 6229 (1973).

6. I.M. Campbell and D.L. Blanch, Specialist Periodical Reports; Gas Kinetics and Energy Transfer Vol. 3. P.J. Ashmore and R.J. Donovan, Eds. (The Chemical Society, London, 1978).

7. U. Dimur, R. Koslott, R.D. Levine and M.J. Berry, Chem. Phys. Lett. 34, 199 (1975).

8. R.J. Donovan, Progr. Reaction Kinetics 10, 255 (1979).

9. V.S. Letokhov, Ann. Rev. Phys. Chem. 28, 133 (1977).

10. R.T. Bailey and F.R. Cruickshank, Ann. Reports Chemical Society 75(A), 49 (1978).

11. D.R. Herschbach, Faraday Disc. Chem. Soc. 55, 233 (1973).

12. M.A.D. Fluendy and K.P. Lawley, Chemical Applications of Molecular Beam Scattering. (Chapman and Hall, London, 1972).

13. M.R. Levy, Prog. Reaction Kinetics 10, 1 (1979).

14. P.J. Kuntz, Modern Theoretical Chemistry Vol 2; Dynamics of Molecular Collisions Pt. B. W.B. Miller, Ed. (Plenum Press, New York, 1976) p. 53.

15. R.J. Tully, op. cit., p. 217.

16. R.N. Porter and L.M. Raff, op. cit., p. 1.

17. P.J. Kuntz, E.M. Nemeth, J.C. Polanyi, S.D. Rosner and C.E. Young, J. Chem. Phys. 44, 1168 (1966).

18. R. Grice, Advan. Chem. Phys. 30, 247 (1975).

19. P. Pechukas, Modern Theoretical Chemistry Vol. 2; Dynamics of Molecular Collisions Pt. B. W.B. Miller, Ed. (Plenum Press, New York, 1976) p. 269.

20. E.E. Nikitin, Theory of Elementary Atomic and Molecular Processes in Gases. (Clarendon Press, Oxford, 1974).

21. R.A. Marcus, Faraday Disc. Chem. Soc. 55, 9 (1973).

22. P. Pechukas and J.C. Light, J. Chem. Phys. 42, 3281 (1965).

23. P. Pechukas, J.C. Light and C. Rankin, J. Chem. Phys. 44, 794 (1968).

24. J.C. Light, Faraday Disc. Chem. Soc. 44, 14 (1968).

25. R.A. White and J.C. Light, J. Chem. Phys. 55, 379 (1971).

26. J.M. Parson, K. Shobotake, Y.T. Lee and S.A. Rice, Faraday Disc. Chem. Soc. 55, 344 (1973).

27. S.A. Safron, N.D. Weinstein, D.R. Herschbach and J.C. Tully, Chem. Phys. Lett. 12, 564 (1972).

28. P.J. Dagdigian, H.W. Cruse, A. Schultz and R.N. Zare, J. Chem. Phys. 61, 4450 (1974).

29. W.H. Miller, J. Chem. Phys. 65, 2216 (1976).

30. D.A. Case and D.R. Herschbach, J. Chem. Phys. 64, 4214 (1976).

31. R.B. Bernstein and R.D. Levine. Advan. Atomic Molec. Phys. 11, 216 (1975).

32. A. Ben-Shaul, R.D. Levine and R.B. Bernstein, J. Chem. Phys. 57, 5427 (1972).

33. R.D. Levine, B.R. Johnson and R.B. Bernstein, Chem. Phys. Lett. 19, 1 (1973).

34. D.A. Case and D.R. Herschbach, J. Chem. Phys. 69, 150 (1978).

35. R.D. Levine and R.B. Bernstein, Chem. Phys. Lett. 29, 1 (1974).

36. A. Ben-Shaul, Chem. Phys. 22, 341 (1977).

37. R.J. Donovan and H.M. Gillespie, Specialist Periodical Reports; Reaction Kinetics Vol. 1. P.J. Ashmore, Ed. (The Chemical Society, London, 1974) p. 14.

38. Y.T. Lee, J.D. McDonald, P.R. LeBreton and D.R. Herschbach, Rev. Sci. Instr. 40, 1402 (1969).

39. J.J. Valentine, Y.T. Lee and D.R. Auerbach, J. Chem. Phys. 67, 4866 (1977).

40. W.B. Miller, S.A. Safron and D.R. Herschbach, Faraday Disc. Chem. Soc. 44, 108 (1967).

41. D.D. Parrish and D.R. Herschbach, J. Am. Chem. Soc. 95, 6133 (1973).

42. D. StA.G. Radlein, J.C. Whitehead and R. Grice, Mol. Phys. 29, 1813 (1975).

43. S.J. Riley and D.R. Herschbach, J. Chem. Phys. 58, 27 (1973).

44. J.M. Birley, R.R. Herm, K.R. Wilson and D.R. Herschbach, J. Chem. Phys. 47, 993 (1967).

45. G.H. Kwei and D.R. Herschbach, J. Chem. Phys. 51, 1742 (1969).

46. S.M. Lin, C.A. Mims and R.R. Herm, J. Chem. Phys. 58, 327 (1973).

47. P.A. Gorry, C.V. Nowikow and R. Grice, Mol. Phys. 37, 329 (1979).

48. P.A. Gorry, C.V. Nowikow and R. Grice, Mol. Phys. 37, 347 (1979).

49. G.A. Fisk, J.D. McDonald and D.R. Herschbach, Faraday Disc. Chem. Soc. 44, 228 (1967).

50. C.F. Carter, M.R. Levy and R. Grice, Faraday Disc. Chem. Soc. 55, 357 (1973).

51. J.D. McDonald, P.R. LeBreton, Y.T. Lee and D.R. Herschbach, J. Chem. Phys. 49, 2447 (1968).

52. K.G. Anlauf, P.J. Kuntz, D.M. Maylotte, P.D. Pacey and J.C. Polanyi, Faraday Disc. Chem. Soc. 44, 183 (1967).

53. K.G. Anlauf, D.S. Horne, R.G. McDonald, J.C. Polanyi and K.B. Woodall, J. Chem. Phys. 57, 1516 (1972).

54. D.H. Maylotte, J.C. Polanyi and K.B. Woodall, J. Chem. Phys. 57, 1547 (1972).

55. J.C. Polanyi and W.J. Skrlac, Chem. Phys. 23, 167 (1977).

56. H.W. Cruse, P.J. Dagdigian and R.N. Zare, Faraday Disc. Chem. Soc. 55, 277 (1973).

57. J.L. Kinsey, Ann. Rev. Phys. Chem. 28, 349 (1977).

58. T.W. Hänsch, App. Optics 11, 895 (1972).

59. L. Stein, J. Wanner, and H. Walther, J. Chem. Phys. 72, 1128 (1980).

60. L. Stein, PLF Report No. 7, Max-Planck-Gesellschaft, Munich (1978).

61. L. Stein, J. Wanner, H. Figger and H. Walther, Springer Series in Chemical Physics Vol. 6; Laser Induced Processes in Molecules, (Springer-Verlag, Berlin, 1979), p. 232.

62. R.B. Bernstein, and M.B. Faist, J. Chem. Phys. 65, 5436 (1976).

63. J.M. Farrar and Y.T. Lee, J. Chem. Phys. 63, 2639 (1975).

64. S.M. Lim, C.A. Mims and R.R. Herm, J. Phys. Chem. 77, 569 (1973).

65. J.G. Pruett and R.N. Zare, J. Chem. Phys. 64, 1774 (1976).

66. K. Lieu and J.M. Parson, J. Chem. Phys. 67, 1814 (1977).

67. J.A. Silver, W.L. Dimpfl, J.H. Brophy and J.L. Kinsey, J. Chem. Phys. 65, 1815 (1976).

68. P.P. Mariella, B. Lautzsch, V.T. Maxson and A.G. Luntz, J. Chem. Phys. 69, 5411 (1978).

69. P.J. Dagdigian and R.N. Zare, J. Chem. Phys. 61, 2464 (1974).

70. G.P. Smith and R.N. Zare, J. Chem. Phys. 64, 2632 (1976).

71. G.P. Smith, J.C. Whitehead and R.N. Zare, J. Chem. Phys. 67, 4912 (1977).

72. Z. Karny and R.N. Zare, J. Chem. Phys. 68, 3360 (1978).

73. J.L. Kinsey, J. Chem. Phys. 66, 1815 (1976).

74. D.A. Case, G.M. McClelland and D.R. Herschbach, Mol. Phys. 35, 541 (1978).

75. M.P. Sinha, C.D. Caldwell and R.N. Zare, J. Chem. Phys. 61, 491 (1974).

76. M.A.A. Clyne and A.H. Curran, Specialist Periodical Reports; Gas Kinetics and Energy Transfer Vol. 2. P.J. Ashmore and R.J. Donovan Eds. (The Chemical Society, London, 1977) p. 239.

77. M.A.A. Clyne and I.S. McDermid, J.C.S. Faraday II 72, 2242 (1976).

78. M.A.A. Clyne and I.S. McDermid, J.C.S. Faraday II 72, 2252 (1976).

79. M.A.A. Clyne and I.S. McDermid, J.C.S. Faraday II 74, 644 (1978).

80. M.A.A. Clyne and I.S. McDermid, J.C.S. Faraday II 74, 664 (1978).

81. M.A.A. Clyne and I.S. McDermid, J.C.S. Faraday II 74, 798 (1978).

82. M.A.A. Clyne and I.S. McDermid, J.C.S. Faraday II 74, 1935 (1978).

83. M.A.A. Clyne and I.S. McDermid, J.C.S. Faraday II 74, 1644 (1978).

84. M.A.A. Clyne and I.S. McDermid, J.C.S. Faraday II 75, 280 (1979).

85. R.F. Barrow, T.C. Clark, J.A. Coxon and K.K. Lee, J. Mol. Spec. 51, 428 (1974).

86. J.A. Coxon, Chem. Phys. Lett. 33, 136 (1975).

87. Y.T. Lee, J.D. McDonald, P.R. LeBreton and D.R. Herschbach, J. Chem. Phys. 51, 455 (1969).

88. J.B. Cross and N.C. Blaise, J. Chem. Phys. 50, 4108 (1969).

89. N.C. Blaise and J.B. Cross, J. Chem. Phys. 52, 3580 (1970).

90. J.B. Cross and N.C. Blaise, J. Chem. Phys. 55, 3970 (1971).

91. H.J. Loesch and D. Beck, Ber. Bunsenges, Phys. Chem. 75, 736 (1971).

92. T.B. Bourne and D.L. Bunker, J. Chem. Phys. 55, 4861 (1971).

93. E.S. Prochaska and L. Andrews, Inorg. Chem. 16, 339 (1977).

94a) S.R. Ungemach and H.F. Schaefer, J. Am. Chem. Soc. 98, 1658 (1977).

b) S.R. Ungemach, Berkely Lab. Rep. LBL, 6699 (1977).

95. L.Y. Nelson and G.C. Pimentel, J. Chem. Phys. 47, 3671 (1967).

96. J.J. Valentini, M.J. Coggiola and Y.T. Lee, Faraday Disc. Chem. Soc. 62, 232 (1977).

97. M.J. Coggiola, J.J. Valentini and Y.T. Lee, Int. J. Chem. Kinetics 8, 605 (1976).

98. C.F. Carter, M.R. Levy, K.B. Woodall and R. Grice, Faraday Disc. Chem. Soc. 55, 381 (1973).

99. C.F. Carter, M.R. Levy, K.B. Woodall and R. Grice, Faraday Disc. Chem. Soc. 55, 385 (1973).

100. Y.C. Wong and Y.T. Lee, Faraday Disc. Chem. Soc. 55, 383 (1973).

101. R. Grice (private communication, 1979).

102. P.C. Nordine, J. Chem. Phys. 61, 224 (1974).

103. E.H. Appelmann and M.A.A. Clyne, J.C.S. Faraday I, 71, 2072 (1975).

104. M.A.A. Clyne and H.W. Cruse, J.C.S. Faraday II, 68, 1377 (1972).

105. M.A.A. Clyne and I.S. McDermid, J.C.S. Faraday II, 74, 1376 (1978).

106. M.A.A. Clyne and I.S. McDermid, J.C.S. Faraday II, 74, 807 (1978).

107. M.A.A. Clyne and M.C. Heaven, J.C.S. Faraday II, 74, 1992 (1978).

108. G.W. King and R.G. McFadden, Chem. Phys. Lett. 58, 119 (1978).

109. M. Broyer, J. Vigue and J.C. Lehman, J. Chem. Phys. 63, 5428 (1975).

110. C.A. Wight, B.S. Ault and L. Andrews, J. Mol. Spec. 56, 239 (1975).

111. G.W. Holleman and J.I. Steinfeld, Chem. Phys. Lett. 12, 431 (1971).

112. J.W. Birks, S.D. Gabelnick and H.S. Johnston, J. Mol. Spec. 57, 23 (1975).

113. L. Pasternack and P.J. Dagdigian, Chem. Phys. 33, 1 (1978).

114a) R.A. Durie, Proc. Phys. Soc. 63, 1292 (1950).

b) R.A. Durie, Proc. Roy. Soc. A207, 388 (1951).

c) R.A. Durie, Can. J. Phys. 44, 337 (1966).

115. M. Schmeisser and E. Scharf, Angew. Chem. 72, 324 (1960).

116. G. Herzberg, Molecular Spectra and Molecular Structure Vol. 1; Spectra of Diatomic Molecules (Van Nostrand, London, 1973).

117. J.A. Coxon, Specialist Periodical Reports; Molecular Spectroscopy Vol. 1. J.F. Barrow Ed., (The Chemical Society, London, 1973) p. 177.

118. M.S. Child and R.B. Bernstein, J. Chem. Phys. 59, 5916 (1972).

119. D.P. Fernie, Ph.D. Thesis, University of Edinburgh, 1980.

120. D.M. Manos and J.M. Parson, J. Chem. Phys. 69, 231 (1978).

121. W.H. Breckenridge, R.P. Blickensderfer, J. Fitzpatrick and D. Oba J. Chem. Phys. 70, 4751 (1979).

122. R. Schlapp, Phys. Rev. 39, 806 (1932).

123. R.J. Leroy and E.R. Viscay, Can. J. Phys. 53, 1560 (1975).

124. N.S. Murthy and L.S. Gouda, J. Phys. B, 10, 491 (1977).

125. C.E. Kolbe and M. Kaufman, J. Phys. Chem. 76, 947 (1972).

126. C.J. Oliver, E.M.I. Technical Report R/P066.

127. L.J. Cline-Love and L.A. Shaver, Anal. Chem. 48, 365A (1976).

128. P.B. Coates, J. Phys. E, 5, 148 (1972).

129. J.A. Giordmaine and T.C. Wang, J. App. Phys. 31, 463 (1960).

130. C.R.C. Handbook of Chemistry and Physics (Chemical Rubber Co. Press, Florida, 1974).

131. J.C. Johnson, A.T. Stairs and J.L. Pritchard, J. App. Phys. 37, 1551 (1966).

132. H. Pauly and J.P. Toennies, Methods Exp. Phys. 7(A), 227 (1968).

133. J.B. Anderson, R.P. Andres and J.B. Fenn, Advan. Chem. Phys. 10, 275 (1966).

134. J.B. Anderson and J.B. Fenn, Phys. Fluids, 8, 780 (1965).

135. R. Compargue, Advan. App. Mech. Vol. 2, Supp. 3, Rarified Gas dynamics, J.H. DeLeeuw, Ed. (Academic Press, London, 1960) p. 279.

136. J.B. French and D.R. O'Keef, op. cit. p. 299.

137. D.E. Roth, Phys. Fluids, 9, 1643 (1966).

138. R. Hialt and S.W. Benson, Int. J. Chem. Kinetics, 4, 479 (1972).

139. N. Basco and F.G.M. Hathorn, Chem. Phys. Lett. 8, 291 (1971).

140. R. Foon and M. Kaufman, Prog. Reaction Kinetics, 8, 81 (1975).

141. F. Kaufman, Progr. Reaction Kinetics, 1, 3 (1966).

142. G.A. Ogryzlo, Can. J. Chem. 39, 2565 (1961).

143. Y.T. Lee, P.R. LeBreton, J.D. McDonald, and D.R. Herschbach, J. Chem. Phys. 49, 2447 (1968).

144. H.C. Berg and D. Kleppner, Rev. Sci. Instruments, 33, 248 (1962).

145. J.B. Kennedy and A.M. Neville, Basic Statistical Methods (Harper and Row, New York, 1976).

146. P.A. Gorry and R. Grice, J. Phys. E, 12, 857 (1979).

147. J.R. Wheeler (private communication).

148. D. Levine, Ann. Rev. Phys. Chem. 29, 59 (1978).

149. M.J. Berry, Chem. Phys. Lett. 29, 327 (1975).

150. H.J. Korsch and R.D. Levine, Chem. Phys. 30, 333 (1978).

151. M.J. Berry, J. Chem. Phys. 61, 3114 (1974).

152. R.D. Levine and J.L. Kinsey, Atom-Molecule Collision Theory - a Guide for the Experimentalist, R.B. Bernstein, Ed. (Plenum Press, New York, 1979) p. 693.

153. A. Ben Shaul, R.D. Levine and R.B. Bernstein, Chem. Phys. Lett. 15, 160 (1972).

154. E. Pollak and R.D. Levine, Chem. Phys. 21, 61 (1977).

155. J.A.N.A.F. Thermochemical Tables (U.S. National Bureau of Standards, 1965).

156. N.B.S. Selected Values of Chemical and Thermodynamic properties (U.S. National Bureau of Standards, 1952).

157. Comprehensive Inorganic Chemistry Vol. 2, A.F. Trotman-Dickenson Ed. (Pergamon Press, Oxford, 1973).

158. N.C. Blaise and D.L. Bunker, J. Chem. Phys. 39, 315 (1963).

159. D.L. Bunker and N.C. Blaise, J. Chem. Phys. 41, 2377 (1964).

161. P.J. Kuntz, M.M. Mok and J.C. Polanyi, J. Chem. Phys. 50, 4623 (1969).

162. R.L. Wilkins, J. Chem. Phys. 58, 2362 (1976).

163. J.J. Valentine, M.J. Coggiola and Y.T. Lee, J. Am. Chem. Soc. 98, 853 (1976).

164. D.A. Dixon, D.D. Parrish and D.R. Herschbach, Faraday Disc. Chem. Soc. 55, 385 (1973).

165. N.H. Hijazi and J.C. Polanyi, J. Chem. Phys. 63, 2249 (1975).

166. N.H. Hijazi and J.C. Polanyi, Chem. Phys. 11, 1 (1975).

167. J.C. Polanyi, Faraday Disc. Chem. Soc. 55, 389 (1973).

168. P.J. Kuntz, J.C.S. Faraday II, 66, 2980 (1970).

169. A.M.G. Ding, L.J. Kirsch, D.S. Perry, J.C. Polanyi and J.L. Schreiber, Farad. Disc. Chem. Soc. 55, 252 (1973).

170. J.C. Polanyi and K.B. Woodall, J. Chem. Phys. 57, 1547 (1972).

171. E.J. Murphy, J.H. Brophy, G.S. Arnold, W.L. Dimpfl, and J.L. Kinsey, J. Chem. Phys. 70, 5910 (1979).

172. M.A.A. Clyne and M.C. Heaven, J.C.S. Faraday II, 76, 49 (1980).

173. P.N. Clough and J. Johnston, Chem. Phys. Letts. 71, 253 (1980).

174. M.A.A. Clyne, M.C. Heaven and E. Martinez, J.C.S. Faraday II, 76, 405 (1980).